Dynamics Analysis of Flexible-Link Cooperating Manipulators

by

Qiao Sun
B.Sc., Shanghai Jiao Tong University, 1982
M.Sc., Shanghai Jiao Tong University, 1986

A Dissertation Submitted in Partial Fulfillment of the
Requirements for the Degree of
DOCTOR OF PHILOSOPHY
in the
Department of Mechanical Engineering.

We accept this dissertation as conforming
to the required standard

Dr. M. Nahon, Co-Supervisor (Dept. of Mech. Eng.)

Dr. I. Sharf, Co-Supervisor (Dept. of Mech. Eng.)

Dr. R. P. Podhorodeski, Departmental Member (Dept. of Mech. Eng.)

Dr. B. Tabarrok, Departmental Member (Dept. of Mech. Eng.)

Dr. W. S. Lu, Outside Member (Dept. of Elec. Eng.)

Dr. J. Y. S. Luh, External Member (Clemson University)

Supervisor: Drs. M. Nahon and I. Sharf

Abstract

Cooperative operation of multiple manipulators has been increasingly used in industrial automation, outer space and hazardous terrestrial applications. Moreover, the requirement for increased speeds of operation and light-weight design of robot manipulators has made structural flexibility a dominant factor in the design and control of cooperating manipulator systems.

When multiple manipulators act cooperatively on an object, a closed-loop chain structure is formed. Redundant actuation is one of the inherent characteristics of such systems. Determining actuator torques necessary to achieve a prescribed object motion is known as the inverse dynamics process. Due to the presence of the redundant actuators, inverse dynamics torques for cooperating manipulator systems admit an infinite number of solutions.

Consideration of flexibility in the links of manipulators, particularly relevant in space applications, not only complicates the dynamics modeling of the system, but also introduces instability in the inverse dynamics solution. In this study, a dynamics model is derived for a flexible-link cooperating manipulator system and the inverse dynamics procedure for such a system is investigated. In particular, the latter is divided into two subproblems — the force distribution problem and the inverse dynamics problem for serial flexible-link manipulators. The approach chosen to the force distribution problem is to formulate it as a linearly constrained local optimization problem. Several objectives particularly relevant to flexible-link cooperating manipulators are proposed. These include minimum strain energy, minimum weighted norm of elastic accelerations and optimal load sharing schemes. The resulting algorithms are shown to be effective in reducing the vibration of the system and stabilizing the inverse dynamics solution.

A stability analysis of the internal dynamics of the inverse dynamics system is also performed by using linearization. Agreement in the behavior of the inverse dynamics system is demonstrated between directly solving the nonlinear dynamics equations with optimal force distribution and calculating the eigenvalues of the plant matrix of the linearized system. A stability approach to the force distribution problem is then proposed which ensures stable behavior of the internal dynamics system under the condition that the number of elastic coordinates of the system is less than or equal to the total number of redundant actuators.

Examiners:

Dr. M. Nahon, Co-Supervisor (Dept. of Mech. Eng.)

Dr. I. Sharf, Co-Supervisor (Dept. of Mech. Eng.)

Dr. R. P. Podhorodeski, Departmental Member (Dept. of Mech. Eng.)

Dr. B. Tabarrok, Departmental Member (Dept. of Mech. Eng.)

Dr. W. S. Lu, Outside Member (Dept. of Elec. Eng.)

Dr. J. Y. S. Luh, External Member (Clemson University)

Table of Contents

List of Tables

List of Figures

Acknowledgements

I would like to thank my supervisors, Dr. M. Nahon and Dr. I. Sharf for their guidance, patience as well as their financial support thoughout the course of my study. I would also like to thank my advisory committee members for their advice and assistance.

I wish to acknowledge the Department of Mechanical Engineering which provided the atmosphere and resources to make my study possible. My thanks also go to the professors and graduate students of the department for many of the interesting and helpful discussions which clarified my understanding of the subject matter.

Finally, my special thanks are due to my family for their understanding, encouragement, and endurance.

To my motherland

and my parents

Nomenclature

$\boldsymbol{c}_i$	position of the ith contact point on the object relative to the mass centre of the object expressed in the fixed frame
i	manipulator index in the arm/object system
P	number of manipulators in the system
$\mathcal{F}_I$	world coordinate frame
$\mathcal{F}_n$	link coordinate frame
n	body index in a single arm
N	number of bodies in a single arm
$\mathcal{F}_E$	end-effector coordinate frame
$\mathcal{F}_B$	object coordinate frame
M	total number of joint degrees of freedom of a single arm
S	total number of elastic coordinates of a single arm
K	total number of generalized coordinates of a single arm
$\boldsymbol{q}_r$	column vector of joint coordinates of a single arm
$\boldsymbol{q}_e$	column vector of elastic coordinates of a single arm
$\mathcal{T}_{n+1,n}$	interbody transformation matrix from body n to body $n+1$ for rigid degrees of freedom
s_n	number of elastic coordinates of body n
$\mathcal{S}_{n+1,n}$	interbody transformation matrix for elastic degrees of freedom

$\mathcal{B}_n$	body n
O_n	origin of $\mathcal{F}_n$
v_n	spatial velocity of $\mathcal{B}_n$ expressed in $\mathcal{F}_n$
v_n	absolute linear velocity of O_n
m_n	degrees of freedom of joint n
$\mathcal{P}_n$	projection matrix for joint n
ω_n	absolute angular velocity of $\mathcal{B}_n$
$\mathcal{C}_{I,E}$	6×6 rotation matrix from end-effector to fixed frame
$\mathrm{C}_{I,E}$	3×3 rotation matrix from end-effector to fixed frame
$\mathbf{J}_r$	rigid Jacobian matrix
$\mathbf{J}_e$	elastic Jacobian matrix
$\mathcal{T}_A$	augmented interbody transformation matrix
$\mathcal{P}_\Sigma$	global projection matrix for a single arm
$\mathcal{S}_\Sigma$	global interbody transformation matrix for elastic degrees of freedom of a single arm
r_B	position vector of O_B expressed in the inertial frame
(α, β, γ)	angles defining the orientation of the object
C_B	rotation matrix from $\mathcal{F}_B$ to the inertial frame
v_B	absolute linear velocity of O_B
ω_B	absolute angular velocity of $\mathcal{B}_B$
$\Omega_B^\times$	cross-product operation matrix of ω_B
r_i	position vector of the ith $\mathcal{F}_E$
v_i	spatial velocity of the ith $\mathcal{F}_E$
$\mathrm{M}_{n,rr}$	6×6 rigid-body mass matrix

$\mathbf{M}_{n,re}$ mass matrix of $\mathcal{B}_n$ associated with equations for *rigid* motion and *elastic* coordinates

$\mathbf{M}_{n,ee}$ mass matrix of $\mathcal{B}_n$ associated with equations for *elastic* motion and *elastic* coordinates

$\mathbf{D}_{n,ee}$ damping matrix of $\mathcal{B}_n$

$\mathbf{K}_{n,ee}$ stiffness matrix of $\mathcal{B}_n$

$f_{nT,r}$ generalized total force on $\mathcal{B}_n$ associated with *rigid* coordinates

$f_{nT,e}$ generalized total force on $\mathcal{B}_n$ associated with *elastic* coordinates

$f_{nI,r}$ generalized nonlinear inertial force on $\mathcal{B}_n$ associated with *rigid* coordinates

$f_{nI,e}$ generalized nonlinear inertial force on $\mathcal{B}_n$ associated with *elastic* coordinates

$\mathbf{M}_{rr}$ global mass matrix of a single arm associated with global equations for *rigid* motion and *rigid* coordinates

$\mathbf{M}_{re}$ global mass matrix of a single arm associated with global equations for *rigid* motion and *elastic* coordinates

$\mathbf{M}_{ee}$ global mass matrix of a single arm associated with global equations for *elastic* motion and *elastic* coordinates

$\mathbf{D}_{ee}$ global damping matrix for a single arm

$\mathbf{K}_{ee}$ global stiffness matrix for a single arm

τ column vector of the actuator torques of a single arm

$f_{I,r}$ global generalized nonlinear inertial force of a single arm associated with *rigid* coordinates

$f_{I,e}$ global generalized nonlinear inertial force of a single arm associated with *elastic* coordinates

$f_{ext,r}$	global generalized external force on a single arm associated with *rigid* coordinates
$f_{ext,e}$	global generalized external force on a single arm associated with *elastic* coordinates
$f_{w,r}$	global generalized force resulting from the tip wrenches on a single arm associated with *rigid* coordinates
$f_{w,e}$	global generalized force resulting from the tip wrenches on a single arm associated with *elastic* coordinates
w	tip wrench applied to the object by a single arm
f	force components of the tip wrench applied to the object by a single arm
n	moment components of the tip wrench applied to the object by a single arm
$f_{N,w}$	tip wrench applied to the arm expressed in $\mathcal{F}_N$
$f_{N,w,r}$	generalized force on $\mathcal{B}_N$ due to tip wrench associated with rigid coordinates
$f_{N,w,e}$	generalized force on $\mathcal{B}_N$ due to tip wrench associated with elastic coordinates
Ψ	matrix of shape functions associated with elastic displacement in $\mathcal{B}_N$
Θ	matrix of shape functions associated with elastic rotation displacement in $\mathcal{B}_N$
$f_{\Sigma,w,r}$	assembled generalized force due to tip wrench on a single arm associated with rigid coordinates

$f_{\Sigma,w,e}$	assembled generalized forces due to tip wrench on a single arm associated with elastic coordinates
$\mathbf{I}_B$	second moment of inertia of the object about its mass center
m_B	mass of the object
$\mathbf{n}_e$	net external moment applied to the object
$\mathbf{f}_e$	net external force applied to the object
$\mathbf{g}$	acceleration due to gravity
$\mathbf{c}_e$	position vector from the object's mass centre to the point of application of $\mathbf{f}_e$
a	width of a rectangular beam
h	height of a rectangular beam
l	length of a beam
m	mass of a beam
EI	bending stiffness of a flexible beam
EA	axial stiffness of a flexible beam
$(x_p,\ y_p)$	coordinates of a point on a planar flexible beam
$\mathbf{u}$	vector of elastic displacements
ξ	x_p/l
Φ	row vector of shape functions for elastic displacement in the Y direction
$y(x_p, t)$	elastic displacement in the Y direction of body frame
$\mathrm{v}(t)$	transverse displacement at a nodal point
$\mathrm{v}'(t)$	slope at a nodal point
$\mathbf{c}_1$	first moment of mass of a single flexible beam
$\mathbf{c}_1^{\times}$	cross-product operation matrix of $\mathbf{c}_1$
$\mathbf{J}_1$	second moment of inertia of a beam
ρ	density of a beam

y	output vector
θ_1	angular displacement of the joint of a single beam
s	Laplace variable
$\boldsymbol{q}$	column vector of the generalized coordinates
$\mathbf{Q}(s)$	Laplace transform of the generalized coordinates
$T(s)$	Laplace transform of actuator torque for a single beam
$Y(s)$	Laplace transform of the output
$H(s)$	transfer function of the forward system
$\hat{H}(s)$	transfer function of the inverse system
$\boldsymbol{x}$	vector of states
$\mathbf{f}(\boldsymbol{x}, t)$	function on the right-hand side of the first-order differential equation
t	time variable
t_a	acceleration period
t_f	terminal time
π	power
W	work
$E(t)$	energy drift
$\epsilon_E(t)$	percentage error in the energy balance
$\epsilon_{E.RMS}$	root mean square value of the energy balance error
$\boldsymbol{\tau}'$	inverse dynamics torques to generate a prescribed tip motion in the absence of tip wrenches
$\ddot{\boldsymbol{q}}'_r$	inverse dynamics solution for rigid accelerations corresponding to a prescribed tip motion in the absence of tip wrenches
$\ddot{\boldsymbol{q}}'_r$	inverse dynamics solution for elastic accelerations corresponding to a prescribed tip motion in the absence of tip wrenches

$\mathbf{J}_1^T$	matrix representing the influence of tip wrenches on the inverse dynamics torques
$\mathbf{J}_2^T$	matrix representing the influence of tip wrenches on the inverse dynamics solution for rigid accelerations
$\mathbf{J}_3^T$	matrix representing the influence of tip wrenches on the inverse dynamics solution for elastic accelerations
τ_Σ	column vector of actuator torques for a multi-arm system
w_Σ	column vector of tip wrenches for a multi-arm system
$\mathbf{A}_1$	matrix of contact force map
n_c	number of degrees of freedom of a closed-loop system
n_a	number of redundant actuators
$R(\mathbf{A}_1)$	range space of $\mathbf{A}_1$
$N(\mathbf{A}_1)$	null space of $\mathbf{A}_1$
z	null space variables
τ_Σ^{lim}	column vector containing the maximum values each actuator can generate
$\mathbf{A}_2$	coefficient matrix on the left-hand side of the inequality constraints of optimization problem
$\mathbf{b}_2$	right-hand side of the inequality constraints of optimization problem
x	vector of design variables for the optimization problem
ζ	damping ratio
$f(\mathbf{x})$	objective function
W	weighting matrix
$\mathbf{c}^T$	coefficient matrix of the linear part of a quadratic objective function

$\boldsymbol{\lambda}$	column vector of Lagrange multipliers
$\mathbf{x}^*$	optimum solution
$\mathbf{x}^+$	resultant components of the grasping wrenches
$\mathbf{x}^-$	internal components of the grasping wrenches
$f_I(\mathbf{x})$	objective function for minimum internal force scheme
$f_T(\mathbf{x})$	objective function for minimum weighted norm of actuator torque scheme
$f_E(\mathbf{x})$	objective function for minimum weighted norm of elastic acceleration scheme
$f_U(\mathbf{x})$	objective function for minimum strain energy scheme
U	strain energy stored in the multi-arm system
$\mathbf{h}_\Sigma$	nonlinear inertial terms in the internal dynamics of system B
$\mathbf{g}_\Sigma$	nonlinear inertial terms in the internal dynamics of system C
$\widehat{\mathbf{M}}_{ee}$	coefficient matrix of the second derivative term in the internal dynamics equations of system B
$\widetilde{\mathbf{M}}_{ee}$	coefficient matrix of the second derivative term in the internal dynamics equations of system C
$\boldsymbol{y}$	vector of state variable of the internal dynamics
$\hat{\boldsymbol{y}}$	equilibrium states
$\delta\boldsymbol{y}$	variation of the state
$\mathbf{A}_A$	plant matrix of the linearized model for system A
$\mathbf{A}_B$	plant matrix of the linearized model for system B
$\mathbf{A}_C$	plant matrix of the linearized model for system C
λ_j	jth eigenvalue of the plant matrix of a linearized system
ω_i	ith modal frequency
$\mathbf{1}$	identity matrix
$\mathbf{0}$	zero matrix
$\dot{(\cdot)}$	time derivative

Chapter 1

Introduction

1.1 Background

Robotic systems are increasingly used in industrial automation, deep-sea exploration, outer space and hazardous terrestrial applications. Common requirements for robot manipulators to be applied in these situations are autonomy and dexterity. Moreover, in order to meet the challenges of rapidly expanded applications, higher operating speeds and productivity, larger payload-carrying capacity, increased positioning accuracy and improved system reliability have become more desirable. Many endeavors have been made to enhance the versatility of potential applications and upgrade the performance of robot manipulators toward these goals. Among them, coordinated operation of multiple manipulators has been recognized as an important technique which offers several advantages over operating a single manipulator in the workspace. These are:

- improved dexterity and manipulability of the system because of the superior capability to assemble sophisticated equipment and handle flexible objects;

- higher payload-carrying capability achieved by sharing the loads within multiple manipulators in the system;
- increased productivity which is evident in assembly tasks where manipulators may insert parts into the same object at different locations and operate in parallel.
- enhanced reliability due to the fact that redundant manipulators are normally involved so that alternative strategies can be adopted by the system if a component failure is detected.

Figure 1.1 illustrates the proposed Mobile Servicing System designed at SPAR Aerospace Ltd., in which the Special Purpose Dextrous Manipulator (SPDM) is attached to the Space Station Remote Manipulator System (SSRMS). The SPDM consists of two manipulator arms which work cooperatively to assemble the space station, repair satellites and perform a variety of maintenance tasks on the space station. The coordinated operation of multiple manipulators gives the potential for improved quality of performance of robot systems. However, it has been realized that the traditional design of both mechanical devices and robot controllers based on the assumption of rigid bodies limits the system performance to a certain level. For example, present generation of serial industrial manipulators are restricted to a load-carrying capacity of only $5-10\%$ of their weight by the requirement of rigidity to ensure a satisfactory performance. The same ratio of payload to weight is retained in cooperating manipulators system. Limitations also exist in the speed of motion of single manipulators and therefore the multiple manipulator systems. When the system is operating beyond these limits, the assumption of rigid links is no longer justified for the dynamics model and the controller design. As well, lightweight and energy efficient design of manipulators is preferable in many situations, most notably, in space applications

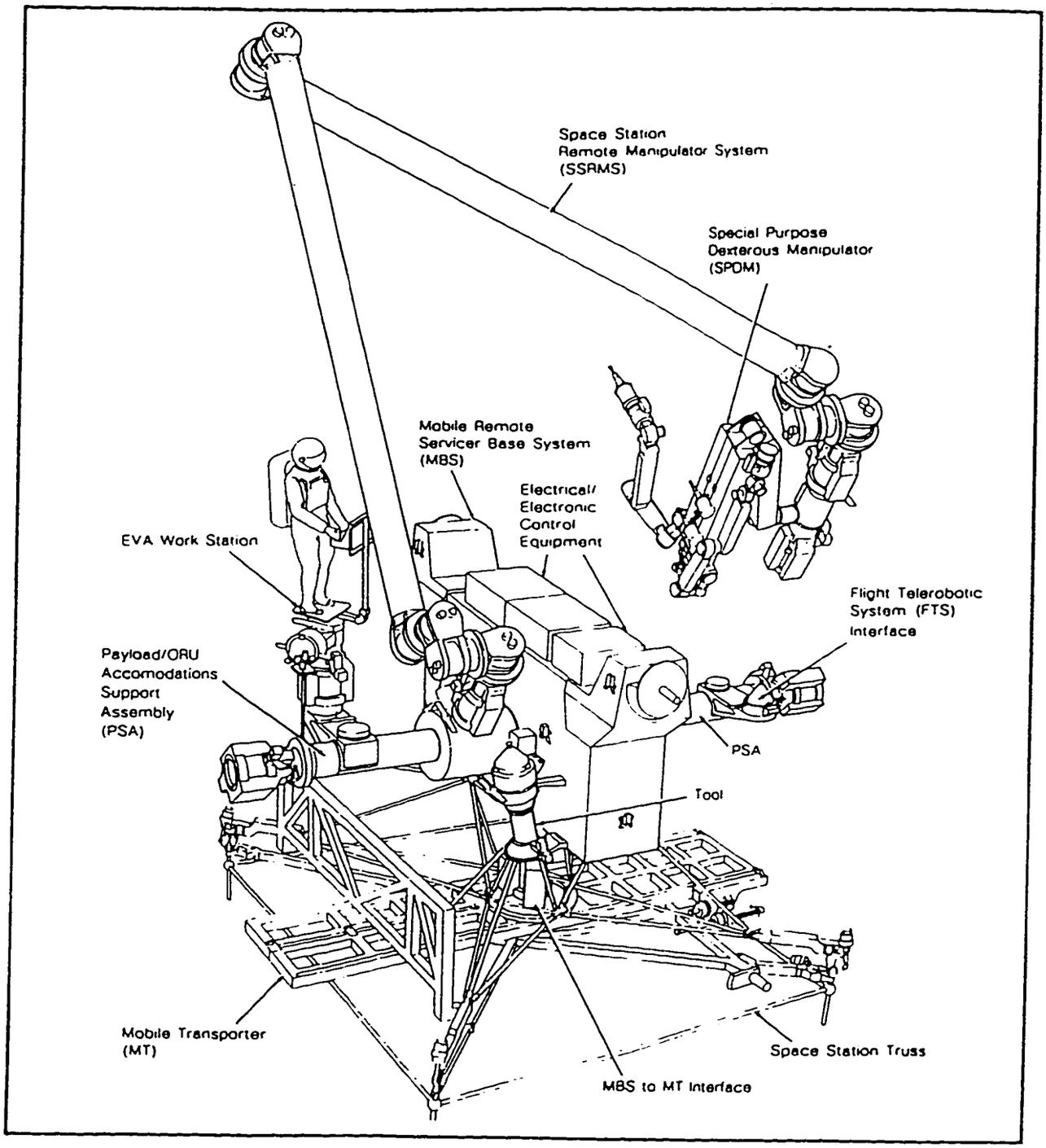

Figure 1.1: The Mobile Servicing System

where links of the manipulators are designed to be long (due to the ineffectiveness of the ground-based wheels and legs) and slender (since the micro-gravity environment of space allows the gravity loads that dominate the design of ground-based mechanical structures to be neglected) [1]. Structural flexibility therefore becomes a dominant factor in modeling and controlling space-based manipulators. Motivated by these facts, this thesis focuses on various aspects of the dynamics analysis of a coordinated multiple manipulator system with flexible links.

1.1.1 System Description

A system of multiple manipulators could be very complicated in terms of its kinematic structure and dynamic features. However, we do not intend to confront all the problems that might stem from considering the most general model. Instead, we still need to specify the system with some assumptions in order to highlight the essential characteristics of the system. Figure 1.2 represents a system of P robotic arms handling a common object. In particular, each manipulator is assumed to be composed of *elastic bodies* connected by *rigid joints*. This is to simulate a situation where link flexibility of the manipulators is a dominant factor as for space applications. The commonly handled object is assumed to be rigid. The manipulator are assumed to be driven by *joint-mounted actuators*. The serial arms are not kinematically redundant that is, the number of degrees of freedom of each serial manipulator is equal to the dimension of the task space. *Rigid grasping* which allows no relative motion between the object and the manipulator end-effectors is also assumed.

Usually, each manipulator is capable of performing certain tasks in its own workspace. However, multiple manipulators become constrained kinematically and dynamically when they form closed loops through a commonly grasped object. When this happens, the total number of degrees of freedom of the system decreases whereas the total

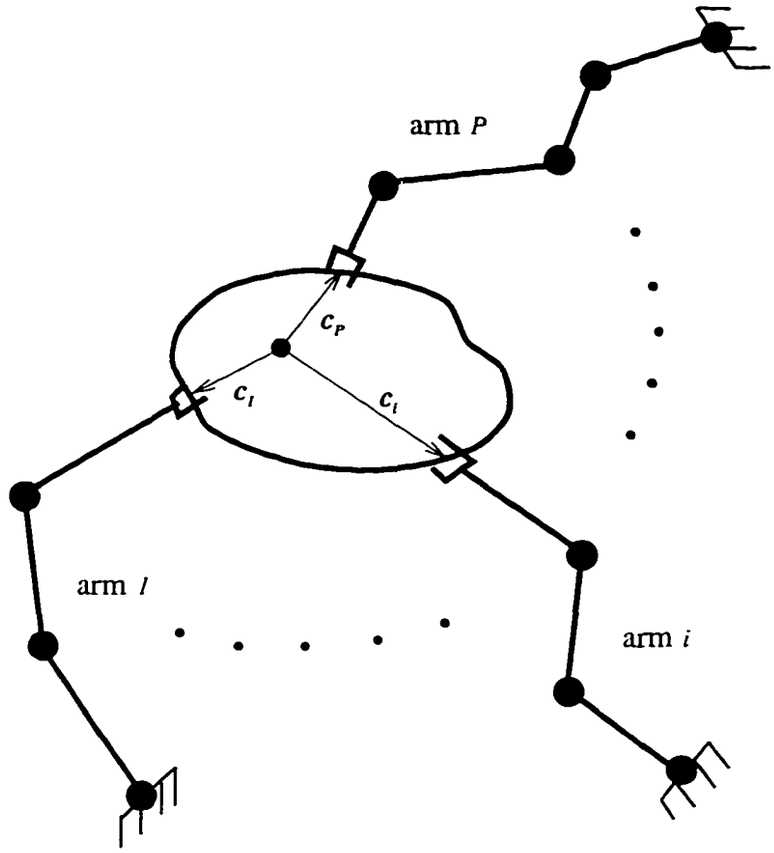

Figure 1.2: Coordinated Multiple Manipulators Handling a Common Object

number of actuators remains unchanged and the system is said to be *redundantly actuated*. We also note that general motion of the system in 3-D space is allowed while the links may undergo bending, extension and torsion.

1.1.2 Introduction to Some Problems

Interest in developing coordinated multiple manipulator systems arise from realizing that some tasks which may be difficult or even impossible for a single manipulator to accomplish can be performed by two or more manipulators operating cooperatively. Hence, a system of coordinated multiple manipulators is normally composed of several

existing serial manipulators. It is the way that manipulators operate makes it a topic of special interest.

Extensive studies have been carried out for rigid cooperating manipulators. These are primarily related to motion planning, coordinated control and application software [2]. On the other hand, studies of flexible-link manipulators are still in the design, simulation and experimental stages. When considering the problem of a coordinated multiple manipulator system while including structural flexibility effects, fundamental issues related to the kinematics and dynamics modeling of the system and its control need to be re-investigated. Dynamics analysis is thus an important consideration and is expected to yield answers to problems ranging from mechanical design to control algorithm development. Since the research issues related to the multiple manipulator systems are mainly of coordinated control type, we are particularly interested in performing the *inverse dynamics analysis* concerned with the driving forces and/or torques for a given trajectory of the reference body — the commonly grasped object. Although this study is directed primarily toward control applications, it also provides useful information for the design engineer with concerns on the control aspects.

Dynamics Modelling

Formulating a concise description of the system dynamics is the first problem we face. Although much research has been conducted on both rigid and flexible multi-body, constrained and unconstrained systems, a concise but effective dynamics model suitable for the inverse dynamics analysis of a flexible-link cooperating manipulator system has not been formulated. On the other hand, in order to analyze and predict the system behavior precisely, an accurate dynamics model is especially useful. However, there always exists a tradeoff between model accuracy and computational efficiency. From the standpoint of system control, it is satisfactory that the dynamics

model be simple to calculate and be reasonably accurate. In this study, finite element method is used to model the elastic links of the manipulators. There is no limitation on the number of elements used to discretize the flexible beams. However, in the simulations carried out to illustrate the performance of inverse dynamics calculation, flexible links are modeled by one or two beam elements as it has been shown by many researchers that the first two modes of vibration are most significant [3].

Planning

In coordinated multiple manipulator systems, two or more manipulators share the same workspace and act in a cooperative manner. Coordination should be ensured both kinematically (*motion planning and tracking*) and in terms of forces (*internal force control*). Motion planning, in this case, differs from what is usually discussed in single kinematically redundant or non-redundant manipulators. Emphasis is placed on coordination within the system rather than optimality associated with individual manipulators. This involves avoiding collisions with other manipulators in the workspace, determining the best set of contact locations on the object for each manipulator [4], *e.g.*, vectors c_i, $(i = 1, \ldots, P)$ in Figure 1.2, and defining a suitable trajectory for the object which minimizes the excitation of the system elastic modes [5]. It is also necessary that the trajectory of the object lie in the common workspace of all the manipulators.

Once the motion is pre-planned for the object, manipulators are required to act in a way to achieve the desired motion of the object. It is important to realize that redundant actuation is an inherent characteristic, once the multiple manipulators contact the common object. By definition, actuation redundancy allows for an infinite set of actuation strategies. This may be beneficial since actuators may share the load evenly so that the overall load carrying capability of the system is enhanced. However,

without force coordination, actuators may act against each other. In the worst case, the manipulators may crush or tear the object and even cause task failure.

Resolution of Actuation Redundancy

Better understanding of actuation redundancy promises better utilization of the redundant actuators. Indeed, this redundancy results in an indeterminacy of the grasping forces and moments (grasping wrenches [6, 7]) for carrying the object over a prescribed trajectory. Nakamura [8] proposed to decompose the total generalized force acting on the object into two orthogonal subsets, the resultant force and the internal force. The resultant force lies in the range space of the grasp matrix [4] of the system and contributes to the motion of the object. It can be uniquely determined for a given object trajectory. By contrast, the internal force lies in the null space of the grasp matrix and produces a squeezing or tearing effect on the object. It is not completely defined by the dynamics equations for the object. Therefore, the term force control in the context of multiple manipulator systems specifically refers to the control of internal forces. It is necessary that the internal forces be controlled to avoid excessive values even if the primary task is simply to track a predefined motion of the object.

The above leads naturally to the *force distribution problem* [9, 10, 11, 12]. It is put forward for determining the set of grasping wrenches to be applied to the object so as to achieve a predefined object motion and ensure satisfactory internal forces. To define the grasping wrenches, the force balance equations, *i.e.*, the dynamics equations of the object should be solved. As mentioned earlier, these equations are underdetermined. Extra constraints need to be imposed to give a unique solution. Evidently, optimization techniques can be used to find the *best* solution. Mathematical descriptions of the optimization problem need to be formulated to define a

solution which minimizes a certain objective function while satisfying some equality and inequality constraints [13]. The force balance equations of the object constitute the primary constraints. They represent a set of linear equality constraints. Depending on the requirements of the particular task and the system under consideration, inequality constraints are optional. One practical concern with the cooperating manipulator systems is the limited capacities of the actuators. When these are included as constraints, dynamics equations of the manipulators are used to relate the actuator forces/torques to the grasping wrenches [14] so that linear inequality constraints in terms of the grasping wrenches are formulated.

Compared with setting up the constraint equations, formulating the objective function is less straightforward. Firstly, it depends on the type of optimization technique to be adopted. Common choices for the objective functions are linear and quadratic functions of design variables (*e.g.*, grasping wrenches). Secondly, interests in obtaining optimal quantities are usually many and their priorities may be different for various systems. Among the many possibilities, commonly implemented ones are the minimal internal forces [15], minimal power consumption [16, 17] and optimal load distribution within the actuators [10, 17, 12]. Attempts have also been made to employ a weighted linear combination of the many objectives to obtain a combined optimal performance [13]. When the system exhibits structural flexibility, intuition suggests that minimizing the system vibration may be critical for upgrading the performance of the system [18, 19]. However, it is not so obvious how this objective should be formulated and how it can be related to other criteria already used in the rigid case.

Stability of the Inverse Dynamics Solution

To clarify the above concerns, a detailed investigation of the problems arising in the inverse dynamics solution of flexible-link manipulators is necessary. Previous research shows that the inherent difficulty with the inverse dynamics solution for flexible-link serial manipulators is its *instability* [20, 21]. This instability results from the fact that the joint-mounted actuators and the required end-effector motion are coupled by structurally flexible links. Hence, there is a time delay for the end-effector to react in response to a given joint actuation. Therefore, the *causal solution* which determines the joint actuator torques according to the *instantaneous* motion of the end-effector exhibits high magnitude and frequency. This is likely to excite the system vibration and result in unbounded values of dynamics variables. Accordingly, Bayo [21] developed a *noncausal* inverse dynamics solution for the joint actuator torques which starts earlier and ends later than does the tip motion. This solution is shown to be unique and stable [21]. However, the noncausal solution requires solving the problem in the frequency domain. This in turn results in extensive computations for the transformation of the dynamics model, trajectory information and the solution between the frequency domain and the time domain. It is also necessary that the complete time history of the desired motion of the end-effector be known before one starts solving the problem, which is not always possible. Therefore, it would still be desirable to find a causal solution with the stability issue resolved.

It has been suggested by several other researchers that the stability of the inverse dynamics solution can be guaranteed if actuator forces/torques are applied at the location where the trajectory is specified [22]. Very interestingly, we noted that when multiple manipulators act cooperatively on a common object, wrenches applied by each arm to the commonly handled object can be viewed as *active* forces and torques applied to the other arms. This thought is supported by the fact that many

possible grasping wrenches exist to achieve the given object motion due to the presence of the redundant actuators. If the grasping wrenches could be chosen arbitrarily, the cooperating manipulators could be viewed as driven by the tip wrenches. This scenario accomplishes a collocation of the actuation and the end-effector motion, which ensures a stable dynamic behavior of the system. In reality however, the grasping wrenches have to satisfy the object dynamics, but the internal forces can be chosen freely. We therefore propose as a goal of the force distribution scheme to ensure stable dynamics of the system by appropriate selection of internal forces.

Another objective is to reduce the system vibration, by which, we mean reducing both the magnitude and the frequency of the responses of significant elastic modes. Minimizing the strain energy stored in the elastic members of the system effectively achieves minimization of elastic deformations. Minimizing the tip deflection may be appropriate for improving the tip trajectory tracking accuracy. Minimizing the elastic accelerations helps to smooth the elastic motion and therefore reduces its frequencies. It is worthwhile to experiment with these choices and their combinations as it helps achieve an effective force distribution scheme for flexible-link cooperating manipulators.

To summarize the above discussion, this thesis primarily endeavors to answer two questions: 1) how does the link flexibility influence the force distribution problem in coordinated multiple manipulator systems? 2) how will the inverse dynamics solution for flexible-link manipulator system be affected by the redundant actuation of the system?

1.2 Research Objectives

In light of the above questions, the principal objectives of the proposed work are summarized as follows:

1. A general and accurate model needs to be formulated to describe the dynamics of the system. The model will allow three dimensional large rigid-body motion and small superimposed link deflection. The model will be 'accurate' in the sense that all the nonlinear terms due to coupling between rigid and elastic motions will be included.

2. Based on the dynamics model, the inverse dynamics problem of serial flexible-link manipulators will first be investigated to gain insight into the various aspects of the inverse dynamics solution arising from relaxing the assumption of structural rigidity.

3. Formulate the force distribution problem for flexible-link multiple manipulator systems. In particular, optimization techniques will be employed to find the best solution for a variety of criteria.

4. Investigate the relationship between actuation redundancy and the instability aspect of the inverse dynamics problem, and the possibility of improving the dynamics behavior of the inverse dynamics system by varying the internal forces.

5. Implement numerical simulations on the proposed force distribution scheme and the inverse dynamics solution. For purposes of mechanical design, these simulations are carried out on examples with various arrangements of flexible and rigid links. Some design guidelines are to be obtained in this respect.

1.3 Review of Previous Work

In view of the aforementioned research objectives, in this section, a detailed literature review is presented on the related topics.

1.3.1 Dynamics of Constrained Multibody Systems

A system of coordinated multiple manipulators handling a common object forms a constrained multi-body system. The fundamental theory of formulating the dynamics of constrained multi-body systems is well established [23, 24, 25, 26]. Lagrange multipliers are commonly used to append the constraint equations to the Lagrange equations for the dynamics equations of the system. Another way to deal with constraints is to insert the constraints into the Lagrange equations by means of a penalty formulation [25].

The solution to the inverse dynamics problem for a closed-chain rigid-body system was first introduced by Luh and Zheng [26]. They proposed the '*virtual cut*' method which involves 'cutting' each kinematic loop in the system at an unactuated joint to produce a kinematic chain with a tree structure. Using the inverse dynamics algorithm for a serial chain and with an explicit calculation of Lagrange multipliers, the forces/torques required at the actuated joints can be found. Based on the same idea of 'virtual cut', Nakamura and Ghodoussi [27] derived the torques applied at the active joints by projecting the generalized torque vector of the unconstrained tree-structure system. This was accomplished with a linear map incorporating the Jacobian of the passive joints with respect to the active joints. The procedure eliminated the necessity of calculating Lagrange multipliers. These methods, however, have only been used in the context of systems without redundant actuation.

Relatively little work has been done in closed-loop systems with structurally flex-

ible members. Kim and Haug [28] derived a recursive formulation for the simulation dynamics of a closed-loop flexible-multibody system. Cut joint constraint equations and the associated Lagrange multipliers are introduced to represent cut joint reaction forces and torques. Bayo *et al.* [29] extended Bayo's inverse dynamics algorithm for serial chain flexible manipulators to the closed-chain case. The method is not suitable for a general inverse dynamics analysis in that it assumes that all the joints follow a nominal predetermined trajectory.

1.3.2 Work on Rigid-Link Cooperating Manipulators

A coordinated multiple manipulator system belongs to a special class of closed-loop mechanisms, in which redundant actuation is a prominent characteristic. The same framework encompasses multi-fingered mechanical hands and multi-legged locomotion vehicles.

Among the many issues relating to the cooperative manipulation by robotic arms, the force distribution problem has received considerable attention. The presence of redundant actuators in a system makes it possible to use optimization techniques to actively distribute the load in the system [30]. Orin and Oh [13] proposed to determine the joint torques while minimizing the energy consumption and the maximum normal tip reaction force for a legged locomotion system. Their method involved solving a linear programming problem to minimize an objective function comprised of a weighted sum of joint torques, joint rates and task space reaction forces. This was done while satisfying equality constraints (force balance equations) and inequality constraints (maximum joint torque capacities and tip reaction force constraints). This approach, while appealing, proved to have the disadvantage of excessive computational expense [31].

Since uniqueness of the solution calculated with linear programming is not ensured, discontinuity of the solution can be observed for small changes in the constraints [14]. By contrast, quadratic programming yields a globally (in the design space) unique solution and proves to be more efficient. It has thus been used to minimize the internal forces [15], the strain energy in the object [32] and the power losses [33, 9, 17]. Taking into account the different capacities of the arms for carrying the loads, an optimal force distribution can be achieved by assigning different weights to the design variables in the objective function [10]. Noticing that only the objective function is non-linear, Luh and Zheng [16] applied the approximate linear programming method to solve the non-linear programming problem. Other researchers have investigated the use of the 'p-norm approach' to solve the constrained optimization problem via unconstrained optimization techniques for multiple arm manipulators [12].

1.3.3 Inverse Dynamics of the Flexible-Link Manipulators

As alluded to in the previous section, the major problem with the inverse dynamics solution for serial flexible-link manipulators is that it may be unstable. To deal with this problem, approaches can be classified into two categories: the non-causal solution and the causal solution. The former approach was proposed by Bayo [21]. Kwon and Book [34] later improved this approach by reducing the computational burden involved in the computationally intensive Fourier transformations. The causal methods have been pioneered by Asada and Park [35, 22], and they have solved the problem in the time domain. The stability of the solution is guaranteed by means of a torque transmission mechanism to accomplish a collocated construction of the sensors and actuators [22].

Another difficulty with the inverse dynamics solution for flexible-body systems

arises because of the coupling effects between the rigid-body motions and the elastic deformations. In contrast to the rigid inverse dynamics solution, the nominal joint motion cannot be determined solely by solving the inverse kinematics equations for the prescribed end-effector motion. Asada *et al.* [35] proposed to use a 'virtual link coordinate system' to decouple the kinematics from the dynamics of a flexible-link manipulator. They also assumed that all the joints follow a nominal predetermined trajectory. Chang and Hamilton [36] also calculated the causal solution by using an 'equivalent rigid link system' to describe the rigid kinematics of the system. Xi and Fenton [37] derived a causal solution by solving the kinematics and dynamics equations simultaneously and integrating them in the time domain. However, most of these studies leave the stability issue unaddressed.

1.4 Outline of the Thesis

The kinematics and the dynamics of a system of multiple flexible-link manipulators to handle a common rigid object are modeled in Chapter 2. As a result, fundamental equations for the system are composed of two sets: that of the manipulators and that of the common object. Constraint forces and torques between the manipulator end-effector and the object are explicitly included in the dynamics equations in view of their significance to the force distribution problem and actuation redundancy resolution. Following Hughes' procedure [38], derivations of the kinematics relations between the end-effector and the variables representing the degrees of freedom of a serial flexible-link manipulator are detailed. In particular, rigid and elastic Jacobians are formulated which map the configuration space velocities into the Cartesian space end-effector velocities. Also, the transpose of the aforementioned Jacobians map the Cartesian tip wrenches into configuration space generalized forces.

In Chapter 3, the inverse dynamics problem is investigated for a serial flexible-link manipulator. We explore analytically the stability issue of the inverse dynamics system driven kinematically by the prescribed end-effector trajectory. Both state space description and the input-output relation for a single flexible link case are established and the latter is used to determine the stability status of the inverse dynamics system. The *causal* inverse dynamics solution for serial flexible-link manipulators is described and written with the view of showing the influence of the tip wrenches on the solution of the prescribed tip trajectory and the effect of the tip wrenches.

The inverse dynamics solutions for the multiple flexible-link manipulators are discussed in chapter 4. In particular, redundancy in choosing the grasping wrenches and in applying the actuator torques required in handling the object along a prescribed trajectory are identified. Moreover, the degree of redundancy in determining the grasping wrenches and in calculating the actuation torques are shown to be the same as the number of components of the internal forces. As a result, the inverse dynamics algorithm for multiple flexible arm system is presented in which tip wrenches are chosen to be the design variables.

In chapter 5, optimization techniques are discussed and used to solve the force distribution problem. After comparing the merits of using the linear and quadratic programming techniques, the latter is adopted. Objective functions are discussed with an emphasis on tackling the particular problems of flexible-link cooperating manipulators, that is, stabilizing and reducing the system vibration. Numerical examples are carried out for each objective function. Comparisons of the inverse dynamics solution by using different objective functions are also made.

The issues related to stability of the internal dynamics of the inverse dynamics system for a cooperating flexible-link manipulator are further discussed in Chapter 6. These are particularly relevant to the inverse dynamics control of flexible ma-

nipulators. Linearization of the internal dynamics equations are performed around equilibrium points. Dynamics behavior of the original nonlinear system can be predicted by examining the behavior of the linearized system. Accordingly, a stability approach to the force distribution problem is proposed which, under certain conditions, ensures a stable dynamic behavior of the causal inverse dynamics systems.

Finally the conclusions are drawn in Chapter 7 together with recommendations for future work.

Chapter 2

Dynamics Modeling

2.1 Introduction

A system composed of multiple flexible-link coordinated manipulators and an object falls into the class of *flexible multibody systems*. In particular, it contains one or more kinematic loops when the multiple arms are handling the common object. Standard methods for deriving the equations of motion of a closed-loop multibody system include two basic steps [23]. First, a *virtual cut* is made at one or more hinges to yield a system with a tree structure. Obviously, this can be done in different ways. One way is to virtually cut the closed loops in such a way that a *reduced system* is produced. In the reduced system, only holonomic constraints remains. This means that places of virtual cuts should at least include all those where nonholonomic constraints are introduced. Dynamics equations are then derived for the reduced system for which modeling techniques have been well developed. In the second step, both kinematic constraints and the internal force relations at the places of virtual cut are re-introduced. In this way, the original system with closed loops is recovered.

For a system of multiple cooperating manipulators, each of the manipulators is considered to be a serial chain. One or more closed loops are formed when the serial manipulators contact the object. Holonomic and/or nonholonomic constraints are introduced where the object is grasped depending on the type of contact between the manipulator end-effectors and the object. *Rigid grasping*, for example, allows no relative motion between the gripper and the object and therefore imposes holonomic constraints, whereas the point contact in multi-fingered mechanical hands introduces both holonomic and nonholonomic constraints. Besides, if the motion of the object is pre-defined, the system is divided by the object into kinematically independent sub-systems. The reduced system defined earlier can then be obtained by virtually cutting the system at the grasp locations. For a system of P manipulators with a rigid grasp, the minimum number of virtual cuts is $P - 1$. However, in order to facilitate the analysis of the constraint forces and torques between the end-effector and the object (grasping wrenches applied by the manipulators), we make virtual cuts at all the places of grasp to allow us to explicitly include all the grasping wrenches in the equations of motion (Figure 2.1). Therefore, the reduced system is composed of P manipulators and the object. Modeling techniques developed for serial flexible-link manipulators are immediately applicable. Some modifications are needed to treat external end-effector wrenches. As well, we need to express the equations of motion in a form which is suitable for the force analysis of multiple manipulator systems which will be discussed in chapter 4.

2.2 Kinematics

While formulating the dynamics equations is the ultimate goal of this chapter, establishing the kinematics relations is an essential step. To start, we first define several

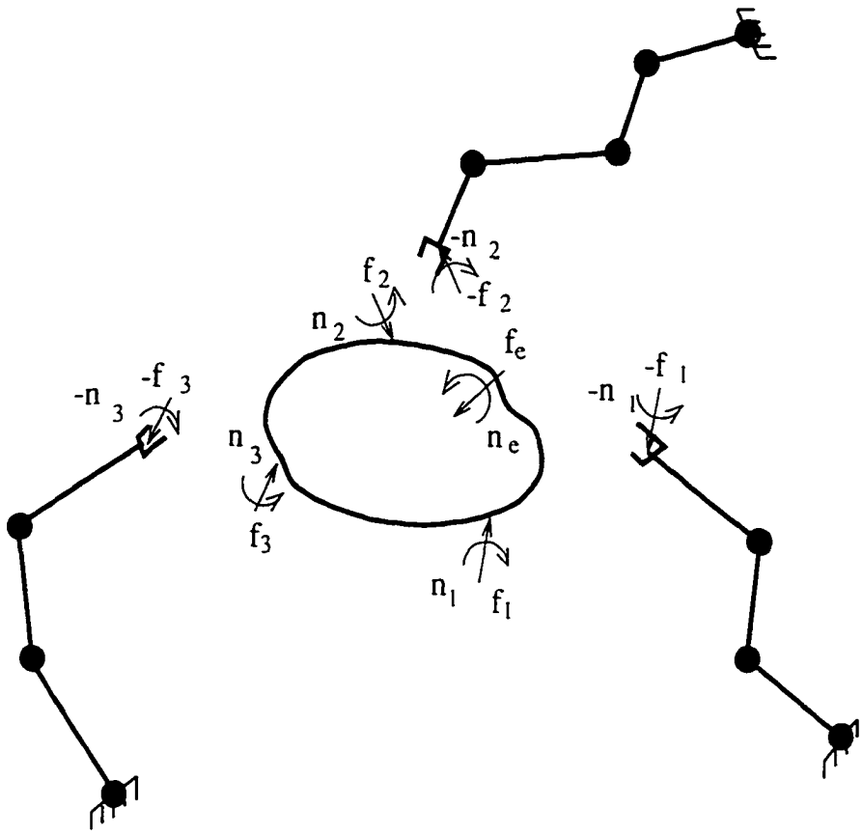

Figure 2.1: Tree Structure of Multiple-Manipulator/Object System

coordinate frames with respect to which the kinematic quantities (position, velocity and acceleration) are expressed. Each of the frames is a three dimensional orthogonal coordinate frame (Figure 2.2).

World coordinate frame $\mathcal{F}_I$ is a frame fixed in inertial space. It represents a unique reference for all the moving bodies in the system. Its origin is denoted by O_I and the three coordinate axes by X_I, Y_I and Z_I. For convenience, we use $\{O_I, X_I, Y_I, Z_I\}$ to represent the origin and three axes of the coordinate system.

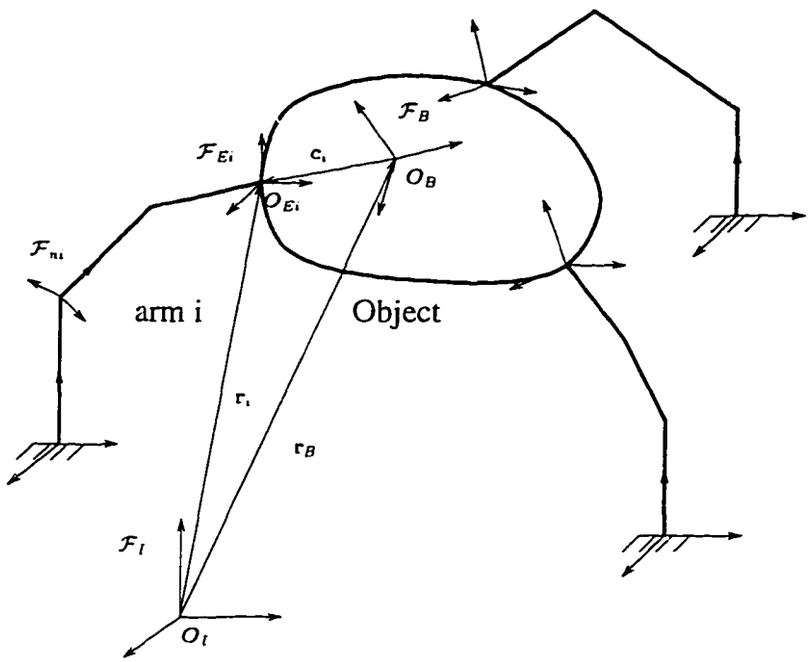

Figure 2.2: Coordinate Frames for Multiple-manipulator System

Link coordinate frame $\mathcal{F}_n$ is a frame attached to the link of the manipulator with its origin located at the proximal end of the link. For link n ($n = 0, 1, \cdots, N_i$) of manipulator i ($i = 1, \cdots, P$), the link frame is denoted by $\mathcal{F}_{ni}$, and the origin and axes by $\{O_{ni}, X_{ni}, Y_{ni}, Z_{ni}\}$. In particular, X_{ni} is oriented in the direction along the line connecting the proximal and distal ends of the link in its undeformed state.

End-effector coordinate frame $\mathcal{F}_{Ei}$ is similar to the link frame except that it is attached to the end-effector of the manipulator. Its origin and axes are denoted by $\{O_{Ei}, X_{Ei}, Y_{Ei}, Z_{Ei}\}$.

Object coordinate frame $\mathcal{F}_B$ is attached to the commonly handled object with its origin located at the mass center of the object. Its origin and axes are

denoted by $\{O_B,\ X_B,\ Y_B,\ Z_B\}$.

We also need to introduce the following definitions which will be used repeatedly in this thesis.

Generalized coordinates For a rigid body system, generalized coordinates are a set of independent variables $q_{r1}, q_{r2}, \cdots, q_{rM}$ which completely define the location and orientation of each rigid body in the system. For a deformable multibody system, the generalized coordinates are composed of $q_{r1}, q_{r2}, \cdots, q_{rM}$ and the set of time-dependent variables $q_{e1}, q_{e2}, \cdots, q_{eS}$ used to approximately model the elastic deformation of the flexible bodies in the system. The total number of generalized coordinates is $K = M + S$.

Configuration space is a K dimensional space in which generalized coordinates $q_{r1}, q_{r2}, \cdots, q_{rM}, q_{e1}, q_{e2}, \cdots, q_{eS}$ correspond to a particular point.

For a multiple-chain system, bodies or joints must be identified by two indices, namely the index i for the individual chain and the index n for the particular body within the chain. Generalized coordinates used to model each body of the system requires the third index. This becomes cumbersome. For this reason, we will omit the chain index i when we investigate a single serial manipulator and will omit body index n when we study the assembled multiple-chain system. In the latter case, each serial chain is treated as a whole.

2.2.1 Kinematics of a Serial Manipulator

As mentioned in the previous chapter, throughout this work, it is assumed that the desired trajectory of the object has been pre-planned. This desired trajectory can be

determined either by off-line path planning or by on-line trajectory generation. In any case, advance knowledge of the desired object trajectory is required, if not for the whole task period, at least for a small interval of future time. In this situation, the multiple manipulators are kinematically independent of each other. Due to the rigid grasp, prescribing the object trajectory is equivalent to prescribing the motion of each end-effector. Therefore, the kinematics relations established in this section are those relating the Cartesian space end-effector motion to the configuration space generalized motion.

The complexity of deriving the kinematics relations for an interconnected flexible multibody system stems from the coupling effects between bodies and those between the rigid motion and the elastic oscillation. Moving frames such as the link coordinate frames introduced above, are usually used to account for the rigid (gross) motion, with respect to which the elastic deformations are expressed. Several ways of setting up these moving frames have been proposed. Book [39] attached frames to the proximal end of every link and extended Denavit and Hartenberg's 4×4 homogeneous transformation matrix notation to describe the kinematics of flexible links connected by *rotary* joints. Hughes and Sincarsin [38] also defined the moving frames attached to each individual body in its rigid configuration. Interbody transformation matrices $\mathcal{T} \in \mathbf{R}^{6\times 6}$ (for rigid degrees of freedom) and $\mathcal{S} \in \mathbf{R}^{6\times s_n}$ (for elastic degrees of freedom where s_n is the number of elastic coordinates for body n) are used to perform transformations of spatial velocities between two interconnected bodies. Their method allows for *general* interjoint motion, that is, arbitrary interjoint displacements and rotations. Chang and Hamilton [36] used an equivalent rigid link system to represent the large motion of the arm. The small motion of the system consists of both small rigid-body motion and elastic deformation. Asada *et al.* [35] and Bayo *et al.* [29] assigned moving frames to each body with one of the axes coinciding with the direction from the

proximal joint to the distal joint of the link in the deformed configuration. In this way, rigid motion can be decoupled from the elastic deformation by assuming that all joints follow their nominal trajectories obtained from the rigid inverse kinematics solution.

To establish an expression for the end-effector motion in terms of the motion in configuration space, a direct method would be to derive equations for the end-effector position and orientation in terms of the configuration space generalized coordinates. For the purpose of inverse dynamics analysis, we are particularly interested in the *inverse kinematics* which determine the generalized coordinates corresponding to the end-effector motion. Using the kinematics expressions at the coordinate level (position) has some disadvantages. One is that only for some specially configured rigid manipulators there exists a closed form formulation of the inverse kinematics solution. The other is that even if a closed-form inverse kinematics equations can be obtained for some particular manipulators, they are nonlinear functions of the generalized coordinates. The generalized coordinates in the inverse kinematics problem admit multiple solutions. For these reasons, the *differential kinematics* relations which describe the differential changes of the position and orientation of the end-effector resulting from the differential changes of the generalized coordinates are advantageous. These are linear algebraic equations. For rigid non-redundant manipulators, a unique solution to the inverse kinematics problem is guaranteed if the system is not at a singular configuration.

For the present study, we adopt the notational scheme and definition of body coordinate frames proposed by Hughes and Sincarsin [38, 40]. Small changes are made to some symbols in order to incorporate traditional robotics notation. As described in reference [38], the velocity kinematics between successive bodies $\mathcal{B}_n$ and $\mathcal{B}_{n+1}$ (Figure 2.3) is:

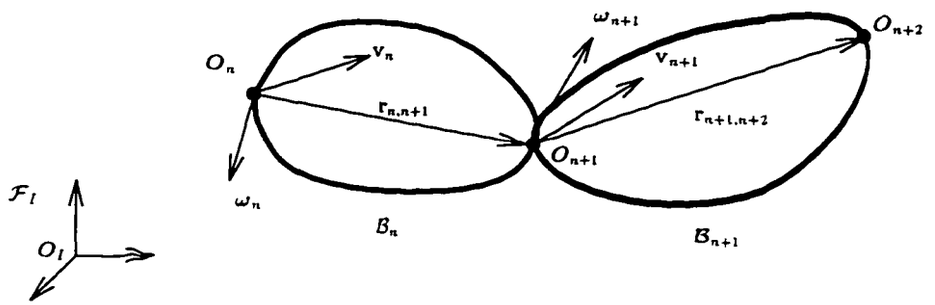

Figure 2.3: Spatial Velocity between Two Successive Bodies

$$v_{n+1} = \mathcal{T}_{n+1,n} v_n + \mathcal{S}_{n+1,n}\, \dot{q}_{n,e} + \mathcal{P}_{n+1}\, \dot{q}_{n+1,r} \tag{2.1}$$

where a spatial vector $v_n \in \mathbf{R}^6$ is used to define a combination of the *absolute* linear and angular velocities of a moving frame expressed in its own frame. That is,

$$v_n = \begin{bmatrix} v_n \\ \omega_n \end{bmatrix} \tag{2.2}$$

Vectors $\dot{q}_{n,e} \in \mathbf{R}^{s_n}$ and $\dot{q}_{n+1,r} \in \mathbf{R}^{m_{n+1}}$ in eq. (2.1) are referred to as generalized velocities associated with the elastic and rigid degrees of freedom, respectively. We also use s_n to denote the number of elastic coordinates used to model the flexible body $\mathcal{B}_n$ and m_n for the number of degrees of freedom of joint O_n. The transformation matrices $\mathcal{T}_{n+1,n} \in \mathbf{R}^{6\times 6}$ and $\mathcal{S}_{n+1,n} \in \mathbf{R}^{6\times s_n}$ as well as the projection matrix $\mathcal{P}_{n+1} \in \mathbf{R}^{6\times m_{n+1}}$ are defined in Appendix A. Conceptually, eq. (2.1) means that the spatial velocity of O_{n+1} in the chain is the summation of three effects: the first due to the velocity of O_n, the second due to the elastic deformation of $\mathcal{B}_n$ and the last due to the relative motion at the joint O_{n+1}. Referring to Figure 2.4, we use eq. (2.1) to define the generalized velocity of $\mathcal{B}_E$ in terms of variables of the previous body, $\mathcal{B}_N$.

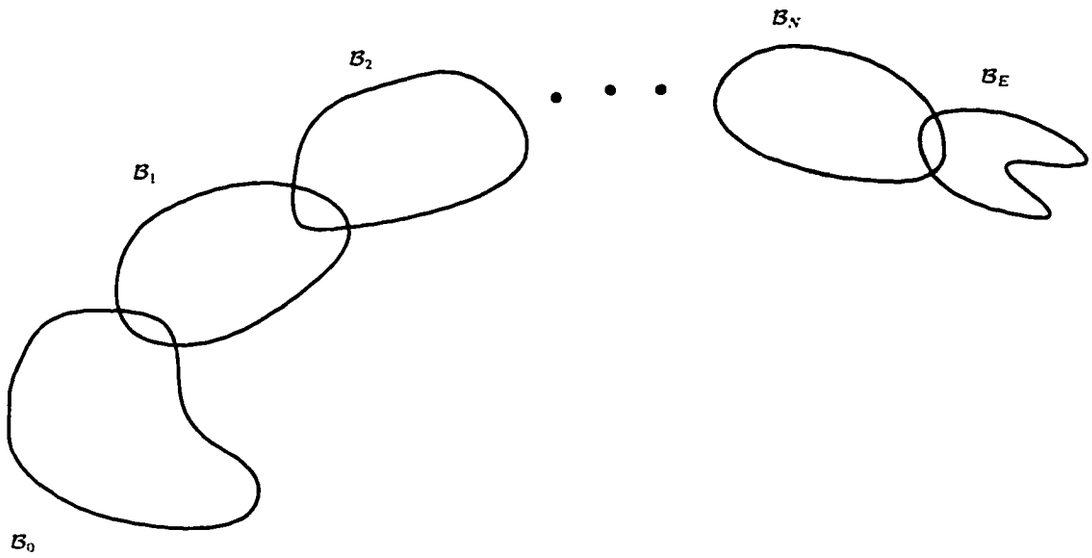

Figure 2.4: A Serial Chain of Flexible Multibodies

Since it is always possible to assume that the end-effector is rigidly attached to the last link of the chain, the spatial velocity of $\mathcal{F}_E$ is

$$v_E = \mathcal{T}_{E,N} v_N + \mathcal{S}_{E,N}\, \dot{q}_{N,e} \tag{2.3}$$

Using eq. (2.1) again to substitute for v_N into the above equation, we obtain

$$v_E = \mathcal{T}_{E,N}\{\mathcal{T}_{N,N-1} v_{N-1} + \mathcal{S}_{N,N-1}\, \dot{q}_{N-1,e} + \mathcal{P}_N\, \dot{q}_{N,r}\} + \mathcal{S}_{E,N}\, \dot{q}_{N,e} \tag{2.4}$$

The same procedure can be applied to replace v_{N-1} and so on until the base body of the chain is reached. In that case, we obtain

$$\begin{aligned} v_E &= \mathcal{T}_{E,0}\mathcal{P}_0\, \dot{q}_{0,r} + \mathcal{T}_{E,1}\mathcal{P}_1\, \dot{q}_{1,r} + \ldots + \mathcal{T}_{E,N}\mathcal{P}_N\, \dot{q}_{N,r} \\ &+ \mathcal{T}_{E,1}\mathcal{S}_{1,0}\, \dot{q}_{0,e} + \mathcal{T}_{E,2}\mathcal{S}_{2,1}\, \dot{q}_{1,e} + \ldots + \mathcal{T}_{E,N}\mathcal{S}_{N,N-1}\, \dot{q}_{N-1,e} + \mathcal{S}_{E,N}\, \dot{q}_{N,e} \end{aligned} \tag{2.5}$$

Introducing vectors q_r and q_e which combine the rigid and elastic coordinates re-

spectively for all bodies in the chain as

$$q_r = \begin{bmatrix} q_{0,r} \\ q_{1,r} \\ \vdots \\ q_{N,r} \end{bmatrix} \qquad q_e = \begin{bmatrix} q_{0,e} \\ q_{1,e} \\ \vdots \\ q_{N,e} \end{bmatrix} \tag{2.6}$$

the quantity v_E can be written in a matrix-vector form as:

$$\begin{aligned} v_E &= \begin{bmatrix} \mathcal{T}_{E,0}\mathcal{P}_0 & \mathcal{T}_{E,1}\mathcal{P}_1 & \cdots & \mathcal{T}_{E,N}\mathcal{P}_N \end{bmatrix} \begin{bmatrix} \dot{q}_{0,r}^T & \dot{q}_{1,r}^T & \cdots & \dot{q}_{N,r}^T \end{bmatrix}^T \\ &+ \begin{bmatrix} \mathcal{T}_{E,1}\mathcal{S}_{1,0} & \cdots & \mathcal{T}_{E,N}\mathcal{S}_{N,N-1} & \mathcal{S}_{E,N} \end{bmatrix} \begin{bmatrix} \dot{q}_{0,e}^T & \dot{q}_{1,e}^T & \cdots & \dot{q}_{N,e}^T \end{bmatrix}^T \end{aligned} \tag{2.7}$$

Since usually the desired end-effector motion is prescribed with respect to a fixed reference frame, we need to transform v_E from $\mathcal{F}_E$ into the inertial frame $\mathcal{F}_I$ by pre-multiplying it by the generalized rotation matrix $\mathcal{C}_{I,E} \in \mathbf{R}^{6\times 6}$. This generalized rotation matrix is defined as $\mathcal{C}_{I,E} = diag\{\mathrm{C}_{I,E}, \mathrm{C}_{I,E}\}$ and $\mathrm{C}_{I,E} \in \mathbf{R}^{3\times 3}$ is the rotation matrix of the end-effector frame relative to the inertial frame. To treat the multiple bodies in a chain as a single entity, we now use v to denote the spatial end-effector velocity expressed in the inertial frame. Finally, the velocity kinematics equation (2.7) can be written more compactly as:

$$v = \mathbf{J}_r \dot{q}_r + \mathbf{J}_e \dot{q}_e \tag{2.8}$$

where $\mathbf{J}_r$ and $\mathbf{J}_e$ are referred to as the rigid and elastic Jacobians. They are defined by

$$\mathbf{J}_r = \mathcal{C}_{I,E}\mathcal{T}_A\mathcal{P}_\Sigma \tag{2.9}$$

$$\mathbf{J}_e = \mathcal{C}_{I,E}\mathcal{T}_A\mathcal{S}_\Sigma + \mathcal{S}'_{E,N} \tag{2.10}$$

where

$$\mathcal{T}_A = \begin{bmatrix} \mathcal{T}_{E,0} & \mathcal{T}_{E,1} & \cdots & \mathcal{T}_{E,N} \end{bmatrix} \tag{2.11}$$

$$\mathcal{S}'_{E,N} = \begin{bmatrix} 0 & 0 & \cdots & 0 & \mathcal{S}_{E,N} \end{bmatrix} \tag{2.12}$$

with $\mathcal{P}_\Sigma$ and $\mathcal{S}_\Sigma$ as defined in Appendix A.

2.2.2 Kinematics of the Object

Specify the Object Motion

As mentioned earlier, throughout this work, we assume that the motion of the object is prescribed; that is, the position of O_B and orientation of $\mathcal{F}_B$ are known as a function of time. One way to define this trajectory is by specifying, in the inertial frame, the position vector $\mathbf{r}_B$ of O_B and the orientation matrix $\mathbf{C}_B \in \mathbf{R}^{3\times3}$ of $\mathcal{F}_B$. Another more compact representation is by a column matrix of six components:

$$r_B(t) = \begin{bmatrix} \mathbf{r}_B \\ \alpha \\ \beta \\ \gamma \end{bmatrix} \tag{2.13}$$

where (α, β, γ) can be Euler angles or roll-pitch-yaw angles. By knowing (α, β, γ) as a function of time, the orientation matrix $\mathbf{C}_B$ can be obtained [41] as a function of time. Since we have decided to consider differential kinematics as a means of defining the motion of the system in its configuration space corresponding to the Cartesian space object motion, the prescribed motion of the object must also be specified at the velocity and/or acceleration level. Assuming the velocity level kinematics, the spatial velocity of $\mathcal{B}_B$ is given as:

$$v_B = \begin{bmatrix} \mathbf{v}_B \\ \omega_B \end{bmatrix} \tag{2.14}$$

where both $\mathbf{v}_B$ and ω_B are expressed in the inertial frame. While it is clear that differentiating $\mathbf{r}_B$ in eq. (2.13) with respect to time gives $\mathbf{v}_B$, differentiating (α, β, γ)

however, does not yield ω_B. To obtain the spatial velocity in eq. (2.14) from eq. (2.13), we need to consider the following

$$\dot{\mathbf{C}}_B = \Omega_B^{\times} \mathbf{C}_B \tag{2.15}$$

from which it follows

$$\Omega_B^{\times} = \dot{\mathbf{C}}_B \mathbf{C}_B^T \tag{2.16}$$

In the above, matrix $\Omega_B^{\times}$ represents a cross-product operation of $\omega_B = [\omega_x \ \omega_y \ \omega_z]^T$ and is defined by

$$\Omega_B^{\times} = \begin{bmatrix} 0 & -\omega_z & \omega_y \\ \omega_z & 0 & -\omega_x \\ -\omega_y & \omega_x & 0 \end{bmatrix} \tag{2.17}$$

and $\dot{\mathbf{C}}_B$ can be obtained from $(\dot{\alpha}, \dot{\beta}, \dot{\gamma})$. Also notice that in eq. (2.16), the orthogonality of the orientation matrix $\mathbf{C}_B$ has been used, that is, $\mathbf{C}_B^{-1} = \mathbf{C}_B^T$.

Define the End-effector Motions

Once the object motion is defined, motions of the manipulator end-effectors are completely determined for the case of a rigid grasp as assumed here. At each grasping location, we have the following constraint equations:

$$\mathbf{r}_i = \mathbf{r}_B + \mathbf{c}_i \tag{2.18}$$

$$\mathbf{C}_{I,Ei} = \mathbf{C}_B \, \mathbf{C}_{B,Ei} \tag{2.19}$$

$$i = 1, \cdots, P$$

Referring to Figure 2.2, $\mathbf{c}_i$ is the vector connecting O_B to O_{Ei} expressed in the inertial frame. In the above, $\mathbf{C}_{B,Ei}$ represents the orientation of $\mathcal{F}_{Ei}$ relative to $\mathcal{F}_B$. The spatial velocity of the ith manipulator end-effector is then given by

$$\boldsymbol{v}_i = \begin{bmatrix} \mathbf{v}_B + \boldsymbol{\omega}_B \times \mathbf{c}_i \\ \boldsymbol{\omega}_B \end{bmatrix} \tag{2.20}$$

Differentiating eq. (2.20) yields the desired acceleration for the ith end-effector:

$$\dot{v}_i = \begin{bmatrix} \dot{v}_B + \dot{\omega}_B \times c_i + \omega_B \times (\omega_B \times c_i) \\ \dot{\omega}_B \end{bmatrix} \tag{2.21}$$

which will be used as the prescribed trajectory for the manipulator end-effectors when solving the inverse dynamics problem for each chain.

2.3 Formulation of the System Dynamics

Difficulties in formulating the dynamics of a flexible multibody system lie in the fact that the constituent bodies are *deformable* and the motions between them are *coupled*. The complexity of the equations increases rapidly as the number of the bodies increases. When reviewing the literature, it becomes evident that both analytical methods, such as Lagrange's equations [39, 42, 43] and Hamilton's Principle [20], and vectorial formulations, such as the Newton-Euler equations [38, 44, 21], have been used extensively to derive the dynamics equations for flexible multibody systems. By assuming that the flexible bodies undergo small deflections (compared with the dimensions of the link), linear theory of elasticity is usually employed. In fact, Euler-Bernoulli beam theory is commonly adopted to represent manipulator links. The dynamics of a flexible body can be written relative to a moving frame which may represent a rigid configuration of the body. A continuous flexible body is typically discretized and approximated by a finite number of degrees of freedom. Assumed modes, finite element method or lumped parameters (masses and springs) are commonly used for this purpose.

2.3.1 Dynamics of A Serial Flexible-Link Manipulator

Considering the tree structure of the reduced system, dynamics equations need to be formulated for the P serial-chain manipulators and for the object. In this section, we study a single serial-chain flexible-link manipulator. The constraint forces between the manipulator end-effector and the rigid object are considered as external forces and torques acting at the end-effector. Following the procedures introduced by Hughes and Sincarsin [38, 40], the Newton-Euler formulation is first applied to each body of the chain to describe the individual body dynamics. The finite element method is used to derive the equations of motion for elastic coordinates relative to the rigid configuration. As a result, the motion equations for an elastic body $\mathcal{B}_n$ are:

$$\mathbf{M}_{n,rr}\dot{\boldsymbol{v}}_n + \mathbf{M}_{n,re}\,\ddot{\boldsymbol{q}}_{n,e} = \boldsymbol{f}_{nT,r} + \boldsymbol{f}_{nI,r} \tag{2.22}$$

$$\mathbf{M}_{n,re}^T\dot{\boldsymbol{v}}_n + \mathbf{M}_{n,ee}\,\ddot{\boldsymbol{q}}_{n,e} + \mathbf{D}_{n,ee}\,\dot{\boldsymbol{q}}_{n,e} + \mathbf{K}_{n,ee}\,\boldsymbol{q}_{n,e} = \boldsymbol{f}_{nT,e} + \boldsymbol{f}_{nI,e} \tag{2.23}$$

where $\mathbf{M}_{n,rr}\in \mathbf{R}^{6\times 6}$,$\mathbf{M}_{n,re}\in \mathbf{R}^{6\times s_n}$ and $\mathbf{M}_{n,ee}\in \mathbf{R}^{s_n\times s_n}$ are the mass matrices while $\mathbf{D}_{n,ee}\in \mathbf{R}^{s_n\times s_n}$ and $\mathbf{K}_{n,ee}\in \mathbf{R}^{s_n\times s_n}$ are the damping and stiffness matrices of $\mathcal{B}_n$ respectively; column matrices $\boldsymbol{f}_{nI,r}$ and $\boldsymbol{f}_{nI,e}$ are the nonlinear inertial forces whereas $\boldsymbol{f}_{nT,r}$ and $\boldsymbol{f}_{nT,e}$ represent the total forces (constraint and external) on $\mathcal{B}_n$. As before, the subscript r stands for rigid, while e stands for elastic.

By including the interbody geometric constraints and interbody force relations, dynamics equations for all the bodies in the chain are then assembled to yield a global formulation of the chain dynamics [40]. The resulting global equations can be written in the following form:

$$\mathbf{M}_{rr}\,\ddot{\boldsymbol{q}}_r + \mathbf{M}_{re}\,\ddot{\boldsymbol{q}}_e = \boldsymbol{\tau} + \boldsymbol{f}_{I,r} + \boldsymbol{f}_{ext,r} + \boldsymbol{f}_{w,r} \tag{2.24}$$

$$\mathbf{M}_{re}^T\,\ddot{\boldsymbol{q}}_r + \mathbf{M}_{ee}\,\ddot{\boldsymbol{q}}_e + \mathbf{D}_{ee}\,\dot{\boldsymbol{q}}_e + \mathbf{K}_{ee}\,\boldsymbol{q}_e = \boldsymbol{f}_{I,e} + \boldsymbol{f}_{ext,e} + \boldsymbol{f}_{w,e} \tag{2.25}$$

Assuming that the manipulator is not kinematically redundant, the total number of independent joint variables in $\boldsymbol{q}_r$ is 6 while the total number of elastic coordinates

in q_e is denoted by $S = \Sigma_{n=1}^{N} s_n$. In eqs. (2.24) and (2.25), $\mathbf{M}_{rr} \in \mathbf{R}^{6\times 6}$, $\mathbf{M}_{ee} \in \mathbf{R}^{S\times S}$ and $\mathbf{M}_{re} \in \mathbf{R}^{6\times S}$ are mass matrices associated with the rigid and elastic coordinates of the chain and the coupling between them; $\mathbf{D}_{ee} \in \mathbf{R}^{S\times S}$ is the damping matrix and $\mathbf{K}_{ee} \in \mathbf{R}^{S\times S}$ is the stiffness matrix; $\tau \in \mathbf{R}^6$ consists of driving forces and/or torques at the joints; vectors $f_{ext,r}$ and $f_{ext,e}$ represent the effect of the external forces applied to the manipulator not including those due to the object, whereas $f_{w,r}$ and $f_{w,e}$ are the generalized forces generated in reaction to the grasping wrench applied to the object. Finally, vectors $f_{I,r}$ and $f_{I,e}$ denote the non-linear inertial forces.

Eqs. (2.24) and (2.25) differ from those given in reference [40] in that the generalized forces due to the external forces (other than the driving forces) are separated into two parts: those due to the tip wrenches and those due to the other external forces *e.g.*, the gravity forces. This is because for a multi-arm system, we are particularly interested in the effect of grasping wrenches. Therefore, vectors $f_{w,r}$ and $f_{w,e}$ are new terms whereas calculations of all coefficient matrices and other generalized external and inertial force terms are described in references [38, 40]. It is thus required to derive the analytical forms of $f_{w,r}$ and $f_{w,e}$ in eqs. (2.24) and (2.25).

Let w represent the grasping wrench *applied to* the object by the manipulator, expressed in the inertial frame and given by

$$w = \begin{bmatrix} \mathrm{f} \\ \mathrm{n} \end{bmatrix} \tag{2.26}$$

Following the procedure used to assemble the chain (global) dynamics from the body dynamics equations [38, 40], we first obtain the generalized force terms appearing in the body dynamics equations of the last body in the chain, $\mathcal{B}_N$, to which the end-effector is rigidly attached. We start by expressing the tip wrenches *applied by*

the object, $-\boldsymbol{w}$, in the body frame $\mathcal{F}_N$ as

$$\boldsymbol{f}_{N,w} = \begin{bmatrix} \mathrm{f}_{N,w} \\ \mathrm{n}_{N,w} \end{bmatrix} = -\boldsymbol{\mathcal{C}}_{N,E}\boldsymbol{\mathcal{C}}_{E,I}\boldsymbol{w} \tag{2.27}$$

and the generalized force terms appearing in the body dynamics equations of $\mathcal{B}_N$ are [38]:

$$\begin{aligned} \boldsymbol{f}_{N,w,r} &:= \begin{bmatrix} \mathrm{f}_{N,w} \\ \mathrm{r}^{\times}_{N,E}\mathrm{f}_{N,w} + \mathrm{n}_{N,w} \end{bmatrix} = \begin{bmatrix} 1 & 0 \\ \mathrm{r}^{\times}_{N,E} & 1 \end{bmatrix} \begin{bmatrix} \mathrm{f}_{N,w} \\ \mathrm{n}_{N,w} \end{bmatrix} \\ &= \mathbf{R}^T_{E,N}\,\boldsymbol{f}_{N,w} \end{aligned} \tag{2.28}$$

$$\begin{aligned} \boldsymbol{f}_{N,w,e} &:= \boldsymbol{\Psi}^T(\mathrm{r}_{N,E})\mathrm{f}_{N,w} + \boldsymbol{\Theta}^T(\mathrm{r}_{N,E})\mathrm{n}_{N,w} \\ &= \begin{bmatrix} \boldsymbol{\Psi}^T(\mathrm{r}_{N.E}) & \boldsymbol{\Theta}^T(\mathrm{r}_{N,E}) \end{bmatrix} \begin{bmatrix} \mathrm{f}_{N,w} \\ \mathrm{n}_{N,w} \end{bmatrix} = \boldsymbol{\Xi}^T_{E,N}\,\boldsymbol{f}_{N,w} \end{aligned} \tag{2.29}$$

In eq. (2.28), $\mathrm{r}^{\times}_{N,E} \in \mathbf{R}^{3\times 3}$ is the matrix form representing the cross product of vector $\mathrm{r}_{N,E}$, a position vector from O_N to O_E. The matrix $\boldsymbol{\Psi} \in \mathbf{R}^{3\times s_N}$ contains the elastic displacement shape functions satisfying cantilevered boundary conditions at the proximal end of the link and $\boldsymbol{\Theta} \in \mathbf{R}^{3\times s_N}$ is defined by

$$\boldsymbol{\Theta} = \frac{1}{2}\nabla^{\times}\boldsymbol{\Psi} \tag{2.30}$$

Substituting from eq. (2.27) and making use of the definitions for the transformation matrices $\mathcal{T}$ and $\mathcal{S}$, eqs. (2.28) and (2.29) become:

$$\boldsymbol{f}_{N,w,r} = -\mathbf{R}^T_{E,N}\boldsymbol{\mathcal{C}}_{N,E}\boldsymbol{\mathcal{C}}_{E,I}\boldsymbol{w} = -\boldsymbol{\mathcal{T}}^T_{E,N}\boldsymbol{\mathcal{C}}_{E,I}\boldsymbol{w} \tag{2.31}$$

$$\boldsymbol{f}_{N,w,e} = -\boldsymbol{\Xi}^T_{E,N}\boldsymbol{\mathcal{C}}_{N,E}\boldsymbol{\mathcal{C}}_{E,I}\boldsymbol{w} = -\boldsymbol{\mathcal{S}}^T_{E,N}\boldsymbol{\mathcal{C}}_{E,I}\boldsymbol{w} \tag{2.32}$$

Then, the generalized force terms in the global dynamics equations due to the grasping wrench are calculated from those in the body dynamics equations of $\mathcal{B}_N$ by

$$\boldsymbol{f}_{w,r} = \boldsymbol{\mathcal{P}}^T_{\Sigma}\boldsymbol{\mathcal{T}}^T_{\Sigma}\,\boldsymbol{f}_{\Sigma,w,r} \tag{2.33}$$

$$\boldsymbol{f}_{w,e} = \boldsymbol{\mathcal{S}}^T_{\Sigma}\boldsymbol{\mathcal{T}}^T_{\Sigma}\,\boldsymbol{f}_{\Sigma,w,r} + \boldsymbol{f}_{\Sigma,w,e} \tag{2.34}$$

where $f_{\Sigma,w,r}$ and $f_{\Sigma,w,e}$ are defined as:

$$f_{\Sigma,w,r} = \begin{bmatrix} 0 \\ \vdots \\ 0 \\ f_{N,w,r} \end{bmatrix} \qquad f_{\Sigma,w,e} = \begin{bmatrix} 0 \\ \vdots \\ 0 \\ f_{N,w,e} \end{bmatrix} \tag{2.35}$$

Following Hughes and Sincarsin's notation, suffix "Σ" is used to symbolize assembled quantities of all the bodies in the chain. Definitions of $\mathcal{T}_\Sigma$, $\mathcal{S}_\Sigma$ and $\mathcal{P}_\Sigma$ are given in Appendix A. Other than that, the "assembled" (chain) matrix is obtained by placing the corresponding body matrices along the diagonal while the assembled vector is formed by aligning the body vectors in sequence.

Expanding the matrix multiplications in eqs. (2.33) and (2.34) and making use of eqs. (2.9)-(2.12), we obtain:

$$\begin{aligned} f_{w,r} &= \begin{bmatrix} \mathcal{P}_0^T & & & \\ & \mathcal{P}_1^T & & \\ & & \ddots & \\ & & & \mathcal{P}_N^T \end{bmatrix} \begin{bmatrix} 1 & \mathcal{T}_{10}^T & \mathcal{T}_{20}^T & \cdots & \mathcal{T}_{N0}^T \\ & 1 & \mathcal{T}_{21}^T & \cdots & \mathcal{T}_{N1}^T \\ & & 1 & \cdots & \vdots \\ & & & \ddots & \mathcal{T}_{N,N-1}^T \\ & & & & 1 \end{bmatrix} \begin{bmatrix} 0 \\ \vdots \\ 0 \\ f_{N,w,r} \end{bmatrix} \\ &= \begin{bmatrix} \mathcal{P}_0^T \mathcal{T}_{N0}^T \\ \mathcal{P}_1^T \mathcal{T}_{N1}^T \\ \vdots \\ \mathcal{P}_{N-1}^T \mathcal{T}_{N,N-1}^T \\ \mathcal{P}_N^T \end{bmatrix} f_{N,w,r} = \begin{bmatrix} \mathcal{P}_0^T \mathcal{T}_{N0}^T \\ \mathcal{P}_1^T \mathcal{T}_{N1}^T \\ \vdots \\ \mathcal{P}_{N-1}^T \mathcal{T}_{N,N-1}^T \\ \mathcal{P}_N^T \end{bmatrix} \mathcal{T}_{E,N}^T \mathcal{C}_{E,I} f_w \\ &= -\mathcal{P}_\Sigma{}^T \mathcal{T}_A^T \mathcal{C}_{E,I} w = -\mathbf{J}_r^T w \end{aligned} \tag{2.36}$$

Similarly,

$$
\begin{aligned}
f_{w,e} &= \begin{bmatrix} 0 & \mathcal{S}_{10}^T & 0 & \cdots & 0 \\ & 0 & \mathcal{S}_{21}^T & \cdots & \\ & & 0 & \ddots & \\ & & & \ddots & \mathcal{S}_{N,N-1}^T \\ & & & & 0 \end{bmatrix} \begin{bmatrix} 1 & \mathcal{T}_{10}^T & \mathcal{T}_{20}^T & \cdots & \mathcal{T}_{N0}^T \\ & 1 & \mathcal{T}_{21}^T & \cdots & \mathcal{T}_{N1}^T \\ & & 1 & \cdots & \vdots \\ & & & \ddots & \mathcal{T}_{N,N-1}^T \\ & & & & 1 \end{bmatrix} \begin{bmatrix} 0 \\ 0 \\ \vdots \\ 0 \\ f_{N,w,r} \end{bmatrix} \\
&+ \begin{bmatrix} 0 \\ 0 \\ \vdots \\ 0 \\ f_{N,w,e} \end{bmatrix} = \begin{bmatrix} \mathcal{S}_{10}^T \mathcal{T}_{N1}^T \\ \mathcal{S}_{21}^T \mathcal{T}_{N2}^T \\ \vdots \\ \mathcal{S}_{N,N-2}^T \mathcal{T}_{N,N-1}^T \\ \mathcal{S}_{N,N-1}^T \end{bmatrix} f_{N,w,r} + \begin{bmatrix} 0 \\ 0 \\ \vdots \\ 0 \\ 1 \end{bmatrix} f_{N,w,e} \\
&= -\begin{bmatrix} \mathcal{S}_{10}^T \mathcal{T}_{N1}^T \\ \mathcal{S}_{21}^T \mathcal{T}_{N2}^T \\ \vdots \\ \mathcal{S}_{N,N-2}^T \mathcal{T}_{N,N-1}^T \\ \mathcal{S}_{N,N-1}^T \end{bmatrix} \mathcal{T}_{E,N}^T \mathcal{C}_{E,I} w - \begin{bmatrix} 0 \\ 0 \\ \vdots \\ 0 \\ 1 \end{bmatrix} \mathcal{S}_{E,N}^T \mathcal{C}_{E,I} w \\
&= -(\mathcal{S}_\Sigma{}^T \mathcal{T}_A^T \mathcal{C}_{E,I} + \mathcal{S}'_{E,N}) w = -\mathbf{J}_e^T w
\end{aligned} \tag{2.37}
$$

Eqs. (2.36), (2.37) and (2.26) represent closed-form relations between the generalized forces $f_{w,r}$ and $f_{w,e}$ and the grasping wrench w. Substituting these into eqs. (2.24) and (2.25), the global form of the dynamics equations of each flexible-link manipulator can be written as:

$$\mathbf{M}_{rr}\,\ddot{q}_r + \mathbf{M}_{re}\,\ddot{q}_e = \tau + f_{l,r} + f_{ext,r} - \mathbf{J}_r^T w \tag{2.38}$$

$$\mathbf{M}_{re}^T\,\ddot{q}_r + \mathbf{M}_{ee}\,\ddot{q}_e + \mathbf{D}_{ee}\,\dot{q}_e + \mathbf{K}_{ee}\,q_e = f_{l,e} + f_{ext,e} - \mathbf{J}_e^T w \tag{2.39}$$

It is not surprising to note that the Jacobian matrices which map the rigid and elastic rates from configuration space to the Cartesian space also relate the generalized

external forces in the Cartesian space to those in the configuration space.

Equations (2.38) and (2.39) represent a compact form of the dynamics equations for a serial-chain flexible-link manipulator interacting with the object through the grasping wrench $\boldsymbol{w}$. However, calculation of the mass matrices, the stiffness matrices and non-linear inertial force terms are quite complicated. The present work is based on a model which includes all the nonlinear inertial terms arising from the coupling between the rigid and elastic motions. Geometric stiffening effects are also accounted for in calculating the stiffness matrix. The reader is referred to Damaren and Sharf [45] for a detailed description of the model.

2.3.2 Dynamics of the Object

In comparison to the dynamics modeling of a flexible-body system, such as a flexible-link manipulator, the derivation of the equations of motion for a rigid body is quite straightforward. By applying Newton's Second Law and Euler's equation to the object, we have

$$\sum_{i=1}^{M} \mathbf{f}_i = m_B(\dot{\mathbf{v}}_B + \mathbf{g}) - \mathbf{f}_e \tag{2.40}$$

$$\sum_{i=1}^{M} (\mathbf{n}_i + \mathbf{c}_i \times \mathbf{f}_i) = \mathbf{I}_B\dot{\boldsymbol{\omega}}_B + \boldsymbol{\omega}_B \times \mathbf{I}_B\boldsymbol{\omega}_B - (\mathbf{n}_e + \mathbf{c}_e \times \mathbf{f}_e) \tag{2.41}$$

where all the vectors are expressed in the inertial frame. The scalar quantity m_B is the mass of the rigid object, the matrix $\mathbf{I}_B$ is the inertia matrix of the object about its mass center and $\mathbf{g}$ represents the gravity effect. Eqs.(2.40) and (2.41) also quantify the dynamic coupling between the individual manipulators since they contain the tip forces $\mathbf{f}_i$ and moments $\mathbf{n}_i$ which represent the wrenches applied by each manipulator. These equations constitute the primary constraints on the force distribution problem as will be discussed later in the thesis.

Chapter 3

Inverse Dynamics of Serial Flexible-Link Manipulators

3.1 Introduction

In the last chapter, the equations of motion for a multiple-arm system were formulated. Given the external forces, solving these differential equations to obtain the motion of the system is known as the *forward dynamics*. In contrast, *inverse dynamics* entails the calculation of the driving forces and/or torques needed to achieve a desired motion. More generally, the inverse dynamics solution can be used in *force analysis*, that is, the study of both driving forces and constraint forces at the joints of a multibody system for a specified motion of a reference body. For robot manipulators, this reference body is normally the end-effector. For a multiple manipulator and object system, achieving a satisfactory motion of the object is a common concern.

The solution of the inverse dynamics has a number of important applications. It allows the determination of the forces to which a multibody system is subjected in

the dynamics and kinematics simulation problems. Force analysis is also a necessary procedure in the design of a mechanical system. Probably the most prominent application of the inverse dynamics solution is in the design of advanced control schemes used for controlling multibody systems. In feed-forward compensation, the actuator torques are calculated to track a prescribed end-effector motion [46, 47]. In feedback control, the inverse dynamics solution provides an inversion of the system dynamics [48, 49, 50]. This gives the control specialist a powerful tool with which he or she can design stable and robust control laws for the motion control of multibody systems.

Although solutions to the inverse dynamics problem have been well developed for rigid multibody systems [51, 26], these become substantially more difficult when structural flexibility in the links is considered. Normally, solving the inverse dynamics problem requires knowledge of the motion of the system, that is, not only the prescribed motion of the end-effector but also the corresponding desired motion in the configuration space of the manipulator. Then, solving the inverse dynamics problem is equivalent to evaluating a set of linear algebraic equations where the generalized coordinates and their first and second derivatives are known as a function of time and the actuator torques must be determined. The Newton-Euler method has been used and proven to be computationally efficient for solving the inverse dynamics problem in the rigid case. Nevertheless, with the same definition of the inverse dynamics problem, obtaining a solution for the flexible multibody system is not so straightforward.

One difficulty is that the desired motion in the configuration space cannot be determined from the prescribed motion of the end-effector because of the unknown deflections of the flexible components. These deflections are, in turn, dependent on the external forces applied to the system including the actuator torques, which are also unknown. It would seem, at this point, that there are more unknowns than equations (dynamics equations) in the inverse dynamics problem for flexible-link manipulators.

To avoid this problem, we could use nominal joint trajectories obtained from the rigid inverse kinematics solution so that the desired joint variables are known when solving the dynamics equations [29, 35, 52, 53]. A more general method is to include the acceleration kinematics equations when solving the inverse dynamics equations [37] so that no assumption is made regarding the desired motion in the configuration space. With this method, the inverse kinematics and inverse dynamics problems for flexible-link manipulators become coupled and the solutions for both the actuator torques and configuration space motions are obtained. In any case, the inverse dynamics solution for flexible-link multibody system differs from that for the rigid case in that it requires integration of the differential equations to produce the configuration space trajectory.

Another difficulty with obtaining inverse dynamics solution for flexible-body systems stems directly from the numerical integration of the derivatives of state variables. Solutions of a set of differential equations may or may not be stable. It has been shown that the inverse dynamics solution for serial flexible-link manipulators with zero initial conditions is *unstable* [21, 22, 52, 54]. In this context, instability implies that the dynamics variables do not remain bounded as $t \rightarrow \infty$. Calculating the feed-forward torques therefore becomes meaningless. As a result, obtaining a stable solution is a key issue in using an inverse dynamics technique to control flexible-link manipulators. Many studies of this issue have been carried out for the past few years. Bayo and his co-workers have developed a so called 'non-causal' solution which has been shown to be unique and stable. Kwon and Book reduced the computational burden of Bayo's method by dividing the solution into a causal and anti-causal parts and integrating them separately. Realizing that an unstable inverse system implies a nonminimum phase forward system which is further caused by the non-collocation of actuation and end-effector motion, Asada *et al.* used a torque transmission mechanism to design a

collocated system [22]. Wang *et al.* proposed a delayed adaptive inverse method which provides a stable and close approximation to the inverse dynamics solution [55].

In this chapter, we focus our attention on the inverse dynamics solution for serial flexible-link manipulators. We begin this study with a single link case for which an analytical formulation of the system dynamics is obtained. Both a state variables description and an input-output description are established and the latter is used for analyzing the stability of the inverse dynamics solution. Based on the analysis of the single link arm and comparison of causal vs. non-causal solutions, we choose to use the causal solutions for the inverse dynamics analysis of flexible multi-body system. Finally, the causal inverse dynamics solutions are formulated for serial flexible-link manipulators.

3.2 Inverse Dynamics of a Single Flexible Link

The study of a single flexible-link manipulator is always a good start. It allows us to obtain an analytic formulation of the system dynamics without undue difficulty. Besides, the model obtained is a set of *linear time-invariant* second-order differential equations. This in turn makes it easier to analyze the system behavior, and in particular, the system stability.

The stability of a system governed by a set of differential equations can be analyzed by directly looking at the time evolution of the system state variables. It can also be analyzed by studying the input-output relations that assigns to each input [56]. These two methods give different insights into how the system works and may lead to solution of some of the problems from different angles. For an *inverse flexible-link dynamics system*, the output driving forces are calculated in response to the input prescribed trajectory of the end-effector. A natural question to consider is whether

or not the output driving forces have similar characteristics to those of the input, say, the boundedness. This motivates us to consider input-output descriptions to investigate the stability issue.

Before proceeding, we need to formulate the dynamics equations of a single flexible-link system for which input-output relations are then established. In many cases, input-output descriptions can also be obtained by direct measurements when deriving the dynamics equations is too complicated. For the present study, we will start with deriving closed-form dynamics equations since this leads to analytical input-output relations. It also helps to understand the procedure of formulating the dynamics model using the method proposed by Hughes and Sincarsin.

3.2.1 State Variable Description

Figure 3.1 shows a single flexible link driven by a torque τ_1 at the hub while the other end of the link is free. The link is assumed to move in a horizontal plane and its joint position is specified by θ_1. The mass, length, and flexural rigidity of the link are m, l and EI respectively. A uniform cross section ($a \times h$) of the link over the length is assumed.

Referring to the same figure, $X_I - Y_I$ and $X_1 - Y_1$ represent the axes of a fixed and a moving (body) frame. It is assumed that the height of the beam is much greater than the width *i.e.*, $a \ll h$, so that the vibration of the beam is constrained to the horizontal plane. Also, the shear deformation and the rotary inertia effects are ignored for simplicity. An arbitrary point P on the link can be located in the moving frame by (x_p, y_p). For simplicity, the deflection of the flexible link is modeled by a single planar beam element with two nodal degrees of freedom. A cubic polynomial shape function is adopted to express the transverse deflection of the beam which

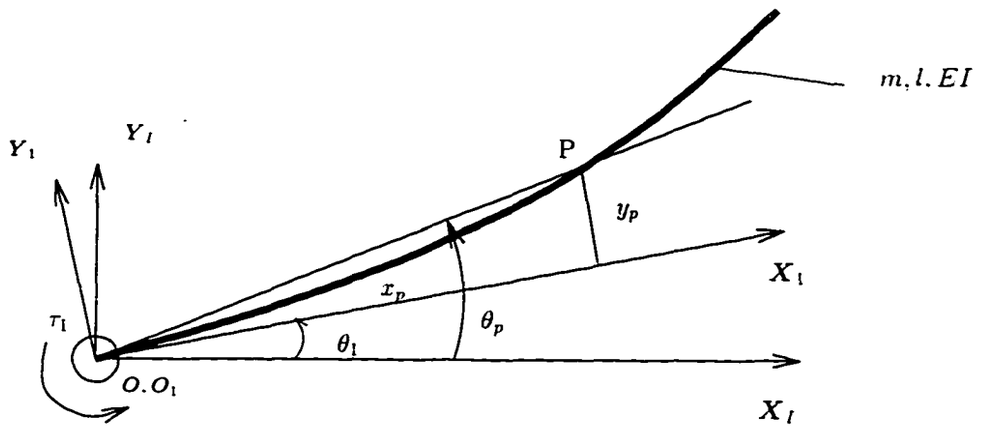

Figure 3.1: Single Flexible Link

satisfies the cantilevered boundary condition. By using the shape function matrix Ψ, elastic displacement u of any point on the link can be calculated from the nodal displacement q_e by:

$$\mathbf{u} = \Psi \, q_e \tag{3.1}$$

For the present case, the shape function matrix is [57]:

$$\Psi(\xi) = \begin{bmatrix} 0 & 0 \\ 3\xi^2 - 2\xi^3 & -(\xi^2 - \xi^3)l \\ 0 & 0 \end{bmatrix} = \begin{bmatrix} 0 \\ \Phi(\xi) \\ 0 \end{bmatrix} \tag{3.2}$$

where $\xi = x/l \in [0, 1]$ represents the location of a point on the link relative to the joint. By defining the shape function matrix Ψ as in eq. (3.2), the deflection of the link takes place only in the Y_1 direction of the body frame and it can be calculated as:

$$y(x_p, t) = \Phi(\xi) \, q_e = [3\xi^2 - 2\xi^3 \;\; -(\xi^2 - \xi^3)l] \begin{bmatrix} \mathrm{v}(t) \\ \mathrm{v}'(t) \end{bmatrix} \tag{3.3}$$

where $(\mathrm{v}, \mathrm{v}')$ are the time-dependent elastic coordinates consisting of the transverse displacement and the slope at the tip of the link. The corresponding cantilevered

element stiffness matrix is [57]

$$\mathbf{K}_{1,ee} = \frac{EI}{l^3}\begin{bmatrix} 12 & -6l \\ -6l & 4l^2 \end{bmatrix} \tag{3.4}$$

Following the derivation of the dynamics equations as described in reference [40], we calculate the mass matrices of the flexible link. The mass matrix associated with the unconstrained rigid degrees of freedom is given by

$$\mathbf{M}_{1,rr} = \begin{bmatrix} m\mathbf{1} & -\boldsymbol{c}_1^{\times} \\ \boldsymbol{c}_1^{\times} & \mathbf{J}_1 \end{bmatrix} \tag{3.5}$$

In the above, $\boldsymbol{c}_1^{\times}$ is the cross product operator of $\boldsymbol{c}_1$, the first moment of mass. The second moment of mass is denoted by $\mathbf{J}_1$. It should be noticed that these quantities are calculated in the body frame, that is, the moving frame $(\boldsymbol{O}_1, \boldsymbol{X}_1, \boldsymbol{Y}_1)$ attached to the joint of the link. In the present case, these are:

$$\boldsymbol{c}_1 = m\begin{bmatrix} \frac{l}{2} \\ 0 \\ 0 \end{bmatrix} \qquad \boldsymbol{c}_1^{\times} = \begin{bmatrix} 0 & 0 & 0 \\ 0 & 0 & -\frac{ml}{2} \\ 0 & \frac{ml}{2} & 0 \end{bmatrix} \qquad \mathbf{J}_1 = \begin{bmatrix} I_{xx} & 0 & 0 \\ 0 & I_{yy} & 0 \\ 0 & 0 & I_{zz} \end{bmatrix} \tag{3.6}$$

and

$$I_{xx} = \int_V (y^2 + z^2)\rho dV \quad I_{yy} = \int_V (x^2 + z^2)\rho dV \quad I_{zz} = \int_V (x^2 + y^2)\rho dV \tag{3.7}$$

The mass matrices associated with the elastic coordinates and the coupling between the rigid and elastic coordinates are defined by

$$\mathbf{M}_{1,ee} = \int \mathbf{\Psi}^T \mathbf{\Psi} dm = m\int_0^1 \mathbf{\Psi}(\xi)^T \mathbf{\Psi}(\xi) d\xi = \begin{bmatrix} \frac{13}{35}m & -\frac{11}{210}ml \\ -\frac{11}{210}ml & \frac{1}{105}ml^2 \end{bmatrix} \tag{3.8}$$

$$\mathrm{M}_{1,re} = \begin{bmatrix} \int \Psi dm \\ \int \mathrm{r}^{\times} \Psi dm \end{bmatrix} = \begin{bmatrix} m \int_0^1 \Psi(\xi) d\xi \\ ml \int_0^1 \mathrm{r}^{\times} \Psi(\xi) d\xi \end{bmatrix} = \begin{bmatrix} 0 & 0 \\ \frac{1}{2}m & -\frac{1}{12}ml \\ 0 & 0 \\ 0 & 0 \\ \frac{7}{20}ml & -\frac{1}{20}ml^2 \end{bmatrix} \tag{3.9}$$

where r denotes the coordinates of point P in the link frame. Since the link is only allowed to rotate in the horizontal plane about the Z_1 axis, the projection matrix is thus defined as:

$$\mathcal{P}_1^T = \begin{bmatrix} 0 & 0 & 0 & 0 & 0 & 1 \end{bmatrix} \tag{3.10}$$

The spatial velocity of the body frame is,

$$v_1 = \begin{bmatrix} \mathrm{v}_1 \\ \omega_1 \end{bmatrix} \qquad \mathrm{v}_1 = \begin{bmatrix} 0 \\ 0 \\ 0 \end{bmatrix} \qquad \omega_1 = \begin{bmatrix} 0 \\ 0 \\ \dot{\theta}_1 \end{bmatrix} \tag{3.11}$$

A vector defined in the inertial frame will be expressed in the moving frame by pre-multiplying it by

$$\mathrm{C}_{1I} = \begin{bmatrix} \cos\theta_1 & \sin\theta_1 & 0 \\ -\sin\theta_1 & \cos\theta_1 & 0 \\ 0 & 0 & 1 \end{bmatrix} \tag{3.12}$$

and the inter-body transformation matrix is calculated by

$$\mathcal{T}_{1I} = \begin{bmatrix} \mathrm{C}_{1I} & -\mathrm{C}_{1I}\,\mathrm{r}_{I1}^{\times} \\ \mathbf{0} & \mathrm{C}_{1I} \end{bmatrix} = \begin{bmatrix} \mathrm{C}_{1I} & \mathbf{0} \\ \mathbf{0} & \mathrm{C}_{1I} \end{bmatrix} \tag{3.13}$$

in which $\mathrm{r}_{I1} = \mathbf{0}$ has been employed. The nonlinear inertial forces are given by

$$f_{1I,r} = \begin{bmatrix} -\omega_1^{\times}(m\mathrm{v}_1 + \omega_1^{\times}\mathrm{c}_1) \\ -(\omega_1^{\times}\mathrm{J}_1\omega_1 + \mathrm{c}_1^{\times}\omega_1^{\times}\mathrm{v}_1) \end{bmatrix} = \begin{bmatrix} \frac{ml}{2}\dot{\theta}_1^{\,2} & 0 & 0 & 0 & 0 & 0 \end{bmatrix}^T \tag{3.14}$$

$$f_{1I,e} = -\int \Psi^T(\omega_1^{\times}\mathrm{v}_1 + \omega_1^{\times}\omega_1^{\times}\mathrm{r})dm = \begin{bmatrix} 0 & 0 \end{bmatrix}^T \tag{3.15}$$

As a convention in the formulation proposed by Hughes and Sincarsin, quantities denoted with a body index, namely, 1 in the above are used to formulate the body dynamics equations. For a single link, there seems to be no difference between the body dynamics and the global dynamics except that quantities are expressed in different frames. This is not really true with Hughes' and Sincarsin's method. Indeed, in their method, equations describing the body dynamics are written in terms of the derivative of the *spatial* velocity of the body frame whereas the global dynamics formulation is expressed in terms of the generalized coordinates and their derivatives in the configuration space. Another notable difference is that in the global formulation, constraint forces are absent while this is not the case in the body dynamics equations.

To obtain the global dynamics formulation of the single link in the configuration space, the assembled projection and inter-body transformation matrices and the assembled mass, stiffness and inertial terms are as follows:

$$\begin{array}{lll} \mathcal{P}_\Sigma = \mathcal{P}_1 & \mathcal{T}_\Sigma = \mathbf{1}_{6\times 6} & \mathcal{S}_\Sigma = \mathbf{0}_{6\times 2} \\ \dot{\mathcal{P}}_\Sigma = \mathbf{0} & \dot{\mathcal{T}}_\Sigma = \mathbf{0} & \dot{\mathcal{S}}_\Sigma = \mathbf{0} \\ \mathrm{M}_{\Sigma,rr} = \mathrm{M}_{1,rr} & \mathrm{M}_{\Sigma,re} = \mathrm{M}_{1,re} & \mathrm{M}_{\Sigma,ee} = \mathrm{M}_{1,ee} \\ \mathrm{K}_{\Sigma,ee} = \mathrm{K}_{1,ee} & f_{\Sigma,I,r} = f_{1,Ir} & f_{\Sigma,I,e} = f_{1,Ie} \end{array} \tag{3.16}$$

By including eq. (3.16), the global mass, stiffness and the inertial forces are [40]:

$$\mathrm{M}_{rr} = \mathcal{P}_\Sigma{}^T \mathcal{T}_\Sigma{}^T \mathrm{M}_{\Sigma,rr} \mathcal{T}_\Sigma \mathcal{P}_\Sigma = \mathcal{P}_1^T \mathrm{M}_{1,rr} \mathcal{P}_1 \tag{3.17}$$

$$\mathrm{M}_{re} = \mathcal{P}_\Sigma{}^T \mathcal{T}_\Sigma{}^T (\mathrm{M}_{\Sigma,re} + \mathrm{M}_{\Sigma,rr} \mathcal{T}_\Sigma \mathcal{S}_\Sigma) = \mathcal{P}_1^T \mathrm{M}_{1,re} \tag{3.18}$$

$$\begin{aligned} \mathrm{M}_{ee} &= \mathcal{S}_\Sigma{}^T \mathcal{T}_\Sigma{}^T \mathrm{M}_{\Sigma,re} + \mathrm{M}_{\Sigma,re}^T \mathcal{T}_\Sigma \mathcal{S}_\Sigma + \mathcal{S}_\Sigma{}^T \mathcal{T}_\Sigma{}^T \mathrm{M}_{\Sigma,rr} \mathcal{T}_\Sigma \mathcal{S}_\Sigma + \mathrm{M}_{\Sigma,ee} \\ &= \mathrm{M}_{1,ee} \end{aligned} \tag{3.19}$$

$$\begin{aligned} f_{I,r} &= \mathcal{P}_\Sigma{}^T \mathcal{T}_\Sigma{}^T \{ f_{\Sigma,I,r} - \mathrm{M}_{\Sigma,rr} (\dot{\mathcal{T}}_\Sigma (\mathcal{P}_\Sigma \dot{\theta}_1 + \mathcal{S}_\Sigma \dot{q}_e) + \mathcal{T}_\Sigma (\dot{\mathcal{S}}_\Sigma \dot{q}_e + \dot{\mathcal{P}}_\Sigma \theta_1)) \} \\ &= \mathcal{P}_1^T f_{1,I,r} = \mathbf{0} \end{aligned} \tag{3.20}$$

$$f_{I,e} = \mathcal{S}_\Sigma{}^T \mathcal{T}_\Sigma{}^T \{ f_{\Sigma,I,r} - \mathrm{M}_{\Sigma,rr} [\dot{\mathcal{T}}_\Sigma (\mathcal{P}_\Sigma \dot{\theta}_1 + \mathcal{S}_\Sigma \dot{q}_e) + \mathcal{T}_\Sigma (\dot{\mathcal{S}}_\Sigma \dot{q}_e + \dot{\mathcal{P}}_\Sigma \theta_1)] \}$$

$$+\{\, \boldsymbol{f}_{\Sigma,I,e} - \mathbf{M}^T_{\Sigma,re}[\dot{\mathcal{T}}_\Sigma(\mathcal{P}_\Sigma\dot{\theta}_1 + \mathcal{S}_\Sigma\,\dot{\boldsymbol{q}}_e) + \mathcal{T}_\Sigma(\dot{\mathcal{S}}_\Sigma\,\dot{\boldsymbol{q}}_e + \dot{\mathcal{P}}_\Sigma\theta_1)]\}$$

$$= \boldsymbol{f}_{1,I,e} = \mathbf{0} \tag{3.21}$$

$$\mathbf{K}_{ee} = \mathbf{K}_{\Sigma,ee} = \mathbf{K}_{1,ee} \tag{3.22}$$

Therefore, the global description of the dynamics of the single flexible link is obtained as

$$\mathbf{M}_{rr}\,\ddot{\boldsymbol{q}}_r + \mathbf{M}_{re}\,\ddot{\boldsymbol{q}}_e = \boldsymbol{\tau} \tag{3.23}$$

$$\mathbf{M}^T_{re}\,\ddot{\boldsymbol{q}}_r + \mathbf{M}_{ee}\,\ddot{\boldsymbol{q}}_e + \mathbf{K}_{ee}\,\boldsymbol{q}_e = \mathbf{0} \tag{3.24}$$

or, in a more compact form

$$\mathbf{M}\,\ddot{\boldsymbol{q}} + \mathbf{K}\,\boldsymbol{q} = \mathbf{B}\boldsymbol{\tau} \tag{3.25}$$

where

$$\mathbf{M} = \begin{bmatrix} I_{zz} & \frac{7}{20}ml & -\frac{1}{20}ml^2 \\ \frac{7}{20}ml & \frac{13}{35}m & -\frac{11}{210}ml \\ -\frac{1}{20}ml^2 & -\frac{11}{210}ml & \frac{1}{105}ml^2 \end{bmatrix} \qquad \boldsymbol{q} = \begin{bmatrix} \theta_1 \\ \mathrm{v} \\ \mathrm{v}' \end{bmatrix}$$

$$\mathbf{K} = \frac{EI}{l^3}\begin{bmatrix} 0 & 0 & 0 \\ 0 & 12 & -6l \\ 0 & -6l & 4l^2 \end{bmatrix} \qquad \mathbf{B} = \begin{bmatrix} 1 \\ 0 \\ 0 \end{bmatrix} \qquad \boldsymbol{\tau} = [\tau] \tag{3.26}$$

A complete description of the system dynamics should include information describing the input, the output and the state variables. Usually, actuation efforts which are used to drive the system are considered as the input and motions that are measurable in response to the input are called the output. As a dynamics problem, definitions for input and output could be different. A dynamics simulation can be 'driven' kinematically by the motion of the system while the solution for the actuator torques can be considered as the output of the system. This is the inverse

dynamics problem which we are interested in looking at. However, we will retain the conventional definition for input and output for now since the inverse system can be investigated by simply reversing the input-output description of the forward system. Therefore, τ in eq. (3.25) is considered as the input to the system and the motion of a point on the link as the output. The output trajectory of P can be defined by the angle θ_p measured from the fixed X_I axis to the line connecting the joint with P (Figure 3.1). It is also the summation of the rigid joint displacement and that due to the elastic displacement, the latter can be calculated by including eq. (3.3):

$$\theta_p(t) \approx \theta_1(t) + \frac{y(x_p,t)}{x_p} = \theta_1(t) + \frac{\Phi(\xi)\, q_e(t)}{l\xi}, \qquad \xi \in [0,1] \tag{3.27}$$

For reasons which will be mentioned shortly when discussing the properties of the transfer function, we define the output y as the angular acceleration of point P:

$$\mathrm{y} = \ddot{\theta}_p = \mathrm{C}\,\ddot{q} \tag{3.28}$$

$$\mathrm{C} = \begin{bmatrix} 1 & \Phi(\xi)/l\xi \end{bmatrix} \quad \in \mathbf{R}^{1\times 3} \tag{3.29}$$

It is evident from eq. (3.27) that the inverse kinematics problem for obtaining the joint motion θ_1 corresponding to the specified motion, θ_p, of a point located other than at the joint cannot be solved due to the unknown deflection of the link. Therefore, the inverse dynamics problem cannot be decoupled from the inverse kinematics solution for even a single flexible-link arm. As mentioned earlier, this certainly complicates the inverse dynamics solution for flexible-link manipulators.

In the above, eqs. (3.25) to (3.28) represent a linear time-invariant system, which is probably the simplest model one can assemble for a flexible-link manipulator. The advantage of obtaining such a model will be proven in subsequent sections where the input-output relation is established and, based on this relationship, the input-output stabilities are investigated.

3.2.2 Transfer Function Representation

The method of Laplace transform can be used for solving linear differential equations. It substitutes a relatively easily solved linear algebraic equations for the more difficult differential equations. The *transfer function* of a linear system is defined as the ratio of the Laplace transform of the output variable to the Laplace transform of the input variable, with all initial conditions assumed to be zero. The zero initial conditions imply that the system is assumed to be *relaxed* or *at rest* before an input is applied. Indeed, for an input-output relation to be valid for investigating key properties of a system, it is necessary that the system be initially relaxed and that the output be excited solely and uniquely by the input applied thereafter. Since all physically possible signals have a Laplace transform, the existence of the Laplace transform is also assumed for the present analysis.

The transfer function of the single flexible arm is obtained from eqs. (3.25) and (3.28), rewritten with zero initial conditions as follows:

$$\mathbf{M}s^2\mathbf{Q}(s) + \mathbf{K}\mathbf{Q}(s) = \mathbf{B}T(s) \tag{3.30}$$

$$Y(s) = \mathbf{C}s^2\mathbf{Q}(s) \tag{3.31}$$

where $\mathbf{Q}(s)$ is the Laplace transform of the generalized coordinates $\boldsymbol{q}$ while $T(s)$ and $Y(s)$ are those of the input τ and the output $\ddot{\theta}_p$. In the present case, we have a single input and a single output. Therefore, $T(s)$ and $Y(s)$ are scalar functions of s, the Laplace variable. Combining eq. (3.30) with eq. (3.31) and solving for $Y(s)$ in terms of $T(s)$, we obtain the transfer function $H(s)$ from input $T(s)$ to the output $Y(s)$ as:

$$H(s) = \frac{Y(s)}{T(s)} = s^2\mathbf{C}(\mathbf{M}s^2 + \mathbf{K})^{-1}\mathbf{B} \tag{3.32}$$

Substituting eq. (3.26) into the above, and expanding, we derive the input-output

description as

$$H(s) = \frac{(0.21\xi^2 - 0.3\xi + 0.1)m^2s^4 + (88.2\xi^2 - 226.8\xi + 122.4)mEIs^2 + 1512EI^2}{(-0.33ml^2 + I_{zz})m^2l^6s^4 + (-390.6ml^2 + 1224I_{zz})ml^3EIs^2 + 15120I_{zz}EI^2} \tag{3.33}$$

This is a rational transfer function. We now introduce several important definitions that are relevant to transfer functions.

Definition 3.1 (Proper Function)

A rational function $H(s)$ is said to be *proper* if $H(\infty)$ is a finite (zero or nonzero) constant. $H(s)$ is said to be *strictly proper* if $H(\infty) = 0$.

Definition 3.2 (Poles)

Poles of a proper transfer function $H(s)$ are numbers (real or complex) which give $|H(s)| = \infty$.

Definition 3.3 (Zeros)

Zeros of a proper transfer function $H(s)$ are numbers(real or complex) which yield $H(s) = 0$.

It can be shown that $H(s)$ defined by eq.(3.33) is proper since $H(\infty)$ equals a constant.

3.2.3 Stability Criteria for the Inverse Dynamics Solution

There are many notions and definitions of 'stability' which are used for defining the properties of dynamic systems. A system that is stable according to one definition of stability may be unstable under some other definitions. Depending on the application, ensuring a 'stable' performance under certain definitions is more appropriate. For

example, an *asymptotically stable* system will return to an equilibrium state no matter how far away the system was initially from the equilibrium state. By contrast, the concept of *Lyapunov stability* is only concerned with the behavior of a system when its initial state is *near* an equilibrium state. A *BIBO* (bounded input and bounded output) stable system demonstrates a bounded output as long as the input is bounded. These are commonly used concepts in system analysis for control purposes.

For an inverse dynamics system, our primary concern is whether the system is BIBO stable or not. This is mainly due to the application of the inverse dynamics solution. For example, when performing force analysis for mechanism design, we are interested in determining the maximum value of the forces needed to be transmitted to the system and the maximum constraint forces on each component in response to a variety of required motions of the system. Boundedness of these forces is one of the major concerns. On the other hand, when the inverse dynamics solution is used as part of the control scheme, boundedness of the actuator torques is essential.

Again, it is of great advantage to use a transfer function to describe the input-output relations of a linear time-invariant system. In terms of the transfer function, the stability criteria are set up by the following theorems [58]:

Theorem 3.1

A relaxed single-variable system that is described by a proper rational function $H(s)$ is BIBO stable if and only if all the poles of $H(s)$ are in the open left-half s plane or, equivalently, all the poles have negative real parts.

Theorem 3.2

If all the poles have nonpositive real parts, but one or more have a zero real part, the system will be BIBO stable if and only if all the poles having zero real parts are simple roots (as opposed to multiple roots) of the characteristic

equation.

For analyzing the inverse system, we need to switch the input with the output that was defined in Section 3.2.2. The input to the inverse dynamics system is now the desired motion of point P, $\ddot{\theta}_p$, while the output is the corresponding joint actuator torques τ. Consequently, the transfer function for the inverse dynamics system, $\hat{H}(s)$, can be obtained from that of the forward system by:

$$\hat{H}(s) = 1/H(s) \tag{3.34}$$

Also, $\hat{H}(s)$ is a proper rational function since $\hat{H}(\infty) \neq 0$. This is the reason why we define the output of the forward system to be the acceleration of point P on the link. Otherwise, the order of the numerator polynomial would be higher than that of the denominator polynomial and $\hat{H}(s)$ would not be proper.

If a proper rational transfer function $\hat{H}(s)$ is irreducible, that is, there is no non-trivial common factor in its numerator and denominator, the poles of the transfer function are known to be the roots of the characteristic equation of $\hat{H}(s)$ obtained by setting the denominator of $\hat{H}(s)$, or equivalently, the numerator of $H(s)$, equal to zero. Thus, in our case, we have:

$$(0.21\xi^2 - 0.3\xi + 0.1)m^2s^4 + (88.2\xi^2 - 226.8\xi + 122.4)mEIs^2 + 1512(EI)^2 = 0 \tag{3.35}$$

In the above, the scalar quantity ξ is a known location of point P on the link relative to the joint. It can also be interpreted as the relative location of the output to the input. We define

$$p = \frac{m}{EI}s^2 \tag{3.36}$$

and substitute it into eq. (3.35) to yield

$$(0.21\xi^2 - 0.3\xi + 0.1)p^2 + (88.2\xi^2 - 226.8\xi + 122.4)p + 1512 = 0 \tag{3.37}$$

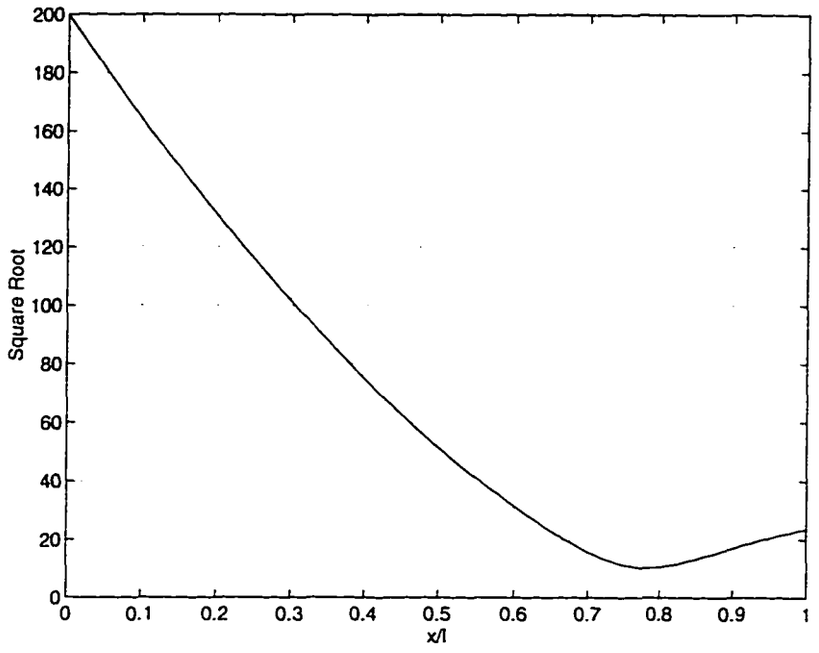

Figure 3.2: Value of Square Root Term

The two roots of eq. (3.37) are obtained as

$$p_{1,2} = \frac{-441\xi^2 + 1134\xi - 612 \pm 3\sqrt{3(7203\xi^4 - 37044\xi^3 + 66444\xi^2 - 49728\xi + 13312)}}{2.1\xi^2 - 3\xi + 1} \tag{3.38}$$

Figure (3.2) depicts the value of the square root term in eq. (3.38) as a function of $\xi \in [0, 1]$. It is shown that this term is always a real positive number. Hence, p from eq. (3.38) is always a real (positive or negative) number. It can be predicted that the poles of the transfer function, calculated from

$$s_{1,2} = \pm(\frac{EI}{m})^{\frac{1}{2}}\sqrt{p_1} \tag{3.39}$$

$$s_{3,4} = \pm(\frac{EI}{m})^{\frac{1}{2}}\sqrt{p_2} \tag{3.40}$$

can either be a real number or a pure imaginary number depending on the value of $\xi (= x/l)$. We now consider the following cases:

1. $\xi = 0$

   This is the case where the joint motion is specified, that is, input and output are collocated at the joint. The poles of the transfer function of the inverse system are: $\pm 34.8j\sqrt{\frac{EI}{m}}$, $\pm 3.53j\sqrt{\frac{EI}{m}}$. According to Theorem 3.2, the system is BIBO stable since all the poles have zero real parts and they are simple roots of the characteristic equation.

2. $\xi = 1$

   This is the case where the tip trajectory is specified and the actuator is located at the joint. This is the most general definition of the inverse dynamics problem. The poles of $\hat{H}(s)$ are: $\pm 9.97\sqrt{\frac{EI}{m}}$, $\pm 38.99\sqrt{\frac{EI}{m}}$. According to Theorems 3.1 and 3.2, we can conclude that the inverse dynamics system is unstable since there are poles located in the right-half s-plane.

3. $0 < \xi < 1$

   When the location of point P is moved from the joint towards the tip of the link, values of $p_{1,2}$ change from being both negative to both positive, which means that the poles of $\hat{H}(s)$ move from the imaginary axis to the open right-half of the s-plane as ξ increases from 0 to 1. A critical position where positive roots of eq. (3.37) start to appear is found to be at $\xi = 0.529$; here, the stability status of the inverse dynamics model changes from being stable to unstable.

From the above analysis, we conclude that stability of the inverse dynamics model of a single flexible link described by eqs. (3.25) and (3.28) is directly affected by the location of specified trajectory relative to the actuator. For the present model, a critical position exists where a change in the stability characteristics of the system is observed. Indeed, for different approximate models, this critical position varies. With a finite element discretization of the elastic link, the critical position moves towards

the actuator as the number of elements used to model the link is increased. Based on this, we predict that with an exact (continuous) model of the link, a stable inverse dynamics system will only be obtained if the actuator and the specified trajectory are collocated.

The other meaning of unstable poles of the transfer function of the inverse system is that the forward system is *nonminimum phase*. For a linear system, if the transfer function has zeros in the open right-half s-plane, the system is said to be nonminimum phase. In practice, the nonminimum phase property often arises in a system where there is a time delay between the input and the output (measured by the sensors). Evidently, when applying a torque at the joint of a flexible link, the tip of the link starts to respond with a time delay. Assuming instantaneous response of the tip motion, the *causal* inverse dynamics solution calculates the joint actuator torques according to the desired tip motion at the same time instant. One can predict this torque to be of high magnitude and frequency in order to overcome the time delay. Such an input signal is likely to excite the elastic vibration and eventually cause unbounded actuator torques. This physical explanation agrees with the conclusion given by the above analysis that collocation between the input and the output guarantees a stable behavior of the inverse dynamics system.

3.3 Introducing Some Solutions

Several methods have been published in the literature to generate stable solutions to the inverse dynamics problem for flexible-link serial manipulators. These methods can be classified into two main categories: the causal solution and the non-causal solution. The first group was introduced by Asada and his research group whereas the non-causal solution was first proposed by Bayo. We now briefly discuss both of

these methods.

3.3.1 Park and Asada's Torque Transmission System

A system is said to be *causal* or non-anticipatory if the output of the system at time t does not depend on input applied after time t, but depends only on the input applied before and at time t. Otherwise, the system is said to be *non-causal.*

Motivated by the work of Spector and Flashner [54] who calculated zero locations of the transfer function of the forward system as a function of the sensor location for tracking control of flexible arms. Park and Asada also investigated the transfer function for a single-link arm [22]. They assumed that actuation efforts could be applied at an arbitrary point on the link. Therefore, they obtained the transfer function for an input being the actuator torque and an output as the tip trajectory. A critical position c was also found (Figure 3.3) which separates stable and unstable regions. They concluded that actuation efforts should be applied as close as possible to the tip. They also pointed out that "as long as the actuator torque is applied at the joint and the endpoint is the control output, the system is nonminimum phase, regardless of how the stiffness and mass of the arm are distributed". In consequence, they proposed to design a torque transmission mechanism to transmit the torques applied by the actuator located at the joint to a point within the stable region. Figure 3.3 shows the basic idea of the mechanism design.

3.3.2 Bayo's Non-causal Solution

In the previous section, we derived the input-output representation of a single flexible-link robot by applying Laplace transformation to the state variable equations. Accordingly, we obtained a transfer function $\hat{H}(s)$ which constitutes the input-output

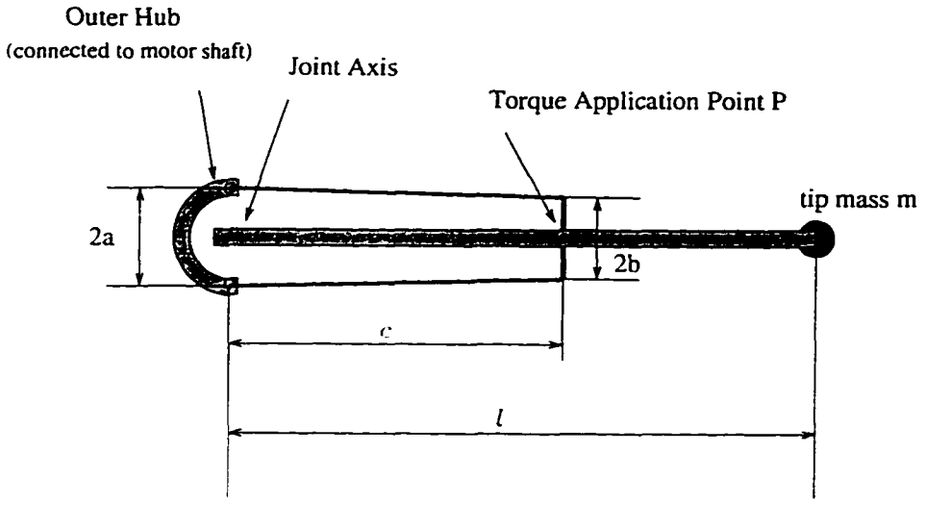

Figure 3.3: Single Link Arm with Transmission Mechanism

relation in the frequency domain. The inverse Laplace transform of the transfer function is known as the impulse-response $\hat{H}(t)$. The time domain output $y(t)$ can be expressed by using the convolution of the impulse-response with the input $u(t)$ as:

$$y(t) = \int_0^t \hat{H}(t-\lambda)u(\lambda)d\lambda. \tag{3.41}$$

In fact, application of this method implicitly assumes that the system is causal. Similarly, the fact that direct integration of the dynamics equations in the time domain only requires the past and the present information about the system also implies that the system is treated as causal.

Because of the existing time lag between the joint actuation and the tip motion, Bayo suggested that the actuator should act before the endpoint motion and continue after it has been completed. Considering the actuator torques as the output of the inverse dynamics solution and the desired endpoint motion as the input, this means that the output is anticipatory. Therefore, the inverse dynamics system for flexible-link manipulators is non-causal and direct integration of motion equations in the time

domain is not applicable.

A single flexible link is again taken as an example to obtain the non-causal solution proposed by Bayo and his co-workers. The method starts by formulating the dynamics equations for the single link arm [59]:

$$\mathbf{M}\ddot{\mathbf{v}} + \mathbf{C}\dot{\mathbf{v}} + \mathbf{K}\mathbf{v} = \mathbf{T} \tag{3.42}$$

Following Bayo's notation, in the above, M, C and K are the mass, damping and stiffness matrices. The column matrix $\mathbf{v} = [\theta_h, x_1, x_2, \cdots, x_n, y]^T$ is composed of the hub rotation angle θ_h, n elastic coordinates $x_1, \cdots, x_n$ for modeling the flexible link using the finite element method, and the tip displacement y. The latter is known as the desired trajectory. The column matrix $\mathbf{T} = [\tau, 0, \cdots, 0]^T$ contains the unknown torque to be applied at the hub. Next, the Fourier transform of eq. (3.42) is obtained for a particular frequency ω as:

$$(\mathbf{M} + \frac{\mathbf{C}}{i\omega} - \frac{\mathbf{K}}{\omega^2})\hat{\mathbf{v}}(\omega) = \hat{\mathbf{T}}(\omega) \tag{3.43}$$

where $\hat{(\cdot)}$ denotes the Fourier transform of a variable. The above represents a linear system of $n+2$ complex equations, the solution of which can be written as:

$$\hat{\mathbf{v}}(\omega) = (\mathbf{M} + \frac{\mathbf{C}}{i\omega} - \frac{\mathbf{K}}{\omega^2})^{-1}\hat{\mathbf{T}}(\omega) = \mathbf{G}(\omega)\hat{\mathbf{T}}(\omega) \tag{3.44}$$

From the last equation in eq. (3.44) we have:

$$\hat{\ddot{y}}(\omega) = G_{n+2,1}(\omega)\hat{T}(\omega) \tag{3.45}$$

where $\hat{T}(\omega)$ is the Fourier transform of the actuator torque τ. Since $\hat{\ddot{y}}(\omega)$ represents the prescribed tip trajectory, the actuator torque is calculated in the frequency domain as

$$\hat{T}(\omega) = H(\omega)\hat{\ddot{y}}(\omega) \tag{3.46}$$

where $H(\omega) = G^{-1}_{n+2,1}(\omega)$. Letting $h(t)$ denote the inverse Fourier transform of $H(\omega)$, the time domain solution $\tau(t)$ is then given by the convolution integral

$$\tau(t) = \int_{-\infty}^{\infty} h(t-\lambda)\ddot{y}(\lambda)d\lambda \tag{3.47}$$

For a typical trajectory defined over a time interval $[t_1,\ t_2]$, this reduces to:

$$\tau(t) = \int_{t_1}^{t_2} h(t-\lambda)\ddot{y}(\lambda)d\lambda \tag{3.48}$$

The difference between the above equation and eq. (3.41) is readily seen. By using eq. (3.48), the noncausality of the solution is captured. The existence and uniqueness of the non-causal solution is proved by Moulin *et al.* [60]. However, we point out that this method requires advance knowledge of the prescribed tip trajectory for the whole task period. Also, as commented by Bayo and Moulin [59], their solution requires heavy computational efforts since it involves the fast Fourier transform, solution of linear systems of complex equations, and the inverse fast Fourier transform.

3.4 Inverse Dynamics Solution for Serial-Chain Flexible Manipulator

Although we were able to formulate and obtain analytical solutions for the inverse dynamics equations of a single flexible-link arm, it is, in general, impossible to do so for a general multiple-link arm. It is well known that the dynamics equations for a multiple-link manipulator are *time-variant* and *nonlinear*. Analysis of the behavior of such a system is very complicated and the method we used for a single flexible-link arm is no longer valid. However, preliminary conclusions can be readily drawn for the inverse dynamics system of a multiple flexible-link arm based on the previous analysis of the single-link arm. These are presented below.

Non-causality of the Inverse Dynamics System

According to the definition of the inverse dynamics problem for a multiple-link manipulator, joint actuator torques are to be determined to generate a prescribed motion of the remotely-located end-effector. Time delays when the end-effector starts to respond to the joint actuation efforts exist as long as at least one of the links is considered to be flexible. It can be further predicted that in order to achieve a desired motion of the end-effector, the joint actuation should start earlier than the specified end-effector trajectory and continue after the input trajectory has been completed. This means that the inverse dynamics solution for the joint actuation efforts depends on not only the past but also the future information of the input and therefore implies non-causality of the system.

Collocation of the Input with Output Improves System Behavior

Since the non-causality of the inverse dynamics system is caused by the time delay between the input actuation and the output response, collocation of the input with the output eliminates this time delay and thereby makes the system causal. It can be predicted that if the actuator efforts are to be applied at the same place as the specified trajectory, solution of the inverse dynamics problem would have better behavior than that of the conventional (noncollocated) case.

From the previous analysis of a single flexible-link arm, we know that the inverse dynamics solution in which we seek a joint actuator torque to achieve a prescribed tip motion is generally unstable. To avoid the instability of the solution, one way is to collocate the actuators at the tip of the manipulator and obtain a causal solution. Another way is to transform the system equations into frequency domain and solve for a non-causal solution. Both methods have been shown to be effective with experimental implementations [22, 21, 29]. A non-causal solution ensures sta-

ble solution but is computationally less efficient than a causal solution. However, a causal solution, due to the instability, is not always applicable unless torques are transmitted to a point close to the tip. Very interestingly, we notice that when multiple manipulators are handling a common object, wrenches applied by each arm to the object can be viewed as *active* forces and torques on the other arms. This can be well illustrated by a two-arm system composed of one flexible and one rigid arm. Assuming both arms are away from the configuration singularities, the rigid arm can be used to manipulate both the object and the flexible arm (through the rigid grasp between the flexible arm and the object). In this situation, actuation wrenches are applied at the tip of the flexible arm through the rigid object by the rigid arm. This scenario implies a collocation between the actuation and the end-effector motion of the flexible arm. Motivated by this observation, we propose to implement the causal inverse dynamics solution while seeking out a way of utilizing redundant actuation to stabilize the solution.

Another important observation is that the behavior of the nonlinear inverse dynamics system may depend critically on the input trajectory assigned to the system, in contrast to the single flexible-link case (linear system) where the input-output relations can be described, for example, by the transfer function, independently of the input. For the present study, we will use smooth acceleration profiles to describe trajectories of the object, starting and ending from rest.

3.4.1 Solutions for the Non-collocated Joint Actuation

As mentioned earlier, the inverse dynamics and the inverse kinematics problems are coupled. Differentiating the velocity kinematics equation (2.8), we obtain the accel-

eration kinematics relation:

$$\dot{\boldsymbol{v}} = \mathbf{J}_r \ddot{\boldsymbol{q}}_r + \mathbf{J}_e \ddot{\boldsymbol{q}}_e + \dot{\mathbf{J}}_r \dot{\boldsymbol{q}}_r + \dot{\mathbf{J}}_e \dot{\boldsymbol{q}}_e \tag{3.49}$$

We repeat here the dynamics equations (2.24) and (2.25) from Chapter 2 for serial manipulators in the absence of the external tip wrenches as:

$$\mathbf{M}_{rr} \ddot{\boldsymbol{q}}_r + \mathbf{M}_{re} \ddot{\boldsymbol{q}}_e = \boldsymbol{\tau} + \boldsymbol{f}_{I,r} + \boldsymbol{f}_{ext,r} \tag{3.50}$$

$$\mathbf{M}_{re}^T \ddot{\boldsymbol{q}}_r + \mathbf{M}_{ee} \ddot{\boldsymbol{q}}_e + \mathbf{D}_{ee} \dot{\boldsymbol{q}}_e + \mathbf{K}_{ee} \boldsymbol{q}_e = \boldsymbol{f}_{I,e} + \boldsymbol{f}_{ext,e} \tag{3.51}$$

These are linear algebraic equations in terms of unknown variables $\ddot{\boldsymbol{q}}_r$, $\ddot{\boldsymbol{q}}_e$ and $\boldsymbol{\tau}$. At every time instant, the mass matrices, the stiffness matrix and the non-linear inertial and generalized external forces are calculated from the known states. Solving for $\ddot{\boldsymbol{q}}_r$, $\ddot{\boldsymbol{q}}_e$, and $\boldsymbol{\tau}$ yields:

$$\boldsymbol{\tau} = \widehat{\mathbf{M}}_{re}\widehat{\mathbf{M}}_{ee}^{-1}(\hat{\mathbf{f}} - \mathbf{M}_{re}^T\mathbf{J}_r^{-1}\hat{\mathbf{a}}) + \mathbf{M}_{rr}\mathbf{J}_r^{-1}\hat{\mathbf{a}} - \mathbf{f}_{I,ext,r} \tag{3.52}$$

$$\ddot{\boldsymbol{q}}_r = \mathbf{J}_r^{-1}[(1 + \mathbf{J}_e\widehat{\mathbf{M}}_{ee}^{-1}\mathbf{M}_{re}^T\mathbf{J}_r^{-1})\hat{\mathbf{a}} - \mathbf{J}_e\widehat{\mathbf{M}}_{ee}^{-1}\hat{\mathbf{f}}] \tag{3.53}$$

$$\ddot{\boldsymbol{q}}_e = \widehat{\mathbf{M}}_{ee}^{-1}(-\mathbf{M}_{re}^T\mathbf{J}_r^{-1}\hat{\mathbf{a}} + \hat{\mathbf{f}}) \tag{3.54}$$

where

$$\begin{aligned} \hat{\mathbf{a}} &= \dot{\boldsymbol{v}} - \dot{\mathbf{J}}_r\dot{\mathbf{q}}_r - \dot{\mathbf{J}}_e\dot{\mathbf{q}}_e & \hat{\mathbf{f}} &= \mathbf{f}_{I,ext,e} - \mathbf{K}_{ee}\,\boldsymbol{q}_e - \mathbf{D}_{ee}\,\dot{\boldsymbol{q}}_e \\ \mathbf{f}_{I,ext,r} &= \boldsymbol{f}_{I,r} + \boldsymbol{f}_{ext,r} & \mathbf{f}_{I,ext,e} &= \boldsymbol{f}_{I,e} + \boldsymbol{f}_{ext,e} \\ \widehat{\mathbf{M}}_{re} &= \mathbf{M}_{re} - \mathbf{M}_{rr}\mathbf{J}_r^{-1}\mathbf{J}_e & \widehat{\mathbf{M}}_{ee} &= \mathbf{M}_{ee} - \mathbf{M}_{re}^T\mathbf{J}_r^{-1}\mathbf{J}_e \end{aligned} \tag{3.55}$$

In the above, we assume $\widehat{\mathbf{M}}_{ee}$ is invertible. Therefore, eq. (3.52) gives the inverse dynamics solution for actuator torques $\boldsymbol{\tau}$. To forward the solution in time, integration of $\dot{\boldsymbol{q}}_r$, $\dot{\boldsymbol{q}}_e$, $\ddot{\boldsymbol{q}}_r$ and $\ddot{\boldsymbol{q}}_e$ is required to calculate the initial states for the next time instant. In fact, we can define a set of state variables to be

$$\boldsymbol{x} = [\boldsymbol{q}_r,\ \boldsymbol{q}_e,\ \dot{\boldsymbol{q}}_r,\ \dot{\boldsymbol{q}}_e]^T \tag{3.56}$$

Then, the equations of motion in state space form can be written as first-order differential equations:

$$\dot{\boldsymbol{x}}(t) = \mathbf{f}(\boldsymbol{x}, t) \tag{3.57}$$

with known initial states as:

$$\boldsymbol{x}(0) = [\boldsymbol{q}_r(0),\ \dot{\boldsymbol{q}}_r(0),\ \boldsymbol{q}_e(0),\ \dot{\boldsymbol{q}}_e(0)]^T \tag{3.58}$$

where $\boldsymbol{q}_e(0)$ represents the static deformation of the links at the beginning of the task. The right-hand side of eq. (3.57) is

$$\mathbf{f}(\boldsymbol{x}, t) = \begin{bmatrix} \dot{\boldsymbol{q}}_r \\ \dot{\boldsymbol{q}}_e \\ \mathbf{J}_r^{-1}[(1 + \mathbf{J}_e\widehat{\mathbf{M}}_{ee}^{-1}\mathbf{M}_{re}^T\mathbf{J}_r^{-1})\hat{\mathbf{a}} - \mathbf{J}_e\widehat{\mathbf{M}}_{ee}^{-1}\hat{\mathbf{f}}] \\ \widehat{\mathbf{M}}_{ee}^{-1}(-\mathbf{M}_{re}^T\mathbf{J}_r^{-1}\hat{\mathbf{a}} + \hat{\mathbf{f}}) \end{bmatrix} \tag{3.59}$$

Eq. (3.57) can be integrated numerically in time and in this way, a time history of both actuator torques and the state variables are obtained which constitute the inverse dynamics solution for a serial chain flexible-body system. Figure (3.4) contains the flow chart of the algorithm for calculating the inverse dynamics solution of a single serial flexible arm. Through the following example, we will illustrate the solution of inverse dynamics problem by using the proposed algorithm.

Example 3.1

Figure 3.5 shows a 3-DOF planar serial flexible arm. It is composed of three links with the first (counted from the base) link flexible. The lengths of the links are $0.5m$, $0.5m$ and $0.1m$ respectively. The geometric dimensions of the flexible link are shown in Figure 3.6, and the inertia properties of the arm are summarized in Table 3.1. In the table, we omitted columns for I_{xy}, I_{xz} and I_{yz} since in the present example, these

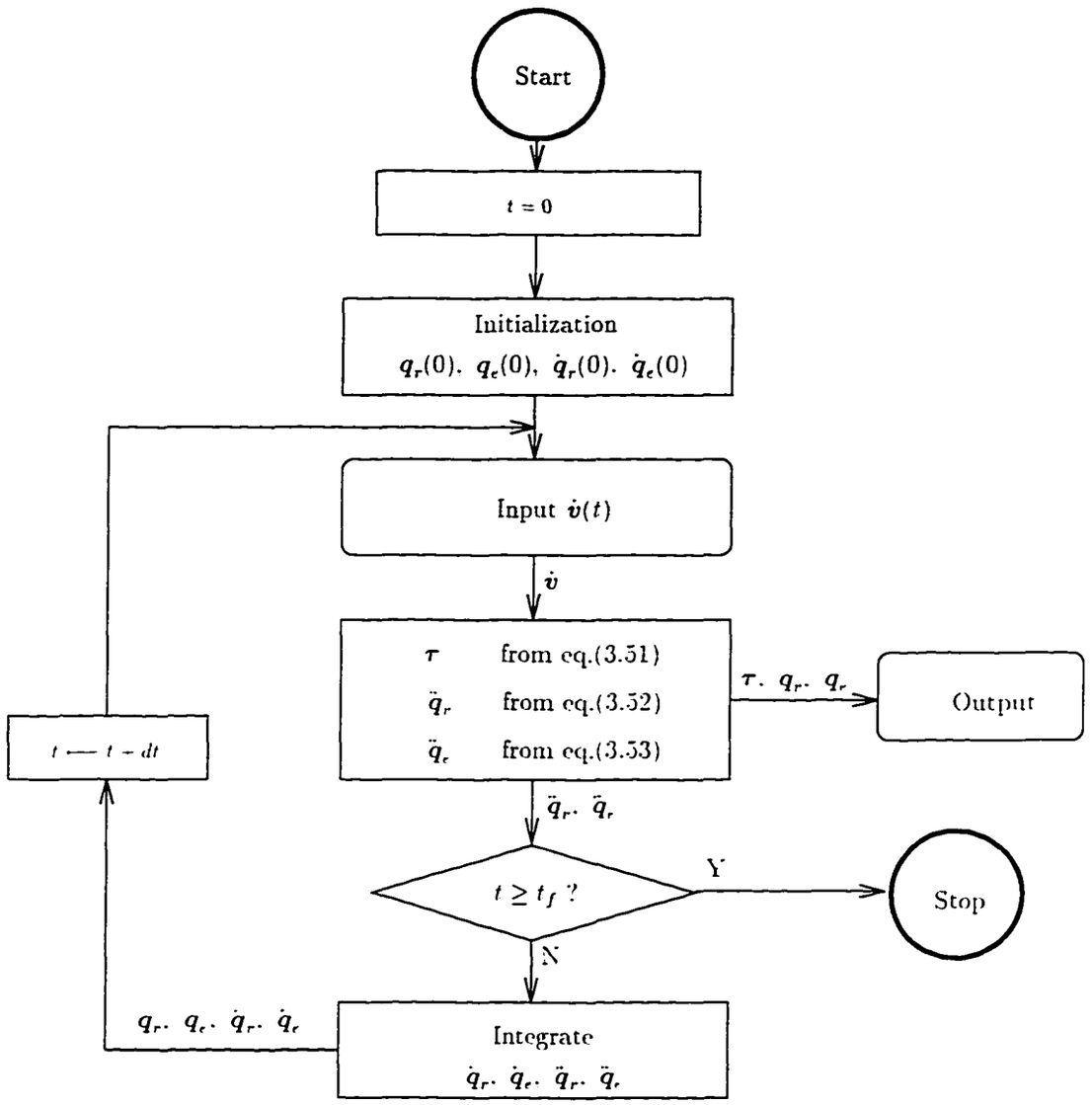

Figure 3.4: Computational Algorithm for Inverse Dynamics Solution of a Serial Flexible Arm

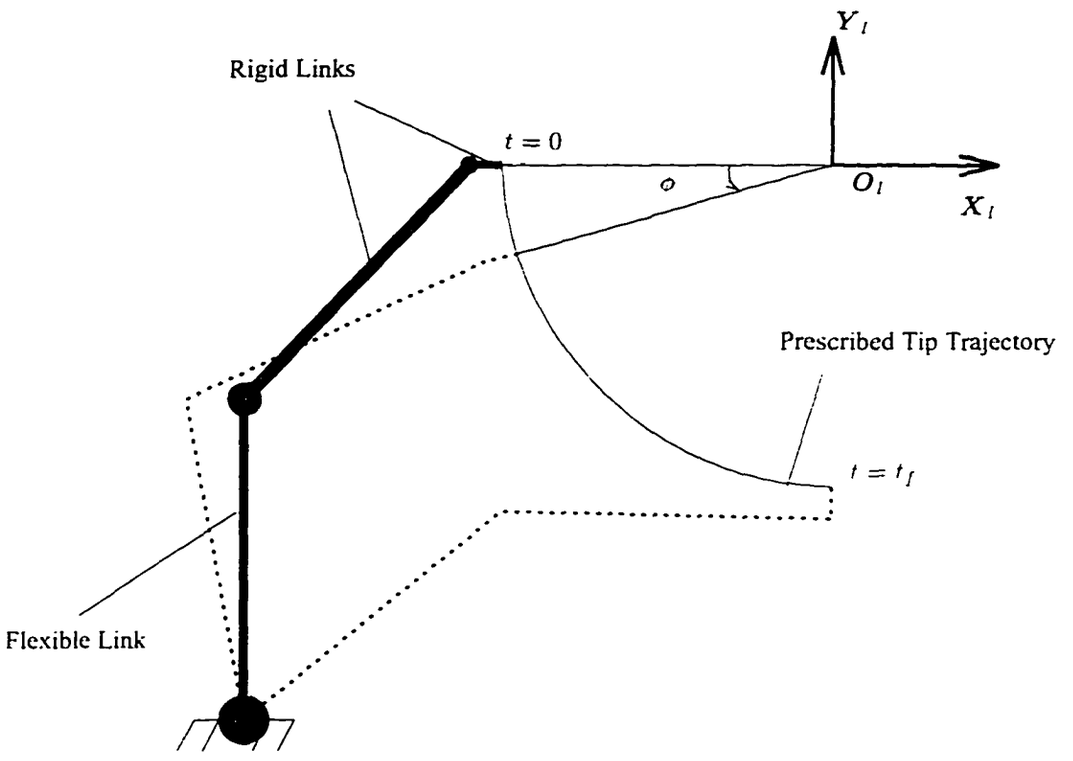

Figure 3.5: A Planar Arm Tracing a 1/4 Circle

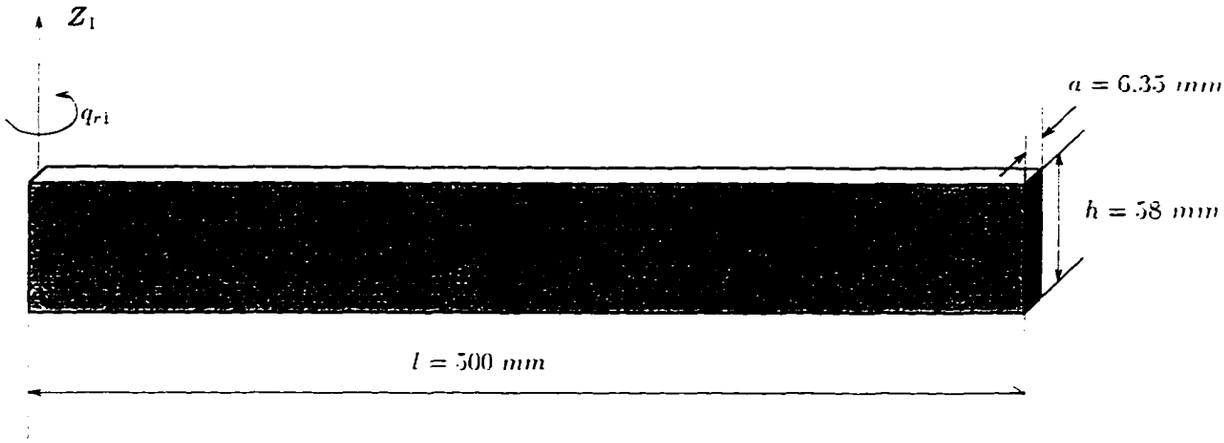

Figure 3.6: Geometric Dimensions of the Flexible Link

values are zeros for all the members. We model the flexible link by using two planar beam elements with a total of four degrees of freedom to allow bending in the plane of motion. The tip of the arm is required to move along a circular arc during time $t \in [0,\ t_f]$. It is also required that the tip of the last link point to the center of the circle during the move. Using a sinusoidal acceleration profile, the angle of rotation around the center of the circle is defined as,

$$o = \frac{h}{\omega}(t - \frac{1}{\omega}\sin(\omega t)), \tag{3.60}$$

the desired tip trajectory (Figure3.5) is then determined by:

$$\dot{v}_x = -d[h\sin(\omega t)\sin o + (\frac{o_f}{t_f})^2(1 - \cos(\omega t))^2\cos o] \tag{3.61}$$

$$\dot{v}_y = -d[h\sin(\omega t)\cos o - (\frac{o_f}{t_f})^2(1 - \cos(\omega t))^2\sin o] \tag{3.62}$$

Table 3.1: Inertia Properties of the Planar Arm

Members	Mass	First Moment of Inertia			Second Moment of Inertia		
	m (kg)	c_x $(kg-m)$	c_y $(kg-m)$	c_z $(kg-m)$	I_{xx} $(kg-m^2)$	I_{yy} $(kg-m^2)$	I_{zz} $(kg-m^2)$
Elastic Link	0.473	0.109	0	0	9.55×10^{-5}	3.65×10^{-2}	3.64×10^{-2}
Rigid Link	0.809	0.214	0	0	4.0×10^{-4}	8.36×10^{-2}	8.37×10^{-2}
End-effector	0.300	0.015	0	0	2.46×10^{-4}	5.02×10^{-2}	1.00×10^{-3}
Base Rotor	11.550	0	0.084	0	5.61×10^{-2}	7.60×10^{-2}	5.61×10^{-2}
Elbow Motor	14.000	0	0.558	0	7.33×10^{-2}	6.05×10^{-2}	7.33×10^{-2}
Wrist Motor	6.500	0	0.289	0	2.66×10^{-2}	1.04×10^{-2}	2.66×10^{-2}

$$C_{I.E} = \begin{bmatrix} \cos\phi & -\sin\phi & 0 \\ \sin\phi & \cos\phi & 0 \\ 0 & 0 & 1 \end{bmatrix} \tag{3.63}$$

where

$$\phi_f = \pi/4 \qquad h = \phi_f/t_f \qquad \omega = 2\pi/t_f \qquad d = 0.5$$

As we are aware of, the actuator torques that we are going to obtain through the causal inverse dynamics algorithm (Figure 3.4) may be unbounded. Depending on the properties of the input, the behavior of the inverse dynamics system may vary significantly. For a desired tip trajectory as defined in eqs. (3.61)-(3.63), a larger value of terminal time t_f implies a slower maneuver. Letting $t_f = 100$ sec and setting the absolute tolerance used for numerical integration to $\epsilon = 10^{-6}$, the numerical integration is carried out with an off-the-shelf routine LSODE. Results for the actuator torques and the tip deformations of the flexible link are shown in Figure 3.7. We observe from Figure 3.7 that the maximum value of the transverse tip deflection is less than 0.0021% of the length of the link because the maneuver is slow enough to allow the arm to behave as 'rigid'. However, if we reduce the duration of the maneuver to 90 sec, the actuator torques become infinite shortly after the maneuver starts. We

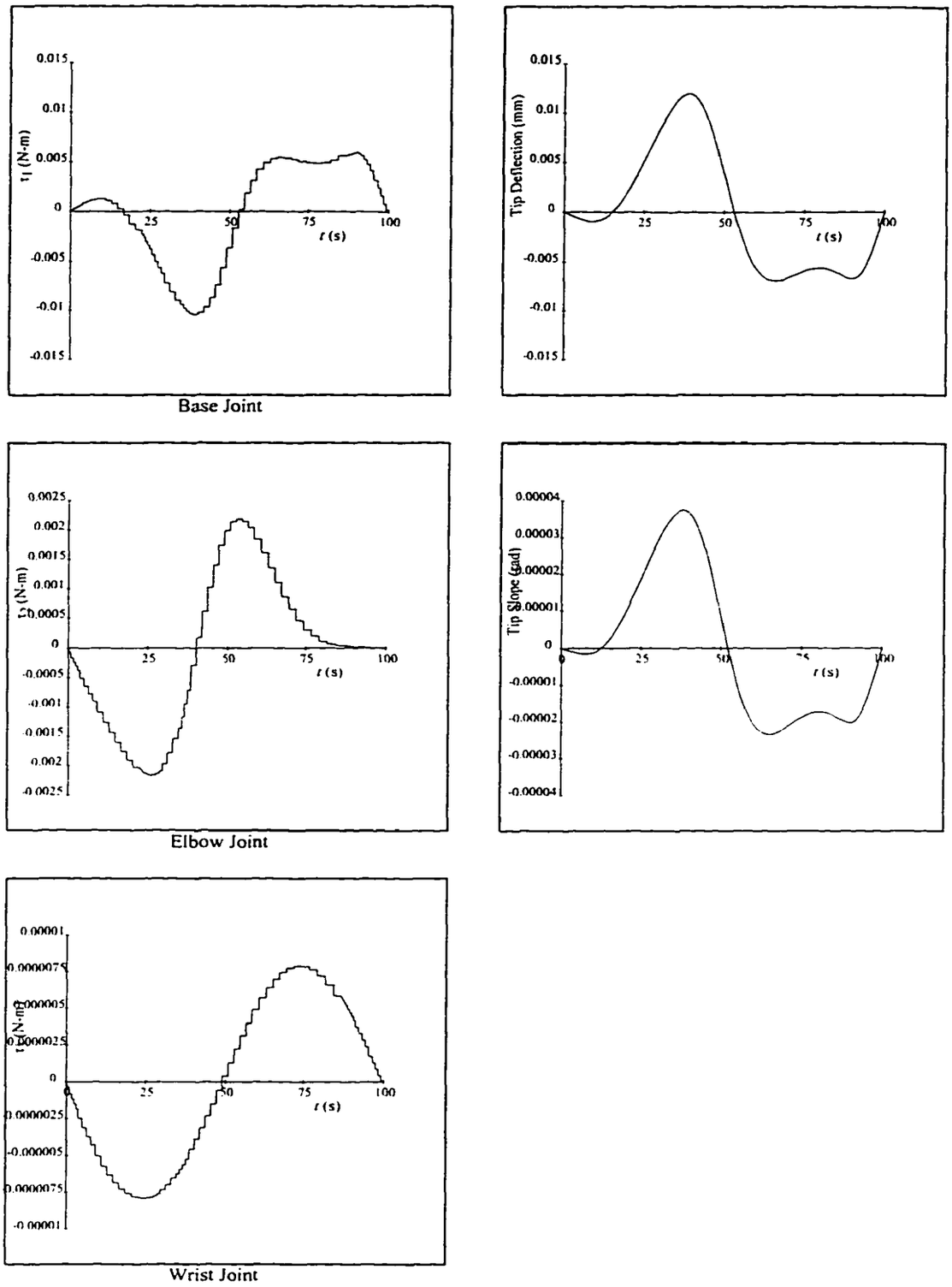

Figure 3.7: Solution for Example 3.1

therefore conclude that the unboundedness of the dynamic variables prohibits the application of causal solutions to the inverse dynamics problem for serial flexible-link manipulators.

3.4.2 Solutions for the Collocated Tip Actuation

As a comparison to the previous example, we now propose a hypothetical situation. Assuming a set of driving wrenches $\boldsymbol{w}$ to be applied at the tip of the arm, we calculate the time profiles of these wrenches necessary to achieve the same tip trajectory used in the previous example. Since the tip wrenches are collocated at the tip of the arm, we expect the behavior of the inverse dynamics system to be improved. Combining the dynamics equations (3.23)and (3.24), in the absence of joint torques $\boldsymbol{\tau}$, together with the acceleration kinematics of eq. (3.49), the driving tip wrenches as well as the rigid and elastic accelerations are calculated, at every time instant, according to:

$$\begin{aligned} \boldsymbol{w} &= \mathbf{J}_r^{-T}[\widehat{\mathbf{M}}_{re}\widetilde{\mathbf{M}}_{ee}^{-T}(\hat{\mathbf{f}} - \mathbf{M}_{re}^T\mathbf{J}_r^{-1}\hat{\mathbf{a}}) + \mathbf{M}_{rr}\mathbf{J}_r^{-1}\hat{\mathbf{a}} - \mathbf{f}_{I,ext,r} \\ &\quad -\widehat{\mathbf{M}}_{re}\widetilde{\mathbf{M}}_{ee}^{-T}(\mathbf{J}_r^{-1}\hat{\mathbf{a}} + \mathbf{J}_e^T\mathbf{J}_r^{-T}\mathbf{f}_{I,ext,r})] \qquad (3.64) \\ \ddot{\boldsymbol{q}}_r &= \mathbf{J}_r^{-1}[(\mathbf{1} + \mathbf{J}_e\widetilde{\mathbf{M}}_{ee}^{-1}\mathbf{M}_{re}^T\mathbf{J}_r^{-1})\hat{\mathbf{a}} - \mathbf{J}_e\widetilde{\mathbf{M}}_{ee}^{-1}\hat{\mathbf{f}} - \mathbf{J}_e\mathbf{J}_e^T\mathbf{J}_r^{-T}\mathbf{f}_{I,ext,r}] \qquad (3.65) \\ \ddot{\boldsymbol{q}}_e &= \widetilde{\mathbf{M}}_{ee}^{-1}(-\mathbf{M}_{re}^T\mathbf{J}_r^{-1}\hat{\mathbf{a}} + \hat{\mathbf{f}}) + \mathbf{J}_e^T\mathbf{J}_r^{-T}\mathbf{f}_{I,ext,r} \qquad (3.66) \end{aligned}$$

where

$$\widetilde{\mathbf{M}}_{ee} = \widehat{\mathbf{M}}_{ee}^T - \widehat{\mathbf{M}}_{re}^T\mathbf{J}_r^{-1}\mathbf{J}_e$$

A similar computational algorithm can be derived by simply replacing $\boldsymbol{\tau}$ by $\boldsymbol{w}$ in Figure 3.4.

Example 3.2

Using equations (3.61)-(3.63) to describe the tip trajectory, we consider a faster maneuver by reducing the terminal time to 1 sec and to 0.5 sec. The resulting solutions

for the tip driving wrenches and the deflections at the tip of the flexible link are shown in Figure 3.8. The left column in the figures corresponds to the maneuver with $t_f = 1\,\text{sec}$ while the right column displays the results for $t_f = 0.5\,\text{sec}$. Higher driving wrenches and tip deflections are observed with the increase of the speed of the maneuver. Compared with example 3.1, bounded solutions are obtained when the arm is driven by tip wrenches for a much faster maneuver. Certainly, this means that tip driven systems have much better behavior than the joint actuated systems.

3.4.3 Validation of the Solution by Energy Check

One direct way of verifying the correctness of the inverse dynamics solution is to apply the *forward dynamics* procedure by inputing the actuator torques obtained as solutions of the inverse dynamics problem to the same dynamics equations under the same initial states. If the output of the forward dynamics simulation gives a response of the system close to that of the input to the inverse dynamics procedure, the inverse dynamics solutions can be considered to be trustable.

The other way which is also effective and probably more efficient is to keep track of the error in the energy balance between the input and output of the inverse dynamics procedure. Without using a separate procedure each time after the inverse dynamics solution is obtained, this check is done within the inverse dynamics calculations. By outputting the profile of the energy drift together with the solution of the actuator torques and generalized coordinates, the inverse dynamics solutions are thus verified. In case when the only external forces applied to the manipulator are the actuator torques, the input energy W is obtained by integrating the power π which is given at every time instant by

$$\pi = \boldsymbol{\tau}\,\dot{\boldsymbol{q}}_r, \qquad W = \int_0^t \pi dt \tag{3.67}$$

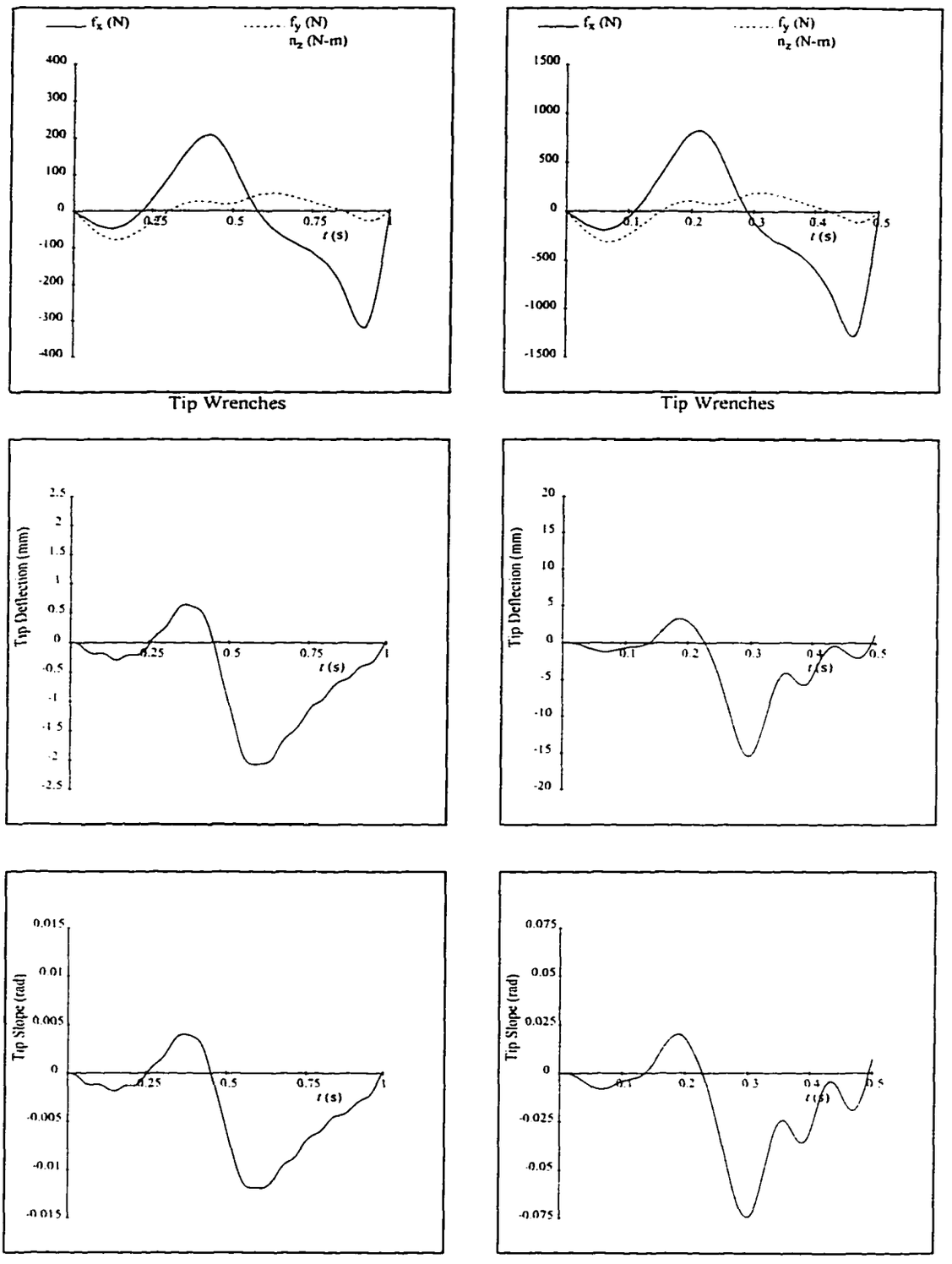

Figure 3.8: Solution for Example 3.2

Part of the above energy is balanced by the dissipative influence such as the modal damping and this can be calculated by

$$W_d = \int_0^t \frac{1}{2} \dot{\mathbf{q}}_e^T \mathbf{D}_{ee} \dot{\mathbf{q}}_e dt \tag{3.68}$$

Assuming the system starts from rest, the error in the energy balance can be calculated from:

$$E(t) = (T(t) + V(t)) - (W - W_d) \tag{3.69}$$

where $T(t)$ and $V(t)$ are the kinetic and potential energies of the system. The kinetic energy at any time instant is defined by

$$T = \frac{1}{2} \dot{\mathbf{q}}^T \mathbf{M} \dot{\mathbf{q}} \tag{3.70}$$

while the potential energy, if in the micro-gravity environment, is that due to the elastic deformation of the links:

$$V = \frac{1}{2} \dot{\mathbf{q}}_e^T \mathbf{K}_{ee} \dot{\mathbf{q}}_e \tag{3.71}$$

Not only can the error in the energy balance be used to verify the inverse dynamics calculation, it can also be used to assess the validity of the dynamics model [45]. Furthermore, in the case of unbounded solution, a large error in the energy balance must result since unbounded solution implies unstable system vibrations.

It is expected that the absolute value of the energy drift is related to the maximum total energy of the system during the maneuver. It is therefore natural that we measure percentage error in the energy balance by comparing the error with the maximum energy of the system:

$$\epsilon_E(t) = \frac{E(t)}{|(T+V)_{peak}|} \times 100\% \tag{3.72}$$

The root mean square value of the energy balance error is then obtained as:

$$\epsilon_{E,RMS} = \sqrt{\frac{\sum_{i=1}^{K} \epsilon_E(t_i)^2}{K}} \tag{3.73}$$

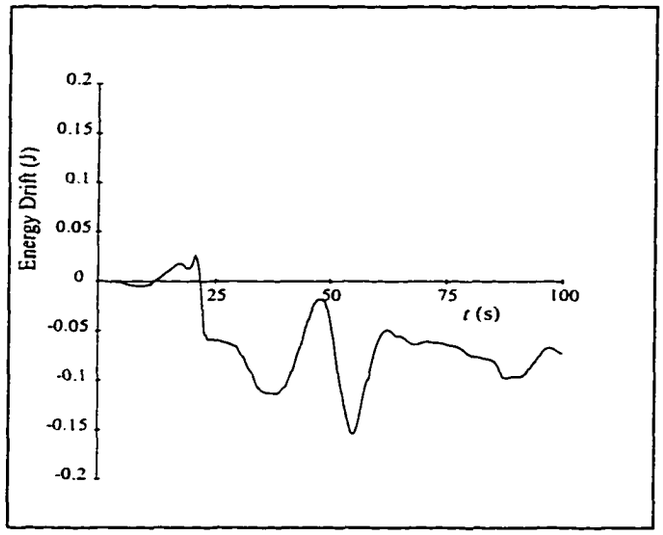

Figure 3.9: Energy Drift for Example 3.1

where K is the total number of points at which the output solution is saved.

Although a sufficiently small error in the energy balance indicates a necessary but not a sufficient condition for a correct inverse dynamics solution, it proves to be efficient in debugging and verifying the inverse dynamics codes. Upon testing the codes with different mechanical set-ups and various maneuvers, the calculation has been proven to be trustable. Still, the energy drift is considered to be part of the inverse dynamics solution and serves as a means of deciding whether the solution is well behaved.

Figure 3.9 illustrates the error in the energy balance between the input and the output for example 3.1. The root mean square value of the percentage energy balance error is 0.07% while the peak value of the system energy is 0.0033 J.

Chapter 4

Inverse Dynamics of Multiple Cooperating Manipulators

In the preceding chapter, we discussed the inverse dynamics solution for a single serial-chain flexible-link manipulator. In particular, we focused on finding the actuator torques required to achieve a desired motion of the end-effector. It was found that the actuator torques needed to produce a prescribed motion of a non-collocated reference body may be unbounded (at this point, we assume that the driving torques are applied at each joint of the manipulator). Along the same line of thought, we define the inverse dynamics problem for multiple cooperating manipulators as: given a motion of the object, find the set of actuator torques for all the arms which will generate the desired object motion. In this chapter, we will first show that this problem is *underspecified* meaning that the number of equations necessary to solve the problem is less than the number of unknown actuator torques. Then, we will discuss in more detail the relationship between the actuation redundancy and the degrees of freedom in choosing the internal forces. Finally, we propose a computational algorithm for calculating the causal inverse dynamics solution for a system of multiple cooperating

manipulators, based on which a numerical example is given.

4.1 Underdeterminacy of the Problem

Based on the discussion in chapter 3, the following work concentrates on finding a *causal* inverse dynamics solution. This implies that direct integration of the dynamics equations with known initial states of the system (positions and velocities) will be carried out in time domain, for a predefined motion of the object. Although it was found that the causal inverse dynamics solution for actuator torques may be unbounded for a serial flexible-link manipulator, we will investigate the possibilities of utilizing the redundant actuation to improve the dynamics behavior of the multiple-arm system.

Repeating, from Chapter 2, the dynamics equations (2.38) and (2.39) for *each* of the decoupled serial chains are:

$$\mathbf{M}_{rr}\ddot{\boldsymbol{q}}_r + \mathbf{M}_{re}\ddot{\boldsymbol{q}}_e = \boldsymbol{\tau} + \boldsymbol{f}_{l.ext.r} - \mathbf{J}_r^T\boldsymbol{w} \tag{4.1}$$

$$\mathbf{M}_{re}^T\ddot{\boldsymbol{q}}_r + \mathbf{M}_{ee}\ddot{\boldsymbol{q}}_e + \mathbf{D}_{ee}\,\dot{\boldsymbol{q}}_e + \mathbf{K}_{ee}\,\boldsymbol{q}_e = \boldsymbol{f}_{l.ext.e} - \mathbf{J}_e^T\boldsymbol{w} \tag{4.2}$$

In the above, $\boldsymbol{f}_{l.ext.r}$ and $\boldsymbol{f}_{l.ext.e}$ have been used to denote the summation of nonlinear inertial forces and the generalized external forces (excluding the tip wrenches) which originally appeared in eqs. (2.38) and (2.39). If we include the acceleration kinematics relations for each serial chain, eq. (3.49), and solve together with the above equations for $\ddot{\boldsymbol{q}}_r$, $\ddot{\boldsymbol{q}}_e$ and $\boldsymbol{\tau}$, we find:

$$\boldsymbol{\tau} = \widehat{\mathbf{M}}_{re}\widehat{\mathbf{M}}_{ee}^{-1}(\hat{\mathbf{f}} - \mathbf{M}_{re}^T\mathbf{J}_r^{-1}\hat{\mathbf{a}}) + \mathbf{M}_{rr}\mathbf{J}_r^{-1}\hat{\mathbf{a}} - \mathbf{f}_{l.ext.r} + \mathbf{J}_3^T\boldsymbol{w} \tag{4.3}$$

$$\ddot{\boldsymbol{q}}_e = \widehat{\mathbf{M}}_{ee}^{-1}\{-\mathbf{M}_{re}^T\mathbf{J}_r^{-1}\hat{\mathbf{a}} + \hat{\mathbf{f}}\} + \mathbf{J}_2^T\boldsymbol{w} \tag{4.4}$$

$$\ddot{\boldsymbol{q}}_r = \mathbf{J}_r^{-1}\{(1 + \mathbf{J}_e\widehat{\mathbf{M}}_{ee}^{-1}\mathbf{M}_{re}^T\mathbf{J}_r^{-1})\hat{\mathbf{a}} - \mathbf{J}_e\widehat{\mathbf{M}}_{ee}^{-1}\hat{\mathbf{f}}\} + \mathbf{J}_1^T\boldsymbol{w} \tag{4.5}$$

where

$$\mathbf{J}_1^T = \mathbf{J}_r^T - \widehat{\mathbf{M}}_{re}\widehat{\mathbf{M}}_{ee}^{-1}\mathbf{J}_e^T \qquad \mathbf{J}_2^T = \mathbf{J}_r^{-1}\mathbf{J}_e\widehat{\mathbf{M}}_{ee}^{-1}\mathbf{J}_e^T \qquad \mathbf{J}_3^T = -\widehat{\mathbf{M}}_{ee}^{-1}\mathbf{J}_e^T \tag{4.6}$$

Comparing with the inverse dynamics formulation for the noncollocated joint actuation system as described in eqs. (3.52)-(3.54), eqs. (4.3)-(4.5) can be written as

$$\boldsymbol{\tau} = \boldsymbol{\tau}' + \mathbf{J}_1^T\boldsymbol{w} \tag{4.7}$$

$$\ddot{\boldsymbol{q}}_r = \ddot{\boldsymbol{q}}_r' + \mathbf{J}_2^T\boldsymbol{w} \tag{4.8}$$

$$\ddot{\boldsymbol{q}}_e = \ddot{\boldsymbol{q}}_e' + \mathbf{J}_3^T\boldsymbol{w} \tag{4.9}$$

where $\boldsymbol{\tau}'$, $\ddot{\boldsymbol{q}}_r'$ and $\ddot{\boldsymbol{q}}_e'$ are as defined in eqs. (3.52)-(3.54). These quantities represent the inverse dynamics solution in the absence of tip wrenches acting between the end-effector and the object.

In the case of a rigid grasp, a given object motion automatically defines the motion of the manipulator end-effectors. Therefore, $\boldsymbol{\tau}'$, $\ddot{\boldsymbol{q}}_r'$ and $\ddot{\boldsymbol{q}}_e'$ can be determined, at every time instant, from the desired motion of the object regardless of the grasping wrenches applied at the end-effectors. The last terms in eqs. (4.7)-(4.9) then represent the effects of the tip wrenches on the solution. In the following, we use 'Σ' to denote assembled quantities for P manipulators, for example,

$$\boldsymbol{\tau}_\Sigma = \mathrm{col}\{\boldsymbol{\tau}_1\ \boldsymbol{\tau}_2\ \cdots \boldsymbol{\tau}_P\} \tag{4.10}$$

$$\mathbf{J}_{1\Sigma}^T = \mathrm{diag}\{\mathbf{J}_{11}^T\ \mathbf{J}_{12}^T\ \cdots\ \mathbf{J}_{1P}^T\} \tag{4.11}$$

It should be pointed out that although 'Σ' was used in Chapter 2 to symbolize assembled quantities over bodies in a single chain, it disappears once the chain dynamics equations have been obtained and each manipulator is treated as a whole. When dealing with multiple arms, 'Σ' is used to denote 'global' quantities for the multiple arms. Thus, assembling eq. (4.7)-(4.9) for all manipulators, we have

$$\boldsymbol{\tau}_\Sigma = \boldsymbol{\tau}_\Sigma' + \mathbf{J}_{1\Sigma}^T\boldsymbol{w}_\Sigma \tag{4.12}$$

$$\tilde{q}_{r\Sigma} = \tilde{q}'_{r\Sigma} + \mathbf{J}^T_{2\Sigma} \boldsymbol{w}_\Sigma \tag{4.13}$$

$$\tilde{q}_{e\Sigma} = \tilde{q}'_{e\Sigma} + \mathbf{J}^T_{3\Sigma} \boldsymbol{w}_\Sigma \tag{4.14}$$

The above relations represent the dynamics of the manipulators constrained by each other through the object. The grasping wrenches $\boldsymbol{w}_\Sigma$ have to satisfy the dynamics equations of the object which are given by eqs. (2.40) and (2.41). These are rewritten here as:

$$\mathbf{A}_1 \boldsymbol{w}_\Sigma = \mathbf{b}_1 \tag{4.15}$$

where

$$\mathbf{A}_1 = \begin{bmatrix} 1 & 0 & 1 & 0 & \dots & 1 & 0 \\ \mathbf{C}_1^\times & 1 & \mathbf{C}_2^\times & 1 & \dots & \mathbf{C}_P^\times & 1 \end{bmatrix} \tag{4.16}$$

$$\mathbf{b}_1 = \begin{bmatrix} m_B(\dot{\mathbf{v}}_B + \mathbf{g}) - \mathbf{f}_e \\ \mathbf{I}_B \dot{\boldsymbol{\omega}}_B + \boldsymbol{\omega}_B \times \mathbf{I}_B \boldsymbol{\omega}_B - (\mathbf{n}_e + \mathbf{c}_e \times \mathbf{f}_e) \end{bmatrix} \tag{4.17}$$

In the above, the matrix $\mathbf{C}_i^\times$ represents the cross-product operator of the relative contact location vector $\boldsymbol{c}_i$. In the literature, matrix $\mathbf{A}_1$ has been called the contact force map [11] or the grasp matrix [4]. It can also be written as

$$\mathbf{A}_1 = [\boldsymbol{\varphi}(\boldsymbol{c}_1)\ \boldsymbol{\varphi}(\boldsymbol{c}_2)\ \cdots\ \boldsymbol{\varphi}(\boldsymbol{c}_P)] \in \mathbf{R}^{6\times 6P} \tag{4.18}$$

with $\boldsymbol{\varphi}(\boldsymbol{c}_i)$ defined by

$$\boldsymbol{\varphi}(\boldsymbol{c}_i) = \begin{bmatrix} 1 & 0 \\ \mathbf{C}_i^\times & 1 \end{bmatrix} \in \mathbf{R}^{6\times 6} \tag{4.19}$$

We note that $\boldsymbol{\varphi}(\boldsymbol{c}_i)$ is invertible and moreover, $\boldsymbol{\varphi}^{-1}(\boldsymbol{c}_i) = \boldsymbol{\varphi}(-\boldsymbol{c}_i)$. The invertability of $\boldsymbol{\varphi}(\boldsymbol{c}_i)$ ensures that $\mathbf{A}_1$ is full rank and $\mathbf{A}_1 \mathbf{A}_1^T \in \mathbf{R}^{6\times 6}$ is always invertible.

We solve the inverse dynamics problem by evaluating eqs. (4.12)-(4.15) for $\boldsymbol{\tau}_\Sigma$, $\ddot{\boldsymbol{q}}_{r\Sigma}$ and $\ddot{\boldsymbol{q}}_{e\Sigma}$ at every time instant. Assuming $\mathbf{J}^T_{1\Sigma}$ is invertible, the constraint tip wrenches $\boldsymbol{w}_\Sigma$ can be further eliminated from equations (4.12)-(4.15) by using

$$\boldsymbol{w}_\Sigma = \mathbf{J}^{-T}_{1\Sigma}(\boldsymbol{\tau}_\Sigma - \boldsymbol{\tau}'_\Sigma) \tag{4.20}$$

and substituting it into eqs. (4.13)-(4.15). Then, the solution of the inverse dynamics problem for the closed-loop multiple arm system can be obtained by solving the linear system:

$$\begin{bmatrix} \mathbf{A}_1\mathbf{J}_{1\Sigma}^{-T} & \mathbf{0} & \mathbf{0} \\ -\mathbf{J}_{2\Sigma}^{T}\mathbf{J}_{1\Sigma}^{-T} & \mathbf{1} & \mathbf{0} \\ -\mathbf{J}_{3\Sigma}^{T}\mathbf{J}_{1\Sigma}^{-T} & \mathbf{0} & \mathbf{1} \end{bmatrix} \begin{bmatrix} \tau_\Sigma \\ \ddot{q}_{r\Sigma} \\ \ddot{q}_{e\Sigma} \end{bmatrix} = \begin{bmatrix} \mathbf{b}_1 + \mathbf{A}_1\mathbf{J}_{1\Sigma}^{-T}\tau'_\Sigma \\ \ddot{q}'_{r\Sigma} - \mathbf{J}_{2\Sigma}^{T}\mathbf{J}_{1\Sigma}^{-T}\tau'_\Sigma \\ \ddot{q}'_{e\Sigma} - \mathbf{J}_{3\Sigma}^{T}\mathbf{J}_{1\Sigma}^{-T}\tau'_\Sigma \end{bmatrix} \tag{4.21}$$

The right hand side of the above is dependent on the prescribed trajectory and the present states of the system. The kinematic constraints at the points of contact have been included in generating the free motion accelerations $\ddot{q}'_{r\Sigma}$ and $\ddot{q}'_{e\Sigma}$ [11]. Hence, eq. (4.21) accounts for all the necessary constraints imposed on the system when the multiple serial chains are closed through grasping the common object. To confirm that the coefficient matrix in eq. (4.21) is not rank deficient, we only need to make sure that the first block entry $\mathbf{A}_1\mathbf{J}_{1\Sigma}^{-T}$ is full rank. This is apparent since

$$\text{rank}(\mathbf{A}_1\mathbf{J}_{1\Sigma}^{-T}) = \min(\text{rank}(\mathbf{A}_1),\ \text{rank}(\mathbf{J}_{1\Sigma}^{-T})) = \min(6,\ 6P) \tag{4.22}$$

We have introduced in Chapter 2 the symbol ΣS_i to denote the total number of elastic coordinates in the assembled system. Then, the number of unknown variables in eq. (4.21) is $6P + 6P + \Sigma S_i$ while the number of equations given by (4.21) is $6 + 6P + \Sigma S_i$. It becomes clear that once $P > 1$, *i.e.*, the system consists of more than one manipulator grasping the object, the number of equations used to solve the inverse dynamics problem is less than the number of unknowns. Therefore, the inverse dynamics problem for a multiple arm system is underdetermined. The degree of this underdeterminacy is equal to the difference between the row and column dimensions of the coefficient matrix in eq. (4.21), that is, $6(P-1)$. In other words, a unique solution of the inverse dynamics problem can only be obtained if additional $6(P-1)$ constraints are imposed on the system.

4.2 Actuation Redundancy and Controllable internal forces

4.2.1 Degrees of Actuation Redundancy

Imposing the closed loop kinematics constraints results in a loss of degrees of freedom of the multiple arms. For a rigid grasp, closing each loop imposes six holonomic constraints on the system, thereby reducing the total degrees of freedom of the system by six. When all P arms are grasping the common object, they form $P-1$ loops and therefore, the number of degrees of freedom of the system is

$$n_c = 6P - 6(P-1) = 6 \tag{4.23}$$

Again, it is assumed that the manipulators are not kinematically redundant. Since the number of actuators driving the system is unaffected by the loop closure, the number of redundant actuators is therefore

$$n_a = 6P - n_c = 6(P-1) \tag{4.24}$$

This number is called the degree of actuation redundancy and it is equal to the total number of arm configuration degrees of freedom lost when the object is grasped. We shall show that the degree of actuation redundancy is also equal to the number of controllable internal forces that exist in the system.

4.2.2 Degrees of Freedom in Choosing Grasping Wrenches

Recall that in deriving the inverse dynamics equations (4.21), we eliminated the constraint wrenches acting between the manipulator end-effectors and the object. This is a logical step to take if only the *driving* wrenches are of interest in the inverse

dynamics analysis. However, it is not appropriate in the case of multiple arm systems. The reasons are twofold: first, if the manipulators are handling a fragile object, the constraint wrenches applied at the contact points must be kept as small as possible. Thus, the constraint wrenches should be part of the output when analyzing the inverse dynamics solution. Secondly, because of the actuation redundancy, it is natural to expect that the constraint wrenches can be altered by applying different actuator torques. This can be an important factor for stabilizing the inverse dynamics solution, as suggested by our previous analysis of the serial flexible-link inverse dynamics. Therefore, we wish to have the arm tip constraint wrenches as part of the inverse dynamics solution.

Another interpretation of eqs. (4.12)-(4.14) is that these equations can be considered as the inverse dynamics solution for *P decoupled* manipulators with *known* external tip wrenches. The solution is for a given set of tip wrenches. Since the object dynamics equations (4.15) constitute the primary constraints on the tip wrenches, they must be solved to yield the grasping wrenches required to produce the desired motion of the object. It is only necessary for the manipulators to supply forces and moments at their end-effectors which, when pre-multiplied by the contact force map give the right hand side of eq. (4.15). The redundancy of the grasping wrenches can be readily observed since only six forces and moments are required to handle the object, while the number of the components of the grasping wrenches is $6P$.

4.2.3 Degrees of Freedom of Internal Force

Nakamura [8] proposed to decompose the contact forces and moments (the grasping wrenches) into resultant ones and internal ones. The resultant forces are those which contribute to the motion of the object while the internal forces represent the squeezing effect on the object. Physically, internal forces do not contribute to the work needed

to move the object through a certain distance. We will use this fact to determine these forces in the analysis below.

Let the manipulators apply the wrenches $\boldsymbol{w}_i$ $(i = 1, \cdots, P)$ to the object and assume the virtual displacements at the contact points are $\delta \boldsymbol{r}_i$ $(i = 1, \cdots, P) \in \mathbf{R}^6$. The total virtual work done by the grasping wrenches is

$$\delta W = \sum_{i=1}^{P} \delta \boldsymbol{r}_i^T \boldsymbol{w}_i \tag{4.25}$$

From the kinematics relations, we know that $\delta \boldsymbol{r}_i$ is related to the set of independent virtual displacements of the object $\delta \boldsymbol{r}_B^T = [\delta \mathbf{r}_B^T \ \delta \boldsymbol{\phi}^T]$, where $\delta \boldsymbol{\phi}$ is the orientation virtual displacement. This is:

$$\delta \boldsymbol{r}_i = \boldsymbol{\varphi}(\boldsymbol{c}_i) \delta \boldsymbol{r}_B \tag{4.26}$$

Then, eq. (4.25) can be rewritten as

$$\delta W = \sum_{i=1}^{P} (\boldsymbol{\varphi}(\boldsymbol{c}_i) \delta \boldsymbol{r}_B)^T \boldsymbol{w}_i = (\sum_{i=1}^{P} \boldsymbol{\varphi}(\boldsymbol{c}_i) \boldsymbol{w}_i)^T \delta \boldsymbol{r}_B = \delta \boldsymbol{r}_B^T \mathbf{A}_1 \boldsymbol{w}_\Sigma \tag{4.27}$$

For an arbitrary $\delta \boldsymbol{r}_B$, the sufficient and necessary condition for the virtual work to vanish is:

$$\mathbf{A}_1 \boldsymbol{w}_\Sigma = \mathbf{0} \tag{4.28}$$

Accordingly, the *internal* forces must lie in the null space of $\mathbf{A}_1$ denoted by $N(\mathbf{A}_1)$. Introducing $\mathbf{A}_1^+$ to denote the pseudoinverse of $\mathbf{A}_1$, the *resultant* wrenches are those which lie in the orthogonal complement of $N(\mathbf{A}_1)$, that is, the range space of $\mathbf{A}_1^+$ denoted as $R(\mathbf{A}_1^+)$. We have shown that $\mathbf{A}_1$ depends only on the relative position of the contact points on the object and is always full rank which equals the row dimension of $\mathbf{A}_1$. The pseudoinverse of $\mathbf{A}_1$ can therefore be calculated by

$$\mathbf{A}_1^+ = \mathbf{A}_1^T (\mathbf{A}_1 \mathbf{A}_1^T)^{-1} \in \mathbf{R}^{6P \times 6} \tag{4.29}$$

The decomposition of the grasping wrenches satisfying eq. (4.15) can now be written as:

$$\boldsymbol{w}_{\Sigma} = \mathbf{A}_1^{+}\mathbf{b}_1 + \mathbf{A}_1^{N}\mathbf{z} \tag{4.30}$$

In the above, the first term on the right hand side represents the projection in the range space of $\mathbf{A}_1^{+}$ while the columns of $\mathbf{A}_1^{N}$ constitute a basis for the null space of $\mathbf{A}_1$. The vector $\mathbf{z} \in \mathbf{R}^{\dim N(\mathbf{A}_1)}$ is arbitrary and it represents the freedom in choosing the internal forces. The dimension of $N(\mathbf{A}_1)$ is determined from

$$\begin{aligned} &\dim R(\mathbf{A}_1) = \operatorname{rank}(\mathbf{A}_1) = 6 \\ &\dim R(\mathbf{A}_1) + \dim N(\mathbf{A}_1) = 6P \end{aligned} \quad \Rightarrow \quad \dim N(\mathbf{A}_1) = 6(P-1) \tag{4.31}$$

The dimension of the null space of $\mathbf{A}_1$ represents the degree of redundancy in determining the grasping wrenches. It also represents the degrees of freedom in controlling the internal forces.

In concluding the above, we have shown that the degree of actuation redundancy equals to the degree of redundancy in determining the grasping wrenches which further represents the degrees of freedom in controlling the internal forces. Hence, in the context of multiple cooperating manipulator systems, resolution of the actuation redundancy, force distribution and internal force control are commonly used terminology, all referring to the same concept of resolving the redundancy in determining the inverse dynamics solution.

Example 4.1 - Decomposition of the Grasping Wrenches

Figure 4.1 shows an example where two planar wrenches are applied to manipulate an object in a vertical plane. A planar wrench is composed of force components in the X_I and Y_I directions and a moment about the Z_I axis, that is, $\boldsymbol{w} = [f_x \; f_y \; n_z]^T$. The assembled column matrix of the grasping wrenches is $\boldsymbol{w}_{\Sigma} = [f_{1x} \; f_{1y} \; n_{1z} \; f_{2x} \; f_{2y} \; n_{2z}]^T$.

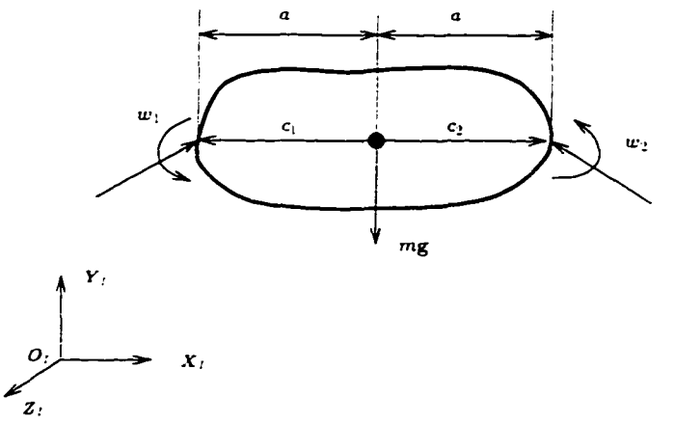

Figure 4.1: Decomposition of Grasping Wrenches

Assuming that the center of mass is at the mid-point of the line segment connecting the two contact points, we have $\mathbf{c}_1 = [-a\ 0\ 0]^T and\, \mathbf{c}_2 = [a\ 0\ 0]^T$. In this case, the matrix of contact force map (grasp matrix) is:

$$\mathbf{A}_1 = \begin{bmatrix} 1 & 0 & 0 & 1 & 0 & 0 \\ 0 & 1 & 0 & 0 & 1 & 0 \\ 0 & -a & 1 & 0 & a & 1 \end{bmatrix} \tag{4.32}$$

If the object is maintained in static equilibrium, the right hand side in eq.(4.15) contains only the external force which is the weight of the object:

$$\mathbf{b}_1^T = \begin{bmatrix} 0 & -(-mg) & 0 \end{bmatrix} \tag{4.33}$$

The pseudoinverse and matrix representation of the null-space of $\mathbf{A}_1$ are:

$$\mathbf{A}_1^+ = \frac{1}{2}\begin{bmatrix} 1 & 0 & 0 \\ 0 & 1 & -a(a^2+1)^{-1} \\ 0 & 0 & (a^2+1)^{-1} \\ 1 & 0 & 0 \\ 0 & 1 & a(a^2+1)^{-1} \\ 0 & 0 & (a^2+1)^{-1} \end{bmatrix} \qquad \mathbf{A}_1^N = \begin{bmatrix} 0 & -1 & 0 \\ -1 & 0 & 0 \\ -2a & 0 & -1 \\ 0 & 1 & 0 \\ 1 & 0 & 0 \\ 0 & 0 & 1 \end{bmatrix} \tag{4.34}$$

Therefore, to keep the object static, the resultant forces are:

$$\mathbf{A}_1^+ \mathbf{b}_1 = \frac{1}{2}\begin{bmatrix} 0 & mg & 0 & 0 & mg & 0 \end{bmatrix}^T \tag{4.35}$$

which shows that only forces in the Y direction are necessary. The internal forces are:

$$\mathbf{A}_1^N \mathbf{z} = \begin{bmatrix} -z_2 & -z_1 & -(2az_1 + z_3) & z_2 & z_1 & z_3 \end{bmatrix}^T \tag{4.36}$$

where z_1, z_2 and z_3 can be chosen freely. It is thus apparent that aside from the resultant forces, there is an infinite number of internal forces which can be applied to the object without affecting its motion. From eq. (4.36), the internal forces at the two grasping points have to be equal and opposite in the X and Y directions while the internal moments at the two points must satisfy:

$$n_{1z} = 2af_{1y} - n_{2z} = -2af_{2y} - n_{2z} \tag{4.37}$$

As a result, eqs. (4.35) and (4.36) are the decomposed orthogonal components of the grasping wrenches — the resultant and the internal forces, respectively.

4.3 Inequality Constraints

Until now, we have only mentioned the primary constraints in solving the inverse dynamics problem for multiple cooperating manipulators, that is, the dynamics equations of the system. Indeed, since the inverse dynamics system satisfying only the primary constraints is underdetermined, it is possible and even desirable that some secondary constraints be taken into consideration in finding an optimal solution. Most commonly considered are the limited actuator capacities which impose inequality constraints on the solution for $\boldsymbol{\tau}_\Sigma$. These can be compactly written as:

$$|\boldsymbol{\tau}_\Sigma| \leq \boldsymbol{\tau}_\Sigma^{lim} \tag{4.38}$$

where $\boldsymbol{\tau}_\Sigma^{lim}$ is a column matrix containing the maximum values of the torques that each actuator of all the arms can generate.

Eq. (4.38) can be expanded into two linear inequalities:

$$\boldsymbol{\tau}_\Sigma \leq \boldsymbol{\tau}_\Sigma^{lim} \tag{4.39}$$

$$\boldsymbol{\tau}_\Sigma \geq -\boldsymbol{\tau}_\Sigma^{lim} \tag{4.40}$$

These equations can be written in terms of the contact wrenches by substituting eq. (4.12) into eqs. (4.39) and (4.40) to yield

$$\mathbf{J}_{1\Sigma}^T \boldsymbol{w}_\Sigma \geq -\boldsymbol{\tau}_\Sigma^{lim} - \boldsymbol{\tau}'_\Sigma \tag{4.41}$$

$$-\mathbf{J}_{1\Sigma}^T \boldsymbol{w}_\Sigma \geq -\boldsymbol{\tau}_\Sigma^{lim} + \boldsymbol{\tau}'_\Sigma \tag{4.42}$$

The assembled inequality constraints for the multiple manipulator system are then

$$\mathbf{A}_2 \boldsymbol{w}_\Sigma \geq \mathbf{b}_2 \tag{4.43}$$

with

$$\mathbf{A}_2 = \begin{bmatrix} \mathbf{J}_{11}^T & \mathbf{0} & \mathbf{0} & \mathbf{0} \\ -\mathbf{J}_{11}^T & \mathbf{0} & \mathbf{0} & \mathbf{0} \\ \mathbf{0} & \mathbf{J}_{12}^T & \mathbf{0} & \mathbf{0} \\ \mathbf{0} & -\mathbf{J}_{12}^T & \mathbf{0} & \mathbf{0} \\ \mathbf{0} & \mathbf{0} & \ddots & \mathbf{0} \\ \mathbf{0} & \mathbf{0} & \ddots & \mathbf{0} \\ \mathbf{0} & \mathbf{0} & \mathbf{0} & \mathbf{J}_{1P}^T \\ \mathbf{0} & \mathbf{0} & \mathbf{0} & -\mathbf{J}_{1P}^T \end{bmatrix} \quad \mathbf{b}_2 = \begin{bmatrix} -\tau_1^{lim} - \tau_1' \\ -\tau_1^{lim} + \tau_1' \\ -\tau_2^{lim} - \tau_2' \\ -\tau_2^{lim} + \tau_2' \\ \vdots \\ -\tau_P^{lim} - \tau_P' \\ -\tau_P^{lim} + \tau_P' \end{bmatrix} \tag{4.44}$$

Other constraints, for example, the maximum normal at the contact points required to prevent damage to the object and the maximum force and moment capabilities of the joints also impose inequality constraints on the solution. These, however, will not be discussed in detail here.

4.4 Computational Algorithms

Summarizing the above analysis, we have shown that the inverse dynamics solution for a multiple arm system is not unique due to the actuation redundancy. The existence of this redundancy complicates the solution procedure. One approach would be to set the torques for the redundant actuators to zero, once they appear in the system, and find a unique solution for the rest of the dynamics variables. However, a better solution might be to optimally use this redundancy to improve the dynamics behavior of the system. To accomplish this, optimization techniques and/or other methods can be used to obtain the inverse dynamics solution.

As alluded to in the previous section, we include explicitly the grasping wrenches in the inverse dynamics equations from which τ_Σ, $\ddot{q}_{r\Sigma}$, $\ddot{q}_{e\Sigma}$ and w_Σ are obtained.

These equations can be written compactly as

$$\begin{bmatrix} 1 & 0 & 0 & -\mathbf{J}_{1\Sigma}^T \\ 0 & 1 & 0 & -\mathbf{J}_{2\Sigma}^T \\ 0 & 0 & 1 & -\mathbf{J}_{3\Sigma}^T \\ 0 & 0 & 0 & \mathbf{A}_1 \end{bmatrix} \begin{bmatrix} \boldsymbol{\tau}_\Sigma \\ \ddot{\boldsymbol{q}}_{r\Sigma} \\ \ddot{\boldsymbol{q}}_{e\Sigma} \\ \boldsymbol{w}_\Sigma \end{bmatrix} = \begin{bmatrix} \boldsymbol{\tau}'_\Sigma \\ \ddot{\boldsymbol{q}}'_{r\Sigma} \\ \ddot{\boldsymbol{q}}'_{e\Sigma} \\ \mathbf{b}_1 \end{bmatrix} \tag{4.45}$$

They are a set of linear algebraic equations in the unknown variables $\boldsymbol{\tau}_\Sigma$, $\ddot{\boldsymbol{q}}_{r\Sigma}$, $\ddot{\boldsymbol{q}}_{e\Sigma}$ and $\boldsymbol{w}_\Sigma$. In particular, the prescribed object trajectory and thereby that of the manipulator end-effectors is included in the right-hand sides of these equations. Coefficient matrices on the left-hand side of the equations are configuration dependent.

The strategy for resolving the actuation redundancy can be applied to the set of design variables $\mathbf{x}$ (here, $\mathbf{x} = [\boldsymbol{\tau}_\Sigma \ \ddot{\boldsymbol{q}}_{r\Sigma} \ \ddot{\boldsymbol{q}}_{e\Sigma} \ \boldsymbol{w}_\Sigma]^T$) while satisfying the constraint equations (4.45) and perhaps (4.43) if required. Selection of the design variables among these dynamics variables is indeed arbitrary. For example, we can also define the design variable to be $\mathbf{x} = [\boldsymbol{\tau}_\Sigma \ \boldsymbol{w}_\Sigma]^T$. In this case, the primary constraints imposed on $\mathbf{x}$ are the first and the last equations in (4.45):

$$\begin{bmatrix} 1 & -\mathbf{J}_{1\Sigma}^T \\ 0 & \mathbf{A}_1 \end{bmatrix} \begin{bmatrix} \boldsymbol{\tau}_\Sigma \\ \boldsymbol{w}_\Sigma \end{bmatrix} = \begin{bmatrix} \boldsymbol{\tau}'_\Sigma \\ \mathbf{b}_1 \end{bmatrix} \tag{4.46}$$

Once $\boldsymbol{\tau}_\Sigma$ and $\boldsymbol{w}_\Sigma$ have been determined, the variables $\ddot{\boldsymbol{q}}_{r\Sigma}$ and $\ddot{\boldsymbol{q}}_{e\Sigma}$ can be obtained uniquely from the second and third equations in (4.45).

The difference in the solution procedures resulting when we choose different sets of design variables can be readily seen now. Although they lead to identical solutions if the same redundancy resolution scheme is applied, the computational cost may be significantly different. For example, if an optimization procedure is used to minimize a certain cost function, the computational expense depends largely on the number of design variables and the number of constraint equations. In fact, an even more compact formulation is obtained by defining the design variables to be only the grasping

wrenches. One reason for this choice is that the grasping wrenches are particularly important in the performance of the inverse dynamics system. Also, none of the other three variables can be determined without knowing the value of $\boldsymbol{w}_\Sigma$. And finally, any cost function formulated in terms of the other variables, namely, $\boldsymbol{\tau}_\Sigma$, $\ddot{\boldsymbol{q}}_{r\Sigma}$ and $\ddot{\boldsymbol{q}}_{e\Sigma}$ can be easily written in terms of $\boldsymbol{w}_\Sigma$ because of the linear relationship between these variables and the grasping wrenches. Therefore, the number of the design variables in our formulation is $6P$ and the primary constraints on the redundancy resolution are reduced to:

$$\mathbf{A}_1\mathbf{x} = \mathbf{b}_1 \tag{4.47}$$

Once the grasping wrenches have been determined, actuator torques and rigid and elastic accelerations can be obtained from the algebraic equations (4.12)-(4.14).

In conclusion, a flowchart of the algorithm for solving the inverse dynamics problem for a multiple-arm system is proposed and shown in Figure 4.2. It can be seen from the flowchart that the solution to the inverse dynamics problem for multiple cooperating flexible arm systems is composed of two parts: the redundancy resolution and the inverse dynamics solution for serial flexible arms.

4.5 Validation of the Numerical Calculation

Again, the percentage error in the energy balance and the root mean square value of the energy drift are used to validate the inverse dynamics solution. The work done by the actuator torques of a multiple-arm system is thus given by

$$\pi = \boldsymbol{\tau}_\Sigma\, \dot{\boldsymbol{q}}_{r\Sigma} \qquad W = \int_0^t \pi dt \tag{4.48}$$

The dissipative work function becomes

$$W_d = \int_0^t \frac{1}{2}\, \dot{\boldsymbol{q}}_{e\Sigma}^T \mathbf{D}_{ee\Sigma}\, \dot{\boldsymbol{q}}_{e\Sigma} dt \tag{4.49}$$

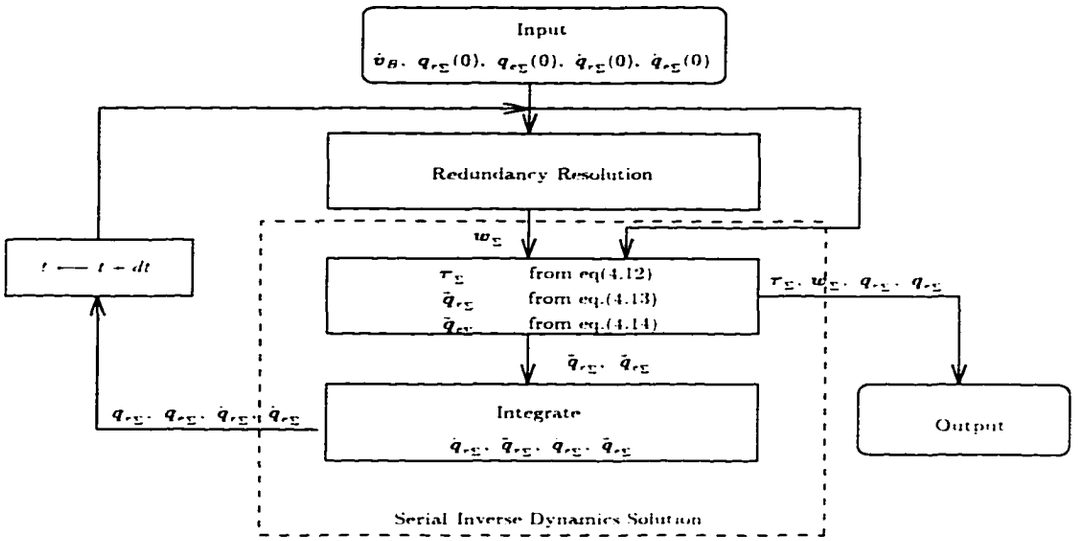

Figure 4.2: Inverse Dynamics Algorithm for Multiple-Arm System

The kinetic energy that the system possesses at every time instant should include that of the rigid object. It is therefore calculated by:

$$T = \frac{1}{2}(\dot{q}_{\Sigma}^{T}\mathbf{M}\,\dot{q}_{\Sigma} + \mathrm{v}_{B}^{T} m_{B} \mathrm{v}_{B} + \omega_{B}^{T}\mathbf{I}_{B}\omega_{B}) \tag{4.50}$$

The potential energy of the system due to the elastic deformation of the links is:

$$V = \frac{1}{2}\,\dot{q}_{e\Sigma}^{T}\mathbf{K}_{ee\Sigma}\,\dot{q}_{e\Sigma} \tag{4.51}$$

Assuming the system starts from rest, the error in the energy balance at every time instant is of the same form as introduced in eq. (3.69):

$$E(t) = (T(t) + V(t)) - (W - W_d)$$

The percentage error and the root mean square error, respectively, are calculated according to eqs. (3.72) and (3.73).

4.6 Ex[illegible]tors

We now des[illegible] which simulations c[illegible] planar and a 3D fl[illegible]pulator system. we a[illegible]re used to illustrate [illegible]hat the present anal[illegible]ems.

4.6.1 Pl[illegible]

The physical [illegible] *or test bed* construct[illegible]ictoria [61]. As show[illegible]r glass top table wh[illegible] links with three r[illegible] other by harmonic-[illegible]ithms for flexible s[illegible]tbed. For the prese[illegible]e use direct-drive [illegible] placed at the joints. [illegible] third joint of each

Special de[illegible] ange-able. Therefo[illegible]xible and one rigid [illegible] iffer-ent mechanic[illegible] and on the difficu[illegible]up is

4.6 Examples of Cooperating Manipulators

We now describe two prototypes of flexible-link cooperating manipulators for which simulations of the inverse dynamics algorithm are carried out. These include a planar and a 3D flexible two-arm and object systems. For each cooperating manipulator system, we also present trajectories for the specified object maneuvers that are used to illustrate the inverse dynamics algorithm. It should be noted, however, that the present analysis and the proposed algorithm are not limited to dual-arm systems.

4.6.1 Planar Dual-Arm

The physical model of this prototype is the *flexible-link cooperating manipulator test bed* constructed in the Subspace Robotics Laboratory at the University of Victoria [61]. As shown in Figure 4.3, both arms are supported by air bearings on a planar glass top table which eliminates the effect of gravity. Each arm is composed of two links with three revolute joints. One arm is driven by direct-drive motors while the other by harmonic-drive motors. Validation of the dynamics models and control algorithms for flexible serial and cooperating manipulators is the main purpose of this testbed. For the present analysis, since actuator dynamics is not our major concern, we use direct-drive motors to actuate both arms and model the motors as rigid bodies placed at the joints. To simulate a general planar motion, we attach a rigid link to the third joint of each arm to represent the end-effector.

Special design of the arms allows the first two links of each arm to be interchangeable. Therefore, each arm can be assembled to have both links flexible, or one flexible and one rigid link, or both rigid links. This allows us to investigate the effect of different mechanical compositions of the arms on the dynamics behavior of the system and on the difficulty of controlling it. The notation used to describe a particular setup is

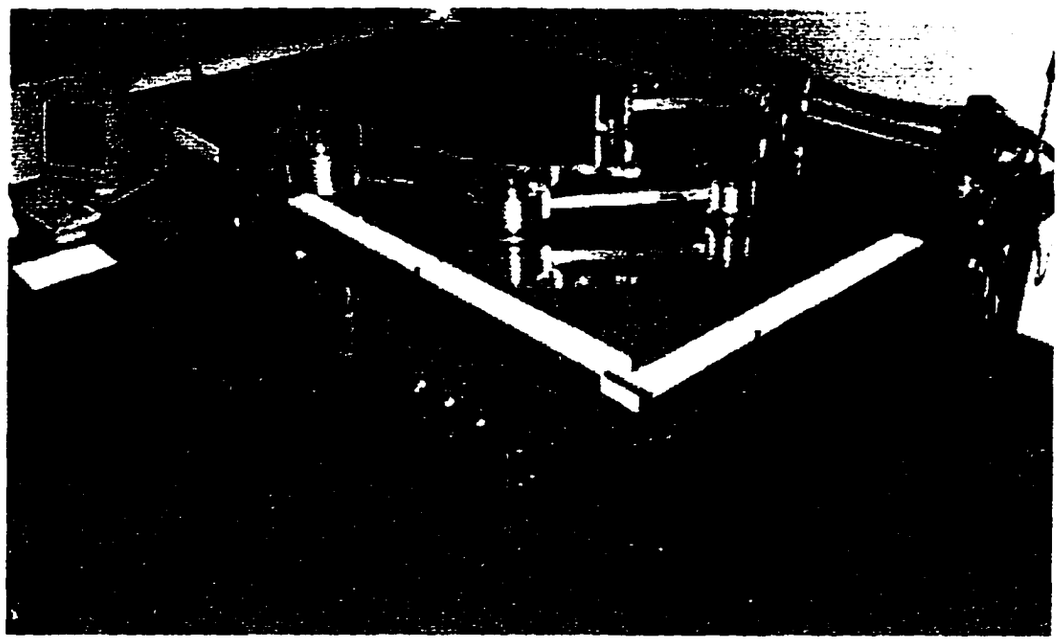

Figure 4.3: Flexible-Link Cooperating Manipulator Test Bed

by counting the links from the first of the left arm, through the object, to the base link of the right arm. We use 'F' to denote a flexible link and 'R' for a rigid link. for example, 'FFR O-RFF' defines a setup with first two links of both arms as flexible.

Figure 4.4 illustrates the architecture of the planar dual arm and object system. The inertia properties of each component of the arm has been shown in Table 4.1. The object considered is a rigid aluminum bar with the following properties:

Length, l:	1.0 m
Mass, m:	13.5 Kg
Moment of inertia, I:	1.128 Kg-m^2

The manipulators are required to rotate the aluminum bar about its center of mass through 90° clockwise in 2 seconds. Therefore, the position of the mass center of the object remains constant. A sinusoidal acceleration profile is used to produce a

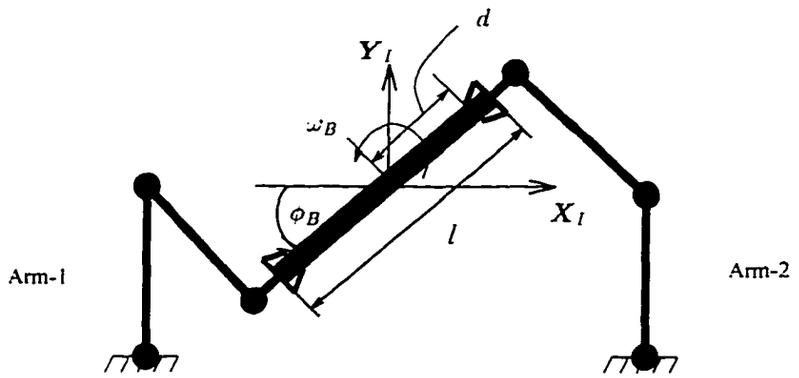

Figure 4.4: Planar Dual-arm/Object System

smooth rotation of the object starting and ending at rest:

$$\dot{\omega}_B = -(\frac{\pi}{2})^2 \sin(\pi t) \qquad 0 \leq t \leq 2 \text{ sec} \tag{4.52}$$

Integrating the above twice yields the prescribed angular velocity and displacement for the object:

$$\omega_B = -\frac{\pi}{4}(1 - \cos(\pi t)) \tag{4.53}$$

$$\phi_B = \frac{\pi}{4} - \frac{\pi}{4}(t - \frac{1}{\pi}\sin(\pi t)) \tag{4.54}$$

The origin O_I of the inertial coordinate frame $X_I - Y_I$ is located at the mass center of the object. The corresponding desired trajectory of the manipulator end-effectors can be determined from the prescribed object trajectory by

$$\begin{cases} \dot{v}_{1x} = d(\sin\phi_B\dot{\omega}_B + \cos\phi_B\omega_B^2) \\ \dot{v}_{1y} = d(-\cos\phi_B\dot{\omega}_B + \sin\phi_B\omega_B^2) \\ \dot{\omega}_{1z} = \dot{\omega}_B \end{cases} \qquad \begin{cases} \dot{v}_{2x} = d(-\sin\phi_B\dot{\omega}_B - \cos\phi_B\omega_B^2) \\ \dot{v}_{2y} = d(\cos\phi_B\dot{\omega}_B - \sin\phi_B\omega_B^2) \\ \dot{\omega}_{2z} = \dot{\omega}_B \end{cases} \tag{4.55}$$

Each flexible link is modeled with two planar beam elements with two degrees of freedom per node, representing the transverse displacement and the slope of the beam. Therefore, each flexible link has four elastic degrees of freedom since the links are cantilevered at the joints.

4.6.2 3D Dual-Arm

Figure 4.5 shows a drawing of a serial 3D flexible arm. The forearm and upper arm (the two shaded links in the figure) are considered to be flexible and have the following properties:

1. Geometric Properties:
   Length: 1.0 m
   Cross Section: 18mm × 18mm
2. Stiffness Properties:
   EI: 603.17 N-m^2
   EA: 2.23×10^7 N
3. Modal Damping Ratio:
   ζ: 0.005%
4. Inertia Properties:
   Mass: 0.878 Kg
   c_x: 0.439 Kg-m
   c_y: 0
   c_z: 0
   I_{xx}: 4.74×10^{-5} Kg-m^2
   I_{yy}: 0.293 Kg-m^2
   I_{zz}: 0.293 Kg-m^2

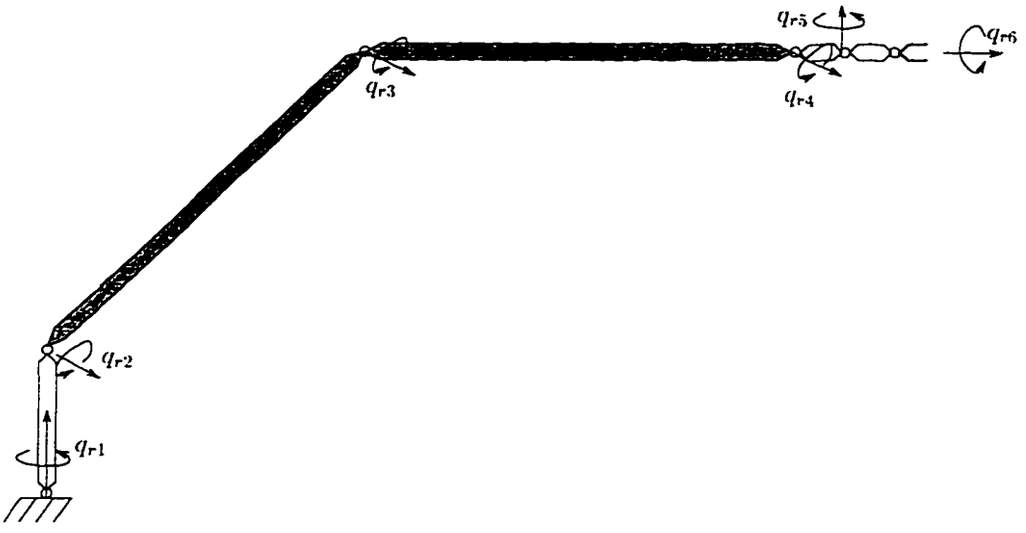

Figure 4.5: Architecture of the 6-DOF Arm

We consider another 3D arm with the same architecture except that the flexible links are replaced by rigid ones. This rigid arm will cooperate with the flexible arm. The object is the same one as introduced earlier for the planar arm (Figure 4.6). Each flexible link is modeled using two 3D beam elements. Bending deflections in the $X-Y$ plane and $X-Z$ plane of the moving frames fixed to the links (with X axis along the length and Z axis of rotation) are referred to as the in-plane and out-of-plane bendings respectively. Therefore, each of the flexible links has eight elastic degrees of freedom.

The maneuver specified for the two arms is to carry the object with its mass center moving along a linear path without changing its orientation in the 3D workspace. The linear part is defined by the following vector equation in the fixed frame:

$$\boldsymbol{l} = \boldsymbol{x} + \boldsymbol{y} + \boldsymbol{z} \tag{4.56}$$

with $\boldsymbol{x}, \boldsymbol{y}, \boldsymbol{z}$ being the displacements in each of the unit directions. Let x, y, z be the magnitudes of displacements of the object center of mass along the three axes

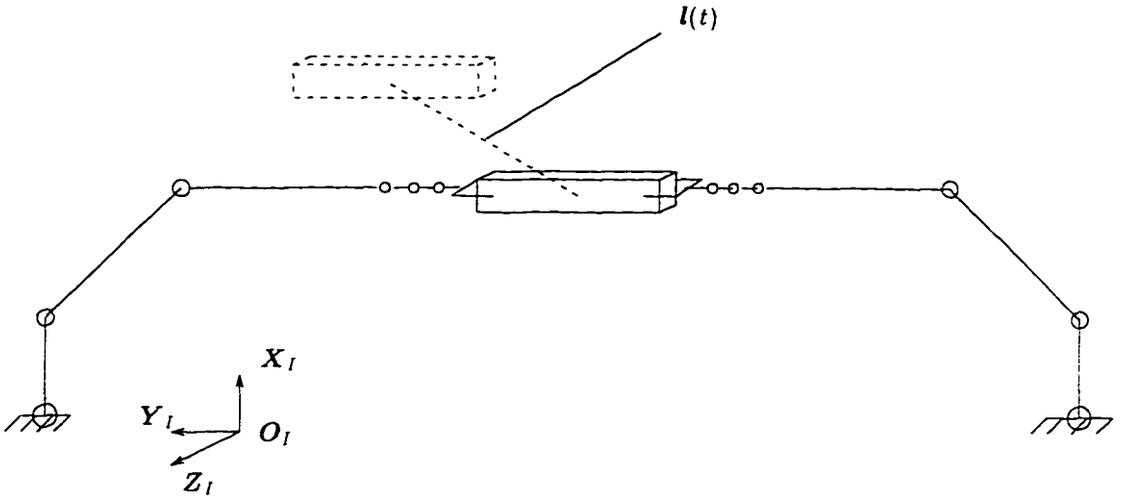

Figure 4.6: 3D Dual-Arm/Object System

respectively and expressed by:

$$x = x(0) + \alpha\phi(t) \qquad y = y(0) + \beta\phi(t) \qquad z = z(0) + \gamma\phi(t) \tag{4.57}$$

where α, β and γ are some constants and $\phi(t)$ is a function of time with continuous first and second derivatives. We define the trajectory to be composed of three segments: the accelerating part, the constant speed part and the decelerating part. The time periods for accelerating and decelerating segments are identical and are denoted by t_a, while t_f represents the terminal time. We use h to denote the maximum value of $\ddot{\phi}(t)$, and accordingly define the second derivative of $\phi(t)$ as:

$$\ddot{\phi}(t) = \begin{cases} h \sin\frac{\pi t}{t_a} & 0 \le t \le t_a \\ 0 & t_a < t \le t_f - t_a \\ h \sin\frac{\pi(t - t_f + 2t_a)}{t_a} & t_f - t_a < t \le t_f \end{cases} \tag{4.58}$$

Figure 4.7 shows ϕ, $\dot{\phi}$ and $\ddot{\phi}$ for $t_f = 2$ and $t_a = 0.4$.

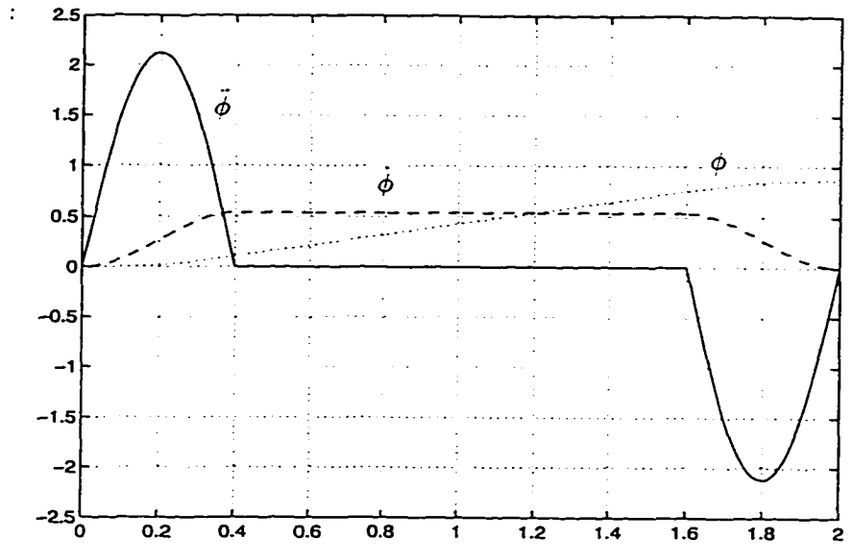

Figure 4.7: Function $\phi(t)$ Used for Defining a Line in 3D Space

4.7 Example 4.2

As an example of calculating the inverse dynamics solution by the proposed algorithm, we use the planar dual-arm (FFR-O-RRR) to demonstrate the performance of the numerical simulation. Figure 4.4 shows the initial configuration of the system. In configuration space, it is defined by the following joint angles:

$$q_{r\Sigma}^T(0) = [\, q_{r1}^T \;\; q_{r2}^T] = [90^o \;\; -135^o \;\; 90^o \;\; 90^o \;\; 45^o \;\; 90^o]$$

The system starts from rest, and no initial deformations are present, therefore,

$$\dot{q}_{r\Sigma} = 0 \qquad q_{e\Sigma} = 0 \qquad \dot{q}_{e\Sigma} = 0$$

The dynamics equations (4.15) of the grasped object are specified by:

$$\mathbf{A}_1 = \begin{bmatrix} 1 & 0 & 0 & 1 & 0 & 0 \\ 0 & 1 & 0 & 0 & 1 & 0 \\ \frac{l}{2}\sin o_B & -\frac{l}{2}\cos o_B & 1 & -\frac{l}{2}\sin o_B & \frac{l}{2}\cos o_B & 1 \end{bmatrix} \quad \mathbf{b}_1 = \begin{bmatrix} 0 \\ 0 \\ I\dot{\omega}_B \end{bmatrix} \tag{4.59}$$

where l denotes the length and I is the moment of inertia of the aluminum bar. The design variables are defined as:

$$\mathbf{x} = \boldsymbol{w}_\Sigma = [\boldsymbol{w}_1^T \ \boldsymbol{w}_2^T]^T = [f_{1x} \ f_{1y} \ n_{1z} \ f_{2x} \ f_{2y} \ n_{2z}]^T$$

In the present case, the number of degrees of freedom of the system is *three* while the system has *six* actuators in total. Once the two arms are grasping the object, three of the actuators become redundant. Equivalently, this redundancy implies arbitrariness in determining the grasping wrenches $\boldsymbol{w}_\Sigma$. According to the proposed algorithm, we need to resolve this redundancy first and then find the corresponding unique solution to the inverse dynamics problem for each of the two manipulators.

Let us suppose that we want all the actuators of arm-1 be turned off, that is:

$$\tau_{11} = \tau_{12} = \tau_{13} = 0 \tag{4.60}$$

From the above, the first three equations in eq.(4.12) then define the additional constraints imposed on the design variables $\mathbf{x}$ as:

$$\begin{bmatrix} \{\mathbf{J}_{11}^T\}_1 & \mathbf{0} \\ \{\mathbf{J}_{11}^T\}_2 & \mathbf{0} \\ \{\mathbf{J}_{11}^T\}_3 & \mathbf{0} \end{bmatrix} \begin{bmatrix} \boldsymbol{w}_1 \\ \boldsymbol{w}_2 \end{bmatrix} = \begin{bmatrix} \tau_{11} - \tau'_{11} \\ \tau_{12} - \tau'_{12} \\ \tau_{13} - \tau'_{13} \end{bmatrix} = \begin{bmatrix} -\tau'_{11} \\ -\tau'_{12} \\ -\tau'_{13} \end{bmatrix} \tag{4.61}$$

where $\{\mathbf{J}_{11}^T\}_i$ represents the ith row of matrix $\mathbf{J}_1^T$ of arm 1 and τ' can be calculated from the known end-effector trajectory at every time instant. If the coefficient matrix of eq.(4.61) is not rank deficient, this equation imposes three constraints on $\boldsymbol{w}_\Sigma$. Together with the dynamics of the object characterized by (4.59), these equations completely determine the value of $\mathbf{x}$. Once $\mathbf{x}$ is obtained, the solutions for τ_Σ, $\ddot{\boldsymbol{q}}_{r\Sigma}$ and $\ddot{\boldsymbol{q}}_{e\Sigma}$ are uniquely determined from eqs.(4.12)-(4.14).

The numerical results for this example are shown in Figures 4.8-4.12. In Figure 4.8, the left column displays the tip wrenches of the left arm (arm-1) while the right column

shows those of the right arm. The force components of the wrenches are equal and opposite since no translational movement of the object mass center is required. It is also observed that the right arm exerts a larger moment in rotating the object because we choose to set the actuator torques of the left arm to zero. Figures 4.9 and 4.10 illustrate the actuator torques generated by the right arm and the joint angle profiles (rigid coordinates) for both arms. From Figures 4.11 and 4.12 where elastic coordinate profiles are shown, we observe that the first flexible link shows larger deformation than the second flexible link. The energy drift for this example is also shown in Figure 4.13, the maximum energy is $(T + V)_{peak} = 7.46$ J and the root mean square value of the error is $e_{E.RMS} = 3.04 \times 10^{-4}\%$. In this example, the relative tolerance used for numerical integration was set to $\epsilon = 10^{-6}$. We consider that the results of numerical simulation are realistic and the inverse dynamics solution is stable.

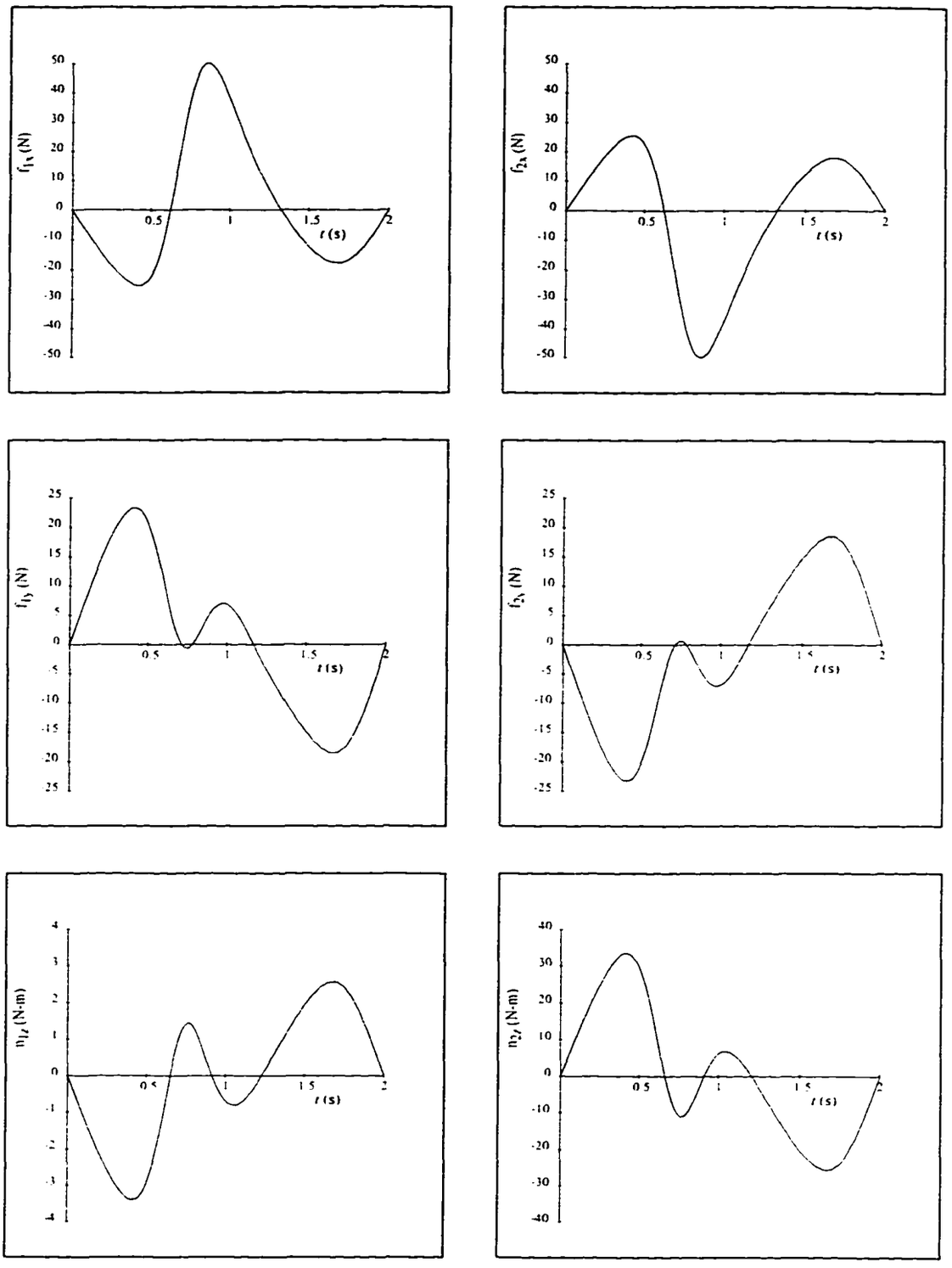

Figure 4.8: Grasping Wrenches

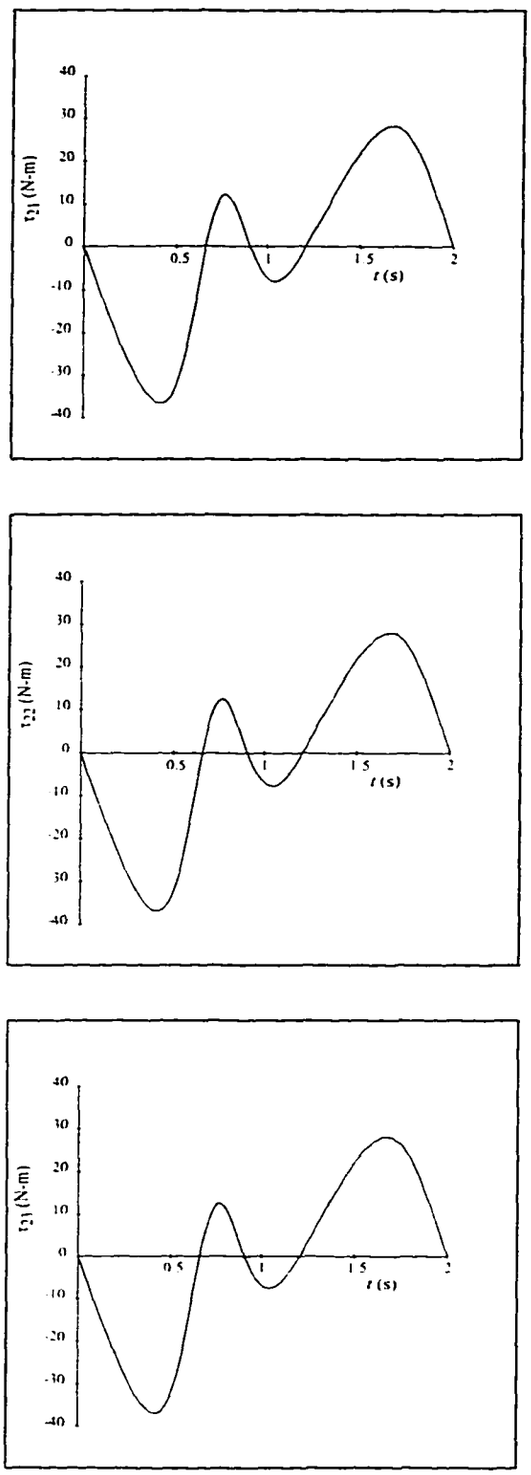

Figure 4.9: Actuator Torques of the Right Arm

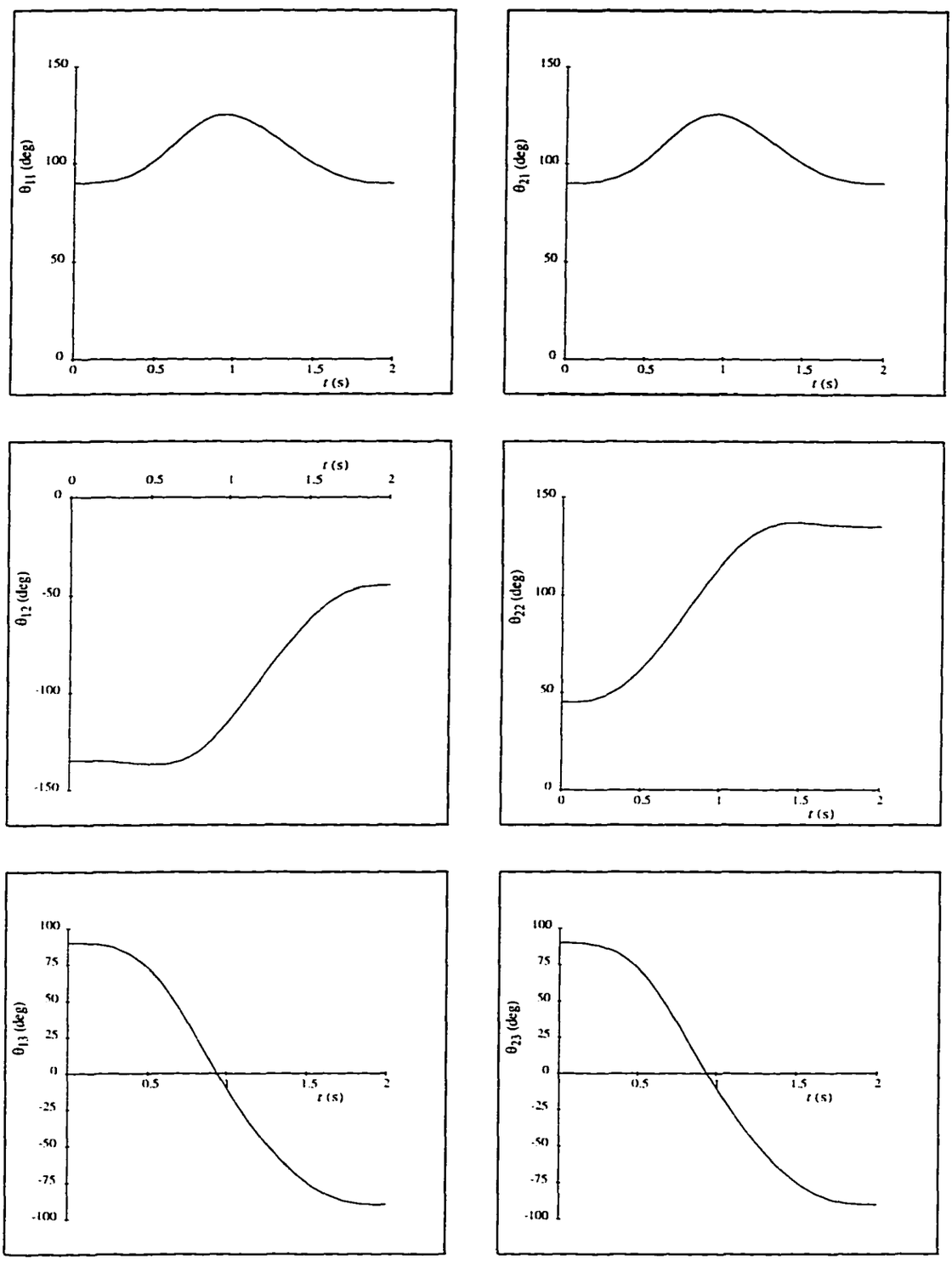

Figure 4.10: Rigid Coordinates

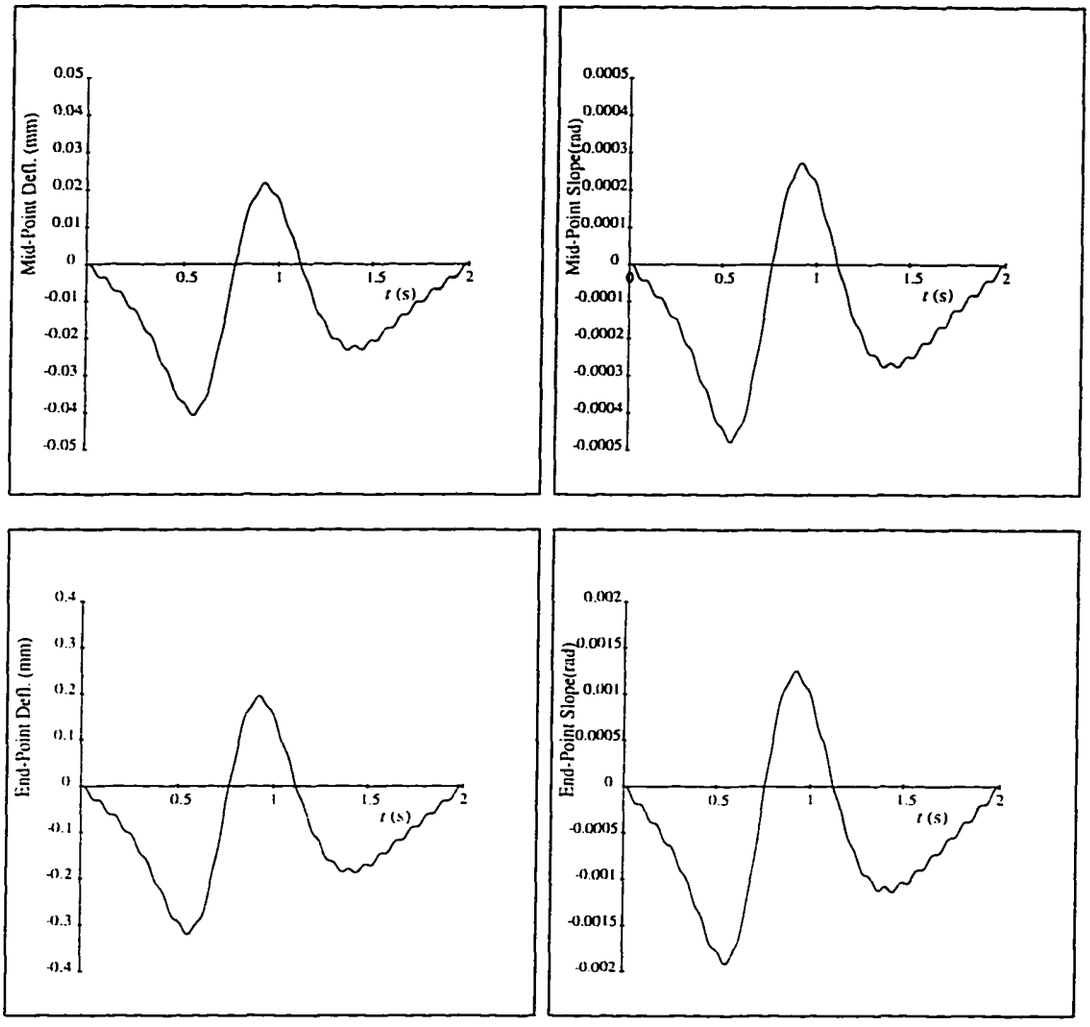

Figure 4.11: Elastic Coordinates of the First Flexible Link

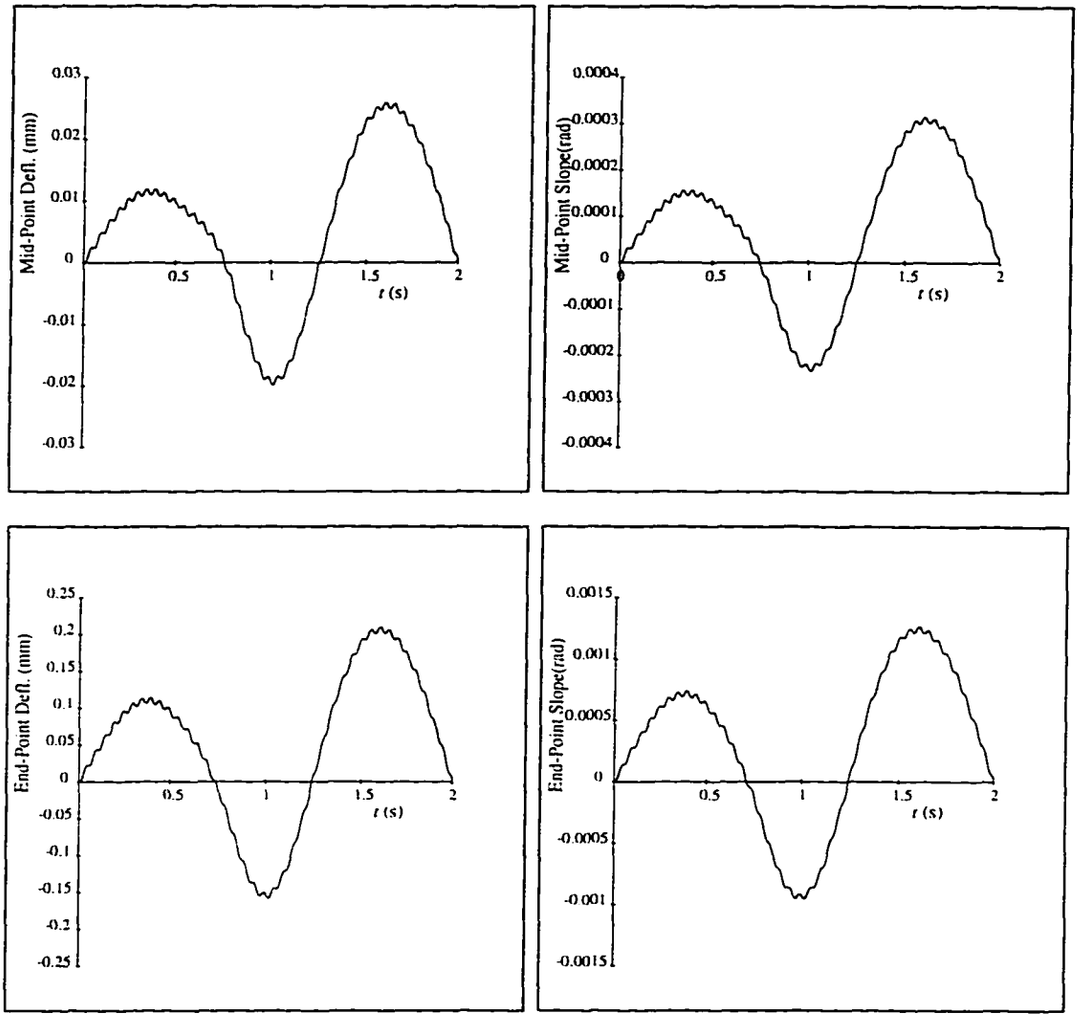

Figure 4.12: Elastic Coordinates of the Second Flexible Link

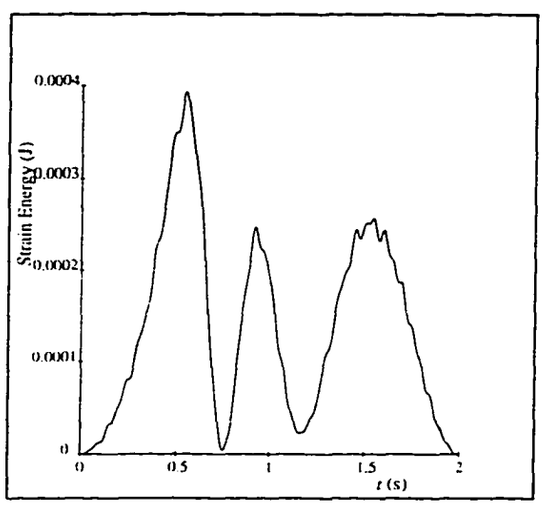

Figure 4.13: Error in the Energy Balance

Chapter 5

Optimization Approach

5.1 Introduction

The concept of optimization has been widely used as a principle to analyze many complex decision or allocation problems. It offers a means for obtaining the 'best' solution to certain mathematically defined problems. Using this concept, one approaches a complex decision making problem by focusing attention on a single objective designed to quantify the outcome or the quality of the decision. This objective is minimized (or maximized, depending on the formulation) subject to certain constraints that may limit the selection of the variables involved in the problem.

Formulation of the inverse dynamics problem for a flexible-link cooperating manipulator system shows that this problem is underdetermined, meaning that an infinite number of solutions exist which generate the same object motion. We demonstrated in the proposed algorithm (Figure 4.2) that resolving the actuation redundancy or determining force distribution is an essential step which requires a decision making procedure. Different sets of solutions for the actuator torques, although generating

the same object motion, can have drastically different effects on the system dynamics. Investigating the performance of the various inverse dynamics solutions is thus an important process which leads to a "better" or even the "best" solution among all the possible ones. Optimization techniques provide a powerful mathematical tool for achieving this goal. This chapter is devoted to the resolution of actuation redundancy via an optimization approach.

As a designer of the optimization problem, our goal is to formulate a simple but physically meaningful and reasonably accurate mathematical model. This model must include most of the significant factors affecting the complex decision on the force distribution within the system. The design procedure includes the following steps:

1. Choose the set of variables which constitute a *design space*. These variables are termed the *design variables*;

2. Determine all the primary and/or secondary constraints which restrict the design variables;

3. Formulate a mathematical statement of the problem in terms of the design variables. This statement must include the objective necessary for evaluating the quality of the decision;

4. Solve the optimization problem with the available resources to obtain a satisfactory solution.

It should be noted that these steps should not be treated independently. For example, when choosing the design variables, one should take into account the complexity of the constraints and the formulation of objectives. Most importantly, one needs to ascertain that it is possible to obtain a solution for a particular problem formulation as well as predict how fast it can be calculated. Good decisions at the design stage

rely on both the knowledge and the experience of the designer. In many instances, the solution of a complex problem cannot be directly treated in its entirety, but instead must be decomposed into subproblems — each subproblem being represented by a particular objective and having constraints that are imposed to restrict its scope.

5.2 Formulation of the Problem

Beginning with the first step of the design process, we propose to choose the set of grasping wrenches $\boldsymbol{w}_\Sigma$ as the design variables. This is a natural choice since many of the quantities we want to minimize can be written as a function of grasping wrenches. As well, these wrenches are primarily constrained by linear equality constraints which we expect to be solved more easily. Considering also the possible secondary constraints, for instance, the limited capacities of the actuators as given in eqs. (4.41) and (4.42), it is not difficult to see that the optimization problem we are facing can be described as a linearly constrained optimization problem, that is, the constraint equations are composed of a set of linear equality and/or inequality equations. In particular, the problem can be mathematically stated as

$$\min_{\mathbf{x}} \quad f(\mathbf{x}) \tag{5.1a}$$

$$\text{Subject to} \quad \mathbf{A}_1\mathbf{x} = \mathbf{b}_1 \tag{5.1b}$$

$$\text{and} \quad \mathbf{A}_2\mathbf{x} \geq \mathbf{b}_2 \tag{5.1c}$$

where $f(\mathbf{x})$ is the *objective function*; vector $\mathbf{x}$ contains the design variables; (5.1*b*) represents the *equality constraints* and (5.1*c*) the *inequality constraints*. Formulation of a practical optimization problem always involves a tradeoff between building a mathematical model sufficiently complex to capture the important features of the physical system and building a model that is *tractable*. We can identify a model, whether tractable or not, by the following characteristics:

Type of Problem

In the most general case, both objective function and the constraint equations may be nonlinear functions of $\mathbf{x}$. Linear functions, by virtue of their simplicity, are often selected as an easy way to start. Indeed, linearity of the constraint equations, as defined for the present study, is most appealing. Linearly constrained problems can be handled through a combination of an elimination method and an active set method [62]. The simplest cases of linearly constrained problems are when the objective function is either linear or quadratic. These are referred to, respectively, as *linear programming or quadratic programming* problems. Methods to handle these simple cases are well-developed and will be mentioned in more detail in Section 5.3. From this standpoint, the reason for excluding the state variables from the design variables is obvious in our case since they are subject to the constraints described by nonlinear differential equations.

Problem Size

One obvious measure of the complexity of an optimization problem is its size, measured in terms of the number of unknown variables and the number of constraints. From this viewpoint, the merits of choosing the grasping wrenches $\boldsymbol{w}_\Sigma$ as the design variables for the present study can be readily seen. In particular, the number of unknown variables is $6P$ (P is the number of manipulators) while the number of equality constraints is 6. If, say, the elastic coordinates $\boldsymbol{q}_{e\Sigma}$ are included in the design variables because reducing the structural vibration is one of our major interests, both the number of unknown variables and the number of constraint equations will be increased by ΣS_i $(i = 1, \ldots, P)$. Besides, these variables are subject to nonlinear differential equations. To avoid these complications, we retain $\boldsymbol{w}_\Sigma$ as the design variables but attempt to reduce the system

vibration by actively choosing the value of grasping wrenches.

Convergence Properties

Most of the algorithms designed to solve large optimization problems are *iterative* in nature. Typically, when seeking the solution to an the optimization problem, an initial vector $\mathbf{x}_0$ is selected and the algorithm generates a sequence of ever-improving points in the design space, $\mathbf{x}_1 \cdots, \mathbf{x}_k \cdots$ that approaches a solution point $\mathbf{x}^*$. As in any interactive scheme, the convergence properties are of primary concern. In particular, one needs to consider the property of *global convergence* and the *rate* of local convergence. A globally convergent algorithm will generate a sequence that converges to a solution point even when initiated far from the solution point. Without an acceptable rate of convergence, however, the algorithm may require an excessive amount of time to reduce the error to a designated tolerance. These seemingly algorithm-related features can sometimes be affected by the inherent structure of the model. For example, if the objective function possesses certain properties, such as *strict convexity*, any algorithm which is locally convergent can be used to find the global solution since a strict convex objective function guarantees a unique optimal solution. In addition, for a given method, the sequence converges to the solution more rapidly for a quadratic than for a linear objective function.

For the present analysis, it is particularly important that the model we build be simple and not require expensive computation. The reasons are two-fold: first, redundancy resolution, for which an optimization problem is to be formulated, constitutes only one step in the inverse dynamics algorithm. For a multiple flexible-link manipulator system, this algorithm is fairly complex already due to the required numerical integration of the state variables. Further complication of the solution procedure should be avoided. Secondly, if the solution is to be used for control purposes and

control efforts are intended to suppress the system vibration, then a higher bandwidth of the controller will be required, thus necessitating a small step size for calculating the torques. Before proceeding to complete the formulation of the optimization problem, we would like to state some fundamental theorems used to solve optimization problems since they influence our decision on how to formulate the optimization problem.

5.3 Linear and Quadratic Programming

Fundamental definitions and theorems relevant to the formulation and solution of the optimization problem are given in Appendix B. In this section, we focus on introducing the linear and quadratic programming techniques.

5.3.1 Linear Programming

The simplest type of constrained optimization problem is obtained when the objective function $f(\mathbf{x})$ and the constraint equations are linear functions of $\mathbf{x}$. The resulting problem is known as a *linear programming* (LP) problem. The term 'programming' here is synonymous with 'optimization'. A linear programming problem can be expressed in the standard form as:

$$\begin{aligned} \min_{\mathbf{x}} \quad & f(\mathbf{x}) = \mathbf{c}^T\mathbf{x} \\ \text{subject to} \quad & \mathbf{A}_1\mathbf{x} = \mathbf{b}_1 \\ \text{and} \quad & \mathbf{x} \geq \mathbf{0} \end{aligned} \tag{5.2}$$

Normally, we consider the case where the matrix $\mathbf{A}_1 \in \mathbf{R}^{m\times n}$ is not rank deficient and $m < n$. Then, the system $\mathbf{A}_1\mathbf{x} = \mathbf{b}_1$ is underdetermined and $n - m$ variables in $\mathbf{x}$ remain free to be determined. Very naturally, we can try to eliminate m variables

by using the equality constraints and determine the remaining $n - m$ variables which give a minimum value of $f(\mathbf{x})$. Since the objective function is linear, it does not have a curvature which can give rise to a minimizing point. It is thus important to realize that the inequality constraints $\mathbf{x} \geq \mathbf{0}$ are *necessary* in linear programming in order to define boundaries of the feasible region.

A solution of the standard LP problem always exists at a particular extreme point or vertex of the feasible region, with at least $n - m$ variables having zero value, and the remaining variables uniquely determined by $\mathbf{A}_1\mathbf{x} = \mathbf{b}_1$ and taking non-negative values. The main difficulty in linear programming is then to find which of the $n - m$ variables should be set to zero at the solution and this is where the various methods for solving the LP problem differ from each other.

Because of the semi-positive definiteness of the Hessian matrix (Appendix B), linear programming problems have non-unique solutions. It has also been shown that for continuous time-varying constraints $\mathbf{A}_1\mathbf{x} = \mathbf{b}_1$, linear programming may generate discontinuous solutions [63]. This is particularly relevant to the present study since our equality constraints are dynamics equations of the object with $\mathbf{A}_1$ and $\mathbf{b}_1$ changing continuously with its desired trajectory.

5.3.2 Quadratic Programming

Another important type of objective function is that of a quadratic form. It can be written as:

$$f(\mathbf{x}) = \mathbf{c}^T\mathbf{x} + \frac{1}{2}\mathbf{x}^T\mathbf{W}\mathbf{x} \tag{5.3}$$

where $\mathbf{W}$ can always be defined as a symmetric matrix. Minimizing such an objective function subject to linear constraints is referred to as *quadratic programming* (QP).

Quadratic programming differs from linear programming in that it is possible

to formulate meaningful problems without the inequality constraints. As shown in the subsequent sections, this will be the basic structure we adopt to solve the force optimization problem. If the problem contains only equality constraints $\mathbf{A}_1\mathbf{x} = \mathbf{b}_1$ and $\mathbf{A}_1$ is full rank, the solution can be obtained by directly using the Lagrange first-order conditions (Appendix B) to yield:

$$\mathbf{W}\mathbf{x} + \mathbf{A}_1^T\boldsymbol{\lambda} + \mathbf{c} = \mathbf{0} \tag{5.4}$$

$$\mathbf{A}_1\mathbf{x} - \mathbf{b}_1 = \mathbf{0} \tag{5.5}$$

If in the above, the matrix $\mathbf{W}$ is positive definite, it can be proven that the matrix

$$\begin{bmatrix} \mathbf{W} & \mathbf{A}_1^T \\ \mathbf{A}_1 & \mathbf{0} \end{bmatrix} \tag{5.6}$$

is nonsingular [62] and therefore, a unique solution for $\mathbf{x}^*$ and $\boldsymbol{\lambda}^*$ exists which satisfies the Lagrange first-order necessary conditions (Appendix B). Indeed, since $\mathbf{W}$ is the Hessian of the objective function, a positive definite $\mathbf{W}$ implies a strict convex objective function (see Appendix B) which ensures that this unique solution is exactly the unique global minimum solution to the problem.

Proceeding to solve the Lagrange conditions, from eq. (5.4) we have

$$\mathbf{x} = -\mathbf{W}^{-1}\mathbf{A}_1^T\boldsymbol{\lambda} - \mathbf{W}^{-1}\mathbf{c} \tag{5.7}$$

Substituting for $\mathbf{x}$ in eq. (5.7) into eq. (5.5) and solving for $\boldsymbol{\lambda}$, we obtain

$$\boldsymbol{\lambda}^* = -(\mathbf{A}_1\mathbf{W}^{-1}\mathbf{A}_1^T)^{-1}(\mathbf{A}_1\mathbf{W}^{-1}\mathbf{c} + \mathbf{b}_1) \tag{5.8}$$

and therefore,

$$\mathbf{x}^* = \mathbf{W}^{-1}\mathbf{A}_1^T(\mathbf{A}_1\mathbf{W}^{-1}\mathbf{A}_1^T)^{-1}(\mathbf{A}_1\mathbf{W}^{-1}\mathbf{c} + \mathbf{b}_1) - \mathbf{W}^{-1}\mathbf{c} \tag{5.9}$$

The above representation is a useful analytical form and will be used in the developments in the next chapter. However, from the numerical efficiency point of view, the solution may be better calculated by some other method.

General quadratic programming with inequality constraints is almost always solved with an active set method [62]. Positive definiteness of matrix $\mathbf{W}$ again simplifies the solution procedure. It is worth mentioning that both linear and quadratic programming can be solved in a finite number of steps which demonstrates well-behaved convergence of these problems.

5.4 Objective Functions

Upon comparing quadratic with linear programming formulations, we chose to adopt the former for solving the force distribution problem. We also chose to consider only the primary constraints, that is, the linear equality constraints in order to capture and highlight the most important features of the force distribution for flexible-link cooperating manipulators. Hence, the resulting optimization problem takes the following form:

$$\min_{\mathbf{x}} \quad \mathbf{c}^T\mathbf{x} + \tfrac{1}{2}\mathbf{x}^T\mathbf{W}\mathbf{x} \qquad (5.10\,a)$$

$$\text{Subject to} \quad \mathbf{A}_1\mathbf{x} = \mathbf{b}_1 \qquad (5.10\,b)$$

where $(5.10\,b)$ comprises the dynamics equations of the object. As was shown in chapter 4, the matrix $\mathbf{A}_1 \in \mathbf{R}^{6\times 6P}$ is always full rank which means that the constraints are linearly independent. The last but very important task which remains is to define suitable quadratic objective functions which will represent criteria for a better force distribution. We will first consider some of the criteria proposed for rigid-link systems, *e.g.*, the minimum internal forces. However, emphasis is placed on implementing new criteria which are particularly relevant to a system consisting of flexible-link manipulators. Here, the ultimate goal is to improve the dynamics behavior and reduce the system vibration. Finally, objective functions which combine many different sub-objectives are proposed and implemented.

5.4.1 Minimizing the Internal Forces

The vector of design variables, $\mathbf{x}$, in eq.(5.10) only includes the wrenches applied to the grasped object. As a result, the force distribution determined by the solution to the optimization problem eq.(5.10) may or may not take into account the dynamics of the manipulators, depending on the objective function. In a situation where manipulators operate at slow speeds and/or carry out delicate tasks, optimality criteria can be formulated which describe how well the object is handled. This is particularly relevant for a multi-fingered mechanical hand grasping an object. In this case, the performance criteria may include any one of the following: (i) the *contact condition* between the fingers and the object to ensure a positive normal contact force [64]; (ii) the *object stability* which ensures that the object remain in a static equilibrium when its position is perturbed [65]; (iii) the *contact stability* which guarantees that the object remains grasped when disturbed by external forces [8] and (iv) the *minimum internal forces* criterion which reduces the potential damage to the object [15]. Internal forces play an important role in achieving all these objectives. For cooperating manipulators with a rigid grasp of the object, the aforementioned contact condition is not needed because the manipulators can apply arbitrary wrenches. As well, the object and contact stability are ensured by the rigid grasp. However, it is desirable to minimize the internal forces because excessive internal forces may damage a fragile object and impose high loads on the system.

As discussed in chapter 4, internal forces are the components of the grasping wrenches in the null space of $\mathbf{A}_1$. These forces do not contribute to the motion of the object but produce a squeezing or tearing effect. Decomposing the grasping wrenches applied to the object into resultant and internal components, denoted by $\mathbf{x}^+$ and $\mathbf{x}^-$ respectively, we have

$$\mathbf{x} = \mathbf{x}^+ + \mathbf{x}^- = \mathbf{A}_1^+ \mathbf{b}_1 + \mathbf{A}_1^N \mathbf{z} \tag{5.11}$$

where the first term $\mathbf{x}^+ (= \mathbf{A}_1^+ \mathbf{b}_1)$ does not vary in the design space. The vector of internal forces $\mathbf{x}^-$ must satisfy:

$$\mathbf{A}_1 \mathbf{x}^- = \mathbf{0} \tag{5.12}$$

Therefore, minimizing the amount of internal forces can be described by minimizing the following quadratic objective function:

$$f_I(\mathbf{x}^-) = \frac{1}{2} \mathbf{x}^{-T} \mathbf{x}^- \tag{5.13}$$

Expanding the above by using eq. (5.11), we obtain:

$$\begin{aligned} f_I(\mathbf{x}^-) &= \frac{1}{2}(\mathbf{x} - \mathbf{x}^+)^T (\mathbf{x} - \mathbf{x}^+) \\ &= \frac{1}{2}(\mathbf{x}^T \mathbf{x} - 2\mathbf{x}^T \mathbf{x}^+ + \mathbf{x}^{+T} \mathbf{x}^+) \end{aligned} \tag{5.14}$$

We now recall that the pseudoinverse of a full rank matrix $\mathbf{A}_1$ maybe calculated by $\mathbf{A}_1^+ = \mathbf{A}_1^T (\mathbf{A}_1 \mathbf{A}_1^T)^{-1}$. We can therefore rewrite the second term in eq. (5.14) as:

$$\mathbf{x}^T \mathbf{x}^+ = \mathbf{x}^T \mathbf{A}_1^T (\mathbf{A}_1 \mathbf{A}_1^T)^{-1} \mathbf{b}_1 = \mathbf{b}_1^T (\mathbf{A}_1 \mathbf{A}_1^T)^{-1} \mathbf{b}_1 \tag{5.15}$$

which is independent on the design variable $\mathbf{x}$. Hence, the only term in eq. (5.14) which is a function of $\mathbf{x}$ is the first term $\frac{1}{2}\mathbf{x}^T \mathbf{x}$. Similarly, the constraint equations (5.12) are rewritten as follows:

$$\begin{aligned} & \mathbf{A}_1 \mathbf{x}^- = \mathbf{A}_1 (\mathbf{x} - \mathbf{x}^+) = \mathbf{0} \\ \Longrightarrow \quad & \mathbf{A}_1 \mathbf{x} = \mathbf{A}_1 \mathbf{x}^+ = \mathbf{A}_1 \mathbf{A}_1^T (\mathbf{A}_1 \mathbf{A}_1^T)^{-1} \mathbf{b}_1 = \mathbf{b}_1 \end{aligned} \tag{5.16}$$

which leads to the equations of the object dynamics. Therefore, the problem of minimizing the internal forces for a multiple cooperating manipulator system can be stated as:

$$\begin{aligned} \min_{\mathbf{x}} \quad & \tfrac{1}{2}\mathbf{x}^T \mathbf{x} \\ \text{subject to} \quad & \mathbf{A}_1 \mathbf{x} = \mathbf{b}_1 \end{aligned} \tag{5.17}$$

Similar formulations to the above were derived by Nakamura [8] to determine a minimum internal force while satisfying the static frictional inequality constraints or the contact stability condition. He also proposed a more physically accurate criterion [32] which minimizes the strain energy stored in the object with the goal of minimizing the possible damage to the object. This is performed by first modeling the object as a rigid body covered with a massless elastic layer. Strain energy is then formulated as a quadratic function of contact wrenches. Nakamura showed that the minimum strain energy criterion is equivalent to the minimum internal force criterion when the stiffness of the elastic layer is the same in all directions at all contact points.

To illustrate the performance of the minimal internal force scheme (5.17), we implement the inverse dynamics algorithm (Figure 4.2) combined with a strategy for minimizing the internal forces. Since this scheme does not take manipulator dynamics into consideration, solution of the serial flexible-link inverse dynamics will be unstable. Therefore, the procedure for minimizing the internal forces will be implemented only for a rigid multiple-arm system. However, as will be shown later, this scheme can be combined with other criteria to produce a useful solution for flexible manipulator systems.

Example 5.1 — Minimum Internal Forces

The same configuration of dual arms and object as shown in Figure 4.4 and the desired object trajectory as defined in eqs. (4.52)-(4.54) are used. The numerical solution is obtained by implementing the minimum internal force scheme. In this example, the two identical arms are considered to be rigid.

Comparing eqs. (5.17) and (5.10), we observe that minimizing internal forces is equivalent to setting $\mathbf{W} = \mathbf{1}$ and $\mathbf{c} = \mathbf{0}$ in eq. (5.10). Obviously, the Hessian matrix $\mathbf{W}$ is positive definite and therefore a unique solution exists to the force optimization

problem. The results for the left arm are displayed in Figure 5.1. It shows the profile of the grasping wrenches compared with those obtained by the method used in example 4.2 where the base motor torque and the elbow motor torque of the left arm were set to zero. It can be seen from the figure that grasping wrenches which give the minimum internal forces are smaller in magnitude than those obtained by the other scheme. The same trend can be observed in the solution of τ_3 but not τ_1 and τ_2 since in the non-minimum internal force scheme, the torques at the base and elbow joints were forced to zero.

5.4.2 Optimal Load Sharing

Task Space Sharing

One of the merits of a multiple-arm system is that the loads can be *shared* among the manipulators. Considering each robot arm as a unit which contributes to carrying the object, it is natural to expect that arms with high load carrying capacities should contribute more than those with low capacities. An optimal load distribution within the arms can be achieved by assigning different weights to the diagonal block of the matrix $\mathbf{W}$. In particular, numbers in the ith block are chosen in inverse proportion to the load carrying capacity of the ith arm, which in turn is quantified by the maximum allowable load it can carry. Each block of $\mathbf{W}$ thus represents a relative 'weight' of wrenches applied by one arm relative to those of the other arms and accordingly, matrix $\mathbf{W}$ is usually called a *weighting matrix*. When all manipulators are identical, the weighting matrix $\mathbf{W}$ is set equal to an identity matrix.

In addition, elements in each 6×6 diagonal blocks of $\mathbf{W}$ represent the relative weights of the components constituting each wrench. To effectively utilize the mechanical advantage provided by multiple arm control, it has been suggested [10] that

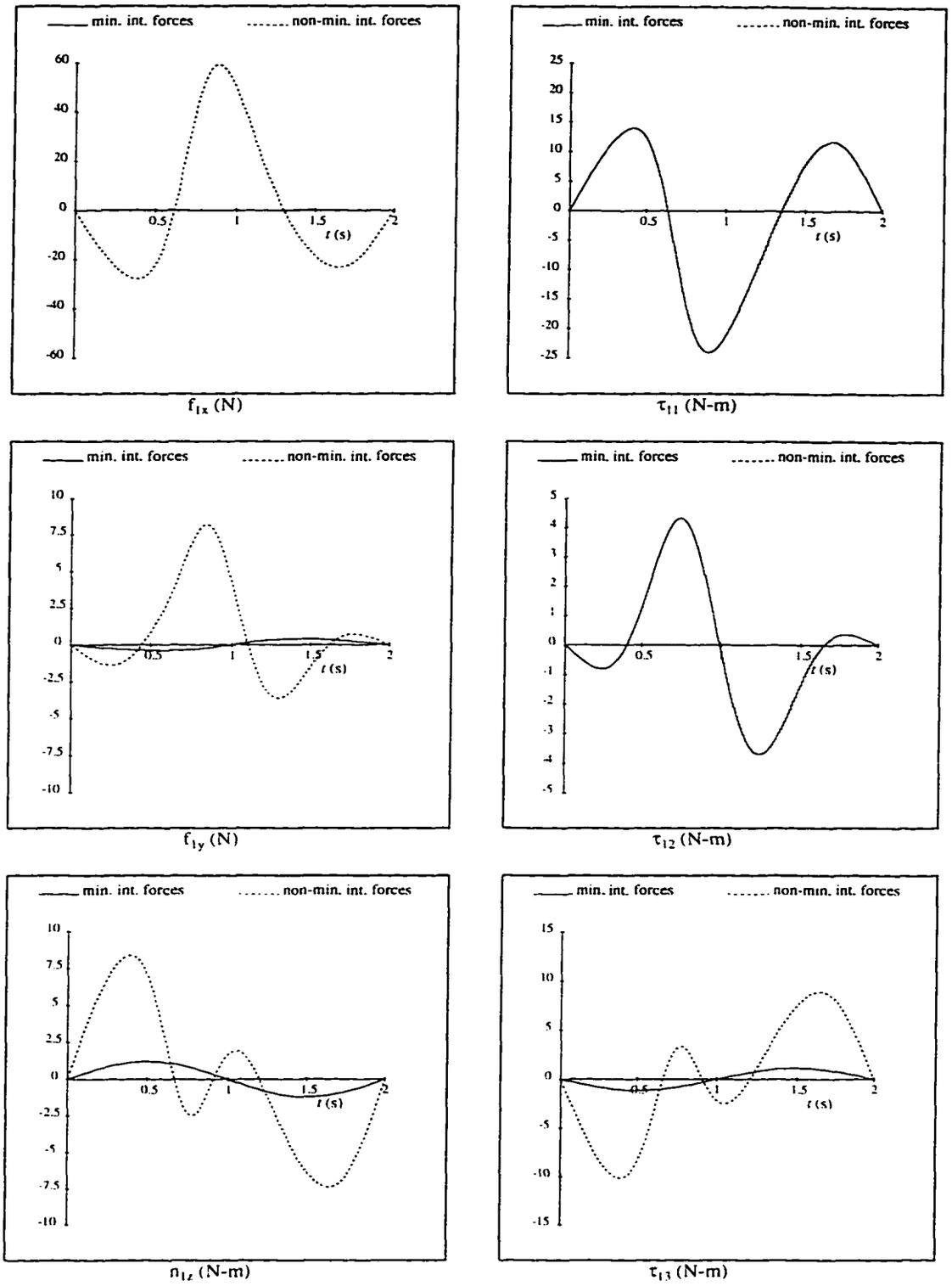

Figure 5.1: Minimal Internal Forces

moments required to handle the object should be attained primarily through the cross product terms $\boldsymbol{c}_i \times \mathbf{f}_i$ in the grasp matrix $\mathbf{A}_1$ of eq.(2.41) rather than the directly applied moments $\mathbf{n}_i$. To enforce a large penalty on the use of $\mathbf{n}_i$ in achieving a desired net moment $\boldsymbol{c}_i \times \mathbf{f}_i + \mathbf{n}_i$, we set

$$\mathbf{W} = \begin{bmatrix} \ddots & & \\ & \frac{1}{w_i}\begin{bmatrix} \mathbf{1} & \mathbf{0} \\ \mathbf{0} & k_i\mathbf{1} \end{bmatrix} & \\ & & \ddots \end{bmatrix} \tag{5.18}$$

where the scalar w_i is the maximum load the ith arm can carry and $k_i \geq 1$. The selection of k_i must also take into consideration the location of the ith contact point on the object. In other words, those end-effectors grasping the object closer to its mass center should be required to supply less moment $\mathbf{n}_i$. A similar argument applies to the components of the grasping forces. At a certain posture (manipulator configuration), a manipulator is more effective in applying, say, a force in the X-direction than in other directions. Thus, in general, the weighting matrix $\mathbf{W}$ can be chosen as diagonal with different weights for each nonzero entry.

Configuration Space Sharing

As can be expected, the above load sharing scheme does not ensure optimal use of the actuators. It is desirable that loads on the actuators be distributed such that motors with a higher capacity support more load than those with smaller capacities. Taking a quadratic function

$$f_T(\boldsymbol{\tau}) = \frac{1}{2}\boldsymbol{\tau}_\Sigma^T \mathbf{W}_T \boldsymbol{\tau}_\Sigma \tag{5.19}$$

as the objective function, an optimal load distribution in the configuration space can be achieved by placing different weights on the diagonal components of $\mathbf{W}_T$.

Analogously to the task space sharing scheme, these weights are selected to be the reciprocals of the maximum torques that the corresponding actuators can generate. For flexible-link manipulators, minimizing and actively distributing the actuator torques is particularly important. The analysis of the inverse dynamics of serial flexible-link manipulators has shown that collocation of the actuation with the end-effector ensures a stable inverse dynamics solution. It has also been shown that in an approximate situation when the elastic links are modeled with finite numbers of elastic modes, a critical point on the arm exists which partitions the stable and unstable regions [22, 66]. A stable region lies between the arm tip and the critical point. A useful inference is that the actuator efforts should be shifted as much as possible towards the end-effectors in order to approximate a collocated case which promises better inverse dynamics behavior. To implement this idea, we suggest that minimizing the norm of the torques required at the joints located prior to the proximal end of the most distal flexible link of a serial arm will shift the actuation efforts toward the end-effectors. An improved dynamics behavior of the inverse system would then be expected.

To incorporate objective (5.19) into the optimization problem (5.10), we need to include the following relations:

$$\boldsymbol{\tau}_\Sigma = \boldsymbol{\tau}'_\Sigma + \mathbf{J}_{1\Sigma}\boldsymbol{w}_\Sigma$$

Note that $\boldsymbol{\tau}'_\Sigma$ is known from the manipulator states. Substituting the above, eq. (5.19) can be written as:

$$f_T(\mathbf{x}) = \frac{1}{2}{\boldsymbol{\tau}'_\Sigma}^T\mathbf{W}_T\boldsymbol{\tau}'_\Sigma + {\boldsymbol{\tau}'_\Sigma}^T\mathbf{W}_T\mathbf{J}_{1\Sigma}^T\boldsymbol{w}_\Sigma + \frac{1}{2}\boldsymbol{w}_\Sigma^T\mathbf{J}_{1\Sigma}\mathbf{W}_T\mathbf{J}_{1\Sigma}^T\boldsymbol{w}_\Sigma \tag{5.20}$$

The first term is independent of the design variables, and therefore does not affect the solution of the optimization problem. Eq. (5.19) can therefore be reduced to:

$$f_T(\mathbf{x}) = \hat{\mathbf{c}}_T^T\mathbf{x} + \frac{1}{2}\mathbf{x}^T\widehat{\mathbf{W}}_T\mathbf{x} \tag{5.21}$$

where

$$\hat{\mathbf{c}}_T = \mathbf{J}_{1\Sigma}\mathbf{W}_T\boldsymbol{\tau}'_\Sigma \qquad \widehat{\mathbf{W}}_T = \mathbf{J}_{1\Sigma}\mathbf{W}_T\mathbf{J}_{1\Sigma}^T \tag{5.22}$$

It remains to be verified whether $\widehat{\mathbf{W}}_T$, the Hessian matrix of the objective function in eq. (5.21) is positive-definite. Referring to eq. (5.22) and recalling that $\mathbf{W}_T$ is chosen to be positive-definite, the same property will be retained for $\widehat{\mathbf{W}}_T$ as long as $\mathbf{J}_{1\Sigma}$ is nonsingular [67]. Since $\mathbf{J}_{1\Sigma}$ is a block diagonal matrix of $\mathbf{J}_{1i}^T$($i = 1, \ldots, P$), $\mathbf{J}_{1\Sigma}^T$ is nonsingular if and only if all $\mathbf{J}_{1i}^T$ have full rank. For a serial manipulator with its end-effector in contact with the environment or a moving object, singularity of $\mathbf{J}_{1i}^T$ implies that the manipulator cannot generate an arbitrary tip wrench. For a rigid manipulator, this happens when the manipulator is at a kinematic singularity.

Example 5.2 — Minimum Norm of Torques

The same rigid dual-arm and object system as used in the previous example is employed to show the numerical performance of the optimal load sharing scheme. First, we minimize the Euclidian norm of actuator torques by setting,

$$f_T(\boldsymbol{\tau}) = \frac{1}{2}\boldsymbol{\tau}_\Sigma{}^T\boldsymbol{\tau}_\Sigma \longrightarrow \mathbf{W}_T = \mathbf{1}$$

The actuator torques obtained with the present scheme are compared with those obtained by the minimum internal forces scheme in example 5.1. Results for the two arms are similar and those for the left arm are shown in Figure 5.2. It is seen from the figure that the scheme of minimum norm of torques generates more evenly distributed loads on the actuators while the minimum internal force scheme generates more evenly distributed tip forces and torques.

Next, considering the actuator capacities given in Table 5.1, the weighting matrix in eq. (5.19) is chosen to be

$$\mathbf{W}_T = \mathrm{diag}\{\frac{1}{150}, \frac{1}{40}, \frac{1}{9.8}, \frac{1}{150}, \frac{1}{40}, \frac{1}{9.8}\} \tag{5.23}$$

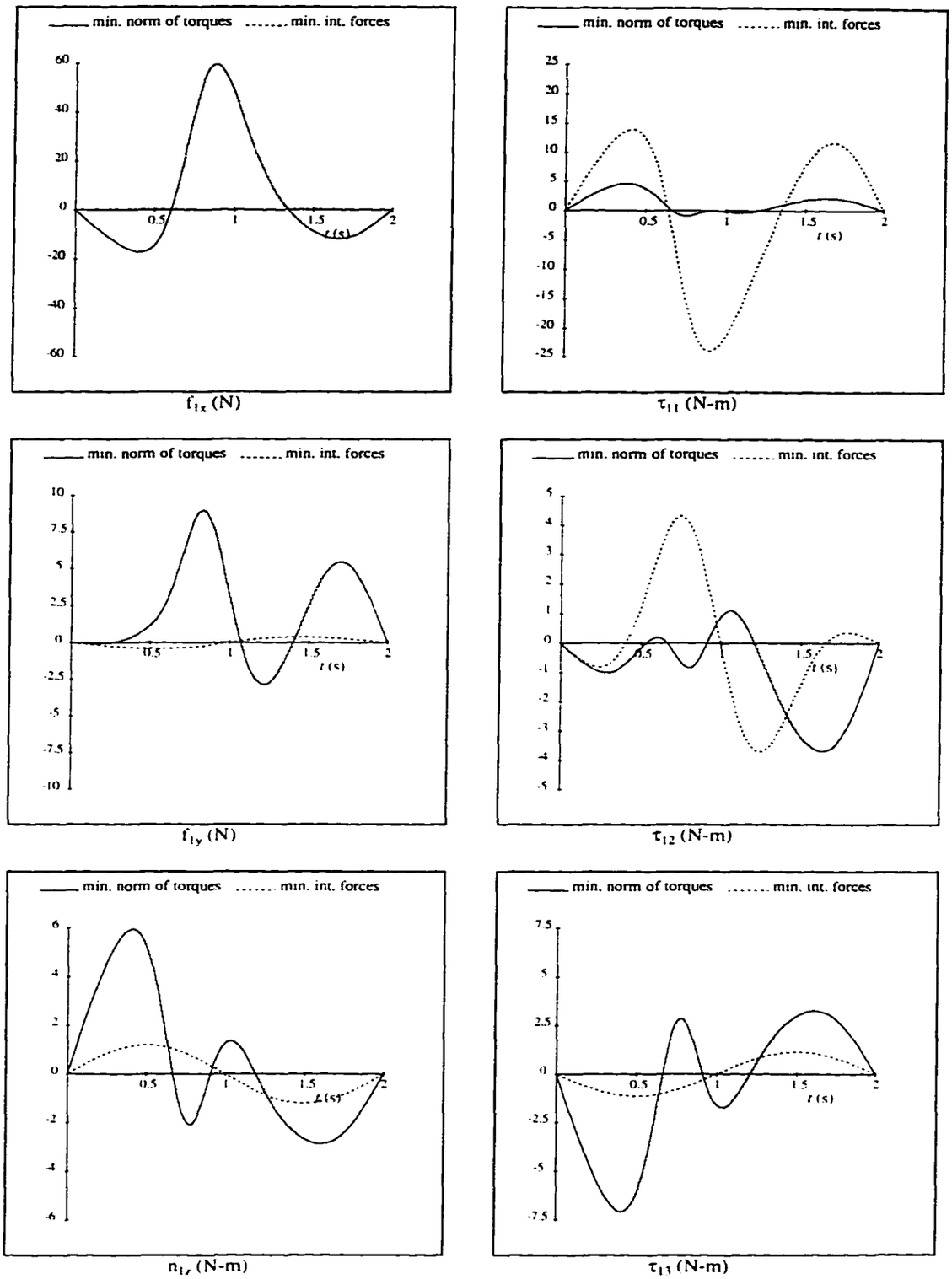

Figure 5.2: Comparison of Minimum Norm of Torques and Minimum Internal Forces

Table 5.1: Maximum Torque of the Motors

Motors	Base	Elbow	Wrist
τ_i^{lim} (N-m)	150	40	9.8

Table 5.2: Maximum Value of Torques in Figure 5.4

Motors	Base	Elbow	Wrist
$(\lvert\tau_i\rvert)_{max}$ (N-m)	13.5	3.14	1.37
$(\lvert\tau_i\rvert)_{max}/\tau_i^{lim}$ (%)	9.0	7.9	13.9

Comparing the torques obtained by using this minimum weighted norm scheme with those of the Euclidian norm scheme implemented above, the results in Figure 5.3 show the loads shifting from motors having lower capacities to those with higher capacities. The torque required at the base and elbow motors increased while the torque at the wrist motor decreased when minimizing the weighted norm of the actuator torques. Also, the maximum values of the torques at each joint (Table 5.2) are all close to 10% of the respective maximum torque values that the actuators can generate. This demonstrates that the actuators contribute according to their abilities.

Example 5.3 — Shifting Torques Towards the End-effectors

Special care needs to be taken when manipulators are composed of flexible links. Numerical experiments conducted with the above weighted-norm or Euclidian norm of torques scheme produce unbounded solutions for joint torques during the maneuver of rotating a rigid object for 90° in 2 seconds. Since a flexible serial arm driven by tip wrenches has a better dynamics behavior, we attempt to shift the actuator loads from those before the proximal end of the last flexible link to those beyond its distal end. In other words, we propose to minimize the actuator torques at the joints located before and including the last flexible link of the arms. In this example, we consider the first

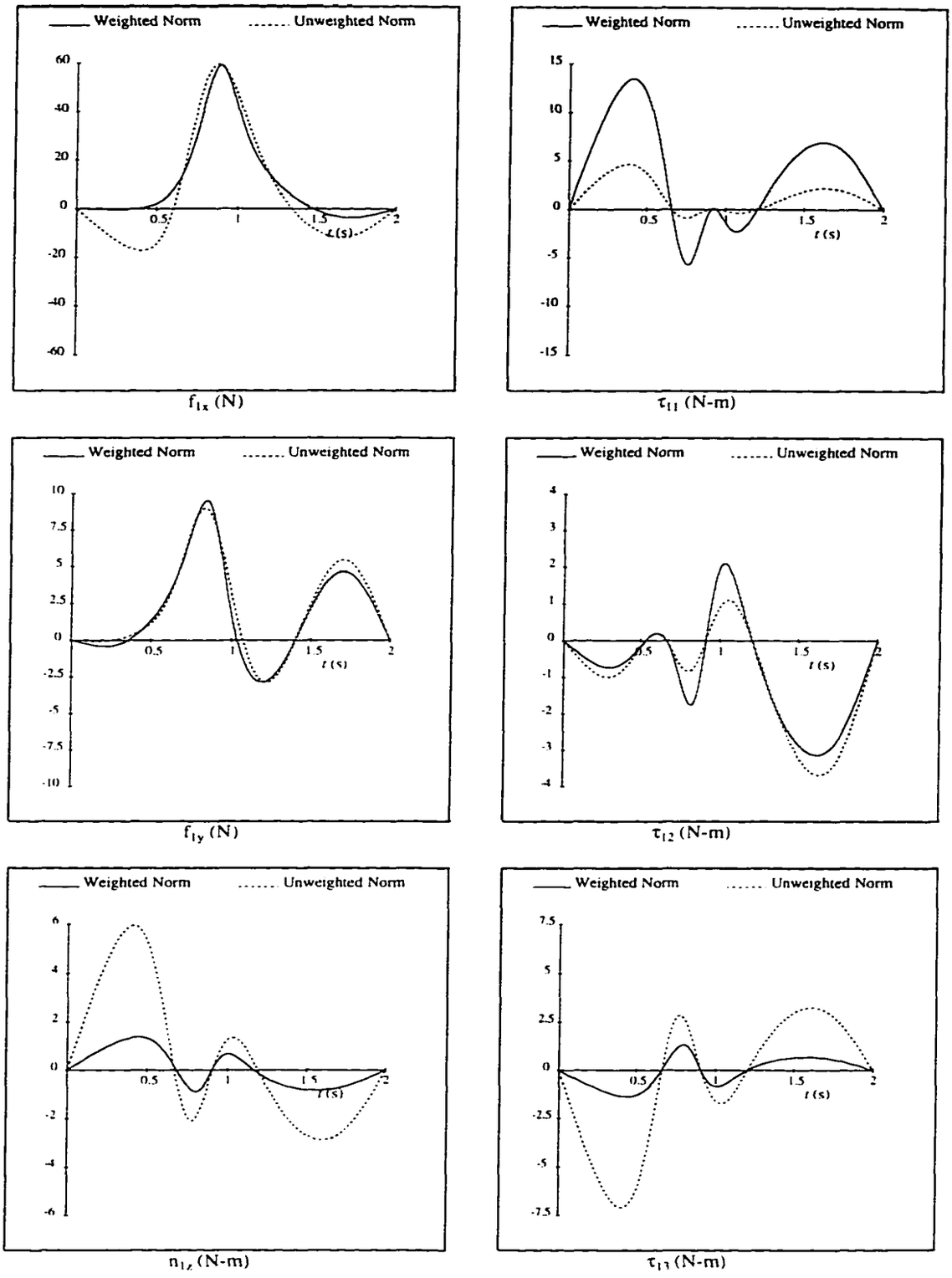

Figure 5.3: Comparison of Minimum Weighted and Unweighted Norm of Torques

and second links of the left arm to be flexible. Since the system has three redundant actuators, in addition to minimizing the base and elbow actuator torques, we also choose to minimize the wrist torques in order to better approximate the situation where the flexible arm is driven by the tip wrench.

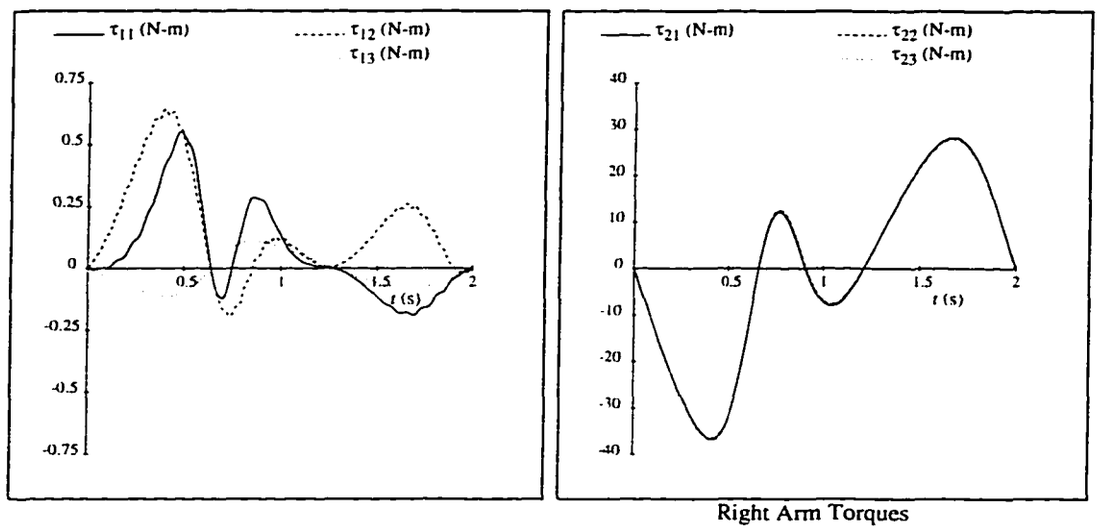

(a) Solution for Torques

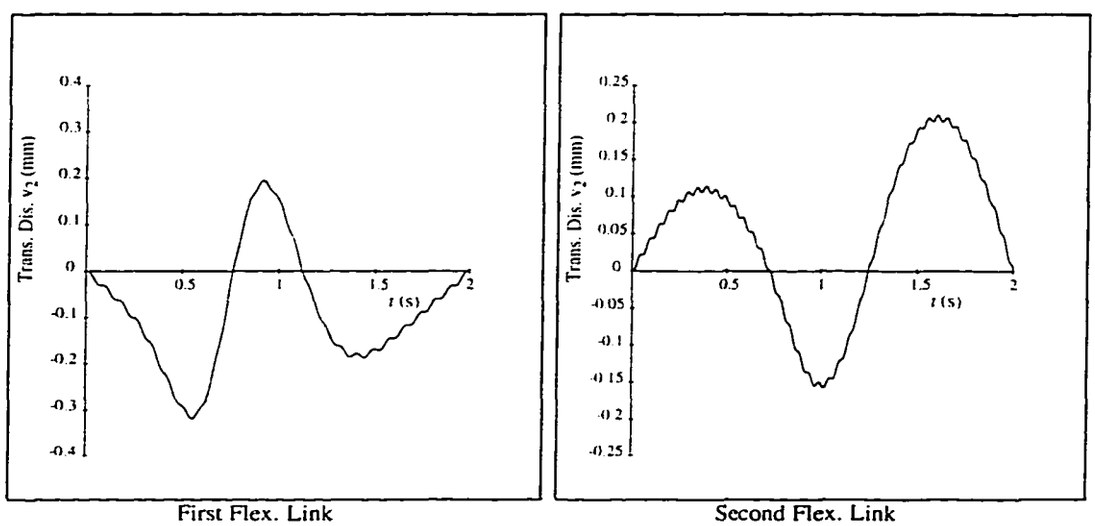

(b) Tip Transverse Displacements of the Flexible Links

Figure 5.4: Shifting Loads on Flexible Links towards the End-effectors

Therefore, the weighting matrix is set to:

$$\mathbf{W}_T = \text{diag}\{1.0,\ 1.0,\ 1.0,\ 10^{-10},\ 10^{-10},\ 10^{-10}\} \tag{5.24}$$

Note that the last three elements in the above are chosen to ensure the positive-definiteness of the matrix $\mathbf{W}_T$. The solution for the torques at both arms and the elastic coordinates of the left arm are shown in Figure 5.4.

5.4.3 Minimizing the Norm of the Elastic Accelerations

Although extensive studies of force optimization schemes have been carried out for rigid cooperating manipulators, relatively little research exists which considers the dynamics of the elastic components in the system. Pfeiffer *et al.* [68] calculated the contact forces for a walking stick insect (a biological model for a multi-legged walking machine) while minimizing the deformation energy stored in the legs. In particular, bending loads on the outer, thin leg segments were minimized based on a *static* relation between the deformation and the loads applied to the leg segments.

It is interesting to note that one of the characteristics of the flexible-link inverse dynamics solution is that the generalized coordinates may be significantly affected by the wrenches applied at the end-effectors of the manipulators. By contrast, in the rigid-link case, a different choice of tip wrenches only affects joint torques since the generalized coordinates (joint variables) are predetermined by the desired motion of the grasped object. Although this fact complicates the inverse dynamics problem, it can be used to advantage. It allows us to actively choose the actuator torques and hence, the wrenches which produce the least excitation of the system vibrations. We therefore set as our goal for a flexible multi-arm system to find a set of wrenches which minimizes the elastic vibration in the flexible links.

Observing that the manipulator dynamics equations are linear in elastic accelerations, we propose to minimize a weighted norm of the elastic accelerations. As in the case of minimizing a weighted norm of the actuator torques, the objective function is written as:

$$f_E(\ddot{q}_e) = \frac{1}{2}\ddot{q}_{e\Sigma}^T \mathbf{W}_E \ddot{q}_{e\Sigma} \tag{5.25}$$

Substituting the elastic accelerations

$$\ddot{q}_{e\Sigma} = \ddot{q}'_{e\Sigma} + \mathbf{J}_{3\Sigma}^T \boldsymbol{w}_\Sigma$$

into the objective function (5.25), we obtain

$$f_E(\mathbf{x}) = \hat{\mathbf{c}}_E^T \mathbf{x} + \frac{1}{2}\mathbf{x}^T \widehat{\mathbf{W}}_E \mathbf{x} \tag{5.26}$$

where

$$\hat{\mathbf{c}}_E = \mathbf{J}_{3\Sigma}\mathbf{W}_E \ddot{q}'_{e\Sigma} \qquad \widehat{\mathbf{W}}_E = \mathbf{J}_{3\Sigma}\mathbf{W}_E\mathbf{J}_{3\Sigma}^T \tag{5.27}$$

Once again, the positive-definiteness of matrix $\widehat{\mathbf{W}}_E$ can be ensured if the matrix $\mathbf{W}_E$ is positive-definite and $\mathbf{J}_{3\Sigma}^T$ has full rank [67]. The matrix $\mathbf{J}_{3\Sigma}^T$ has full rank equaling to its row dimension provided that $\mathbf{J}_{3i}$ ($i = 1, \ldots, P$) are not rank deficient. Since as defined in eq. (4.6), $\mathbf{J}_{3i}^T = -\widehat{\mathbf{M}}_{eei}^{-1}\mathbf{J}_{ei}^T$ and we assume the existence of $\widehat{\mathbf{M}}_{eei}^{-1}$, $\mathbf{J}_{3i}^T$ has full rank as long as $\mathbf{J}_{ei}^T$ is of full rank. The rank deficiency of $\mathbf{J}_{ei}^T$ corresponds to a situation where some of the elastic degrees of freedom cannot be affected by any tip wrench. Recalling that $\mathbf{J}_{ei}$ is the elastic Jacobian matrix which maps configuration space elastic rates into a corresponding workspace end-effector velocity, $\mathbf{J}_{ei}$ becomes rank deficient when the elastic motion of the ith manipulator only generates end-effector motion in a subspace of the Cartesian space. Figure 5.5 provides an illustration of a planar two-link arm in a rigid singular configuration (X_1 and X_2 are aligned). Assuming that only bending is modeled for the links, any nonzero elastic rates of the arm will only produce tip velocity in one direction, as shown by $\mathbf{v}_E$. In this case, $\mathbf{J}_e$ is rank deficient.

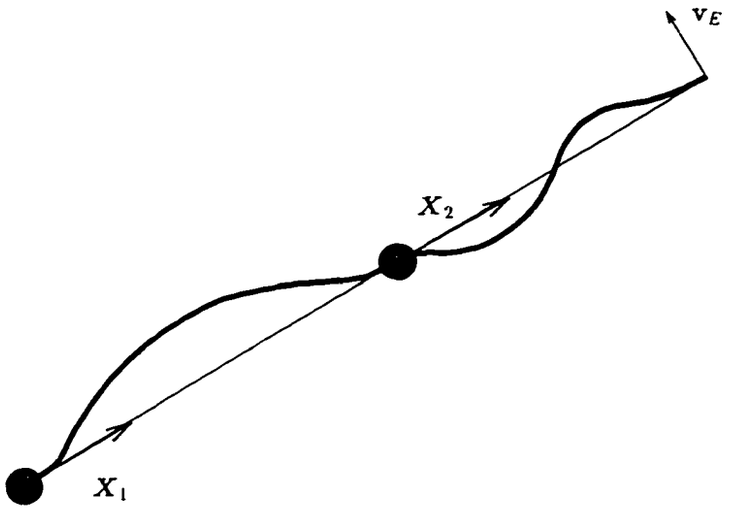

Figure 5.5: Singularity of the Elastic Jacobian Matrix

Example 5.4

As in the previous example, the left arm is considered to have two flexible links while the right arm has rigid links only. Since each flexible link is modeled with two planar beam elements in bending, the total number of elastic coordinates is 8. We implement the scheme of minimum norm of elastic accelerations with an identity weighting matrix $\mathbf{W}_E$. Figure 5.6 shows the resulting profile of the transverse displacements at the midpoint and the tip of each flexible link, as well as the strain energy of the system. Although increasing elastic deformations in the elastic links are observed in the figure, they still appear to be bounded within the specified time of the maneuver. This behavior is characteristic of a *short time stable* system [69]. The short time stability deals with determining whether a system response lies within specified bounds over specified intervals of time when the inputs are within specified bounds. In investigating the inverse dynamics solution, this concept is very useful since the system behavior within specified time intervals is our main concern.

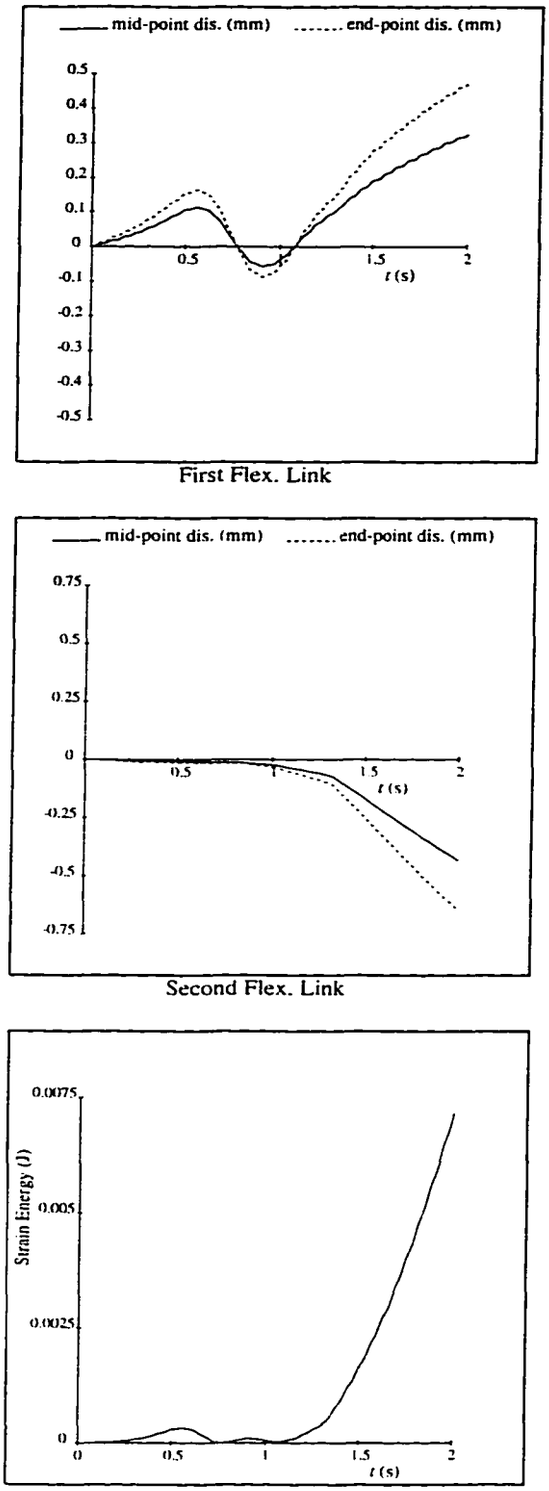

Figure 5.6: Results with Minimal Norm of Elastic Accelerations

5.4.4 Minimizing the Strain Energy Stored in the Flexible Links

If we accept that minimizing elastic accelerations smoothes the profile of elastic displacements, then minimizing elastic displacements should decrease the magnitude of deformations. For this purpose, it would be desirable to express the objective in terms of the elastic coordinates $\boldsymbol{q}_e$, that is,

$$f(\boldsymbol{q}_e) = \frac{1}{2}\boldsymbol{q}_e^T \mathbf{W}\, \boldsymbol{q}_e \tag{5.28}$$

Since $\ddot{\boldsymbol{q}}_e$ is linearly related to the design variables $\mathbf{x}$, double integration of $\mathbf{x}$ over the time history is required to determine the effects of $\mathbf{x}$ on $\boldsymbol{q}_e$. In other words, the elastic deformation of a manipulator at time t depends not only on the present value but also on the history of its end-effector wrenches. Ideally, the force distribution problem should be solved to produce the minimum vibration excitation in the system over the complete trajectory, *i.e.*, *globally*. However, as mentioned in the beginning of the thesis, in the present work, we have focused on the development of local force optimization schemes because of their simpler formulation, their lighter computational requirements, and the fact that they can be implemented without knowing the object trajectory apriori.

Since the solution to the optimization problem must be carried out numerically, we discretize time into intervals and approximate $\boldsymbol{q}_e$ at a time instant t_k by its second-order Taylor expansion at time t_{k-1}:

$$\boldsymbol{q}_e^k \approx \boldsymbol{q}_e^{k-1} + \Delta t\, \dot{\boldsymbol{q}}_e^{k-1} + \frac{1}{2}(\Delta t)^2\, \ddot{\boldsymbol{q}}_e^{k-1} \tag{5.29}$$

where $\Delta t = t_k - t_{k-1}$ and the superscript k denotes quantities evaluated at t_k. In formulating a quadratic objective function of the form (5.28), we note that using identical weights on all the elastic coordinates may be unacceptable. This is partly

due to the fact that these coordinates are likely to represent different quantities and hence have different dimensions. For instance, some components of $\boldsymbol{q}_e$ represent linear displacement measured in millimeters, while others represent angular displacement measured in radians. Also, the importance of each elastic coordinate will be very different for links with different stiffnesses.

Given that the strain energy can be used as a measure of the elastic deformation, we could set as our goal to minimize the strain energy in the flexible links. This can be achieved with the following objective

$$f_U(\boldsymbol{q}_e) = U = \frac{1}{2}\boldsymbol{q}_{e\Sigma}^T \mathbf{K}_{ee\Sigma}\boldsymbol{q}_{e\Sigma} \tag{5.30}$$

Substituting eq. (5.29) into the above, the strain energy at time t_k, U^k, in terms of the design variables $\mathbf{x}$ at time t_{k-1} becomes:

$$\begin{aligned} U^k \approx\ & \{(\frac{1}{2}(\Delta t)^2\,\ddot{\boldsymbol{q}}'_{e\Sigma} + \Delta t\,\dot{\boldsymbol{q}}_{e\Sigma} + \boldsymbol{q}_{e\Sigma})^T \mathbf{K}_{ee\Sigma}\mathbf{J}_{3\Sigma}^T\mathbf{x} \\ & + \frac{1}{4}(\Delta t)^2\mathbf{x}^T\mathbf{J}_{3\Sigma}\mathbf{K}_{ee\Sigma}\mathbf{J}_{3\Sigma}^T\mathbf{x} + g(\boldsymbol{q}_{e\Sigma}, \dot{\boldsymbol{q}}_{e\Sigma}, \ddot{\boldsymbol{q}}'_{e\Sigma})\}^{k-1} \end{aligned} \tag{5.31}$$

In the above, the matrix $\mathbf{J}_{3\Sigma}$ is of dimension $6P \times \Sigma_{i=1}^{P} S_i$. The expression for U^k represents an approximation for the strain energy at t_k in terms of the variables evaluated at the previous time instant. Thus, minimizing the value on the right-hand side of eq. (5.31) amounts to minimizing the strain energy at the next time instant. The last term in the above equation, $g(\boldsymbol{q}_e, \dot{\boldsymbol{q}}_e, \ddot{\boldsymbol{q}}'_e)$, is independent of $\mathbf{x}$ and its detailed form is omitted as it has no influence on the solution. The resulting objective function can be expressed in the form (5.10a) with the following definitions:

$$\hat{\mathbf{c}}_U = \mathbf{J}_{3\Sigma}\mathbf{K}_{ee\Sigma}(\frac{1}{2}(\Delta t)^2\,\ddot{\boldsymbol{q}}'_{e\Sigma} + \Delta t\,\dot{\boldsymbol{q}}_{e\Sigma} + \boldsymbol{q}_{e\Sigma}) \tag{5.32}$$

$$\widehat{\mathbf{W}}_U = \frac{1}{2}(\Delta t)^2\mathbf{J}_{3\Sigma}\mathbf{K}_{ee\Sigma}\mathbf{J}_{3\Sigma}^T \tag{5.33}$$

Once again, since $\mathbf{K}_{ee\Sigma}$ is a positive definite matrix, $\mathbf{W}_U$ will be positive-definite as long as $\mathbf{J}_{3\Sigma}$ has full rank.

Table 5.3: Coefficients of the Object Trajectory

t_f (sec)	t_a (sec)	α	β	γ	h (m)
1.0	0.5	−1.0	0.5	1.0	1.0

Example 5.5 — Minimum Strain Energy

We implement the minimum strain energy scheme on the 3D dual-arm and object system first introduced in section 4.5.2. The forearm and the upper arm of the left arm are considered to be flexible while the right arm is rigid. For this example, the object trajectory is defined with the trajectory constants given in Table 5.3. The resulting maneuver has no constant speed segment and the total motion in the Y direction is smaller than in the other directions. The weighting matrix is invariant with time and is defined as:

$$\mathbf{W}_U = \text{diag}\{\mathbf{K}_{ee11},\ \mathbf{K}_{ee12}\}$$

with the two diagonal blocks given by:

$$\mathbf{K}_{ee1i} = \begin{bmatrix} 115809.5 & 0.0 & 0.0 & 0.0 & -57904.8 & 0.0 & 0.0 & 14476.2 \\ 0.0 & 115809.5 & 0.0 & 0.0 & 0.0 & -57904.8 & -14476.2 & 0.0 \\ 0.0 & 0.0 & 9650.8 & 0.0 & 0.0 & 14476.2 & 2412.7 & 0.0 \\ 0.0 & 0.0 & 0.0 & 9650.8 & -14476.2 & 0.0 & 0.0 & 2412.7 \\ -57904.8 & 0.0 & 0.0 & -14476.2 & 57904.8 & 0.0 & 0.0 & -14476.2 \\ 0.0 & -57904.8 & 14476.2 & 0.0 & 0.0 & 57904.8 & 14476.2 & 0.0 \\ 0.0 & -14476.2 & 2412.7 & 0.0 & 0.0 & 14476.2 & 4825.4 & 0.0 \\ 14476.2 & 0.0 & 0.0 & 2412.7 & -14476.2 & 0.0 & 0.0 & 4825.4 \end{bmatrix}$$

Numerical results were generated with $\Delta t = 0.0002$ (reasons for this will be given after the analysis of the stability of the inverse system). Solutions for the transverse displacement and the slopes at the end-point of both flexible links are shown in

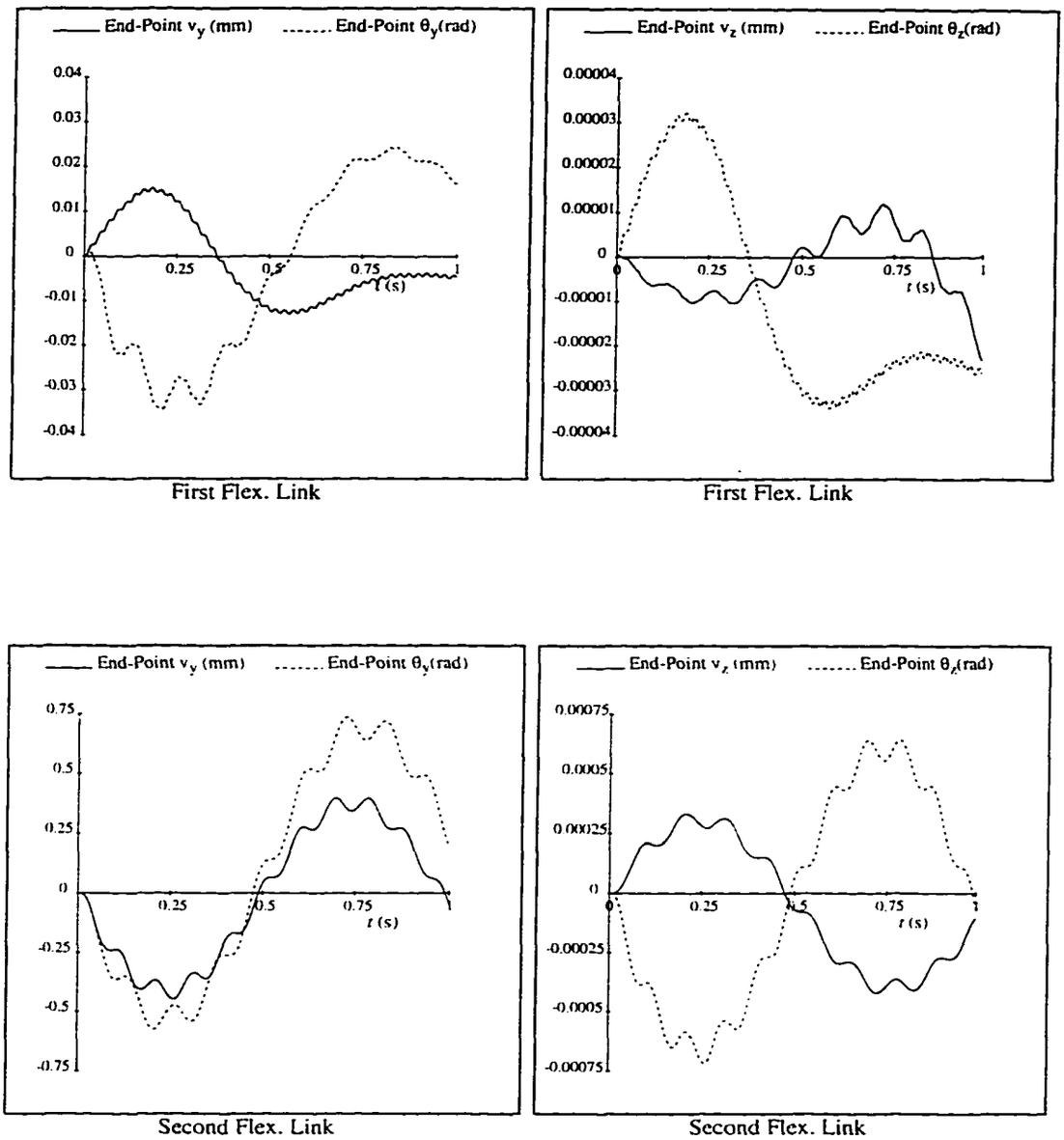

Figure 5.7: End-Point Deflections with Minimum Strain Energy Scheme

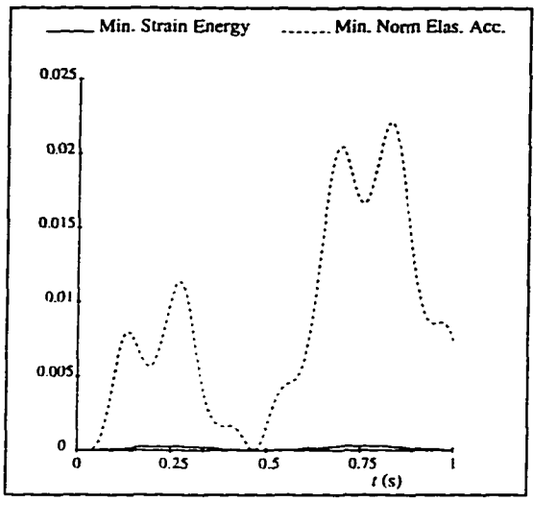

Figure 5.8: Comparison of the Strain Energy (J)

Figure 5.7. It is observed that in-plane deflections (v_y) are much larger than the out-of-plane deflections (v_z), since faster motion in the X_I direction is required for the flexible links than in the Z_I direction. As a result of minimizing the strain energy, the strain energy stored in the flexible links is kept to less than 3×10^{-4} Joule. When compared to the results obtained using the minimum Euclidian norm of the elastic acceleration scheme (Figure 5.8, 5.9 and 5.10), it is apparent that the minimum strain energy scheme is effective in reducing both strain energy and the elastic deformations.

5.4.5 Combination of Various Objectives

One can take a weighted combination of the aforementioned individual objectives to form a new objective function. This objective function represents a combined criterion which is particularly relevant to optimal performance of the system. The choice of the relative weights on each component of the objective depends largely on the particular manipulator system and numerical experiments are required to "tune"

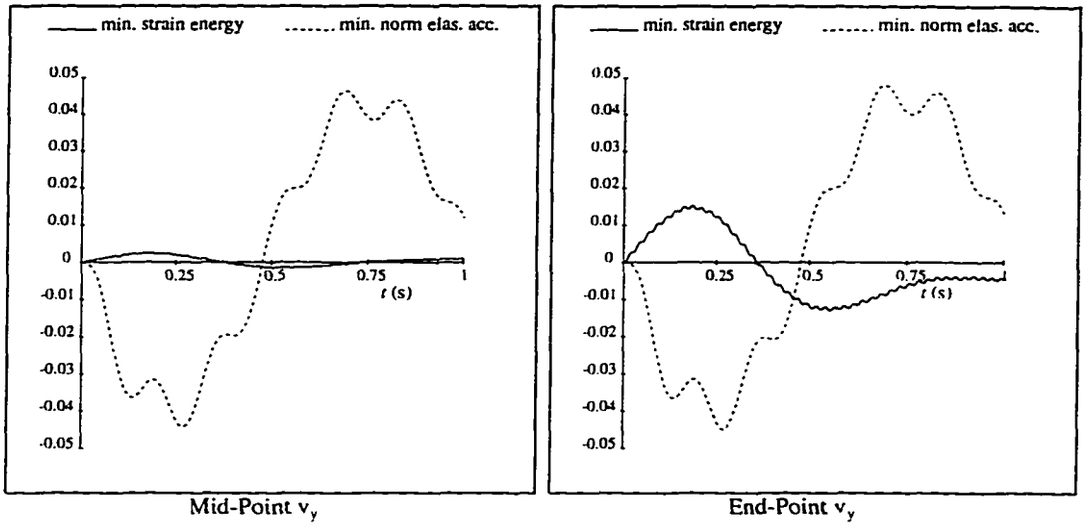

Figure 5.9: In-Plane Deflections of the First Flexible Link

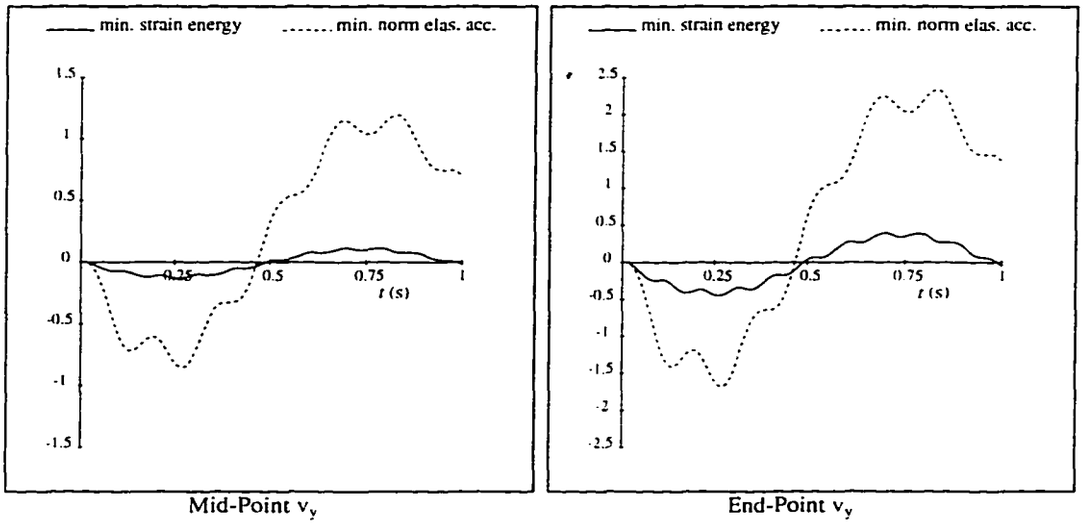

Figure 5.10: In-Plane Deflections of the Second Flexible Link

the weights. The resultant objective function can be formulated as:

$$f(\mathbf{x}) = a f_I(\mathbf{x}) + b f_T(\boldsymbol{\tau}) + c f_E(\ddot{\boldsymbol{q}}_e) + d f_U(\boldsymbol{q}_e) \tag{5.34}$$

where the weights a, b, c, d are positive numbers, some of which can be set to zero. The terms in eq. (5.34) represent component objectives of minimum internal forces, optimal load sharing, minimum elastic acceleration and minimum strain energy. Since each individual term is a strictly convex function, the combined objective function is also strictly convex and it is characterized by:

$$\mathbf{c} = b\hat{\mathbf{c}}_T + c\hat{\mathbf{c}}_E + d\hat{\mathbf{c}}_U \tag{5.35}$$

$$\mathbf{W} = a\mathbf{W}_I + b\widehat{\mathbf{W}}_T + c\widehat{\mathbf{W}}_E + d\widehat{\mathbf{W}}_U \tag{5.36}$$

The definitions for each term in the above have been given in Sections 5.4.1 to 5.4.4. We now present some examples to illustrate the performance of the combined objective function scheme.

Example 5.6 — Combined Objective

To demonstrate the performance with the combined objectives, we consider two cases:

Case 1 : $f(\mathbf{x}) = \tau_{11}^2 + \tau_{12}^2 + \tau_{13}^2 + U$

According to eq. (5.34), the relative weights on each of the four objectives are: $a = 0$, $b = 1$, $c = 0$ and $d = 1$. The weighting matrices for the combined objective function are:

$$\mathbf{W}_T = \text{diag}\{\mathbf{W}_{T1}, \mathbf{W}_{T2}\} \tag{5.37}$$

$$\mathbf{W}_U = \text{diag}\{\mathbf{K}_{ee11}\ \mathbf{K}_{ee12}\} \tag{5.38}$$

where

$$\mathbf{W}_{T1} = \text{diag}\{2,\ 2,\ 2,\ 10^{-10},\ 10^{-10},\ 10^{-10}\}$$
$$\mathbf{W}_{T2} = 10^{-10}\ \mathbf{1}_{6\times 6}$$

It can be seen from Figure 5.11 that the torques driving the flexible arm are kept small in magnitude since the norm of torques at the first three joints is minimized. The torques for the rigid arm are shown in Figure 5.12. The tip transverse deflections (in-plane and out-of-plane) for both links are shown in Figure 5.13. Larger deflections in the out-of-plane direction occur because the end-effectors are required to move faster in the $X_I - Z_I$ plane than in the $X_I - Y_I$ plane.

Case 2 — $f(\mathbf{x}) = 10^{-5}(\frac{1}{2}\mathbf{x}^T\mathbf{x}) + U$

We have mentioned in the first example (Example 5.1) that minimum internal force scheme by itself is not suitable for solving the force distribution problem for flexible-link cooperating manipulators. However, sometimes it can be combined with other schemes to yield a compromise performance between lower internal forces and other objectives. To illustrate this idea, we propose case 2 which sets $a = 10^{-5}$. The time histories of the tip deflections at each flexible link and the strain energy for this case are shown in Figure 5.14. Without the second term in the objective function, the minimum internal force scheme almost always generates unbounded solution. However, comparing these results with those obtained in example 5.5 when using the minimum strain energy scheme, the dynamic response of the system is dramatically different for the two schemes, even though only a small change to the objective function was made.

Based on the large number of numerical simulations performed with two-arm (planar and 3D) cooperating manipulators (only representative results are shown

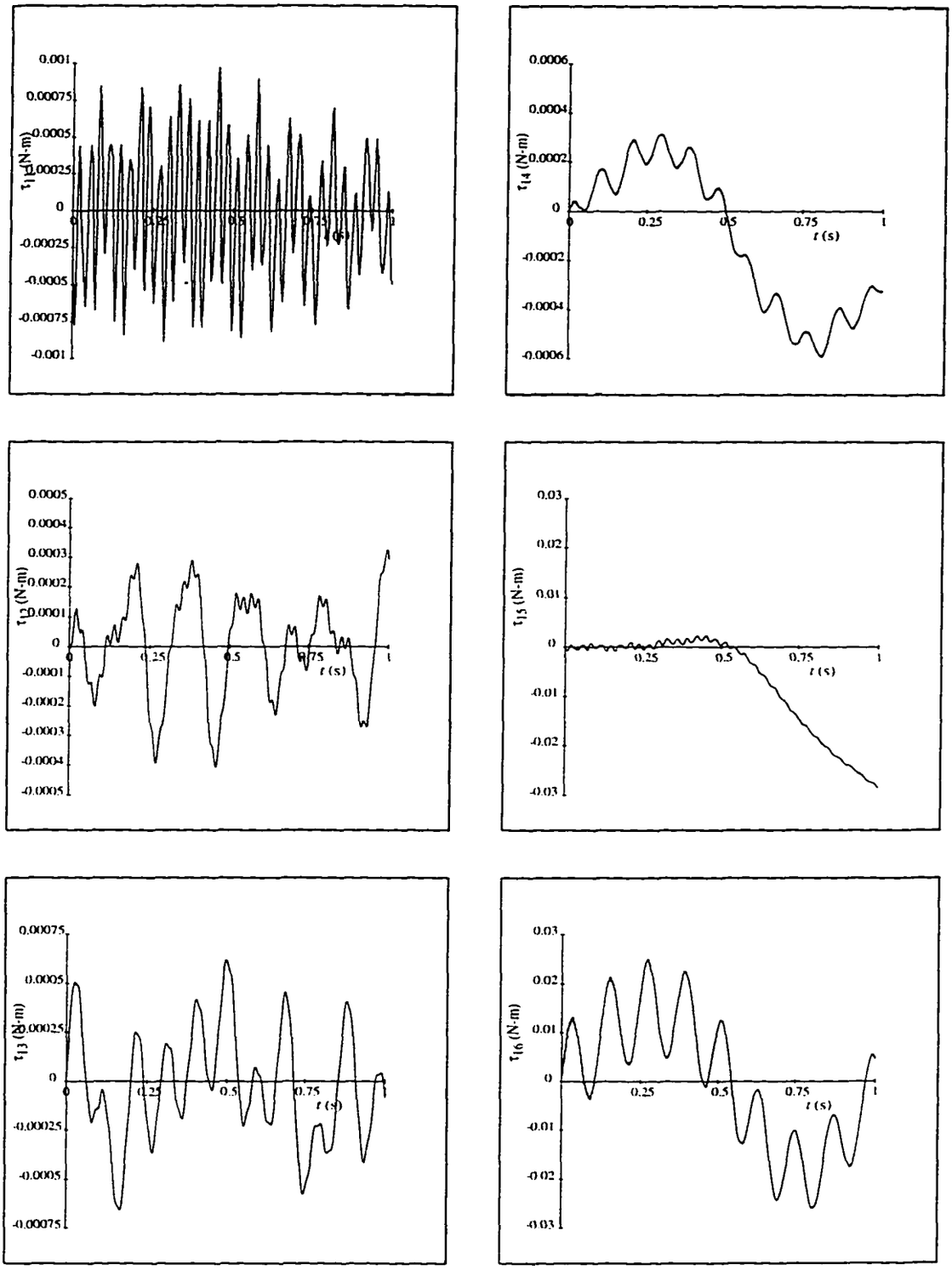

Figure 5.11: Actuator Torques of the Flexible Arm in Case 1

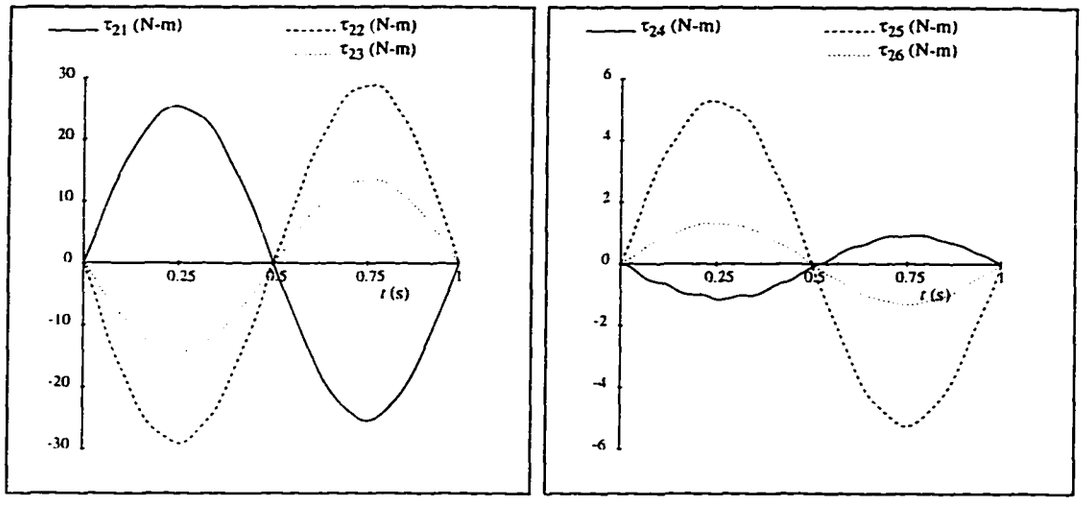

Figure 5.12: Actuator Torques of the Rigid Arm in Case 1

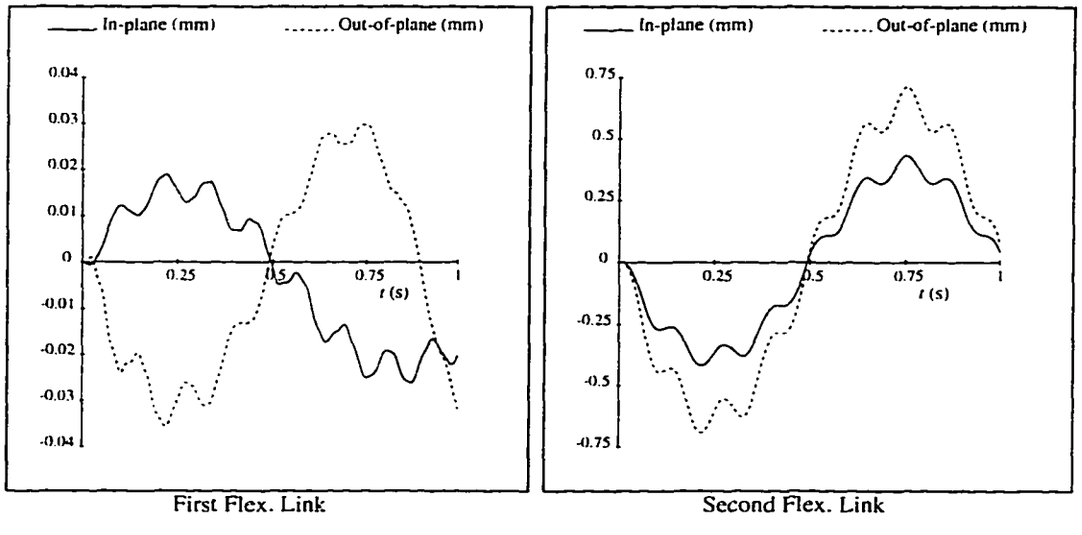

Figure 5.13: Tip Deflections of the Flexible Links in Case 1

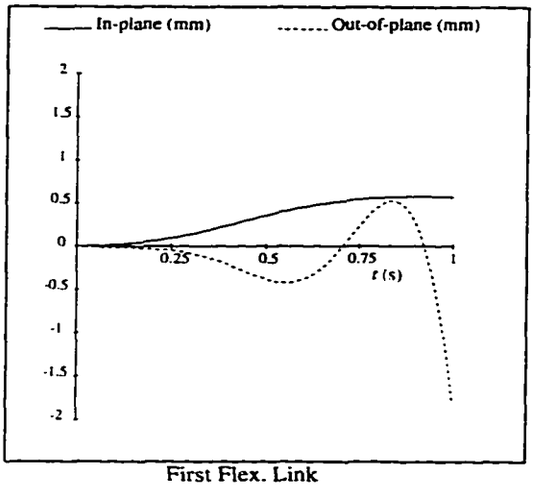

First Flex. Link

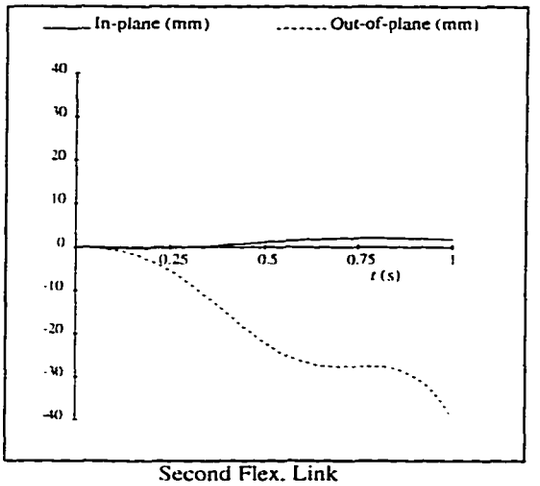

Second Flex. Link

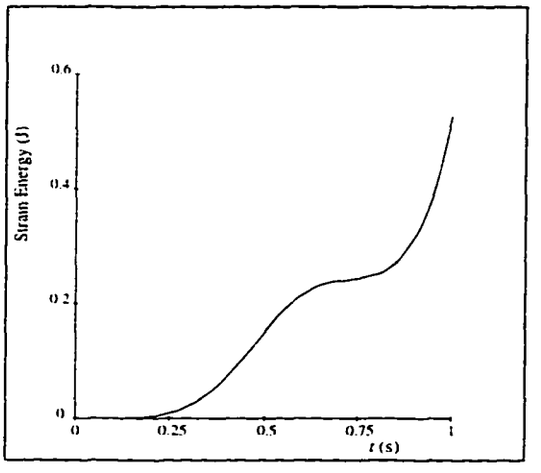

Figure 5.14: Results of Case 2

in the thesis), the following conclusions which are particularly relevant to the force optimization issue for flexible cooperating manipulators may be drawn:

- Minimizing the strain energy is one of the better objectives to use for flexible cooperating manipulators. Strain energy is a more physically meaningful measure than the elastic accelerations. Furthermore, in many cases, the minimum strain energy scheme provides a bounded solution while the other schemes do not.

- Shifting loads from the joint actuators before the last flexible link to beyond the distal end of the last flexible link of the arm helps to obtain a bounded inverse dynamics solution.

- To obtain a bounded solution, either the minimum strain energy or the load shifting scheme should be used in combination with other objectives.

- Systems with different mechanical setups in terms of the location of the flexible links behave differently with the same force optimization scheme.

- For a system with only one flexible link, better behavior is obtained when the flexible link is connected to the base. This can be explained with the same argument as that used to design the load shifting scheme. When the flexible link is closer to the base, there is a better chance that the load can be shifted to beyond its distal end and therefore, the system more closely approximates a collocated situation.

Chapter 6

Stability Approach

One of the important applications of the inverse dynamics solution is for trajectory tracking control of nonlinear dynamics systems. The well-known *computed torque* method [70], also known as *inverse dynamics control* is basically designed to achieve feedback linearization of a nonlinear plant. A prerequisite for this method to be applicable in controlling a robot manipulator is that a bounded solution for the inverse dynamics torques be obtained during the specified time period, which is usually the period over which the reference trajectory is defined. The computed torque technique has been successfully employed to control rigid manipulator systems. For a serial flexible-link manipulator, however, we have observed that the nonlinear inversion of input-output map does not exist because of the nonminimum phase zeros of the input-output map. Hence, the inverse dynamics torques are no longer guaranteed to be bounded.

In this chapter, further discussion on the stability of the inverse dynamics system for flexible manipulator system is performed. In particular, we aim at obtaining a stable inverse dynamics solution for flexible-link cooperating manipulator system with an emphasis on its control applications.

6.1 Description of Internal Dynamics

In the context of control, it is known that the invertability of the input-output map is closely related to the stability of the *zero dynamics*, also called the *internal dynamics* The definition of the zero dynamics is as follows:

Definition 6.1 (Zero Dynamics) [56]

> If we divide the system states into the observable and unobservable parts. the zero dynamics represents the dynamics of the unobservable states when: 1) the input is set equal to zero. and 2) the output is constrained to be identically zero.

As mentioned earlier. the instability of the causal inverse dynamics solution for flexible-link manipulators is due to the inherent nonminimum phase property of the system. Indeed, according to its definition, the nonminimum phase *linear* system is that which has zeros of the input-output transfer function in the right half of s-plane whereas a nonminimum phase *nonlinear* system means that the system has *unstable* zero dynamics. Therefore. stabilizing the internal dynamics (zero dynamics) is related to changing a nonminimum phase system into a minimum phase system for which stable causal inverse dynamics solutions can be obtained.

In tip trajectory tracking control of a flexible manipulator. the output equations are those which define the tip position and orientation. or their first and second derivatives since the latter are easier to formulate. The unobservable state variables are the coordinates and their rates which define the elastic motion. Therefore. the internal dynamics is described by the elastic equations of motion with the joint torques (input) and the tip velocity (output) both set to zero. It is found that the design of a stable closed-loop control scheme is critically dependent on the stability of the internal elastic dynamics [56. 71. 72. 73].

The importance of the elastic response can also be observed when considering the inverse dynamics solution for flexible manipulators. In the inverse dynamics system, the tip motion is predefined (this is also true in multiple-arm systems with rigid grasp). The rigid states (the joint coordinates and speeds, $\boldsymbol{q}_{ri}$ and $\dot{\boldsymbol{q}}_{ri}$) of the i-th manipulator are dependent on the elastic states (elastic coordinates and speeds, $\boldsymbol{q}_{ei}$ and $\dot{\boldsymbol{q}}_{ei}$) through the kinematics relations. The behavior of the inverse dynamics solution, comprising rigid states and actuator torques, is determined by the elastic motion. In other words, if the equations describing the evolution of elastic coordinates produce a stable trajectory in the time domain, the inverse dynamics solution for actuator torques is ensured to be stable as well. To analyze the stability of the internal dynamics, we first present its state-space description. We assume in the following analysis that there are no external forces acting on the manipulator system other than the actuator efforts. This is done in order to exclude the dependency of the system behavior on the external forces.

It can be found in the literature that some researches have focused on modifying the output of the system in order to realize a minimum phase property. Joint-based control [71] accomplishes collocation of the input and output at the joint. Reflected tip position is used to allow precise tracking of a close-to-equivalent tip position [74]. Torque transmission mechanism is also used to transfer the actuation efforts to the tip so that the input is transferred to be collocated with the output [22]. For the multiple arm system, we are interested in investigating the possibility of stabilizing the internal dynamics by actively choosing the tip wrenches. For the purpose of analyzing the inherent properties of various systems, we propose the following three typical cases:

System A: Collocation at the Joints

In this case, actuators are located at the joints and the joint variables (displacements, velocities and accelerations) are predefined as functions of time. This is not impractical and in fact, most of the existing inverse dynamics control schemes for serial flexible manipulators adopt such a scheme. Not only is joint collocation simple to implement since the actuators and sensors can be easily set up at the joints of the manipulator, but more significantly, it results in a stable internal dynamics system. Therefore, a stable closed-loop behavior can be obtained by designing a robust linear PD controller [71, 53]. The principal limitation is that the resulting controller only ensures tracking of a prescribed joint motion. For tip trajectory tracking control, a modification is made to allow precise tracking of the nominal joint trajectory while the dynamics equations describing the elastic motion are written with respect to the moving frames attached to the *virtual* links [35, 29]. Some researchers have tried to control the motion of some virtual point (not a real point on the manipulator) the coordinates of which can be expressed as a linear combination of the joint variables. For example, the reflected tip motion [74] has been used so that a linear combination of the joint motions is predefined and controlled [75, 66].

To put in place this situation in a multiple-arm system, we consider that the manipulators are decoupled to follow their own joint trajectories without interfering with each other. This is imposed because, for a multiple-arm system, the joint coordinates can only be freely specified if the manipulators are not constrained by each other, that is, when there are no constraint wrenches acting at the tip of each manipulator. This seems artificial since the multiple arms are not arranged to cooperate on the common task. However, we do this primarily to gain an understanding on why the internal dynamics is stable in this case.

To investigate the inherent properties of such a system with joint motion specified, we consider the dynamics equation for the elastic motion, eq. (4.2). We assign suffix

Σ to each matrix and vector variable to represent a multiple-arm system, and set $\ddot{q}_{r\Sigma} = \mathbf{0}$ since it is the output of the forward collocated system. The internal dynamics is then described by:

$$\mathbf{M}_{ee\Sigma}\,\ddot{q}_{e\Sigma} + \mathbf{D}_{ee\Sigma}\,\dot{q}_{e\Sigma} + \mathbf{K}_{ee\Sigma}\,q_{e\Sigma} = f_{I,e\Sigma} \tag{6.1}$$

We point out the difference between the nonlinear forcing term in the above equation, $f_{I,e\Sigma}$, and that in eq. (4.2), $f_{I,ext,e\Sigma}$. The latter includes the effect of external forces on the manipulators. It is evident that if eq. (6.1) gives a stable trajectory for $q_{e\Sigma}$, then the inverse dynamics torques τ_{Σ} calculated from the algebraic equation (4.1), will be bounded.

System *B*: Noncollocation of the Joint Actuation and Tip Trajectory

As implied by tip trajectory tracking, the joint variables in this system are not explicitly prescribed. Instead, the desired output is a nonlinear function of both rigid and elastic coordinates. For rigid manipulators, tip tracking control can be implemented by tracking the prescribed joint trajectories since the joint variables are uniquely defined by the tip trajectory (assuming the manipulators are not kinematically redundant). However, this is not the case for flexible-link manipulators because of the unknown elastic variables appearing in the kinematics equations. In a multiple-arm system, the reference trajectory is prescribed for the object. With the assumption of a rigid grasp, this is equivalent to defining the reference trajectory for the respective end-effectors of the arms. To derive the equations of internal dynamics for system *B*, we set $\dot{v}_{\Sigma}$ to zero. In chapter 4, we derived the solution for the elastic accelerations which is represented by eq. (4.9). Expanding this equation by substituting the expressions for $\ddot{q}'_{e\Sigma}$ and $\mathbf{J}^T_{3\Sigma}$ from eq. (3.54) and eq. (4.6), respectively, the governing equation for the elastic motion becomes:

$$\widehat{\mathbf{M}}_{ee\Sigma}\,\ddot{q}_{e\Sigma} + \mathbf{D}_{ee\Sigma}\,\dot{q}_{e\Sigma} + \mathbf{K}_{ee\Sigma}\,q_{e\Sigma} = h_{\Sigma} + \mathbf{J}^T_{e\Sigma} w_{\Sigma} \tag{6.2}$$

where

$$\begin{aligned} \boldsymbol{h}_{\Sigma} &= \mathrm{col}\{\boldsymbol{h}_1, \cdots \boldsymbol{h}_P\} && (6.3)\\ \widehat{\mathbf{M}}_{ee\Sigma} &= \mathrm{diag}\{\widehat{\mathbf{M}}_{ee1}, \cdots . \widehat{\mathbf{M}}_{eeP}\} && (6.4)\\ \boldsymbol{h}_i &= \boldsymbol{f}_{I,ei} + \mathbf{M}_{rei}^T \mathbf{J}_{ri}^{-1}(\dot{\mathbf{J}}_{ri}\,\dot{\boldsymbol{q}}_{ri} + \dot{\mathbf{J}}_{ei}\,\dot{\boldsymbol{q}}_{ei}) && (6.5)\\ \widehat{\mathbf{M}}_{eei} &= \mathbf{M}_{eei} - \mathbf{M}_{rei}^T \mathbf{J}_{ri}^{-1}\mathbf{J}_{ei} && (6.6)\\ & \quad i = 1, 2, \cdots, P \end{aligned}$$

Eq. (6.2) represents the internal dynamics for the system when the actuators and the specified object trajectory are noncollocated.

System C: Collocation at the Tip

This again represents a hypothetical situation where the manipulators are driven by wrenches at the tips. The motivation for investigating such a system is due to the successful design of a stable PD controller by Park and Asada [22] for a one-link flexible arm with the actuator torque transmitted to the tip of the arm. It is implied that the internal dynamics of such a system is stable. To derive the internal dynamics equations for system C, we simply set $\boldsymbol{\tau}_{\Sigma} = \mathbf{0}$ in eq. (4.12) to nullify the actuation at the joints. Solving the resulting equations for the "actuation" at the tip *i.e.*, the tip wrenches $\boldsymbol{w}_{\Sigma}$, we obtain:

$$\begin{aligned} \boldsymbol{w}_{\Sigma} &= -\mathbf{J}_{1\Sigma}^{-T}\boldsymbol{\tau}'_{\Sigma}\\ &= \mathbf{J}_{r\Sigma}^{-T}(\mathbf{M}_{re\Sigma} - \mathbf{M}_{rr\Sigma}\mathbf{J}_{r\Sigma}^{-1}\mathbf{J}_{e\Sigma})\,\ddot{\boldsymbol{q}}_{e\Sigma} && (6.7)\\ &\quad + \mathbf{J}_{r\Sigma}^{-T}(\mathbf{M}_{rr\Sigma}\mathbf{J}_{r\Sigma}^{-1}(\dot{\boldsymbol{v}}_{\Sigma} - \dot{\mathbf{J}}_{r\Sigma}\,\dot{\boldsymbol{q}}_{r\Sigma} - \dot{\mathbf{J}}_{e\Sigma}\,\dot{\boldsymbol{q}}_{e\Sigma}) - \boldsymbol{f}_{I,r\Sigma}) \end{aligned}$$

Upon substituting the above into the elastic dynamics equation (4.14) and setting $\dot{\boldsymbol{v}}_{\Sigma}$ to zero, we obtain:

$$\widetilde{\mathbf{M}}_{ee\Sigma}\,\ddot{\boldsymbol{q}}_{e\Sigma} + \mathbf{D}_{ee\Sigma}\,\dot{\boldsymbol{q}}_{e\Sigma} + \mathbf{K}_{ee\Sigma}\,\boldsymbol{q}_{e\Sigma} = \boldsymbol{g}_{\Sigma} \qquad (6.8)$$

where

$$\widetilde{\mathbf{M}}_{ee\Sigma} = \widehat{\mathbf{M}}_{ee\Sigma} - \mathbf{J}_{e\Sigma}^T \mathbf{J}_{r\Sigma}^{-T} \widehat{\mathbf{M}}_{re\Sigma} \tag{6.9}$$

$$\boldsymbol{g}_\Sigma = \boldsymbol{h}_\Sigma - \mathbf{J}_{e\Sigma}^T \mathbf{J}_{r\Sigma}^{-T} (\boldsymbol{f}_{I,r\Sigma} - \mathbf{M}_{rr\Sigma} \mathbf{J}_{r\Sigma}^{-1} (\dot{\mathbf{J}}_{r\Sigma}\, \dot{\boldsymbol{q}}_{r\Sigma} + \dot{\mathbf{J}}_{e\Sigma}\, \dot{\boldsymbol{q}}_{e\Sigma})) \tag{6.10}$$

In the above, $\widetilde{\mathbf{M}}_{ee\Sigma}$ is symmetric which can be shown by substituting the expressions for $\widehat{\mathbf{M}}_{ee\Sigma}$ and $\widehat{\mathbf{M}}_{re\Sigma}$ into eq. (6.9) to yield:

$$\widetilde{\mathbf{M}}_{ee\Sigma} = \mathbf{M}_{ee\Sigma} - \mathbf{M}_{re\Sigma}^T \mathbf{J}_{r\Sigma}^{-1} \mathbf{J}_{e\Sigma} - \mathbf{J}_{e\Sigma}^T \mathbf{J}_{r\Sigma}^{-T} \mathbf{M}_{re\Sigma} + \mathbf{J}_{e\Sigma}^T \mathbf{J}_{r\Sigma}^{-T} \mathbf{M}_{rr\Sigma} \mathbf{J}_{r\Sigma}^{-1} \mathbf{J}_{e\Sigma} \tag{6.11}$$

and noting that $\mathbf{M}_{rr\Sigma}$ and $\mathbf{M}_{ee\Sigma}$ are both symmetric in nature. As a result, eq. (6.8) describes the internal dynamics of system C in which the manipulators are driven by the wrenches collocated with the specified trajectory at the tip of the end-effectors.

6.2 Properties of the Internal Dynamics

Since closed-form solutions to the internal dynamics equations (6.1), (6.2) or (6.8) do not exist, we shall analyze the behavior of the internal dynamics through an approximation method, in particular, the linearization method in the neighbourhood of *equilibrium points* of the nominal configurations. To develop an effective linearised model of the internal dynamics, it is necessary to identify the properties of the internal dynamics equations by reviewing the procedure for deriving these equations.

For notational convenience, we now drop the suffix Σ used to denote the assembled quantities for the *multiple* manipulator system and focus our discussion on a single "decoupled" manipulator. We note that equations (6.1), (6.2), and (6.8) represent a set of second-order ordinary differential equations for the elastic coordinates $\boldsymbol{q}_r$.

6.2.1 Constant $\mathbf{K}_{ee}$ and $\mathbf{D}_{ee}$

We have observed that when multiple manipulators are in contact with a common object, they form several closed-loop chains. The multi-arm mechanism as a whole is stiffened because of the constraints that manipulators impose on each other. It is therefore reasonable to expect smaller elastic deformations than in the situation where manipulators are decoupled to follow the same end-effector trajectory. Although the present study of the inverse dynamics solution for flexible manipulators is not limited to a particular dynamics model, to render the stability analysis more tractable, we use linear theory of elasticity to derive *body* mass, stiffness and modal damping matrices. Therefore, these body matrices are assumed to be constant.

Furthermore, according to the assembly procedure of the global dynamics equations for a serial-chain manipulator [40], the stiffness and damping matrices in the *global* dynamics equations are formed by placing the body matrices along the diagonals. Therefore, the global stiffness and damping matrices are constant and depend only on the material and geometric properties of the links.

6.2.2 Configuration Dependent $\mathbf{M}_{ee}$, $\widehat{\mathbf{M}}_{ee}$, and $\widetilde{\mathbf{M}}_{ee}$

We consider the coefficient matrices of the acceleration terms in the internal dynamics equations for the foregoing three systems and repeat the expressions for $\mathbf{M}_{ee}$, $\widehat{\mathbf{M}}_{ee}$, and $\widetilde{\mathbf{M}}_{ee}$ as.

$$\mathbf{M}_{ee} = \mathcal{S}_{\Sigma}^{T}\mathcal{T}_{\Sigma}^{T}\mathbf{M}_{\Sigma,re} + \mathbf{M}_{\Sigma,re}^{T}\mathcal{T}_{\Sigma}\mathcal{S}_{\Sigma} + \mathcal{S}_{\Sigma}^{T}\mathcal{T}_{\Sigma}^{T}\mathbf{M}_{\Sigma,rr}\mathcal{T}_{\Sigma}\mathcal{S}_{\Sigma} + \mathbf{M}_{\Sigma,ee} \quad (6.12)$$

$$\widehat{\mathbf{M}}_{ee} = \mathbf{M}_{ee} - \mathbf{M}_{re}^{T}\mathbf{J}_{r}^{-1}\mathbf{J}_{e} \quad (6.13)$$

$$\widetilde{\mathbf{M}}_{ee} = \widehat{\mathbf{M}}_{ee}^{T} - \widehat{\mathbf{M}}_{re}^{T}\mathbf{J}_{r}^{-1}\mathbf{J}_{e} \quad (6.14)$$

Note that in eq. (6.14), we made use of the symmetry of the matrix $\widetilde{\mathbf{M}}_{ee}$. The suffix Σ appearing in eq. (6.12) denotes the assembled quantities over all the *bodies* in a single serial chain. The dependence of these matrices on the configuration variables $\boldsymbol{q}_r$ and $\boldsymbol{q}_e$ is through the coordinate transformation matrices $\boldsymbol{\mathcal{T}}_\Sigma$ and $\boldsymbol{\mathcal{S}}_\Sigma$ and the Jacobian matrices $\mathbf{J}_r$ and $\mathbf{J}_e$. Although generally, these are functions of both $\boldsymbol{q}_r$ and $\boldsymbol{q}_e$, in an approximate situation, they can be evaluated at a nominal rigid configuration while ignoring the effects of elastic deformations. For the same reason that a closed-loop multiple-arm system is stiffer than the individual serial manipulators, we ignore the variation of the body transformation matrices on the body deformations and focus on analyzing the dominant factors governing the internal dynamics. Therefore, the coefficient matrices are assumed to be dependent on *rigid* configurations only.

6.2.3 Nonlinear Inertial Terms

In the equations of internal dynamics, the right hand sides contain the nonlinear inertial forces and in the case of system B, another term of tip wrenches. For the nonlinear inertial forces in eqs. (6.3) and (6.10), we repeat the following expressions for calculating $\boldsymbol{f}_{I,r}$ and $\boldsymbol{f}_{I,e}$ [40]:

$$\boldsymbol{f}_{I,r} = \mathcal{P}_\Sigma{}^T \boldsymbol{\mathcal{T}}_\Sigma{}^T \{ \boldsymbol{f}_{\Sigma,I,r} - \mathbf{M}_{\Sigma,rr}[\dot{\boldsymbol{\mathcal{T}}}_\Sigma(\mathcal{P}_\Sigma \dot{\boldsymbol{q}}_r + \boldsymbol{\mathcal{S}}_\Sigma \dot{\boldsymbol{q}}_e) + \boldsymbol{\mathcal{T}}_\Sigma(\dot{\boldsymbol{\mathcal{S}}}_\Sigma \dot{\boldsymbol{q}}_e + \dot{\mathcal{P}} \dot{\boldsymbol{q}}_r)]\} \quad (6.15)$$

$$\begin{aligned} \boldsymbol{f}_{I,e} = {} & \boldsymbol{\mathcal{S}}_\Sigma{}^T \boldsymbol{\mathcal{T}}_\Sigma{}^T \{ \boldsymbol{f}_{\Sigma,I,r} - \mathbf{M}_{\Sigma,rr}[\dot{\boldsymbol{\mathcal{T}}}_\Sigma(\mathcal{P}_\Sigma \dot{\boldsymbol{q}}_r + \boldsymbol{\mathcal{S}}_\Sigma \dot{\boldsymbol{q}}_e) + \boldsymbol{\mathcal{T}}_\Sigma(\dot{\boldsymbol{\mathcal{S}}}_\Sigma \dot{\boldsymbol{q}}_e + \dot{\mathcal{P}} \dot{\boldsymbol{q}}_r)]\} \\ & + \boldsymbol{f}_{\Sigma,I,e} - \mathbf{M}_{\Sigma,re}[\dot{\boldsymbol{\mathcal{T}}}_\Sigma(\mathcal{P}_\Sigma \dot{\boldsymbol{q}}_r + \boldsymbol{\mathcal{S}}_\Sigma \dot{\boldsymbol{q}}_e) + \boldsymbol{\mathcal{T}}_\Sigma(\dot{\boldsymbol{\mathcal{S}}}_\Sigma \dot{\boldsymbol{q}}_e + \dot{\mathcal{P}} \dot{\boldsymbol{q}}_r)] \end{aligned} \quad (6.16)$$

In the above, $\boldsymbol{f}_{\Sigma,I,r}$ and $\boldsymbol{f}_{\Sigma,I,e}$ are composed of the body nonlinear inertial forces which in turn include only the rigid motion nonlinearities, that is, terms of $O(\| \dot{\boldsymbol{q}}_r \|^2)$. With the earlier assumptions, it is not difficult to see that the nonlinear inertial forces $\boldsymbol{f}_{I,e}$, $\boldsymbol{h}$ and $\boldsymbol{g}$ contain terms that are $O(\| \dot{\boldsymbol{q}}_r \|^2)$ and $O(\| \dot{\boldsymbol{q}}_r \| \| \dot{\boldsymbol{q}}_e \|)$. The coefficients

of these terms are, again, generally functions of the variables q_r and q_e but are approximated to be dependent only on the rigid coordinates q_r.

It is also worth repeating here that in system B, the tip wrenches appear in the internal dynamics equations. Keeping in mind that we have some degrees of freedom in choosing these wrenches, the potential benefit is that these wrenches may be actively chosen to stabilize the internal dynamics which is the key objective of this chapter.

6.3 Linearization

The main purpose of analyzing the internal dynamics for the three different systems described in section 6.2 is to predict whether the internal dynamics possesses a stable behavior. For the multiple-arm system, we are also aiming to find a force distribution scheme which, based on the stability analysis, will ensure improved behavior of the system. However, as shown in section 6.2, the internal dynamics equations are nonlinear even though we made several approximations in deriving them. The analytical solution of the internal dynamics equations is impossible to obtain. In view of the much greater simplicity and tractability of linear, as opposed to nonlinear equations, it is desirable to make use of the linear approximation. The behavior of the solution to the original nonlinear equations about a nominal configuration can be investigated by considering the linearized model.

Reinstating the use of suffix Σ for a multiple-arm system, we now define a vector of state variables of the internal dynamics as:

$$y \triangleq [y_1\ y_2]^T = [q_{e\Sigma}\ \dot{q}_{e\Sigma}]^T \tag{6.17}$$

It is not difficult to rewrite equations (6.1), (6.2), and (6.8) in the form:

$$\dot{\boldsymbol{y}} = \mathbf{f}(\boldsymbol{y}) \tag{6.18}$$

For instance, in system A, the function $\mathbf{f}(\boldsymbol{y})$ on the right hand side of eq. (6.18) is

$$\mathbf{f}_A(\boldsymbol{y}) = \begin{bmatrix} \boldsymbol{y}_2 \\ -\mathbf{M}_{ee\Sigma}^{-1}[(\mathbf{K}_{ee\Sigma}\boldsymbol{y}_1 + \mathbf{D}_{ee\Sigma}\boldsymbol{y}_2) + \boldsymbol{f}_{I,e\Sigma}] \end{bmatrix} \tag{6.19}$$

We emphasize that $\mathbf{f}(\boldsymbol{y})$ is evaluated at a nominal rigid configuration with state variable $\hat{\boldsymbol{q}}_{r\Sigma}$ satisfying the kinematics relations in the absence of elastic deformations and $\dot{\hat{\boldsymbol{q}}}_{r\Sigma} = \mathbf{0}$. Eq. (6.18) also represents an *autonomous* system since time variable t does not appear explicitly in the function $\mathbf{f}$.

Definition 6.2 (Equilibrium Point)

Suppose an autonomous system is described by the vector differential equation

$$\dot{\boldsymbol{y}} = \mathbf{f}(\boldsymbol{y}) \tag{6.20}$$

$\hat{\boldsymbol{y}}$ is said to be an equilibrium point of the system if

$$\mathbf{f}(\hat{\boldsymbol{y}}) = \mathbf{0} \tag{6.21}$$

It can be shown that $\hat{\boldsymbol{y}} = (\hat{\boldsymbol{q}}_{e\Sigma}, \dot{\hat{\boldsymbol{q}}}_{e\Sigma}) = (\mathbf{0}, \mathbf{0})$ is one of the equilibrium points of the internal dynamics equations eqs. (6.1),(6.2) and (6.8). In other cases, for example, where gravity effects have not been dropped, $\hat{\boldsymbol{q}}_{e\Sigma}$ may not be zero but would represent the static deformation of the flexible structure. Analyzing the system behavior in the neighbourhood of equilibrium points is particularly important in the situation where damping out the system vibration at an operating point is of specific interest.

The local stability properties of equilibrium point can be obtained by linearisation. We therefore linearize the internal dynamics equations around the equilibrium point

$(\hat{\boldsymbol{q}}_{e\Sigma}, \dot{\hat{\boldsymbol{q}}}_{e\Sigma}) = (\mathbf{0}, \mathbf{0})$ by taking variations of the variables from the nominal values and letting

$$\ddot{\boldsymbol{q}}_{e\Sigma} = \ddot{\hat{\boldsymbol{q}}}_{e\Sigma} + \delta\ddot{\boldsymbol{q}}_{e\Sigma} \tag{6.22}$$

$$\dot{\boldsymbol{q}}_{e\Sigma} = \dot{\hat{\boldsymbol{q}}}_{e\Sigma} + \delta\dot{\boldsymbol{q}}_{e\Sigma} \tag{6.23}$$

$$\boldsymbol{q}_{e\Sigma} = \hat{\boldsymbol{q}}_{e\Sigma} + \delta\boldsymbol{q}_{e\Sigma} \tag{6.24}$$

$$\boldsymbol{w}_{\Sigma} = \widehat{\boldsymbol{w}}_{\Sigma} + \delta\boldsymbol{w}_{\Sigma} \tag{6.25}$$

We will use eq. (6.2) which is the internal dynamics equation for system B to illustrate the derivation of the linearized model. Expanding eq.(6.2) into a Taylor series, for small variations of the state variables as in eqs. (6.22)-(6.25), the original nonlinear model can be approximated by the first-order expansion about the nominal state. For the sake of simplicity, the circumflex for denoting nominal values is omitted in the following. Thus, we have:

$$\widehat{\mathbf{M}}_{ee\Sigma}\delta\ddot{\boldsymbol{q}}_{e\Sigma} + (\mathbf{D}_{ee\Sigma} + \frac{\partial \boldsymbol{h}_{\Sigma}}{\partial \dot{\boldsymbol{q}}_{e\Sigma}})\delta\dot{\boldsymbol{q}}_{e\Sigma} + \mathbf{K}_{ee\Sigma}\delta\boldsymbol{q}_{e\Sigma} = \mathbf{J}_{e\Sigma}^{T}\delta\boldsymbol{w}_{\Sigma} \tag{6.26}$$

where we observe that $\frac{\partial \boldsymbol{h}_{\Sigma}}{\partial \dot{\boldsymbol{q}}_{e\Sigma}} = \mathbf{0}$ since $\boldsymbol{h}_{\Sigma}$ contains nonlinear coupling terms of $O(\| \dot{\boldsymbol{q}}_{r\Sigma}\| \| \dot{\boldsymbol{q}}_{e\Sigma}\|)$ which vanish when evaluated at $\dot{\hat{\boldsymbol{q}}}_{r\Sigma} = \mathbf{0}$. Once again, all the coefficient matrices in eq. (6.26) are calculated at the nominal states. The resultant linearized model of eq.(6.2) can be written as:

$$\begin{bmatrix} \delta\dot{\boldsymbol{q}}_{e\Sigma} \\ \delta\ddot{\boldsymbol{q}}_{e\Sigma} \end{bmatrix} = \begin{bmatrix} \mathbf{0} & \mathbf{I} \\ -\widehat{\mathbf{M}}_{ee\Sigma}^{-1}\mathbf{K}_{ee\Sigma} & -\widehat{\mathbf{M}}_{ee\Sigma}^{-1}\mathbf{D}_{ee\Sigma} \end{bmatrix} \begin{bmatrix} \delta\boldsymbol{q}_{e\Sigma} \\ \delta\dot{\boldsymbol{q}}_{e\Sigma} \end{bmatrix} + \begin{bmatrix} \mathbf{0} \\ \mathbf{J}_{3\Sigma}^{T} \end{bmatrix} \delta\boldsymbol{w}_{\Sigma} \tag{6.27}$$

In the same manner, the linearized model of system A, that is, the case of joint collocation is described by:

$$\begin{bmatrix} \delta\dot{\boldsymbol{q}}_{e\Sigma} \\ \delta\ddot{\boldsymbol{q}}_{e\Sigma} \end{bmatrix} = \begin{bmatrix} \mathbf{0} & \mathbf{I} \\ -\mathbf{M}_{ee\Sigma}^{-1}\mathbf{K}_{ee\Sigma} & -\mathbf{M}_{ee\Sigma}^{-1}\mathbf{D}_{ee\Sigma} \end{bmatrix} \begin{bmatrix} \delta\boldsymbol{q}_{e\Sigma} \\ \delta\dot{\boldsymbol{q}}_{e\Sigma} \end{bmatrix} \tag{6.28}$$

Finally for system C where the input and output are collocated at the tip, eq. (6.8) is approximated by:

$$\begin{bmatrix} \delta\dot{\boldsymbol{q}}_{e\Sigma} \\ \delta\ddot{\boldsymbol{q}}_{e\Sigma} \end{bmatrix} = \begin{bmatrix} \mathbf{0} & \mathbf{I} \\ -\widetilde{\mathbf{M}}^{-1}_{ee\Sigma}\mathbf{K}_{ee\Sigma} & -\widetilde{\mathbf{M}}^{-1}_{ee\Sigma}\mathbf{D}_{ee\Sigma} \end{bmatrix} \begin{bmatrix} \delta\boldsymbol{q}_{e\Sigma} \\ \delta\dot{\boldsymbol{q}}_{e\Sigma} \end{bmatrix} \tag{6.29}$$

For systems A and C, the linearized model can be written compactly as:

$$\delta\dot{\boldsymbol{y}} = \mathbf{A}\delta\boldsymbol{y} \tag{6.30}$$

It can be seen from eq. (6.27) which is the actual case for multiple flexible arms, that the tip wrenches influence the value of the state variables. The linearized model for system B is accordingly given by

$$\delta\dot{\boldsymbol{y}} = \mathbf{A}\delta\boldsymbol{y} + \mathbf{B}\delta\boldsymbol{w}_{\Sigma} \tag{6.31}$$

where

$$\mathbf{B} = \begin{bmatrix} \mathbf{0} \\ \mathbf{J}^{T}_{3\Sigma} \end{bmatrix} \tag{6.32}$$

The coefficient matrices $\mathbf{A}$ in the three different cases denoted by $\mathbf{A}_A$, $\mathbf{A}_B$ and $\mathbf{A}_C$ respectively are:

$$\mathbf{A}_A = \begin{bmatrix} \mathbf{0} & \mathbf{I} \\ -\mathbf{M}^{-1}_{ee\Sigma}\mathbf{K}_{ee\Sigma} & -\mathbf{M}^{-1}_{ee\Sigma}\mathbf{D}_{ee\Sigma} \end{bmatrix} \tag{6.33}$$

$$\mathbf{A}_B = \begin{bmatrix} \mathbf{0} & \mathbf{I} \\ -\widehat{\mathbf{M}}^{-1}_{ee\Sigma}\mathbf{K}_{ee\Sigma} & -\widehat{\mathbf{M}}^{-1}_{ee\Sigma}\mathbf{D}_{ee\Sigma} \end{bmatrix} \tag{6.34}$$

$$\mathbf{A}_C = \begin{bmatrix} \mathbf{0} & \mathbf{I} \\ -\widetilde{\mathbf{M}}^{-1}_{ee\Sigma}\mathbf{K}_{ee\Sigma} & -\widetilde{\mathbf{M}}^{-1}_{ee\Sigma}\mathbf{D}_{ee\Sigma} \end{bmatrix} \tag{6.35}$$

The differences between these are in the "mass" matrix which premultiplies the stiffness and damping matrices, that is, the matrices $\mathbf{M}_{ee\Sigma}$, $\widehat{\mathbf{M}}_{ee\Sigma}$ and $\widetilde{\mathbf{M}}_{ee\Sigma}$. For system

B. since we have some freedom in choosing the tip wrenches and in particular, if they are chosen to be a function of the state variables $q_{e\Sigma}$ and $\dot{q}_{e\Sigma}$, then it is possible to change the inherent behavior of the linearized internal dynamics around the equilibrium points.

6.4 Stability Issue Revisited

We stated in chapter 3 that in considering the inverse dynamics solution, we were particularly interested in obtaining a bounded solution when a bounded input is applied. From a practical point of view, it is perhaps more useful to require that the solution be bounded over a specified *finite* time interval. In terms of the behavior of the internal dynamics of the inverse dynamics system about an equilibrium point, what is more relevant is whether the elastic variables will approach zero as time goes to infinity. At this point, it is necessary to review some definitions and related stability theorems.

6.4.1 Stability of Linear Time-Invariant Systems

Definition 6.2 (Stable Equilibrium)

An equilibrium point $\hat{\boldsymbol{y}}$ is *stable* if, given any $\epsilon > 0$, there exists $\delta > 0$ such that $|\boldsymbol{y}(0) - \hat{\boldsymbol{y}}| < \delta$ implies $|\boldsymbol{y}(t) - \hat{\boldsymbol{y}}| < \epsilon$ for all $t > 0$.

The physical interpretation of a stable equilibrium point is that a trajectory described by eq. (6.18) can be made to remain within an arbitrarily small region about $\hat{\boldsymbol{y}}$ by starting sufficiently close to it.

Definition 6.3 (Asymptotically Stable Equilibrium)

For a stable equilibrium point $\hat{\boldsymbol{y}}$, if there exists $\Delta > 0$ such that $|\boldsymbol{y}(0) - \hat{\boldsymbol{y}}| < \Delta$

implies that $\boldsymbol{y}(t) \rightarrow \hat{\boldsymbol{y}}$ as $t \rightarrow \infty$, then the equilibrium point $\hat{\boldsymbol{y}}$ is said to be asymptotically stable.

Evidently, asymptotic stability requires that a trajectory starting in a sufficiently close region of the equilibrium point not only remain close enough to $\hat{\boldsymbol{y}}$, but that it also approaches $\hat{\boldsymbol{y}}$ asymptotically.

If the original nonlinear system (6.18) is approximated by a *time-invariant* linear system at the equilibrium point, it is well-known that the local stability of the equilibrium point $\hat{\boldsymbol{y}}$ of the given nonlinear system can be examined by checking the eigenvalues of the plant matrix $\mathbf{A}$. The system is unstable if $\mathbf{A}$ has at least one eigenvalue with a positive real part and it is asymptotically stable if all the eigenvalues of $\mathbf{A}$ have negative real parts. If some of the eigenvalues are purely imaginary and the others have negative real parts, then the linearization technique is inconclusive. In this case, the stability of the equilibrium is determined by the higher order terms that are neglected in the linearization process.

For end-point positioning control, the dynamics model is required at the desired terminal rigid configuration. In many trajectory tracking control algorithms the dynamics model of the system must be evaluated at several nominal rigid configurations. In this case, linear time-invariant equations approximating the nonlinear equations are obtained at the equilibrium $\hat{\boldsymbol{y}} = [\hat{\boldsymbol{q}}_{e\Sigma}\ \dot{\hat{\boldsymbol{q}}}_{e\Sigma}]^T$. These applications justify the analysis of the linearized internal dynamics of the inverse dynamics problem and we therefore concentrate on calculating the eigenvalues of the plant matrix $\mathbf{A}$. It should be realized that since the linear model is configuration dependent, ideally, we should check the complete workspace of the manipulator for the stability status at the equilibrium points. However, because of certain properties of the linearised system, there exist certain patterns of the eigenvalues of the plant matrix, which will be discussed shortly.

Table 6.1: Stable Eigenvalues of $\mathbf{A}_A$

Eigenvalues	$\lambda_{1,2}$	$\lambda_{3,4}$	$\lambda_{5,6}$	$\lambda_{7,8}$
$\zeta = 0$	$\pm 3032.45j$	$\pm 842.25j$	$\pm 20.54j$	$\pm 8.72j$
$\zeta = 0.5\%$	$-12.9 \pm 3032.43j$	$-3.1 \pm 842.24j$	$-0.0036 \pm 20.54j$	$-0.05 \pm 8.72j$

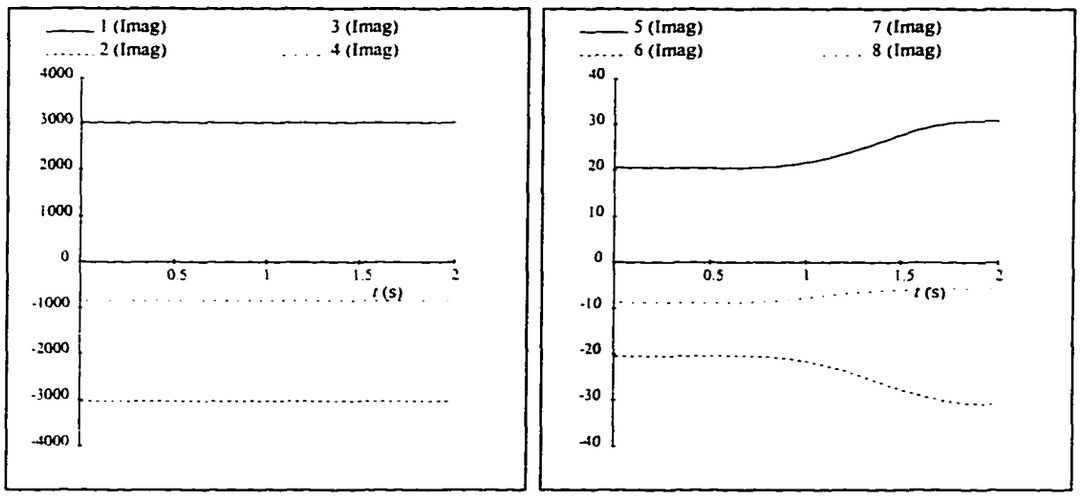

Figure 6.1: Eigenvalues of System A

6.4.2 Configuration Dependent Eigenvalues

We now present some sample results obtained for the planar dual-arm architecture used in the previous chapter (FRR-O-RRF). As before, the trajectory specified for the end-effectors is to rotate the object about its mass center through 90° in 2 seconds. For systems A and C, the two arms are not carrying the object but are required to follow the same trajectory as if they were handling a common object. Since the flexible link in each arm is modeled with two planar beam elements and hence 4 elastic degrees of freedom in total, the number of eigenvalues of the plant matrices is 8. The eigenvalues of the undamped system are calculated along the trajectory and shown for systems A, C and B in Figure 6.1-6.3 respectively.

Table 6.2: Stable Eigenvalues of $\mathbf{A}_C$

Eigenvalues	$\lambda_{1,2}$	$\lambda_{3,4}$	$\lambda_{5,6}$	$\lambda_{7,8}$
$\zeta = 0$	$\pm 5275.49j$	$\pm 2162.64j$	$\pm 582.75j$	$\pm 77.11j$
$\zeta = 0.5\%$	$-321.0 \pm 5753.35j$	$-58.5 \pm 2162.84j$	$-5.5 \pm 582.81j$	$-0.05 \pm 77.11j$

For system A, where the actuators and the specified trajectories are collocated at the joints, the eigenvalues of the undamped system are purely imaginary since in eq. (6.28), the mass and stiffness matrices are symmetric and positive definite. Indeed, the eigenvalues λ of the plant matrix are related to the natural frequencies of the arm by:

$$\lambda_j^2 = -\omega_i^2 \qquad i = 1, \cdots, S \qquad j = (2i-1), 2i \tag{6.36}$$

where $\omega_i \geq 0$ is the ith modal frequency and S is the total number of elastic coordinates used to model the flexible links of the arm. It is also known that when damping is included, the eigenvalues are shifted to the left half of the complex plane since the damping matrix $\mathbf{D}_{ee_\Sigma}$ is always positive definite. Table 6.1 compares the eigenvalues of the plant matrix $\mathbf{A}_A$ at the initial configuration, with and without damping. We therefore conclude that system A is always stable since this is ensured by the aforementioned properties of the system matrices. Figure 6.1 also shows that the eigenvalues vary little with the rigid configurations.

Figure 6.2 illustrates the eigenvalues for plant C (eq. (6.29)) — a system where actuators and the specified trajectories are collocated at the tip of the end-effector. Interestingly, we have verified numerically that matrix $\widetilde{\mathbf{M}}_{ee_\Sigma}$ possesses similar properties to the mass matrix $\mathbf{M}_{ee_\Sigma}$, in particular, it is also symmetric and positive definite. The same conclusion as for plant A can be drawn for the system with collocation at the tip: the nonlinear equations of motion in the region of equilibrium points are stable (See also Table 6.2).

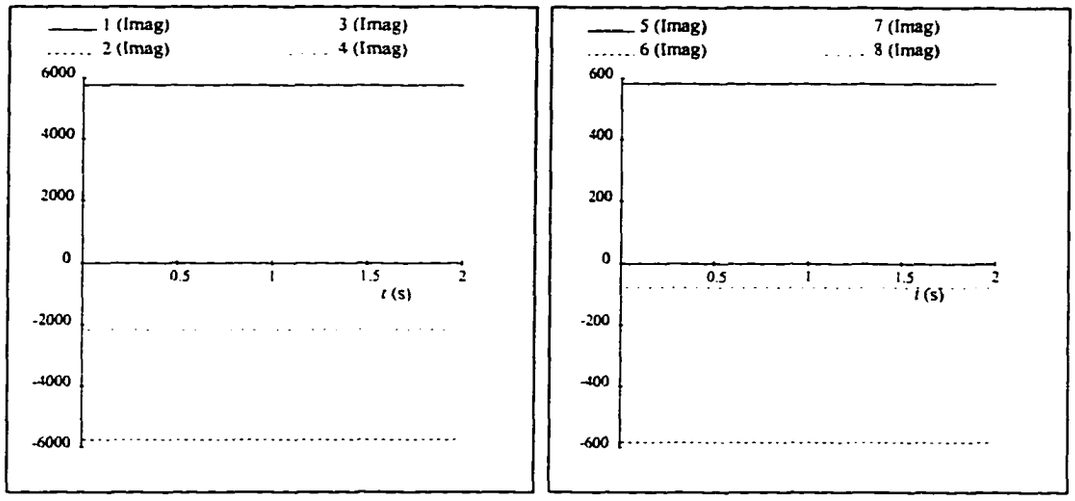

Figure 6.2: Eigenvalues of System C

Figure 6.3 illustrates the eigenvalues of the plant matrix $\mathbf{A}_B$. The linearized model for system B is characterized by $\mathbf{A}_B$ if the tip wrenches are *independent* of the elastic state variables ($\boldsymbol{q}_{e\Sigma}$, $\dot{\boldsymbol{q}}_{e\Sigma}$) since then the second term on the right hand side of eq. (6.27) vanishes. From Figure 6.3, we conclude that if the tip wrenches aren't chosen to vary with the elastic state variables, the internal dynamics at equilibrium points are unstable because of the eigenvalues in the right half s-plane. We also note from Figures 6.3 and 6.2 that the eigenvalues of the corresponding linearised systems are nearly constant with the rigid configuration.

6.4.3 Changing the Linear Plant of System B by Force Distribution Schemes

In chapter 5, we discussed and demonstrated the performance of various optimization schemes used for force distribution to determine the tip wrenches. As it turns out, some of the schemes are not effective for flexible cooperating manipulator systems.

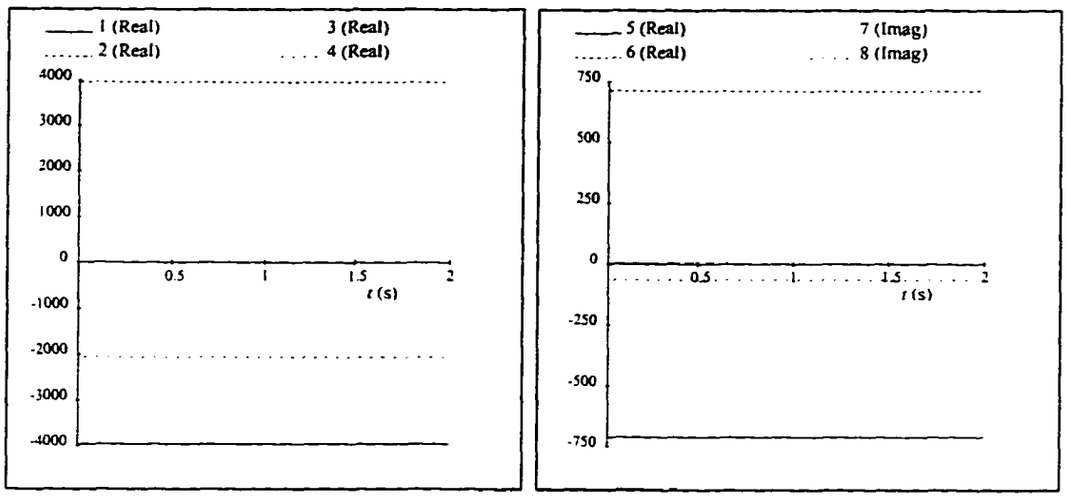

Figure 6.3: Eigenvalues of System B

For example, a scheme which only considers minimizing the internal forces produces unbounded inverse dynamics solutions. We have also shown that some other schemes designed to account for the dynamics variables of the manipulators, yield bounded solutions. This motivated us to consider the following question. What is the connection between the behavior of the inverse dynamics solution and the stability of the linearized system? To look for the answer, we consider how the tip wrenches produced by different optimization schemes affect the plant matrix of the linear system. Let the tip wrenches be a function of $\boldsymbol{y}$, and therefore

$$\delta \boldsymbol{w}_{\Sigma} = \frac{\partial \boldsymbol{w}_{\Sigma}}{\partial \boldsymbol{y}} \delta \boldsymbol{y} \tag{6.37}$$

Substituting the above into eq. (6.31), the linearized model for a real situation of multiple-arm and object system is characterized by the following plant matrix:

$$\mathbf{A} = \mathbf{A}_B + \mathbf{B} \frac{\partial \boldsymbol{w}_{\Sigma}}{\partial \boldsymbol{y}} \tag{6.38}$$

In chapter 5, the tip wrenches are obtained as the optimal solution of the linearly-constrained quadratic optimization problem. To find out how the tip wrenches $\boldsymbol{w}_{\Sigma}$

are related to the internal state variables $\boldsymbol{y}$, we repeat eq. (5.9).

$$\boldsymbol{w}_\Sigma^* = \mathbf{W}^{-1}\mathbf{A}_1^T(\mathbf{A}_1\mathbf{W}^{-1}\mathbf{A}_1^T)^{-1}(\mathbf{A}_1\mathbf{W}^{-1}\mathbf{c} + \mathbf{b}_1) - \mathbf{W}^{-1}\mathbf{c}$$

where $\mathbf{A}_1$ is the grasp matrix. Since matrix $\mathbf{A}_1$ is not related to the elastic variables of the manipulators, the dependence of $\boldsymbol{w}_\Sigma^*$ on $\boldsymbol{y}$ can only be due to the weighting matrix $\mathbf{W}$ and the column matrix $\mathbf{c}$. In the minimum internal force scheme, $\mathbf{W}$ is an identity matrix while $\mathbf{c}$ is a zero vector. From eq. (6.38), the plant matrix in this case is equal to $\mathbf{A}_B$ which has previously been demonstrated to be unstable, thereby explaining why this approach yields unbounded solutions. It is evident that in order to improve the behavior of the inverse dynamics system, the tip wrenches must be chosen to be functions of the elastic variables.

Let us now consider the optimal load sharing scheme for which the objective function is characterized by (eq. (5.22)):

$$\hat{\mathbf{c}}_T = \mathbf{J}_{1\Sigma}\mathbf{W}_T\boldsymbol{\tau}'_\Sigma \qquad\qquad \widehat{\mathbf{W}}_T = \mathbf{J}_{1\Sigma}\mathbf{W}_T\mathbf{J}_{1\Sigma}^T$$

where $\mathbf{W}_T$ is a constant matrix. By ignoring the dependence of $\mathbf{J}_{1\Sigma}$ on $\boldsymbol{q}_{e\Sigma}$, as was done in deriving the linear internal dynamics equations, the partial derivative of $\boldsymbol{w}_\Sigma^*$ with respect to $\boldsymbol{y}$ is obtained as

$$\begin{aligned}\frac{\partial \boldsymbol{w}_\Sigma^*}{\partial \boldsymbol{y}} &= (\widehat{\mathbf{W}}_T{}^{-1}\mathbf{A}_1^T(\mathbf{A}_1\widehat{\mathbf{W}}_T{}^{-1}\mathbf{A}_1^T)^{-1}\mathbf{A}_1 - \mathbf{1})\widehat{\mathbf{W}}_T{}^{-1}\frac{\partial \hat{\mathbf{c}}_T}{\partial \boldsymbol{y}} \\ &\triangleq \mathbf{A}_W\frac{\partial \hat{\mathbf{c}}_T}{\partial \boldsymbol{y}} \end{aligned} \tag{6.39}$$

Eq. (3.52) for calculating $\boldsymbol{\tau}'_\Sigma$ for a multiple-arm system can be rewritten as:

$$\boldsymbol{\tau}'_\Sigma = -\widehat{\mathbf{M}}_{re\Sigma}\widehat{\mathbf{M}}_{ee\Sigma}^{-1}(\mathbf{K}_{ee\Sigma}\,\boldsymbol{q}_{e\Sigma} + \mathbf{D}_{ee\Sigma}\,\dot{\boldsymbol{q}}_{e\Sigma}) + \hat{\mathbf{g}}_\Sigma$$

where $\hat{\mathbf{g}}_\Sigma$ includes the nonlinear terms of $O(\|\dot{\boldsymbol{q}}_{r\Sigma}\|^2)$, and $O(\|\dot{\boldsymbol{q}}_{e\Sigma}\|^2)$ as well as the coupling terms of $O(\|\dot{\boldsymbol{q}}_{r\Sigma}\;\dot{\boldsymbol{q}}_{e\Sigma}\|)$. Taking the partial derivative of $\boldsymbol{\tau}'_\Sigma$ with respect to

$\boldsymbol{y}$, eq. (6.39) becomes:

$$\frac{\partial \boldsymbol{w}_\Sigma^*}{\partial \boldsymbol{y}} = \mathbf{A}_W \mathbf{J}_{1\Sigma} \mathbf{W}_T \widehat{\mathbf{M}}_{re\Sigma} \begin{bmatrix} -\widehat{\mathbf{M}}_{ee\Sigma}^{-1} \mathbf{K}_{ee\Sigma} & -\widehat{\mathbf{M}}_{ee\Sigma}^{-1} \mathbf{D}_{ee\Sigma} \end{bmatrix} \tag{6.40}$$

Substituting the above into eq. (6.27), the plant matrix of the noncollocated multiple-arm inverse system becomes:

$$\begin{aligned} \mathbf{A} &= \mathbf{A}_B + \mathbf{B} \frac{\partial \boldsymbol{w}_\Sigma^*}{\partial \boldsymbol{y}} \\ &= \mathbf{A}_B + \begin{bmatrix} \mathbf{0} \\ \mathbf{J}_{3\Sigma}^T \end{bmatrix} \mathbf{A}_W \mathbf{J}_{1\Sigma} \mathbf{W}_T \widehat{\mathbf{M}}_{re\Sigma} \begin{bmatrix} -\widehat{\mathbf{M}}_{ee\Sigma}^{-1} \mathbf{K}_{ee\Sigma} & -\widehat{\mathbf{M}}_{ee\Sigma}^{-1} \mathbf{D}_{ee\Sigma} \end{bmatrix} \\ &= \begin{bmatrix} \mathbf{0} & \mathbf{1} \\ -(\mathbf{1} + \mathbf{J}_{3\Sigma}^T \mathbf{A}_W \mathbf{J}_{1\Sigma} \mathbf{W}_T \widehat{\mathbf{M}}_{re\Sigma}) \widehat{\mathbf{M}}_{ee\Sigma}^{-1} \mathbf{K}_{ee\Sigma} & -(\mathbf{1} + \mathbf{J}_{3\Sigma}^T \mathbf{A}_W \mathbf{J}_{1\Sigma} \mathbf{W}_T \widehat{\mathbf{M}}_{re\Sigma}) \widehat{\mathbf{M}}_{ee\Sigma}^{-1} \mathbf{D}_{ee\Sigma} \end{bmatrix} \end{aligned} \tag{6.41}$$

The above equation can be written compactly as

$$\mathbf{A} = \mathbf{A}_T \mathbf{A}_B \tag{6.42}$$

where

$$\mathbf{A}_T = \begin{bmatrix} \mathbf{1} & \mathbf{0} \\ \mathbf{0} & \mathbf{1} + \mathbf{J}_{3\Sigma}^T \mathbf{A}_W \mathbf{J}_{1\Sigma} \mathbf{W}_T \widehat{\mathbf{M}}_{re\Sigma} \end{bmatrix} \tag{6.43}$$

The plant matrix in eq. (6.42) represents that for the linearized model of the internal dynamics when optimal load sharing scheme is applied to determine the grasping wrenches within the system.

As shown in Example 5.3, we successfully implemented a torque shifting scheme for the dual-arm system with one arm flexible and the other rigid. This scheme minimizes the norm of actuator torques of the flexible arm. The idea underlying the torque shifting scheme is that it emulates a collocated situation where the flexible arm is driven by the tip wrenches (applied through the object by the rigid arm). While we were unable to establish analytically a relationship between the eigenvalues

of the plant matrix in eq. (6.42) for this scheme and for the collocated system $\mathbf{A}_C$, numerical experiments revealed some interesting results. One interesting observation was that the eigenvalues of the two plants were identical. However, based on this special case, we cannot draw a general conclusion that one can predict the behaviour of the nonlinear system from the eigenvalues of the linear plant matrix.

Table 6.3 lists the eigenvalues of the plant matrix of eq. (6.42) calculated for two load sharing schemes and different mechanical setups of the flexible dual-arm system. Since the eigenvalues do not change significantly along the trajectory, we include here sample calculations at the beginning of the trajectory only. From Table 6.3, we conclude that minimizing $\boldsymbol{\tau}_1^T\boldsymbol{\tau}_1$ is effective for one flexible and one rigid arm but becomes ineffective if both arms are flexible. However, minimizing $\boldsymbol{\tau}_\Sigma^T\boldsymbol{\tau}_\Sigma$ gives unstable eigenvalues for all three setups.

In the same way, we can formulate the plant matrix which corresponds to the optimization scheme which minimizes the norm of the elastic accelerations. Towards this end, we first express $\frac{\partial \boldsymbol{w}^*}{\partial \boldsymbol{y}}$ as:

$$\frac{\partial \boldsymbol{w}^*}{\partial \boldsymbol{y}} = \mathbf{A}_W \mathbf{J}_{3\Sigma} \mathbf{W}_E \frac{\partial \ddot{\boldsymbol{q}}'_{e\Sigma}}{\partial \boldsymbol{y}} \tag{6.44}$$

Then, the corresponding plant matrix is obtained as

$$\mathbf{A} = \mathbf{A}_E \mathbf{A}_B \tag{6.45}$$

where

$$\mathbf{A}_E = \begin{bmatrix} 1 & 0 \\ 0 & 1 + \mathbf{J}_{3\Sigma}^T \mathbf{A}_W \mathbf{J}_{3\Sigma} \mathbf{W}_E \end{bmatrix} \tag{6.46}$$

Similarly, the scheme of minimum strain energy yields a plant matrix

$$\mathbf{A} = \mathbf{A}_U \mathbf{A}_B \tag{6.47}$$

Table 6.3: Eigenvalues of **A** with Minimum Norm of Torque Scheme

Optimization Scheme	Mechanical Setup		
	FRR-O-RRR	RFR-O-RRR	FRR-O-RRF
	$\mathbf{A}_{T\,8\times8}$	$\mathbf{A}_{T\,8\times8}$	$\mathbf{A}_{T\,16\times16}$
$\min \boldsymbol{\tau}_1^T \boldsymbol{\tau}_1$	$\pm 5752.49j$ $\pm 2161.64j$ $\pm 582.74j$ $\pm 77.11j$	$\pm 5754.24j$ $\pm 2165.48j$ $\pm 595.77j$ $\pm 124.84j$	± 3958.27 ± 2059.26 ± 710.94 ± 582.74 -3.1×10^{-12} $\pm 2161.64j$ -2.1×10^{-9} $\pm 5752.49j$ $\pm 77.11j$ $\pm 64.39j$
$\min \boldsymbol{\tau}_\Sigma^T \boldsymbol{\tau}_\Sigma$	$2741.0 \pm 1352.4j$ $-2741.0 \pm 1352.4j$ ± 489.6 $\pm 64.5j$	$1680.3 \pm 2351.0j$ $-1680.3 \pm 2351.0j$ ± 383.0 $\pm 49.6j$	± 3958.0 $2326.1 \pm 2211.9j$ $-2326.1 \pm 2211.9j$ ± 2059.6 ± 710.8 ± 229.1 $\pm 57.7j$ $\pm 64.3j$

Table 6.4: Eigenvalues for Various Optimization Schemes

Objective Function	Mechanical Setup			
	FRR-O-RRR	RFR-O-RRR	FRR-O-RRF	FFR-O-RRR
$\ddot{q}_e^T \ddot{q}_e$	56.5	1178.1	0.1	4.0×10^{-8}
$U(\Delta t = 0.0002)$	0.77	59.8	0.1	5.7×10^{-10}
$\tau_\Sigma^T \tau_\Sigma + \ddot{q}_e^T \ddot{q}_e$	0.25	0.12	1.96	0.6
$\tau_1^T \tau_1 + U$	1.7×10^{-8}	0.0	$1424.1 \pm 1994.1j$	1.5×10^{-7}

with

$$\mathbf{A}_U = \begin{bmatrix} \mathbf{1} & \mathbf{0} \\ \mathbf{0} & \mathbf{1} + \frac{1}{2}\Delta t^2 \mathbf{J}_{3\Sigma}^T \mathbf{A}_W \mathbf{J}_{3\Sigma} \mathbf{K}_{ee\Sigma} \end{bmatrix} \tag{6.48}$$

We note in the above, that the plant matrix $\mathbf{A}$ in eq. (6.47) depends on the value of Δt. Recall that Δt is used in the minimum strain energy scheme to approximate elastic coordinates in terms of velocities and accelerations at the previous step. For a better approximation, one would expect that Δt should be as small as possible within the requirements of computational efficiency. However, from eq. (6.48) we observe that as Δt becomes very small, the matrix $\mathbf{A}_U$ approaches identity and the plant matrix $\mathbf{A}$ reduces to $\mathbf{A}_B$ which in turn is unstable. Indeed, this phenomenon was verified numerically when we implemented the scheme of minimum strain energy — decreasing Δt below a certain value would result in unbounded solutions. Based on our experience with the simulations, it is found $\Delta t = 0.0002$ sec is a suitable value in most of the cases.

The eigenvalues of the plant matrices in eq. (6.45) and eq. (6.47) have been calculated for various mechanical setups and for several of the optimization schemes with which inverse dynamics solutions were attempted. In Table 6.4, we present for each case only the eigenvalue which has the largest real part. We shall adopt the term *almost stable* [75] to refer to the eigenvalues with a very small positive real part. In

this case, the internal dynamics is said to be *very lightly unstable* and a linear stabilizer can still be applied to obtain a stable closed-loop behavior [75]. From Table 6.4, we observe that minimizing a combined objective of the total strain energy and the norm of the actuator torques of the left arm ($\boldsymbol{\tau}_l^T\boldsymbol{\tau}_l + U$) gives stable or almost stable behavior of the linearized system except for the setup where both arms have the base link flexible. This is predictable since minimizing the torque in one arm results in a heavier burden on the other arm which also has a flexible link. Very likely, the elastic vibrations are excited first in the arm whose actuators are required to supply the majority of the torques which the system needs. Although our previous findings indicated that minimizing the norm of the actuator torques alone (min. $\boldsymbol{\tau}_\Sigma^T\boldsymbol{\tau}_\Sigma$) was not feasible, the results in Table 6.4 show that minimizing the combination of $\boldsymbol{\tau}_\Sigma^T\boldsymbol{\tau}_\Sigma$ and $\ddot{\boldsymbol{q}}_{e\Sigma}^T\ddot{\boldsymbol{q}}_{e\Sigma}$ produces an almost stable linearized internal dynamics. Furthermore, minimizing the strain energy U has better performance than minimizing the norm of elastic accelerations $\ddot{\boldsymbol{q}}_{e\Sigma}^T\ddot{\boldsymbol{q}}_{e\Sigma}$. This is in complete accordance with our conclusions in chapter 5.

6.5 Stability Approach

The stability analysis based on the eigenvalues of the plant matrices of the linearised models shows some agreement with the conclusions of other researchers and those drawn from the numerical results in chapter 5. These can be summarized as follows:

- Collocation at either the joints (system A) or at the tip (system C) of a serial flexible manipulator ensures a stable behavior of the nonlinear internal dynamics at the equilibrium points.
- Noncollocation of the joint actuators with the specified tip trajectory (system B) results in unstable behavior of the internal dynamics.

- For cooperating flexible manipulators, stability properties of the system can be modified by optimizing the force distribution. This essentially allows us to choose the relationship between the tip wrenches and the internal state $\boldsymbol{y}$.

- Depending on the optimization scheme used, the force distribution solution may produce a stable or unstable behavior of the system. Agreement in stability characteristics has been demonstrated between nonlinear simulation and the eigenvalues of the plant matrices of the linearized system.

- Various mechanical arrangements of flexible and rigid links produce responses with different stability characteristics. Again agreement has been demonstrated between directly solving the nonlinear equations and calculating the eigenvalues of the linear plant matrix. For a manipulator with only one flexible link, better behavior is obtained when this link is located closer to the base.

- Although the internal dynamics is defined as the dynamics of the internal states when both input and output are set to zero, the stability of the internal dynamics around equilibrium still allows us to predict the behavior of the inverse dynamics system along a nominal trajectory. Once again, this is supported by the agreement we obtained between the inverse dynamics solution via optimization approach and the stability analysis of the corresponding linear system.

Motivated by the above, we set out to find a force distribution scheme which would allow the tip wrench $\boldsymbol{w}_{\Sigma}$ to be dependent on the states so as to give a stable plant matrix of the linearised system.

6.5.1 Changing the Plant Matrix

Recall from chapter 4, that the grasping wrenches can be calculated as

$$\boldsymbol{w}_\Sigma = \mathbf{A}_1^+ \mathbf{b}_1 + \mathbf{A}_1^N \mathbf{z} \tag{6.49}$$

where the arbitrarily chosen vector $\mathbf{z}$ in the null space of $\mathbf{A}_1$ represents the degrees of freedom in determining the grasping wrenches. Based on the stability analysis, it is apparent that it would be desirable to let the tip wrenches vary in a way which forces the plant matrix of the manipulator system to be equal to the plant matrix of the system with tip collocation. This requires that we set:

$$\mathbf{A} = \mathbf{A}_C = \mathbf{A}_B + \mathbf{B}\frac{\partial \boldsymbol{w}_\Sigma}{\partial \boldsymbol{y}} \tag{6.50}$$

From eq. (6.49), the partial derivative of $\boldsymbol{w}_\Sigma$ with respect to $\boldsymbol{y}$ should satisfy

$$\frac{\partial \boldsymbol{w}_\Sigma}{\partial \boldsymbol{y}} = \mathbf{A}_1^N \frac{\partial \mathbf{z}}{\partial \boldsymbol{y}} \triangleq \mathbf{A}_1^N \mathbf{K} \tag{6.51}$$

where $\mathbf{K}$ is an arbitrary matrix of dimension $6P \times \Sigma_{i=1}^{P} S_i$. With this approach, we essentially attempt to vary the internal force in the multiple arm system in accordance with the internal state variables $\boldsymbol{y}$. Substituting eq. (6.51) into eq. (6.50), we have

$$\mathbf{A}_C = \mathbf{A}_B + \mathbf{B}\mathbf{A}_1^N \mathbf{K} \triangleq \mathbf{A}_B + \mathbf{B}'\mathbf{K} \tag{6.52}$$

Solving for $\mathbf{K}$ from the above and replacing $\mathbf{A}_B$ and $\mathbf{A}_C$ with eq. (6.34) and eq. (6.35) respectively leads to:

$$\mathbf{K} = (\mathbf{J}_{3\Sigma}^T \mathbf{A}_1^N)^+ \mathbf{G} \tag{6.53}$$

with

$$\mathbf{G} = \begin{bmatrix} -(\widetilde{\mathbf{M}}_{ee\Sigma}^{-1} - \widehat{\mathbf{M}}_{ee\Sigma}^{-1})\mathbf{K}_{ee\Sigma} & -(\widetilde{\mathbf{M}}_{ee\Sigma}^{-1} - \widehat{\mathbf{M}}_{ee\Sigma}^{-1})\mathbf{D}_{ee\Sigma} \end{bmatrix} \tag{6.54}$$

Substituting eq.(6.53) back into eq.(6.49) gives the following solution for $\boldsymbol{w}_\Sigma$:

$$\boldsymbol{w}_\Sigma = \mathbf{A}_1^+ \mathbf{b}_1 + \mathbf{A}_1^N (\mathbf{J}_{3\Sigma}^T \mathbf{A}_1^N)^+ \mathbf{G}\boldsymbol{y} \tag{6.55}$$

with $\boldsymbol{y} = [\boldsymbol{q}_{e\Sigma}^T \; \dot{\boldsymbol{q}}_{e\Sigma}^T]^T$.

Whether the above grasping wrenches will guarantee a stable solution of the inverse dynamics depends on the properties of matrix $\mathbf{J}_{3\Sigma}^T \mathbf{A}_1^N$. Here, $\mathbf{J}_{3\Sigma}^T$ is of dimension $\Sigma_{i=1}^P S_i \times 6P$ where recall S_i denotes the total number of elastic coordinates of arm i. The dimension of $\mathbf{A}_1^N$ is $6P \times \dim N(\mathbf{A}_1)$. It is also known that $\dim N(\mathbf{A}_1)$, the dimension of the null space of $\mathbf{A}_1$ is equal to the order of the actuation redundancy of the system. Therefore, the rank of $\mathbf{J}_{3\Sigma}^T \mathbf{A}_1^N$ must satisfy the inequality below:

$$rank(\mathbf{J}_{3\Sigma}^T \mathbf{A}_1^N) \leq min(\Sigma_{i=1}^P S_i, \dim N(\mathbf{A}_1)) \tag{6.56}$$

Assuming, as is usually the case, that $\mathbf{J}_{3\Sigma}^T \mathbf{A}_1^N$ is not rank deficient, we can define the following cases:

- $\Sigma_{i=1}^P S_i = \dim N(\mathbf{A}_1)$

  In this case, $(\mathbf{J}_{3\Sigma}^T \mathbf{A}_1^N)^+ = (\mathbf{J}_{3\Sigma}^T \mathbf{A}_1^N)^{-1}$ and eq.(6.55) has a unique solution for $\boldsymbol{w}_\Sigma$ which satisfies the requirements of both the primary task (handling the common object) and secondary task (stabilizing the elastic motions).

- $\Sigma_{i=1}^P S_i < \dim N(\mathbf{A}_1)$

  When the order of actuation redundancy is greater than the number of elastic coordinates in the system, there is an infinite number of choices for $\mathbf{K}$ which will produce the plant matrix $\mathbf{A}$ equal to $\mathbf{A}_C$. The extra degrees of freedom in choosing $\mathbf{K}$ can be further used to accomplish other tasks, such as, minimizing the actuator torques or the elastic deformations.

- $\Sigma_{i=1}^P S_i > \dim N(\mathbf{A}_1)$

  This is the case when the degree of actuation redundancy is insufficient to alter the plant matrix of the linearized model exactly as desired. Instead, eq.(6.55) will produce a close (in the least-square sense) approximation of $\mathbf{A}$ to $\mathbf{A}_C$. This, however, does not guarantee a stable behavior of the elastic motion.

Example 6.1 — Varying the plant matrix

We now implement the force distribution scheme of eq.(6.55) to solve the inverse dynamics problem. We consider the planar dual-arm example (RFR-O-RRR), first introduced in section 4.5.1 to demonstrate its performance. The elastic link is modeled with one beam element which allows considering stretching and bending deformations. This gives a total of 3 elastic coordinates. The same trajectory profile as described in section 4.5.1 (rotating the object for 90° in 2 seconds) is employed to specify the object trajectory. As mentioned earlier, the degrees of actuation redundancy for a planar dual-arm is 3 which is the same as the total number of elastic coordinates. From the aforementioned conditions, it is concluded that there exists a unique solution for grasping wrenches which will generate the plant matrix of the linearized elastic motion identical to that of a collocated system C'. The solutions for actuator torques, the elastic coordinates and the tip moment are shown in Figures 6.4 and 6.5. From Figure 6.4, we observe that in the present case, the actuators of the rigid arm (right column in the figure) contribute more to moving the object that those of the flexible arm. The same conclusion can be made by comparing (5a) with (5b) in Figure 6.5 for the tip moment. This means that in order for the joint actuated flexible arm to have the same behavior as that of the tip collocated system, driving forces for controlling the flexible arm must be shifted towards the end-effector of the flexible arm. Plot (5f) of figure 6.5 shows the actual trajectory of the object generated by calculated actuator torques.

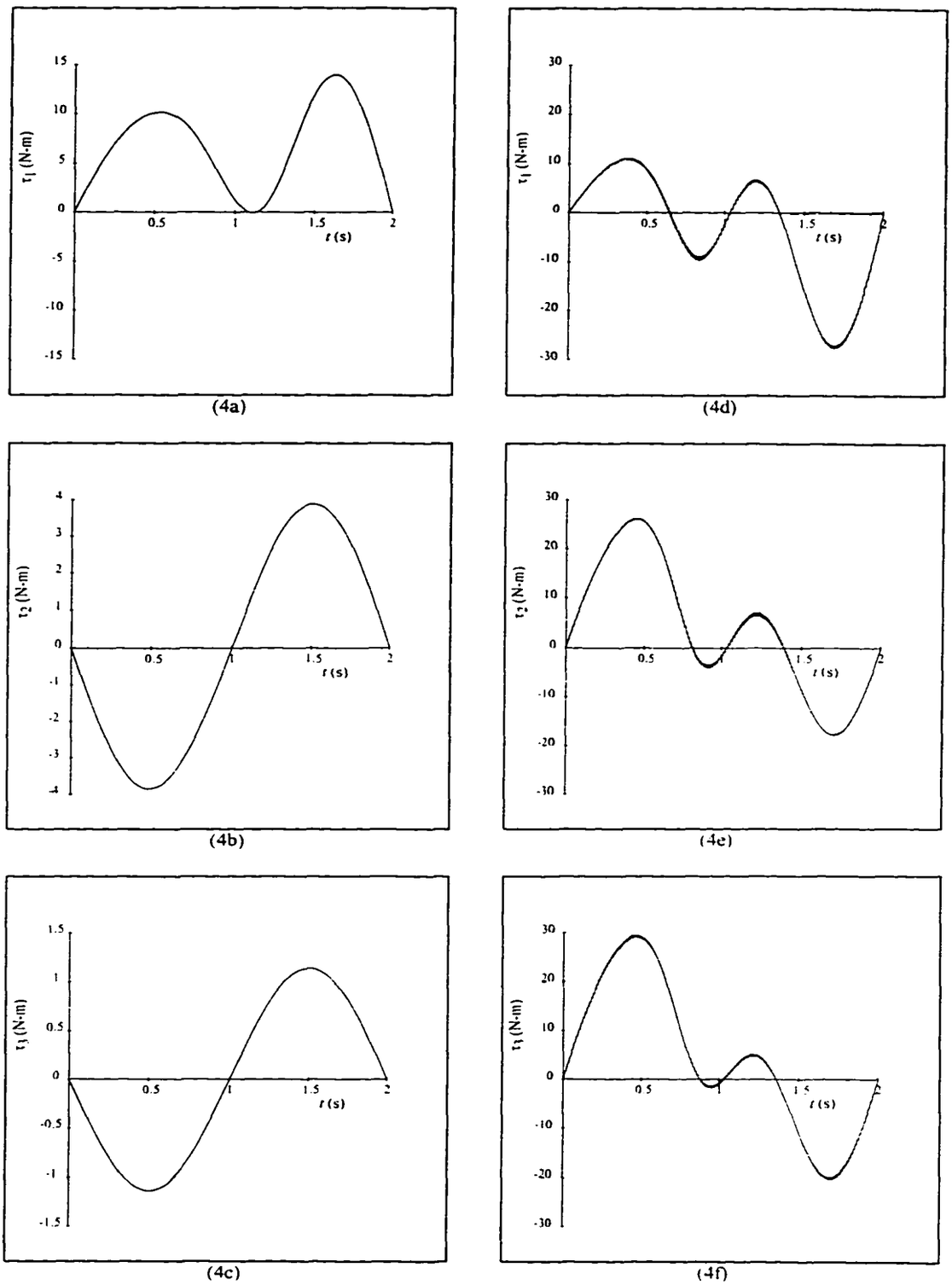

Figure 6.4: Actuator Torques via Stability Approach

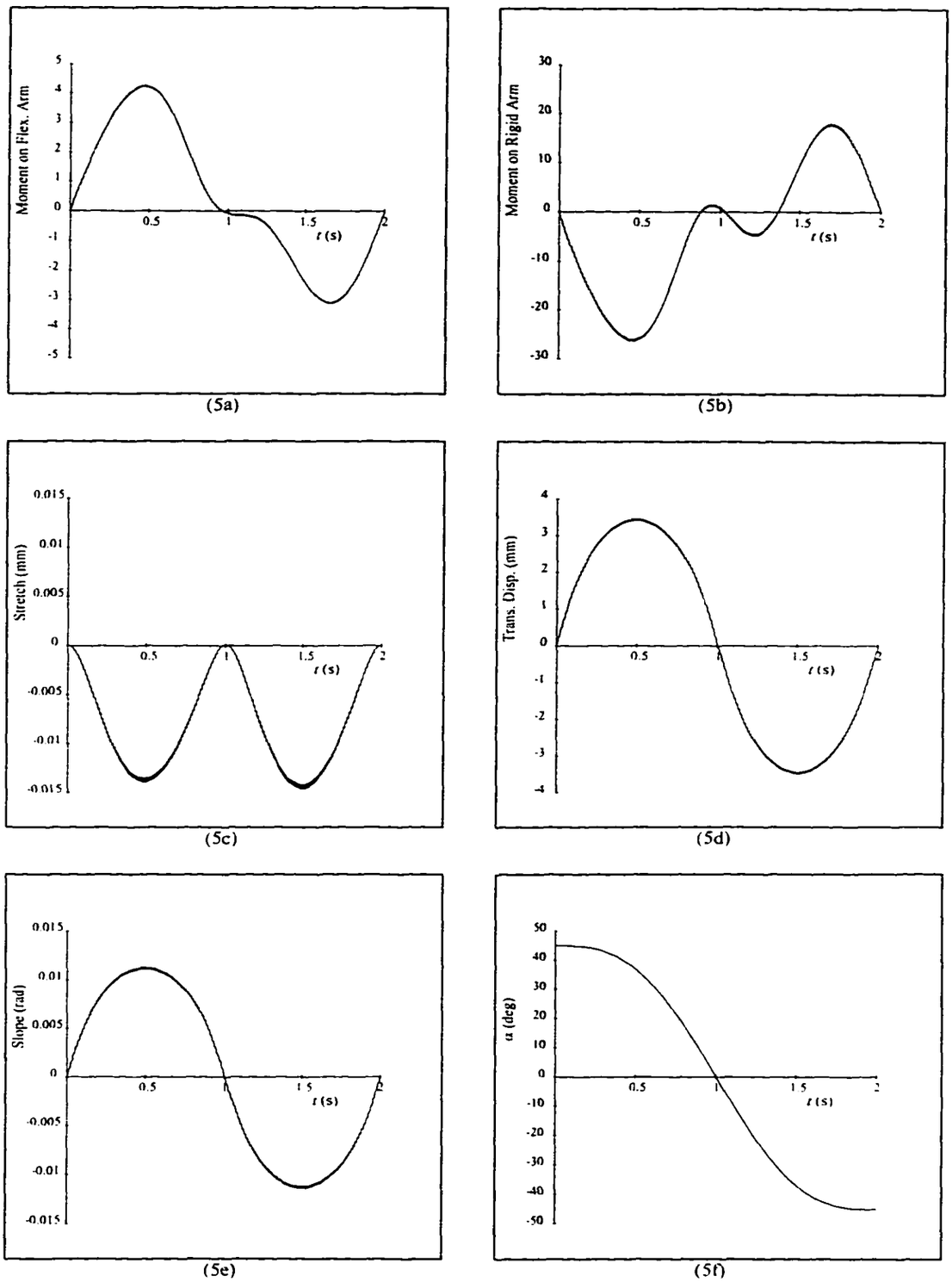

Figure 6.5: Stable Elastic Motion via Stability Approach

Chapter 7

Conclusions

The present work has focused on investigating the inverse dynamics solutions for multiple cooperating manipulators with flexible links. Although extensive studies have been carried out in the past on the rigid cooperating manipulators, little has been done to account for the structural flexibility in the manipulators. Including link flexibility in the analysis is not a trivial extension of the case for a rigid multiple arm system. In fact, the key issues which motivated this study were the complications introduced by the structural flexibility in the inverse dynamics problem and the ways in which redundant actuation could be used to improve the dynamics behavior of the system.

We began by modeling the dynamics of the system. These dynamics are composed of two parts: that of the manipulators and that of the commonly grasped object. The dynamics equations of the manipulators are formulated in terms of the generalized coordinates for every serial chain while the coupling effects between the serial arms are represented by the grasping wrenches applied to the object. The rigid and elastic Jacobian matrices are derived which transform the Cartesian space tip wrenches into the generalized forces associated with the generalized coordinates.

To gain a thorough understanding of the inverse dynamics problem in the presence of link flexibility, the analytical approach to the inverse dynamics problem of a flexible single-link arm was formulated. Both the state space description and the input-output relation are derived for a flexible beam. The latter was used to identify the issue of causality and the resulting the instability of the causal inverse dynamics solution. Correlation between the instability and the collocation of the input and output was demonstrated by expressing the dependency of the nonminimum phase zeros of the forward system on the location of the prescribed trajectory relative to the joint. Upon comparing the advantages and disadvantages of the noncausal and causal solutions, and in view of the potential of a multiple arm system to improve the causal behavior, the causal solution for the inverse dynamics of the multiple flexible arm system was adopted in this study.

In chapter 4, the inverse dynamics solution is formulated for a multiple flexible arm system. In particular, the inverse dynamics torques as well as the rigid and elastic accelerations are found to be a combination of those required to achieve a prescribed object trajectory and those associated with the required tip wrenches, which in turn are determined by a force distribution scheme. The underdeterminacy of the inverse dynamics problem is revealed by comparing the number of unknowns with the number of equations used to obtain the solution. It is also demonstrated, for kinematically non-redundant manipulators rigidly grasping the object, that the degree of redundant actuation is equal to the degree of freedom in choosing the tip wrenches as well as the dimension of the internal force vector.

Therefore, the inverse dynamics problem which determines the actuator torques necessary to realize a desired motion of the object in a multiple arm system admits an infinite number of solutions. Unlike the rigid case, different solutions affect the dynamics behaviors of the arms due to the flexibility of the arms. The problem is

then formulated as a linearly constrained optimization problem by choosing the tip wrenches as the design variables. Quadratic programming is employed to solve the resulting optimization problem in light of its simplicity, uniqueness of the optimal solution and computational efficiency. Besides the objectives commonly used for rigid cooperating manipulators, special attention is given to improving the dynamics behavior of the flexible manipulator system, in particular, to reducing and stabilizing the system vibrations. We illustrate with various numerical examples that the minimum strain energy, minimum weighted norm of elastic accelerations and the optimal load sharing schemes are effective in achieving these goals.

Stability of the internal dynamics of a inverse dynamics system is then investigated in chapter 6. The internal dynamics is described by the equations of elastic motion in the absence of both input (tip trajectory) and the output (joint actuator torques). Linearization was used to approximate the state space trajectories around equilibrium points. In many cases, the stability status of the nonlinear internal dynamics in the neighbourhood of equilibrium points can be determined by the eigenvalues of the plant matrix of the linearized system. In fact, agreement in the behavior of the inverse dynamics system was obtained between directly solving the nonlinear dynamics equations and by calculating the eigenvalues of the linear plant matrix. The stability analysis helped to explain why some of the optimization schemes are not suitable for flexible multiple-arm systems, for example, minimizing the internal force alone cannot be used as the objective of the optimization problem. In practice, calculating the eigenvalues of the plant matrix of the linearized internal dynamics allows us to predict the behavior of the nonlinear inverse dynamics system in response to various force distribution schemes.

In view of the application of the inverse dynamics solution in control of nonlinear dynamics systems, a stability approach was proposed to actively distribute grasping

wrenches in such a way that the plant matrix of the linearized internal dynamics is stable. The idea here is that tip wrenches should vary in accordance with the states of the internal dynamics. In the case where the degree of actuation redundancy is equal to or larger than the total number of elastic coordinates, stable internal dynamics can be ensured by the stability approach. Numerical examples were used to illustrate the performance of the stability approach.

Directions for Future Work

It is known that for a rigid cooperating manipulator system, actuation redundancy resolution is formulated as a local optimization problem. The solution for forces and moments at $t = t_1$ does not affect the solution at $t > t_1$. By contrast, introducing link flexibility causes a drastic change in the characteristics of the force optimization problem. Because of the different behaviors of the internal dynamics in response to different sets of forces and moments (the grasping wrenches), the actuation redundancy resolution is no longer local in nature. Determination of the grasping wrenches at $t = t_1$ influences the solution of force optimization problem at $t > t_1$. Therefore, force optimization problem for flexible cooperating manipulator systems should be further investigated by formulating it as a *global* optimization problem, that is, with a cost function optimized over the complete trajectory of the object.

Possible selections of the cost function would be the elastic deflection of the system over the whole trajectory which would serve as a criterion for minimum excitation of the system vibration. It can also be viewed as a means of avoiding unstable inverse dynamics solution. It would also be interesting to compare the global force optimization approach with Bayo's noncausal inverse dynamics solution and to determine if there is any correlation between the two approaches. From the practical standpoint, it would be significant to determine if there exists a local optimization

approach which approximates the solution to the global optimization problem in order to combine the merits of the global solution with the computational simplicity of the local optimization.

To demonstrate the significance of the proposed inverse dynamics solution for flexible-link cooperating manipulator systems, it would also be worthwhile to extend the present work to the control of a flexible-link cooperating manipulator system. Especially relevant is the application of the stability approach presented in chapter 6. Performance of this approach can be better illustrated by implementing it together with a robust controller which guarantees that the states of the system stay in a region close to the equilibrium point. Further development of this approach would also consider cases where the degree of actuation redundancy is less than the number of elastic coordinates.

Another extension of the present work is to investigate cases where joint flexibility is significant. Justification for considering the structural flexibility in either the manipulator links or the joints or both lies in the relevant applications. For instance, in space applications, link flexibility is dominant because of the requirement for long and slender manipulator structure. By contrast, in most industrial manipulators, joint flexibility is more prominent because of the elastic transmission components and because the links of industrial manipulators tend to be heavy and stiff. However, when manipulators are required to move at fast speeds, both joint and link flexibilities could significantly affect the performance of the system. Although control of cooperating manipulators with flexible joints has been tackled by some researchers [76, 77], consideration of both joint and link flexibility in the manipulators has been left unaddressed.

References

[1] W. J. Book. Controlled motion in an elastic world. *Journal of Dynamic Systems, Measurement, and Control*, 115:252-261, 1993.

[2] A. J. Koivo and G. A. Bekey. Report of workshop on coordinated multiple robot manipulators: Planning, control, and applications. *IEEE Journal of Robotics and Automation*, 4(1):91-93, February 1988.

[3] A. R. Fraser and R. W. Daniel. *Perturbation Techniques for Flexible manipulators*. Kluwer Academic Publishers, 1991.

[4] Ping Hsu. Control of multi-manipulator systems - trajectory tracking, load distribution, internal force control, and decentralized architecture. In *Proceedings of IEEE Intternational Conference on Robotics and Automation*, volume 2, pages 1234-1239, 1989.

[5] O. Al-Jarrah, Y. F. Zheng, and K-Y. Yi. Efficient trajectory planning for two manipulators to deform flexible materials with experiments. In *Proceedings 1995 IEEE International Conference on Robotics and Automation*, volume 1, pages 312-317, Nagoya, Aichi, Japan, May 1995.

[6] M. T. Mason and J. K. Salisbury. *Robot Hands and the Mechanics of Manipulation*. MIT Press, 1985.

[7] Zexiang Li, Ping Hsu, and Shankar Sastry. Grasping and coordinated manipulation by a multifingered robot hand. *The International Journal of Robotics Research*, 8(4):33-49, 1989.

[8] Y. Nakamura. *Advanced Robotics: Redundancy and Optimization*. Addison-Welsley Publishing Company, 1991.

[9] Y. F. Zheng and J. Y. S. Luh. Optimal load distribution for two industrial robots handling a single object. In *Proceedings of the 1988 IEEE International Conference on Robotics and Automation*, pages 344-349, Philadelphia, Pa., 1988.

[10] T. E. Alberts and D. I. Soloway. Force control of a multi-arm robot system. In *Proceedings of the 1988 IEEE International Conference on Robotics and Automation*, pages 1490–1496, Philadelphia, Pa, 1988.

[11] K. Kreutz and A. Lokshin. Load balancing and closed chain multiple arm control. In *Proceedings of the 1988 American Control Conference*, pages 2148–2155, 1988.

[12] W. S. Lu and Q. H. M. Meng. An improved load distribution scheme for coordinating manipulators. In *Proceedings 1993 IEEE International Conference on Robotics and Automation*, pages 523–528, Atlanta, Georgia, May 1993.

[13] D. E. Orin and S. Y. Oh. Control of force distribution in robotic mechanisms containing closed kinematic chains. *Journal of Dynamic Systems, Measurement, and Control*, 103(2):134–141, 1981.

[14] M. Nahon and J. Angeles. Real-time force optimization in parallel kinematic chains under inequality constraints. *IEEE Transactions on Robotics and Automation*, 8(4):439–450, 1992.

[15] Y. Nakamura, K. Nagai, and T. Yoshikawa. Mechanics of coordinative manipulation by multiple robotic mechanisms. In *Proceedings 1987 IEEE International Conference on Robotics and Automation*, pages 991–998, Raleigh, 1987.

[16] J. Y. S. Luh and Y. F. Zheng. Load distribution between two coordinating robots by nonlinear programming. In *Proceedings of the 1988 American Control Conference*, pages 479–482, Atlanta, Georgia, June 1988.

[17] M. Nahon and J.Angeles. Minimization of power losses in cooperating manipulators. *Journal of Dynamic Systems, Measurement, and Control*, 114:213–219, 1992.

[18] Q. Sun, M. Nahon, and I. Sharf. Force optimization in multi-armed manipulators with flexible links. In *Intelligent Automation and Soft Computing*, pages 183–187, Hawaii, August 1994.

[19] Q. Sun, I. Sharf, and M. Nahon. A stable solution for the inverse dynamics problem of flexible-link cooperating manipulators. In *Proceedings of the 15th Canadian Congress of Applied Mechanics*, volume 1, pages 798–799, Victoria, B.C., May 1995.

[20] R. H. Cannon and E. Schmitz. Initial experiments on the end-point control of a flexible one-link robot. *The International Journal of Robotics Research*, 3(3):62–75, 1984.

[21] E. Bayo. A finite-element approach to control the end-point motion of a single-link flexible robot. *Journal of Robotic Systems*, 4:63–75, 1987.

[22] J.-H. Park and H. Asada. Dynamic analysis of noncollocated flexible arms and design of torque transmission mechanisms. *Journal of Dynamic Systems, Measurement, and Control*, 116:201–207, 1994.

[23] J. Wittenburg. *Dynamics of Systems of Rigid Bodies.* B. G. Teubner Stuttgart, 1977.

[24] A. A. Shabana. *Dynamics of Multibody Systems.* John Wiley & Sons, 1989.

[25] E. Bayo, J. G. de Jalon, and M. Serna. A modified lagrangian formulation for the dynamic analysis of constrained mechanical systems. *Computer Methods in Applied Mechanics and Engineering*, 71:183–195, 1988.

[26] J. Y. S. Luh and Y. F. Zheng. Computation of input generalized forces for robots with closed-kinematic chain mechanisms. *IEEE Journal of Robotics and Automation*. RA-a(2):95–103, June 1985.

[27] Y. Nakamura and M. Ghodoussi. Dynamics computation of closed-link robot mechanisms with nonredundant and redundant actuators. *IEEE Transactions on Robotics and Automation*, 5(3):294–302, June 1989.

[28] S. S. Kim and E. J. Haug. A recursive formulation for flexible multibody dynamics, part ii: Closed-loop system. *Computer Methods in Applied Mechanics and Engineering*, 74:251–269, 1989.

[29] E. Bayo, P. Papadopoulos, J. Stubbe, and M. A. Serna. Inverse dynamics and kinematics of multi-link elastic robots: An iterative frequency domain approach. *The International Journal of Robotics Research*, 8(6):49–62, 1989.

[30] R. J. Williams and A. Seireg. Interactive modeling and analysis of open or closed loop dynamic systems with redundant actuators. *Journal of Mechanical Design*, 101:407–416, July 1979.

[31] S. Hayati. Hybrid position/force control of multi-arm cooperating robots. In *Proceedings 1986 IEEE International Conference on Robotics and Automation*, pages 82–89, San Fransisco, April 1986.

[32] Y. Nakamura. Minimizing object strain energy for coordination of multiple robotic manipulators. In *Proceedings of the 1988 American Control Conference*, pages 499–504, 1988.

[33] C. D. Kopf. Two-arm hybrid position/force control with dynamic compensation. In *Proceedings of the Second International Symposium on Robotics and Manufacturing*, pages 371–381, Albuquerque, NM, 1988.

[34] Dong-Soo Kwon and Wayne J. Book. A time-domain inverse dynamic tracking control of a single-link flexible manipulator. *Journal of Dynamic Systems, Measurement, and Control*, 116:193–200, June 1994.

[35] H. Asada, Z.-D. Ma, and H. Tokumaru. Inverse dynamics of flexible robot arms: Modeling and computation for trajectory control. *Journal of Dynamic Systems, Measurement, and Control*, 112:177–185, June 1990.

[36] Liang-Wey Chang and J. F. Hamilton. The kinematics of robotic manipulators with flexible links using an equivalent rigid link system (ERLS) model. *Journal of Dynamic Systems, Measurement, and Control*, 113:48–52, March 1991.

[37] F. Xi and R. G. Fenton. A sequential integration method for inverse dynamic analysis of flexible link manipulators. *Proceedings 1993 IEEE International Conference on Robotics and Automation*, 3:473–478, May 1993.

[38] P. C. Hughes and G. B. Sincarsin. Dynamics of an elastic multibody chain: Part A - body motion equations. *Dynamics and Stability of Systems*, 4(3 & 4):209–226, 1989.

[39] W. J. Book. Recursive lagrangian dynamics of flexible manipulator arms. *The International Journal of Robotics Research*, 3(3):87–101, 1984.

[40] P. C. Hughes and G. B. Sincarsin. Dynamics of an elastic multibody chain: Part B - global dynamics. *Dynamics and Stability of Systems*, 4(3 & 4):227–244, 1989.

[41] T. Yoshikawa. *Foundation of Robotics — Analysis and Control*. Corona Publishing Co. Ltd., 1988.

[42] W. Sunada and S. Dubowsky. The application of finite element methods to the dynamic analysis of flexible spatial and co-planar linkage systems. *Journal of Mechanical Design*, 103:643–651, July 1981.

[43] D. Wang and M. Vidyasagar. Modeling of a 5-bar-linkage manipulator with one flexible link. In *Proceedings 1988 IEEE International Conference on Robotics and Automation*, volume 1, pages 21–26, 1988.

[44] A. A. Shabana. Dynamics of flexible bodies using generalized newton-euler equations. *Journal of Dynamic Systems, Measurement, and Control*, 112(3):496–503, 1990.

[45] C. Damaren and I. Sharf. Simulation of flexible-link manipulators with inertial and geometric nonlinearities. *Journal of Dynamic Systems, Measurement, and Control*, 117:74–87, March 1995.

[46] B. Gebler. Feed-forward control, strategy for an industrial robot with elastic links and joints. In *Proceedings 1987 IEEE International Conference on Robotics and Automation*, pages 923–928, Raleigh, NC., April 1987.

[47] C.-H. Menq and J. Chen. Precision tracking control of discrete time nonminimum-phase systems. In *Proceedings of the 1992 American Control Conference*, pages 1097–1101, Chicago, Il, June 1992.

[48] S. N. Singh and A. A. Schy. Decomposition and state variable feedback control of elastic robotic systems. In *Proceedings of the 1985 American Control Conference*, pages 375–380, Boston, MA, June 1985.

[49] D. Wang and M. Vidyasagar. Control of a class of manipulators with a single flexible link — part I: Feedback linearization. *Journal of Dynamic Systems, Measurement, and Control*, 113:655–661, December 1991.

[50] D. Chen. An iterative solution to stable inversion of nonminimum phase systems. In *Proceedings of the 1993 American Control Conference*, pages 2960–2964. San Francisco, CA, June 1993.

[51] Y. Stepanenko and M. Vukovratović. Dynamics of articulated open-chain active mechanisms. *Mathematical Biosciences*, 28:137–170, 1976.

[52] D. S. Kwon and W. J. Book. An inverse dynamic method yielding flexible manipulator state trajectories. In *Proceedings of American Control Conference*, volume 1, pages 186–193, 1990.

[53] W. Gawronski, C.-H. C. Ih, and S. J. Wang. On dynamics and control of multi-link flexible manipulators. *Journal of Dynamic Systems, Measurement, and Control*, 117:134–142, June 1995.

[54] V. A. Spector and H. Spector. Modeling and design implications of noncollocated control in flexible systems. *Journal of Dynamic Systems, Measurement, and Control*, 112:186–193, 1990.

[55] D. S. Wang, G.-B. Yang, and M. Donath. Non-collocated flexible beam motion control based on a delayed adaptive inverse method. In *Proceedings of the 1993 American Control Conference*, pages 552–559, San Francisco, CA, June 1993.

[56] M. Vidyasagar. *Nonlinear Systems Analysis*. Simon and Schuster, 1993.

[57] L. Meirovitch. *Elements of vibration analysis.* McGraw-Hill, 1986.

[58] C.-T. Chen. *Linear System Theory and Design.* Holt, Rinehart and Winston, 1984.

[59] E. Bayo and H. Moulin. An efficient computation of the inverse dynamics of flexible manipulators in the time domain. In *Proceedings 1989 IEEE International Conference on Robotics and Automation*, pages 710–715, Scottsdale, AZ, 1989.

[60] H. C. Moulin, Eduardo Bayo, and Bradley Paden. Existence and uniqueness of solutions of the inverse dynamics of multilink flexible arms: Convergence of a numerical scheme. *Journal of Robobic Systems*, 10(1):73–102, 1993.

[61] M. Nahon, C. Damaren, A. Bergen, and J. Gonçalves. A test facility for multi-armed space-based manipulators. *Canadian Aeronautic and Space Journal*, pages 391–400, 1995.

[62] D. G. Luenberger. *Linear and Nonlinear Programming.* Addison-Wesley Publishing Company, 1984.

[63] M. Nahon. *Optimization of Force Distribution in Redundantly-Actuated Robotic System.* PhD thesis, McGill University, Montréal, Canada, February 1991.

[64] J. K. Salisbury and J. J. Craig. Articulated hands: Force control and kinematic issues. *The International Journal of Robotics Research*, 1(1):4–17, 1982.

[65] H. Hanafusa and H. Asada. Stable prehension by a robot hand with elastic fingers. In *Proceedings of the 7th International Symposium on Industrial Robots*, pages 361–368, Tokyo, October 1977.

[66] W. Yim and S. N. Singh. Inverse force and motion control of constrained elastic robots. *Journal of Dynamic Systems, Measurement, and Control*, 117:374–383, September 1995.

[67] G. Strang. *Linear Algebra and its Applications.* Academic Press Inc., 1976.

[68] F. Pfeiffer, H.-J. Weidemann, and P. Danowski. Dynamics of the walking stick insect. In *Proceedings of the 1990 IEEE International Conference on Robotics and Automation*, volume 3, pages 1458–1463, Cincinnati, Ohio, May 1990.

[69] H. D'Angelo. *Linear Time-Varying Systems: Analysis and Synthesis.* Allyn and Bacon Inc., 1970.

[70] M. W. Spong and M. Vidyasagar. *Robot Dynamics and Control.* New York: Wiley, 1989.

[71] A. De Luca and B. Siciliano. Joint-based control of a nonlinear model of a flexible arm. In *Proceedings of the 1988 American Control Conference*, pages 935–940. Atlanta, GA, June 1988.

[72] J. Z. Xia and C.-H. Menq. Real time estimation of elastic deformation for end-point tracking control of flexible two-link manipulators. *Journal of Dynamic Systems, Measurement, and Control*, 115:385–393, September 1993.

[73] M. W. Vandegrift, F. L. Lewis, and S. Q. Zhu. Flexible-link robot arm control by a feedback linearization/singular perturbation approach. *Journal of Robotic Systems*, 11(7):591–603, 1994.

[74] D. Wang and M. Vidyassagar. Passive control of a stiff flexible link. *The International Journal of Robotics Research*, 11(6):572–578, 1992.

[75] S. K. Madhavan and S. N. Singh. Inverse trajectory control and zero dynamic sensitivity of an elastic manipulator. *The International Journal of Robotics and Automation*, 6(4):179–192, 1991.

[76] K. P. Jankowski, H. A. ElMaraghy, and W. H. ElMaraghy. Dynamic coordination of multiple robot arms with flexible joints. *The International Journal of Robotics Research*, 12(6):505–528, 1993.

[77] Y.-R. Hu adn A. A. Goldenberg. An approach to motion and force control of coordinated robot arms in the presence of joint flexibility. In *IRIS Workshop on Dynamics and Control of Flexible Manipulators*, Vancouver, BC, April 1993.

Appendix A

Interbody Matrices and Projection Matrices

In this appendix, we introduce various sets of matrices which are used to relate the geometric properties of the bodies in a chain to one another and to describe the chain kinematics.

A.1 Rotation Matrices

We associate with each body frame $\mathcal{F}_n$ $(n = 0, 1, \ldots, N)$ a corresponding *vectrix* — a column of three dextral, orthogonal unit vectors. We denote by $\mathbf{F}_n$ the vectrix corresponding to the frame $\mathcal{F}_n$.

Components of any vector in any frame can be transformed into the components in any other frame by means of the rotation matrix $\mathbf{C}_{n,m}$, defined as follows:

$$\mathbf{C}_{n,m} \triangleq \mathbf{F}_n \mathbf{F}_m^T \qquad (n, m = 0, 1, \ldots, N) \qquad (A.1)$$

This rotation matrix is orthonormal so that

$$\mathbf{C}_{n,m}^{-1} = \mathbf{C}_{n,m}^{T} = \mathbf{C}_{m,n} \tag{A.2}$$

It is also convenient to define the following 6×6 rotation matrix:

$$\mathcal{C}_{n,m} = \begin{bmatrix} \mathbf{C}_{n,m} & \mathbf{0} \\ \mathbf{0} & \mathbf{C}_{n,m} \end{bmatrix} \tag{A.3}$$

A.2 Matrix $\mathbf{R}_{n+1,n}$

It is helpful in the dynamics analysis of multibody systems to define the following 6×6 matrices:

$$\mathbf{R}_{n+1,n} = \begin{bmatrix} \mathbf{1} & -\mathbf{r}_{n,n+1}^{\times} \\ \mathbf{0} & \mathbf{1} \end{bmatrix} \qquad (n = 0, 1, \ldots, N) \tag{A.4}$$

We also define

$$\mathbf{R}_{n,n+1} = \begin{bmatrix} \mathbf{1} & -\mathbf{r}_{n+1,n}^{\times} \\ \mathbf{0} & \mathbf{1} \end{bmatrix} \qquad (n = 0, 1, \ldots, N) \tag{A.5}$$

The transpose and inverse of $\mathbf{R}_{n+1,n}$ are respectively

$$\mathbf{R}_{n+1,n}^{T} = \begin{bmatrix} \mathbf{1} & \mathbf{0} \\ \mathbf{r}_{n,n+1}^{\times} & \mathbf{1} \end{bmatrix} \tag{A.6}$$

and

$$\mathbf{R}_{n+1,n}^{-1} = \begin{bmatrix} \mathbf{1} & \mathbf{r}_{n+1,n}^{\times} \\ \mathbf{0} & \mathbf{1} \end{bmatrix} \tag{A.7}$$

A.3 Interbody Transformations

The interbody transformation matrix $\mathcal{T}_{n+1,n}$ is defined as

$$\mathcal{T}_{n+1,n} = \mathcal{C}_{n+1,n}\mathbf{R}_{n+1,n} \tag{A.8}$$

Also, it is not difficult to show that

$$\mathcal{T}_{n,n+1} = \mathcal{C}_{n,n+1}\mathbf{R}_{n,n+1} \tag{A.9}$$

and

$$\mathcal{T}^{-1}_{n+1,n} = \mathcal{T}_{n,n+1} \tag{A.10}$$

Moreover, for $m > n+1$, the following is also true

$$\mathcal{T}_{m,n} = \mathcal{T}_{m,m-1}\mathcal{T}_{m-1,m-2}\cdots\mathcal{T}_{n+2,n+1}\mathcal{T}_{n+1,n} \tag{A.11}$$

and

$$\mathcal{T}^{-1}_{m,n} = \mathcal{T}_{n,m} \tag{A.12}$$

A.4 Generalized Transformation Matrix for Elastic Bodies

The generalized transformation matrix for elastic body is used to determine the effect of the elastic deformation on the spatial velocity at the joint. It is defined as:

$$\mathcal{S}_{n+1,n} = \mathcal{C}_{n+1,n}\Xi_{n+1,n} \tag{A.13}$$

where

$$\Xi_{n+1,n} = \begin{bmatrix} \Psi(\mathbf{r}_{n,n+1}) \\ \Theta(\mathbf{r}_{n,n+1}) \end{bmatrix} \tag{A.14}$$

In the above, $\Psi(\mathbf{r}_{n,n+1})$ is the shape function matrix at $\mathbf{r}_{n,n+1}$ associated with the elastic deformation and Θ is defined by:

$$\Theta = \frac{1}{2}\nabla^{\times}\Psi \tag{A.15}$$

A.5 Projection Matrix

A projection matrix is used to define the geometric constraints imposed at each joint. Columns span the subspace of allowable interbody motion. Therefore, the dimension of $\mathcal{P}_n$ is $6 \times m_n$ where m_n (< 6) is the number of allowable degrees of freedom.

In a typical case of robotics application, the following is commonly used:

$$\mathcal{P}_n = \begin{bmatrix} 0 & 0 & 0 & 0 & 0 & 1 \end{bmatrix}^T \tag{A.16}$$

The above implies that only one rotational degree of freedom about the third axis is allowed.

A.6 Global Transformation Matrices

The global transformation matrices for a multibody chain are defined as follows:

$$\mathcal{T}_{\Sigma} = \begin{bmatrix} \mathbf{1} & \mathbf{0} & \mathbf{0} & \cdots & \mathbf{0} \\ \mathcal{T}_{1,0} & \mathbf{1} & \mathbf{0} & \cdots & \mathbf{0} \\ \mathcal{T}_{2,0} & \mathcal{T}_{2,1} & \mathbf{1} & \cdots & \mathbf{0} \\ \vdots & \vdots & \vdots & \cdots & \vdots \\ \mathcal{T}_{N,0} & \mathcal{T}_{N,1} & \mathcal{T}_{N,2} & \cdots & \mathbf{1} \end{bmatrix} \tag{A.17}$$

and

$$\mathcal{S}_{\Sigma} = \begin{bmatrix} \mathbf{0} & \mathbf{0} & \cdots & \mathbf{0} & \mathbf{0} \\ \mathcal{S}_{1,0} & \mathbf{0} & \cdots & \mathbf{0} & \mathbf{0} \\ \mathbf{0} & \mathcal{S}_{2,1} & \cdots & \mathbf{0} & \mathbf{0} \\ \vdots & \vdots & \cdots & \vdots & \vdots \\ \mathbf{0} & \mathbf{0} & \cdots & \mathcal{S}_{N,N-1} & \mathbf{0} \end{bmatrix} \tag{A.18}$$

Appendix B

Definitions and Theorems of Optimization

B.1 General Form of Optimization Problem

We now introduce some basic definitions and fundamental theorems used in solving the constrained optimization problems. A general form of such a problem is given as [62]:

$$\min_{\mathbf{x}} \quad f(\mathbf{x}) \qquad \mathbf{x} \in \mathbf{R}^n \tag{B.1a}$$

$$\text{Subject to} \quad h_i(\mathbf{x}) = 0 \qquad i = 1, \cdots, m \tag{B.1b}$$

$$\text{and} \quad g_j(\mathbf{x}) \leq 0 \qquad j = 1, \cdots, p \tag{B.1c}$$

where $m \leq n$ and functions f, h_i $(i = 1, \cdots, m)$ and g_j $(j = 1, \cdots, p)$ are continuous, and are usually assumed to possess continuous second partial derivatives. For the objective function, we define a *gradient vector* $\nabla f \in \mathbf{R}^n$ of the objective function f

at $\mathbf{x}$:

$$\nabla f = \begin{bmatrix} \partial f/\partial \mathrm{x}_1 \\ \partial f/\partial \mathrm{x}_2 \\ \vdots \\ \partial f/\partial \mathrm{x}_n \end{bmatrix} \tag{B.2}$$

and the *Hessian matrix* of f:

$$\mathbf{H}(f) = \begin{bmatrix} \partial^2 f/\partial^2 \mathrm{x}_1 & \partial^2 f/\partial \mathrm{x}_1 \partial \mathrm{x}_2 & \cdots & \partial^2 f/\partial \mathrm{x}_1 \partial \mathrm{x}_n \\ \partial^2 f/\partial \mathrm{x}_2 \partial \mathrm{x}_1 & \partial^2 f/\partial^2 \mathrm{x}_2 & \cdots & \partial^2 f/\partial \mathrm{x}_2 \partial \mathrm{x}_n \\ \vdots & \vdots & \cdots & \vdots \\ \partial^2 f/\partial \mathrm{x}_n \partial \mathrm{x}_1 & \partial^2 f/\partial \mathrm{x}_n \partial \mathrm{x}_2 & \cdots & \partial^2 f/\partial^2 \mathrm{x}_n \end{bmatrix} \tag{B.3}$$

Constraints on the design variables separate the design space into *feasible* and *infeasible* regions which are defined below.

Definition B.1 (Feasible Point and Feasible Region)

If any point $\mathbf{x}'$ satisfies all the constraints in (B.1b) and (B.1c), it is said to be a *feasible point*. The set of all such points is referred to as the *feasible region* and is denoted by Ω.

An inequality constraint can be characterized according to the following definition:

Definition B.2 (Active and Inactive Constraint)

A constraint $g_j(\mathbf{x}) \leq 0$ is said to be *active* at a feasible point $\mathbf{x}$ if $g_j(\mathbf{x}) = 0$ and *inactive* at $\mathbf{x}$ if $g_j(\mathbf{x}) < 0$. By convention, any equality constraint $h_i(\mathbf{x}) = 0$ is *active* at any feasible point.

In the investigation of the general problem (B.1), we distinguish two kinds of solution points: *local minimum points* and *global minimum points*.

Definition B.3 (Local Minimum Point)

A point $\mathbf{x}^* \in \Omega$ is said to be a *local minimum point* of f over Ω if there is an $\varepsilon > 0$ such that $f(\mathbf{x}) \geq f(\mathbf{x}^*)$ for all $\mathbf{x} \in \Omega$ within a distance ε of $\mathbf{x}^*$ (that is, $\mathbf{x} \in \Omega$ and $|\mathbf{x} - \mathbf{x}^*| < \varepsilon$). If $f(\mathbf{x}) > f(\mathbf{x}^*)$ for all $\mathbf{x} \in \Omega$, $\mathbf{x} \neq \mathbf{x}^*$, within a distance ε of $\mathbf{x}^*$, then $\mathbf{x}^*$ is said to be a *strict local minimum point* of f over Ω.

Definition B.4 (Global Minimum Point)

A point $\mathbf{x}^* \in \Omega$ is said to be a *global minimum point* of f over Ω if $f(\mathbf{x}) \geq f(\mathbf{x}^*)$ for all $\mathbf{x} \in \Omega$. If $f(\mathbf{x}) > f(\mathbf{x}^*)$ for all $\mathbf{x} \in \Omega$, $\mathbf{x} \neq \mathbf{x}^*$, then $\mathbf{x}^*$ is said to be a *strict global minimum point* of f over Ω.

In formulating and attacking problem (B.1) we are, by definition, seeking a global minimum point of f over the feasible region Ω. An ideal situation is when a strict global minimum point exists which means the minimum point is *unique* over the feasible region. In reality, however, searching for the minimum point by comparison of the values of nearby points is all that is possible when using a convergent stepwise procedure. Therefore, the optimality conditions which will be introduced in the following section are all related to local minima. Global minimum solutions can only be found if the problem possesses certain convexity properties which essentially guarantee that any local minimum is a global minimum.

B.2 Optimality Conditions

In studying the properties of a local minimum point, it is clear that only the active constraints need to be considered. This is illustrated in Figure B.1 where the local properties satisfied by the solution $\mathbf{x}^*$ do not depend on the inactive constraints g_2 and g_3. This observation suggests that optimality conditions can be derived by considering

the equality constraints alone and subsequently making additions to account for the selection of the active inequality constraints. We begin with the following definition.

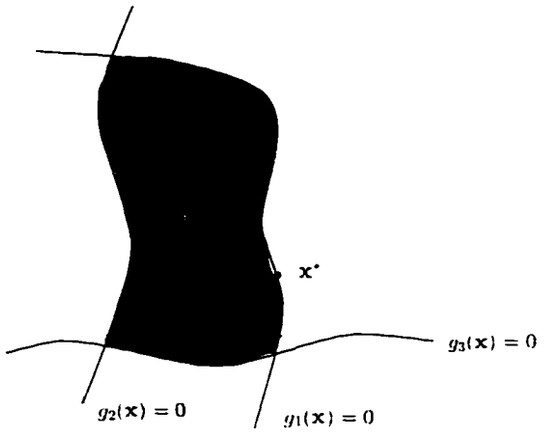

Figure B.1: Example of Inactive Constraints

Definition B.5 (Regular Point)

A point $\mathbf{x}^*$ satisfying the constraint (B.1b) is said to be a *regular point* of the constraint if the gradient vectors $\nabla h_1(\mathbf{x}^*), \nabla h_2(\mathbf{x}^*), \cdots \nabla h_m(\mathbf{x}^*)$ are linearly independent.

For a problem constrained by linear equality equations of the form in (5.1*b*), the above condition for a regular point is equivalent to the matrix $\mathbf{A}_1$ having a full rank. From the simplest optimization problem — the unconstrained one-dimensional optimization — we know that a local minimum point requires zero slope and positive curvature. We would also expect similar optimality conditions for the constrained multi-dimensional problems.

Theorem B.1 (Lagrange First-Order Necessary Conditions)

Let $\mathbf{x}^*$ be a *local extremum point* (a minimum or maximum) of f subject to the

constraint ($B.1b$) written compactly as $\mathbf{h}(\mathbf{x}) = \mathbf{0}$ with $\mathbf{h} = \text{col}\{h_1, h_2, \cdots, h_m\}$. Assume further that $\mathbf{x}^*$ is a regular point of these constraints, then there exists $\boldsymbol{\lambda} = \text{col}\{\lambda_1, \lambda_2 \ldots, \lambda_m\}$ such that

$$\nabla f(\mathbf{x}^*) + \nabla \mathbf{h}(\mathbf{x}^*)\boldsymbol{\lambda} = \mathbf{0} \tag{B.4}$$

where the elements of $\boldsymbol{\lambda}$ are called the *Lagrange multipliers*.

In the above, the gradient of $\mathbf{h}$ is evaluated at $\mathbf{x}^*$ according to

$$\nabla \mathbf{h}(\mathbf{x}^*) = \begin{bmatrix} \partial h_1/\partial \mathrm{x}_1 & \partial h_2/\partial \mathrm{x}_1 & \cdots & \partial h_m/\partial \mathrm{x}_1 \\ \partial h_1/\partial \mathrm{x}_2 & \partial h_2/\partial \mathrm{x}_2 & \cdots & \partial h_m/\partial \mathrm{x}_2 \\ \vdots & \vdots & \cdots & \vdots \\ \partial h_1/\partial \mathrm{x}_n & \partial h_2/\partial \mathrm{x}_n & \cdots & \partial h_m/\partial \mathrm{x}_n \end{bmatrix} \tag{B.5}$$

In the case that (B.1b) is a set of linear equations, that is,

$$\mathbf{h}(\mathbf{x}) = \mathbf{A}_1\mathbf{x} - \mathbf{b}_1 = \mathbf{0} \tag{B.6}$$

the gradient matrix composed of ∇h_i is then a constant matrix:

$$\nabla \mathbf{h} = \mathbf{A}_1^T \tag{B.7}$$

Therefore, the first-order necessary condition of eq. (B.4) becomes

$$\nabla f(\mathbf{x}^*) = -\mathbf{A}_1^T\boldsymbol{\lambda} \tag{B.8}$$

This means that the gradient vector of f must lie in the range space of $\mathbf{A}_1^T$, or equivalently, $\nabla f(\mathbf{x}^*)$ is orthogonal to the null space of $\mathbf{A}_1$.

The information supplied by the first-order necessary condition is not sufficient to determine whether or not the extremum point is a local minimum since eq. (B.4) will be satisfied by both the minima and maxima in the feasible region. Therefore, we introduce a sufficient condition for obtaining a strict local minimum point:

Theorem B.2 (Second-Order Sufficiency Conditions)

Suppose there is a point $\mathbf{x}^*$ satisfying $\mathbf{h}(\mathbf{x}^*) = \mathbf{0}$, and $\boldsymbol{\lambda} \in \mathbf{R}^m$ such that

$$\nabla f(\mathbf{x}^*) + \nabla \mathbf{h}(\mathbf{x}^*)\boldsymbol{\lambda} = \mathbf{0} \tag{B.9}$$

Suppose also that the matrix $\mathbf{L}(\mathbf{x}^*) = \mathbf{H}(f(\mathbf{x}^*)) + \mathbf{H}(\mathbf{h}(\mathbf{x}^*))\boldsymbol{\lambda}$ is *positive definite* on $M = \{\mathbf{y} : \nabla \mathbf{h}(\mathbf{x}^*)\mathbf{y} = \mathbf{0}\}$, that is, for $\mathbf{y} \in M$, $\mathbf{y} \neq 0$, we have $\mathbf{y}^T\mathbf{L}(\mathbf{x}^*)\mathbf{y} > 0$. Then $\mathbf{x}^*$ is a strict local minimum of f subject to $\mathbf{h}(\mathbf{x}) = \mathbf{0}$.

In the above theorem, the Hessian matrix of $\mathbf{h}$ is calculated as:

$$\mathbf{H}(\mathbf{h}(\mathbf{x}^*)) = \sum_{j=1}^{m} \mathbf{H}(h_j(\mathbf{x}^*)) \tag{B.10}$$

The second term in the matrix $\mathbf{L}$ represents the following expansion [62]:

$$\mathbf{H}(\mathbf{h})\boldsymbol{\lambda} = \sum_{j=1}^{m} \lambda_j \mathbf{H}(h_j(\mathbf{x}^*)) \tag{B.11}$$

Again, in the case when $\mathbf{h}$ is linear in $\mathbf{x}$, $\mathbf{H}(\mathbf{h}) = \mathbf{0}$. Hence, the condition for the positive definiteness of $\mathbf{L}(\mathbf{x}^*)$ on M reduces to:

$$\mathbf{y}^T\mathbf{H}(f(\mathbf{x}^*))\mathbf{y} > 0 \tag{B.12}$$

The significance of introducing Lagrange multipliers can be observed from Theorem B.1 which reduces a minimization (or maximization) problem subject to equality constraints to a constraint-free stationary value problem. The Lagrange multipliers are also important in determining how much a cost function f varies with a small variation in the constraint equations. Therefore, the Lagrange multipliers are also interpreted as a marginal *price* [62].

B.3 Extended Optimality Conditions

We consider now the problems of the form (B.1), that is, an optimization problem subject to both equality *and* inequality constraints. We start by extending the definition B.5 of a regular point as follows:

Definition B.6 (Regular Point Extended)

Let $\mathbf{x}^*$ be a point satisfying the constraints

$$\mathbf{h}(\mathbf{x}^*) = \mathbf{0} \qquad \mathbf{g}(\mathbf{x}^*) \leq \mathbf{0} \tag{B.13}$$

and let J be the set of indices j for which $g_j(\mathbf{x}^*) = 0$. Then $\mathbf{x}^*$ is said to be a *regular point* of the constraints (B.13) if the gradient vectors $\nabla h_i(\mathbf{x}^*)$, $\nabla g_j(\mathbf{x}^*)$, $1 \leq i \leq m$, $j \in J$ are linearly independent.

We note that according to the definition for active constraints given in definition B.2, a point $\mathbf{x}^*$ is a regular point if the gradients of the active constraints are linearly independent. For a linearly constrained problem, if we collect all active constraints as columns of a single matrix, the condition for a regular point of these constraints is that the resulting matrix has a full rank. For the extended first-order necessary conditions, the following theorem is given.

Theorem B.3 (Kuhn-Tucker Conditions)

Let $\mathbf{x}^*$ be a local minimum point for the problem as defined in eq. (B.1) and suppose $\mathbf{x}^*$ is a regular point for the constraints. Then there is a vector $\boldsymbol{\lambda} \in \mathbf{R}^m$ and a vector $\boldsymbol{\mu} \in \mathbf{R}^p$ with $\boldsymbol{\mu} \geq \mathbf{0}$ such that

$$\nabla f(\mathbf{x}^*) + \nabla \mathbf{h}(\mathbf{x}^*)\boldsymbol{\lambda} + \nabla \mathbf{g}(\mathbf{x}^*)\boldsymbol{\mu} = \mathbf{0} \tag{B.14}$$

$$\boldsymbol{\mu}^T \mathbf{g}(\mathbf{x}^*) = 0 \tag{B.15}$$

We note that, since $\boldsymbol{\mu} \geq \mathbf{0}$ and $\mathbf{g}(\mathbf{x}^*) \leq \mathbf{0}$, eq. (B.15) is equivalent to the statement that a component of $\boldsymbol{\mu}$ may be nonzero only if the corresponding constraint is active. Similarly, the second-order sufficient conditions are extended for the situation with inequality constraints as follows:

Theorem B.4 (Extended Second-Order Sufficiency Conditions)

Let f, $\mathbf{g}$, $\mathbf{h}$ have continuous second partial derivatives. Sufficient conditions for a point $\mathbf{x}^*$ satisfying (B.1b) and (B.1c) to be a strict relative minimum of the problem (B.1) is that there exist $\boldsymbol{\lambda} \in \mathbf{R}^m$ and $\boldsymbol{\mu} \in \mathbf{R}^p$, such that

$$\boldsymbol{\mu} \geq \mathbf{0} \tag{B.16}$$

$$\boldsymbol{\mu}^T \mathbf{g}(\mathbf{x}^*) = 0 \tag{B.17}$$

$$\nabla f(\mathbf{x}^*) + \nabla \mathbf{h}(\mathbf{x}^*)\boldsymbol{\lambda} + \nabla \mathbf{g}(\mathbf{x}^*)\boldsymbol{\mu} = \mathbf{0} \tag{B.18}$$

and the Hessian matrix

$$\mathbf{L}(\mathbf{x}^*) = \mathbf{H}(f(\mathbf{x}^*)) + \mathbf{H}(\mathbf{h}(\mathbf{x}^*))\boldsymbol{\lambda} + \mathbf{H}(\mathbf{g}(\mathbf{x}^*))\boldsymbol{\mu} \tag{B.19}$$

is positive definite on the subspace

$$M' = \{\mathbf{y} : \nabla \mathbf{h}(\mathbf{x}^*)\mathbf{y} = \mathbf{0}, \nabla g_j(\mathbf{x}^*)\mathbf{y} = \mathbf{0} \text{ for all } j \in J\}$$

where

$$J = \{j : g_j(\mathbf{x}^*) = 0, \mu_j > 0\}$$

Once again, for a linearly constrained problem, the condition for the positiveness of the Hessian matrix $\mathbf{L}(\mathbf{x}^*)$ reduces to $\mathbf{H}(f(\mathbf{x}^*))$ being positive definite on the subspace M'. In summary, we note that the inequalities are treated by determining which of them are active at a solution. An active inequality constraint is then treated just like an equality constraint, except that its associated Lagrange multiplier can never be negative.

B.4 Convex Functions

Based on the above optimality theorems, a constrained optimization problem can be approached by solving directly the Lagrange first-order necessary conditions. The second-order sufficient conditions are then used to determine whether or not point $\mathbf{x}^*$ satisfying the Lagrange first-order conditions is a local minimum. This procedure is known as the Lagrange method. In some cases, if the objective function takes a special form, the second step can be omitted. An ideal situation arises for a particular objective function, when a solution of the Lagrange first-order necessary conditions is guaranteed to produce a unique global minimum point in the design space. Such objective function is known as a convex function as defined below.

Definition B.6 (Convex Set)

A set Ω in $\mathbf{R}^n$ is said to be *convex* if for every $\mathbf{x}_1, \mathbf{x}_2 \in \Omega$ and every real number α, $0 < \alpha < 1$, the point $\alpha\mathbf{x}_1 + (1-\alpha)\mathbf{x}_2 \in \Omega$.

With this definition, it is trivial to show that the design space $\mathbf{R}^n$ is always convex since any point on the line connecting two other points in $\mathbf{R}^n$ is also a member of $\mathbf{R}^n$.

Definition B.7 (Convex Function)

A function f defined on a convex set Ω is said to be *convex* if for every $\mathbf{x}_1, \mathbf{x}_2 \in \Omega$ and every α, $0 \leq \alpha \leq 1$, the following holds

$$f(\alpha\mathbf{x}_1 + (1-\alpha)\mathbf{x}_2) \leq \alpha f(\mathbf{x}_1) + (1-\alpha) f(\mathbf{x}_2) \tag{B.20}$$

The function f is said to be strictly convex if for every α, $0 < \alpha < 1$, and $\mathbf{x}_1 \neq \mathbf{x}_2$, the following holds

$$f(\alpha\mathbf{x}_1 + (1-\alpha)\mathbf{x}_2) < \alpha f(\mathbf{x}_1) + (1-\alpha) f(\mathbf{x}_2) \tag{B.21}$$

In addition, convex functions can be combined to yield new convex functions. For a function which is twice continuously differentiable, an alternative characterization of convexity can be stated in terms of the function's Hessian matrix: a positive semidefinite Hessian implies a convex function, while a positive definite Hessian implies a strictly convex function.